

INTERIM
IN 507
507
P 90

Annual Progress Report

January 1, 1994- December 31, 1994

FEB 08 1995
NCC 2-651

Grant Title: Comparative transduction mechanisms of vestibular otolith hair cells

Grant number: NASA grant 2-651

Principal Investigator: Richard A. Baird
Associate Scientist

Institution: R.S. Dow Neurological Sciences Institute
Legacy Good Samaritan Hospital and Medical Center
1120 NW 20th Avenue
Portland, OR 97209
(503) 229-8205 (VOICE)
(503) 229-7229 (FAX)
Bairdr@ohsu.edu (INTERNET)

Principal Investigator

Richard A Baird

1/25/95

Richard A. Baird, Associate Scientist

Date

Institutional Officer

Lutz L. Kiesow

2/2/95

Lutz Kiesow, M.D., Ph.D., Chief, Legacy Research

Date

(NASA-CR-197980) COMPARATIVE
TRANSDUCTION MECHANISMS OF
VESTIBULAR OTOLITH HAIR CELLS
Annual Report, 1 Jan. - 31 Dec.
1994 (Legacy Good Samaritan
Hospital) 90 p

N95-26727
--THRU--
N95-26732
Unclass

Description of Research:

The vertebrate utricle transduces the linear forces produced by static head displacement relative to gravity and by dynamic translational head acceleration into neural signals. Utricular hair cells with differing hair bundle morphology differ in their voltage-dependent conductances. These conductances, by acting as frequency-dependent filters of the receptor current, modify the sensitivity and frequency selectivity of hair cells. Utricular hair cells also differ in their rate of adaptation to sustained head displacement. Nonadapting hair cells are most sensitive to static gravity and adapting hair cells, because they do not retain information about maintained displacement, are most sensitive to changes in linear acceleration. The dual encoding functions of the vestibular otolith organs are therefore largely accomplished by varying the rate and extent of adaptation in different hair cell phenotypes.

Hair cells in the bullfrog vestibular otolith organs regenerate following aminoglycoside ototoxicity. Hair cells in these organs are differentially sensitive to gentamicin, with saccular hair cells and hair cells in the utricular striola being damaged at lower gentamicin concentrations than hair cells in the utricular extrastriola. Regenerating hair cells in these organs have short hair bundles and can be classified into a number of phenotypes using the same morphological criteria used to identify their mature counterparts. BrdU-labeling studies in living animals and *in vitro* organ cultures indicate that hair cell recovery in the vestibular otolith organs is accomplished by both mitotic and non-mitotic mechanisms. The former mechanism is known to produce hair cells through the mitotic division of precursor cells. Our studies also suggest that some supporting cells can convert, or *transdifferentiate*, into hair cells without an intervening cell division. By stimulating these processes in humans, clinicians may be able to alleviate human deafness and peripheral vestibular disorders by regenerating and replacing lost hair cells.

Accomplishments:**(1) *In vivo* studies of cell proliferation and hair cell regeneration**

The results of earlier *in vivo* studies suggested that hair cell regeneration in the vestibular otolith organs might involve the mitotic production of new hair cells. To examine the role of mitotic division in hair cell recovery, we injected bullfrogs with 5-bromo-2'-deoxyuridine (*BrdU*), a thymidine analogue incorporated into mitotic cells. Using BrdU immunocytochemistry, we then measured the number, macular location, and cell morphology of BrdU-labeled cells at varying survival times.

Cell proliferation was seen in normal and gentamicin-treated animals. BrdU-labeling in the sacculus was more extensive than in the utricle, consistent with the greater damage caused by gentamicin to the former organ. BrdU-labeled cells were initially seen in the macular margins and, within the maculae, immediately adjacent to the basement membrane. The latter cells had spherical cell bodies and, unlike typical supporting cells, did not project to the lumenal surface. At later survival times, BrdU-labeled cells were located further from the basement membrane and displayed mitotic figures, suggesting that progenitor cells underwent cell division at more apical positions.

The total number of BrdU-labeled cells in normal and gentamicin-treated animals increased with survival time. This increase, which was first observed 3-5 days postinjection, was largely due to an increase in progenitor progeny. Cell proliferation, however, was insufficient to explain the amount of hair cell regeneration seen in the vestibular otolith organs. At early survival times, large numbers of hair cells with immature hair bundles were seen in gentamicin-treated animals *before* the arrival of progenitor progeny. Moreover, the total number of proliferating progeny at late survival times was still significantly lower than the number of regenerating hair cells. The great majority of regenerating hair cells in the vestibular otolith organs were therefore not BrdU-labeled, suggesting that hair cell recovery in these organs was primarily determined by non-mitotic mechanisms. These mechanisms might include hair cell migration from undamaged macular regions, hair bundle repair

in damaged hair cells, or the conversion (*transdifferentiation*) of undamaged supporting cells into hair cells (see below). The results of these studies were reported in preliminary form at the 1993 Annual meeting of the Society for Neuroscience (D) and the 1994 Mechanisms of Sensory Regeneration Conference (B). We will soon submit these studies in manuscript form to the *Journal of Comparative Neurology* (I).

(2) Morphological studies of scar formation and hair cell regeneration

We used rhodamine-conjugated phalloidin to label filamentous actin in normal and gentamicin-treated organs. This technique clearly differentiated hair cells and supporting cells and improved the visibility of immature hair bundles, allowing us to more closely examine the processes of hair cell degeneration, scar formation, and hair cell regeneration. In normal animals, phalloidin strongly labeled filamentous actin in intercellular adherens junctions at the apical surfaces of marginal cells and, within the sensory epithelium, the apical surfaces of hair cells and supporting cells. It also strongly labeled the sensory hair bundles and the cuticular plates of hair cells. By contrast, little phalloidin staining was observed within supporting cells.

The distribution of phalloidin staining changed dramatically in gentamicin-treated animals. In the sacculus, little phalloidin staining was seen above the luminal surface 24-48 hours after gentamicin treatment, confirming that this treatment resulted in a profound loss of hair bundles throughout the central sacculus and, less extensively, in the peripheral saccular margins. Phalloidin staining in the utricular striola was similarly depleted. In the medial and lateral extrastriolar regions, on the other hand, phalloidin staining was largely unaffected by gentamicin treatment. Phalloidin staining of hair bundles was largely restored in both the saccular and utricular macula at later survival times, consistent with the re-appearance of hair cells.

We also examined the luminal surfaces of phalloidin-labeled organs at higher magnification to more closely study the processes of hair cell degeneration, scar formation, and hair cell regeneration. In normal animals, the luminal surfaces of hair cells and supporting cells in the sacculus and formed a complex mosaic pattern. Hair cells were seldom in contact with other hair cells. The luminal surfaces of hair cells were circular while those of supporting cells were polygonal in shape, ranging from four to six sides. At lower levels, a narrow actin-free zone, demarcating the borders between adjacent cells, was visible between hair cells and supporting cells.

Hair cells in the central sacculus, although they were all the same phenotypes, differed markedly in the size of their hair bundles. Most saccular hair cells in normal animals had mature hair bundles. A few hair cells had smaller luminal surfaces and hair bundles than those of mature hair cells. Immature hair cells, like mature hair cells, were seldom in contact with other hair cells and typically had circular apical surfaces. Hair cells with small hair bundles were, however, surrounded by fewer supporting cells than hair cells with more mature hair bundles. Immature saccular hair cells, for example, typically had four neighboring supporting cells, although they could be surrounded by from three to six supporting cells. Mature hair cells, on the other hand, typically had five neighboring supporting cells.

We observed a near-complete loss of hair bundles in the central sacculus one to two days after gentamicin treatment, although hair bundles in the peripheral macular margins were still present. Despite the loss of their hair bundles, hair cells in these animals could still be differentiated from supporting cells by their cuticular plates and their circular apical surfaces. The few remaining hair cells in the central sacculus had small hair bundles. Except in regions of extensive hair cell damage, the distribution of filamentous actin in intercellular adherens junctions was continuous throughout the confines of the sensory macula. Small epithelial holes, presumably left by individual extruded hair cells, were observed throughout the saccular macula. The number of supporting cells surrounding small epithelial holes in gentamicin-treated animals was similar to that surrounding mature hair cells in normal animals.

Scar formations, composed of the expanded processes of neighboring supporting cells, were commonly seen surrounding the degenerated remnants of hair cells or the epithelial holes left by extruded hair cells. In these regions, the apical surfaces of supporting cells had expanded in size to fill the spaces previously occupied by hair cells. Different scarring patterns were seen in gentamicin-treated animals depending on the number of supporting cells taking part in the scar formation. The number of supporting cells taking part in scar formations ranged from four to eight and was similar to the number of supporting cells surrounding mature hair cells in normal animals.

Scar formations in the bullfrog vestibular otolith organs, unlike those in mammalian vestibular organs, were rapidly replaced by regenerating hair cells. By seven days postinjection, hair bundles were seen throughout the saccular macula, although the mean density of hair cells was less than in normal animals and epithelial holes and scar formations were still visibly apparent. Hair cells with small hair bundles were far more common in these animals than in normal animals, particularly in areas with extensive hair cell damage. As in normal animals, hair cells with immature hair bundles in gentamicin-treated animals were surrounded by fewer supporting cells than mature hair cells.

In heavily damaged regions, unlabeled supporting cells with immature hair bundles and cellular morphology transitional between that of hair cells and supporting cells were often seen, suggesting that hair cell recovery in these regions was primarily determined by the transdifferentiation of undamaged supporting cells into hair cells. Supporting cells have long apical projections which have extensive surface contact with hair cells. We hypothesize that the loss of this contact due to local hair cell death may trigger intercellular signals which initiate the transdifferentiation of supporting cells into hair cells. The results of these studies were reported in preliminary form at the 1994 Mechanisms of Sensory Regeneration Conference (D) and the 1995 ARO Midwinter research meeting (H). We will soon submit these studies in manuscript form to the *Journal of Comparative Neurology* (J).

(3) *In vitro* studies of cell proliferation and hair cell regeneration

In earlier *in vivo* studies, regenerating hair cells were seldom BrdU-labeled, suggesting that hair cell regeneration was largely due to non-mitotic mechanisms. We considered the possibility that BrdU, because it was not administered continuously, was not equally available to all proliferating cells. To rule out this possibility, we repeated our *in vivo* experiments of cell proliferation and hair cell regeneration in saccular and utricular organ cultures.

Excised organs were incubated in Wolfe-Quimby incubation media (GIBCO) and placed, hair bundles upward, in lab-built culture chambers. Cultured organs were maintained for 7-14 days, replacing half of the culture medium with fresh culture medium every two days. We assessed the morphological integrity of normal cultures using Nomarski optics and their vitality with vital dye exclusion. Saccular and utricular cultures were maintained with little cell damage for up to 7 and 11 days, respectively. Within this time frame, the otolith membranes of cultured maculae were only marginally restored, allowing good visibility of hair cells and their sensory hair bundles. In cross-section, the cell and hair bundle morphology of cultured organs was similar to that of normal animals although there was a tendency at longer times for the cultured sacculus to round up and transform into an de-differentiated epithelium. This tendency was suppressed in saccular maculae incubated in amphibian culture medium supplemented with non-essential amino acids. Saccular maculae cultured with intact otolith membranes and nervous innervation also maintained normal cell and hair bundle morphology for longer periods than other saccular maculae.

Organ cultures incubated for 6 or 12 hrs in amphibian culture medium supplemented with 200 or 400 μM gentamicin sulfate displayed extensive cell and hair bundle damage by 2 days. This damage, as *in vivo*, was seen throughout the saccular macula but was restricted in the utricular macula to the striolar region. Gentamicin-treated cultures tended to round up earlier than normal cultures. This tendency was reduced by culturing gentamicin-treated organs in amphibian culture

medium supplemented with sodium pyruvate.

Cell proliferation in both normal and gentamicin-treated cultures consisted of a small number of condensed BrdU-labeled progenitor cells and a large number of diffuse BrdU-labeled progeny. BrdU-labeled cells in normal saccular cultures were seen in the macular margins and, with the exception of the abneural margin, throughout the sensory macula. In the utricle, BrdU labeling was scattered throughout the medial extrastriola and concentrated on the medial striolar border. Cell proliferation, especially in the saccular and utricular margins, was higher than *in vivo* and was up-regulated in gentamicin-treated cultures. The majority of BrdU-labeled progeny, as *in vivo*, were basement and supporting cells, although BrdU-labeled progeny were seen in both normal and gentamicin-treated cultures. As *in vivo*, BrdU-labeled macular cells were more lightly labeled than BrdU-labeled marginal cells, implying that the former cells undergo more rounds of mitotic division than the latter cells.

Gentamicin-treated organs had many hair cells with immature hair bundles, indicating that both cell proliferation and hair cell regeneration were supported by our culture conditions. Hair cell recovery, as *in vivo*, was more complete in the utricle than the sacculus and, in the sacculus, was less complete in the central macula than in the macular margins. Hair cell recovery under *in vitro* conditions was less complete than that seen *in vivo*. *In vivo*, for example, hair cell recovery began within 1-2 days of gentamicin treatment and hair bundle density returned to 75-100% of its normal value by 7-9 days. By contrast, hair bundle density in organ culture returned to only 50% of its normal value in the same time period. The distribution of stereociliary height in gentamicin-treated cultures was also shifted to lower values than in normal cultures, reflecting the loss of existing hair cells and the creation of new hair cells with immature hair bundles. This distribution was also broader than that in normal cultures, suggesting that immature hair cells were forming and maturing throughout the incubation period.

To determine if hair cell regeneration could take place in the absence of cell proliferation, we cultured saccular and utricular maculae in amphibian culture medium supplemented with aphidicolin, a blocker of DNA replication. In these experiments, normal and gentamicin-treated organs were cultured for 7-9 days in amphibian culture medium supplemented with 25 μ M aphidicolin. Aphidicolin was highly successful in blocking cell proliferation, eliminating diffuse BrdU-labeling in both normal and gentamicin-treated organs. Condensed BrdU-labeled cells, on the other hand, were similar in number in organs cultured with and without aphidicolin. Condensed cells, as *in vivo*, were found adjacent to the basement membrane or at the luminal surface. The latter cells exhibited mitotic figures, indicating that they were in the process of cell division. Normal organs cultured in aphidicolin-supplemented medium had normal cell and hair bundle morphology. Hair cell recovery, measured by hair bundle density, was similar in gentamicin-treated organs cultured in normal or aphidicolin-supplemented amphibian culture medium. These preliminary results confirm that mitotic division is not required for hair cell regeneration and suggest that early hair cell recovery after gentamicin ototoxicity is largely due to non-mitotic mechanisms. Preliminary results of our aphidicolin studies were presented at the 1994 Mechanisms of Sensory Regeneration Conference (D) and the 1995 ARO Midwinter research meeting (H). We will soon submit these studies in manuscript form to *Science* magazine (L).

References

Conference Proceedings:

- (A) Baird, R.A. (1994) Hair cell determinants of afferent response dynamics, Mechanisms of Vestibular Function and Dysfunction, Waikoloa, Hawaii.
- (B) Baird, R.A. (1994) Cell proliferation and hair cell regeneration in the bullfrog vestibular otolith organs, Mechanisms of Sensory Regeneration Conference, University of Virginia,

Charlottesville, Virginia.

(C) **Baird, R.A.** (1994) Gravity responses of vestibular otolith hair cells, Gordon Conference on Gravitational Effects on Living Systems, Colby-Sawyer College, New Hampshire.

Manuscripts and abstracts in print:

(D) **Baird, R.A.**, Torres, M.A., and Schuff, N.R. (1993) On-going and gentamicin-induced hair cell regeneration in the bullfrog vestibular otolith organs. *Soc. Neurosci. Abstr.* 19: 1580.

(E) **Baird, R.A.** and Schuff, N.R. (1994) Peripheral innervation patterns of vestibular afferents in the bullfrog utricle. *J. Comp. Neurol.* 342: 279-298.

(F) **Baird, R.A.** (1994) Comparative transduction mechanisms of utricular hair cells. I. Responses to intracellular current. *J. Neurophysiol.* 71: 666-684.

(G) **Baird, R.A.** (1994) Comparative transduction mechanisms of utricular hair cells. II. Sensitivity and response dynamics to hair bundle displacement. *J. Neurophysiol.* 71: 685-705.

(H) **Baird, R.A.** (1995) *In vivo* and *in vitro* evidence for non-mitotic hair cell regeneration of vestibular otolith hair cells, *Assoc. Res. Otolaryngol. Abstr.* 18: 50.

Manuscripts in preparation:

*(I) **Baird, R.A.**, Torres, M.A., and Schuff, N.R. Ongoing and gentamicin-induced hair cell regeneration in the bullfrog vestibular otolith organs. I. Relationship to cellular proliferation. *J. Comp. Neurol.* (Manuscript in preparation).

*(J) **Baird, R.A.**, Torres, M.A., and Schuff, N.R. Ongoing and gentamicin-induced hair cell regeneration in the bullfrog vestibular otolith organs. II. Contribution of non-mitotic mechanisms. *J. Comp. Neurol.* (Manuscript in preparation).

*(K) **Baird, R.A.** and Schuff, N.R. Intracellular distributions and putative functions of calcium-binding proteins in the bullfrog vestibular otolith organs. *Hear. Res.* (Submitted).

*(L) **Baird, R.A.**, Bales, S., Fiorillo, C., and Schuff, N.R. Hair cell regeneration in the bullfrog vestibular otolith organs does not require cell proliferation. *Science Washington DC* (Manuscript in preparation).

I have enclosed copies of manuscripts 4-8 and abstracts of manuscripts 9-12 with this report; full pre-prints of manuscripts 9-12 will be sent to NASA upon final journal submission.

51-5'
N95-26728

P-13

HEARES 01863

Regional differences in lectin binding patterns of vestibular hair cells

R.A. Baird, N.R. Schuff and J. Bancroft

R.S. Dow Neurological Sciences Institute, Good Samaritan Hospital and Medical Center, Portland, Oregon, USA

(Received 4 June 1992; Revision received 11 September 1992; Accepted 16 September 1992)

Surface glycoconjugates of hair cells and supporting cells in the vestibular endorgans of the bullfrog were identified using biotinylated lectins with different carbohydrate specificities. Lectin binding in hair cells was consistent with the presence of glucose and mannose (CON A), galactose (RCA-I), *N*-acetylglucosamine (WGA), *N*-acetylgalactosamine (VVA), but not fucose (UEA-I) residues. Hair cells in the bullfrog sacculus, unlike those in the utricle and semicircular canals, did not stain for *N*-acetylglucosamine (WGA) or *N*-acetylgalactosamine (VVA). By contrast, WGA and, to a lesser extent, VVA, differentially stained utricular and semicircular canal hair cells, labeling hair cells located in peripheral, but not central, regions. In mammals, WGA uniformly labeled Type I hair cells while labeling, as in the bullfrog, Type II hair cells only in peripheral regions. These regional variations were retained after enzymatic digestion. We conclude that vestibular hair cells differ in their surface glycoconjugates and that differences in lectin binding patterns can be used to identify hair cell types and to infer the epithelial origin of isolated vestibular hair cells.

Lectins; Glycoconjugates; Otolith organs; Semicircular canals; Bullfrog; Guinea pig

Introduction

The surface coat of eukaryotic cells consists of extracellular carbohydrate chains of membrane-bound or membrane-associated glycoconjugates (Luft, 1976; Hook et al., 1984). These cell surface glycoconjugates include the glycolipids, glycoproteins, and the proteoglycans with their glycosaminoglycan groups (Glick and Flowers, 1978). A common feature of the glycoconjugates is the presence of negatively-charged carbohydrates bound to either protein or lipid molecules. Although few of these functions have been directly demonstrated, cell surface glycoconjugates are suspected of subserving important functions in neural development, including cell differentiation, recognition, and adhesion (Edelman, 1984; Dodd and Jessell, 1986; Peinado et al., 1987).

The presence of a glycoconjugate-rich surface coat surrounding hair cells and supporting cells of the vertebrate inner ear has been well documented. Hirokawa and Tilney (1982), using frozen, unfixed tissue, described a network of fibrils associated with the plasma membrane of hair cell stereocilia in the chick vestibular organs. The presence of negatively-charged glycoconjugates associated with the plasma membrane of cochlear and vestibular hair cells has also been indirectly demonstrated by binding experiments with poly-

cationic ferritin (Flock et al., 1977), ruthenium red (Slepecky and Chamberlain, 1985; Khan et al., 1990), alcian blue (Santi and Anderson, 1986; 1987) and tannic acid (Prieto and Merchan, 1986; Khan et al., 1990).

Lectins, non-immune proteins able to recognize specific carbohydrate structures, have been widely used as biochemical tools to identify and localize specific glycoconjugates in cell membranes (Sharon and Lis, 1982; Lis and Sharon, 1986). Lectins have previously been used to examine carbohydrates present in the tectorial (Gil-Loyzaga et al., 1985a; Khalkhali-Ellis et al., 1987; Sugiyama et al., 1991; Tachibana et al., 1987a,c) and cupular and otolith membranes (Gil-Loyzaga et al., 1985b; Tachibana et al., 1987b). They have also been used to study the expression of specific glycoconjugates in the inner ear endorgans during postnatal development (Rueda and Lim, 1988; Lim and Rueda, 1990; Prieto et al., 1990; Endo et al., 1991). More recently, investigators have used lectins to demonstrate the presence of a number of carbohydrates on the apical surface of hair cells in the cochlea and vestibular endorgans (Gil-Loyzaga and Brownell, 1988; Khan et al., 1991). They have not, however, attempted to examine regional variations in the glycoconjugate composition of hair cells within individual inner ear endorgans. This is of critical importance in the vestibular endorgans, where Type I and Type II hair cells with differing hair bundle and cell body morphology are located in close proximity to one another (Lindeman, 1969a; Wersall and Bagger-Sjoberg, 1974). Variations in hair bundle morphology are particularly striking in the bullfrog

Correspondence to: Richard A. Baird, R.S. Dow Neurological Sciences Institute, 1120 NW 20th Avenue, Portland, OR 97209, USA.

otolith organs, where several types of Type II hair cells differing in hair bundle morphology (Lewis and Li, 1975; Baird and Lewis, 1986) and physiological response properties (Baird, 1992, 1993a,b) have been described.

In our laboratory, we are studying the development and differentiation of hair cell types in the vestibular endorgans. These studies have been hampered by a lack of cell specific markers that could be used to identify subpopulations of vestibular hair cells. Separation methods used to date have used differences in cell body and hair bundle morphology. It would be highly desirable to separate and characterize subpopulations of hair cells on the basis of their biochemical phenotype. We were also interested in determining whether enzymatically dissociated hair cells maintained their ability to bind specific lectins and, if so, whether differences in lectin binding patterns could be used to infer the epithelial origin of isolated vestibular hair cells. As recent patch-clamp studies have found, it is difficult to infer the epithelial origin of a hair cell once it has been isolated from the sensory epithelium. This problem is compounded in higher vertebrates, where Type I hair cells (Correia and Lang, 1989; Valat et al., 1989; Rennie and Ashmore, 1991) do not retain their cellular morphology after enzymatic dissociation.

In the present study, we used biotinylated lectin probes to identify and characterize the surface glycoconjugates of hair cells in the vestibular endorgans. The primary aim of these studies was to determine if hair cells in different epithelial regions could be distinguished by their surface glycoconjugates. Our results demonstrate that vestibular hair cells in central and peripheral epithelial regions differ in their lectin binding patterns. These differences are preserved after enzymatic dissociation, demonstrating that they can be used to separate Type I and Type II hair cells and to infer the epithelial origin of isolated vestibular hair cells.

Preliminary accounts of portions of this data have been presented in abstract form (Baird et al., 1991).

Methods

Removal of the vestibular endorgans

Adult bullfrogs (*Rana catesbeiana*) were anesthetized by immersion in 0.2% MS-222; guinea pigs (*Cavia porcellus*) received intraperitoneal injections of Nembutal (50 mg/kg body wt). Anesthetized animals were decapitated and the sacculus, utriculus, and horizontal and anterior vertical semicircular canals were dissected from the membranous labyrinth and maintained in cold, oxygenated physiological saline. The cupular and otolith membranes of vestibular endorgans

were removed with gentle mechanical agitation following a 15–45 min proteolytic digestion in 50 $\mu\text{g}/\text{ml}$ subtilopectidase BPN' (Sigma). Vestibular endorgans were then trimmed of excess nerve and connective tissue to improve the visibility of hair bundles and, in some experiments, sectioned with a teflon-coated double-edge razor to separate central and peripheral regions of the sensory epithelium.

Isolation of vestibular hair cells

Hair cells and supporting cells were isolated from the sacculus and horizontal and anterior vertical semicircular canals by enzymatically dissociating the appropriate endorgan for 20–45 min with 500 $\mu\text{g}/\text{ml}$ papain (CalBiochem) and 300 $\mu\text{g}/\text{ml}$ L-cysteine (Sigma) dissolved in Ca^{2+} -free, PIPES-buffered saline (pH = 7.25). The utricular macula was pre-treated for 5 min with 250 $\mu\text{g}/\text{ml}$ collagenase (Sigma, Fraction IV) dissolved in the same buffer. After enzymatic dissociation, endorgans were washed for 10–20 min each in 500 $\mu\text{g}/\text{ml}$ bovine serum albumin (BSA) and 2 $\mu\text{g}/\text{ml}$ DNase 1 (Sigma) dissolved in standard HEPES-buffered saline. They were then mechanically triturated with fire-polished pasteur pipettes, depositing isolated cells into small cover-slipped chambers. Isolated cells were allowed 15–20 min to settle to the chamber bottom. In early studies, chamber bottoms were coated with 1 mg/ml poly-L-lysine (Sigma, > 300,000 mol.wt.). In later experiments, isolated cells were embedded in a 1% solution of low-temperature agarose (BioRad). This change did not affect lectin binding patterns, but did enable larger numbers of isolated cells to survive histological processing.

Lectin histochemistry

Vestibular endorgans and isolated vestibular hair cells were fixed by immersion for 1–4 h in 4% PFA and rinsed with 0.02M phosphate buffered saline containing 0.5 mM CaCl_2 (PBS). If desired, vestibular endorgans were pre-treated for 1 h with 0.1 U/ml neuraminidase (Calbiochem, *Vibrio cholerae*) to remove sialic acid residues. Endorgans were then pre-treated for 1 h in 3% BSA to block non-specific binding sites, rinsed briefly in PBS, and incubated for 1 h in biotinylated lectins (E-Y Labs) diluted 50–100 $\mu\text{g}/\text{ml}$ in PBS. Lectins from other suppliers produced weaker responses than those from E-Y Laboratories. The lectins studied, their carbohydrate specificities, and their inhibitory sugars are listed in Table I.

Biotinylated lectins were visualized by incubating vestibular endorgans for 1 h in 10 $\mu\text{g}/\text{ml}$ streptavidin-Texas Red conjugate (Amersham). Agarose-embedded hair cells were reacted with biotinylated lectins as above except that all incubation times were halved

TABLE I
Lectins used for characterization of vestibular hair cells

Lectin (common name)	Abbreviation	Carbohydrate specificity	Inhibitory sugar
<i>Canavalia ensiformis</i> (jack bean)	CON A	α -Man \gg α -Glc	α -methyl mannopyranoside
<i>Galanthus nivalis</i> (snowdrop)	GNA	α -Man	α -methyl mannopyranoside
<i>Griffonia simplicifolia</i> (no common name)	GS-II	α, β -GlcNAc	β -GlcNAc
<i>Ricinus communis-1</i> (castor bean)	RCA-I	β -Gal	β -Gal
<i>Ulex europaeus</i> (gorse seed)	UEA-I	α -Fuc	α -Fuc
<i>Vicia villosa</i> (hairy vetch)	VVA	α -GalNAc	α -GalNAc
<i>Triticum vulgare</i> (wheat germ)	WGA	β -GlcNAc, Neu5Ac	β -GlcNAc, Neu5Ac

Fuc, fucose; Gal, galactose; GalNAc, *N*-acetylgalactosimine; Glc, glucose; GlcNAc, *N*-acetylglucosamine; Man, mannose; Neu5Ac, neuraminic (sialic) acid.

from those used for vestibular endorgans. Controls for lectin staining included: (1) exposure of tissue to streptavidin-Texas Red conjugate without lectin and (2) pre-incubation of lectins with 0.1 M–1.0 M of the appropriate inhibitory sugar (Table I).

At the completion of histological procedures, vestibular endorgans and agarose-embedded hair cells were mounted in Fluoromount (Fischer Scientific) and examined with $\times 40$ and $\times 63$ oil-immersion objectives using Nomarski optics and epifluorescent illumination. Vestibular endorgans were also dehydrated in ethanol, embedded in glycol methacrylate (Polysciences, JB-4), and serially sectioned at 5–10 μ m. In sectioned material, Type I hair cells were identified by the presence of a calyx ending (Lindeman, 1969a; Wersall and Bagger-Sjoberg, 1974). Type II hair cell subtypes were identified, as in previous studies (Baird, 1992; Baird 1993a,b), from their macular location and hair bundle morphology (Fig. 1). Nomarski photomicrographs were taken with Tech-Pan film developed to ASA 50 with HC-110 developer. Fluorescent photomicrographs were photographed, whenever possible, at similar illumination and exposure times with T-Max 400 and 3200 film (Kodak).

TABLE II
Lectin binding patterns in the vestibular endorgans

Lectin	Sacculus		Utriculus			Semicircular Canals		
	HC	SC	HC		S	HC		SC
			S	ES		I	P	
CON A	+++ ++	++	+++ ++	++++ ++	+	+++ ++	++++ ++	+
GNA	++ +	+	+ +	++ +	-	+ +	++ +	-
GS-II	- +	-	- +	- +	-	- +	- +	-
RCA-I	+++ -	++	++++ -	++++ -	+	++++ -	++++ -	-
UEA-I	- +	-	- +	- +	-	- +	- +	-
VVA	++	-	+ +	++ +	-	+ +	+ +	-
WGA	- -	-	- -	++ -	++	- -	++ -	++
WGA & neuraminidase	+ -	+ -	- -	+++ -	+++	- -	+++ -	+++

Degree of lectin binding on apical surface of hair cells (HC) and supporting cells (SC) based on a visual assessment of relative staining intensity on a scale from +, least stained, to + + + + +, most stained, with - corresponding to no staining. Each value was obtained from examination of ten or more stained sections. Where applicable, HC staining is separated into hair bundle (top) and apical surface, (bottom) staining, respectively. S, striola; ES, extrastriola; I, Isthmus; P, Planum semilunatum.

Results

In agreement with earlier studies (Gil-Loyza et al., 1985b; Takumida et al., 1989c), significant lectin staining was observed in the cupular and otolithic membranes. For many lectins, this staining was so intense that it obscured the lighter staining of the sensory epithelium. This was particularly true for CON A, RCA-I, and WGA. By contrast, little or no staining of these structures was seen with UEA-I.

With the cupular or otolithic membrane removed, lectin binding was generally confined to the apical surfaces of hair cells and supporting cells. The lectin binding patterns of lectins in the sacculus, utricle, and horizontal and anterior vertical semicircular canals are summarized in Table II. Endorgans incubated without lectins or lectins pre-incubated with their inhibitory sugars exhibited no specific staining (Fig. 3d).

Amphibian vestibular endorgans

Sacculus

The hair bundle morphology and macular distribution of hair cells in the bullfrog sacculus are illustrated in Fig. 1. The saccular macula is composed largely of hair cells with short stereocilia and bulbed kinocilia no longer than their longest stereocilia (Type D). These hair cells occupy the entire central region of the macula inside the first 2–4 rows of its perimeter. A second type of hair cell, located on the perimeter of the saccular macula, has very short stereocilia and kinocilia longer than its longest stereocilia (Type A).

Lectin binding patterns in the sacculus are illustrated in Fig. 2. Two lectins – CON A and RCA-I – strongly labeled peripheral remnants of the otolithic membrane and, less strongly, supporting cells and the hair bundles of hair cells (Figs. 2a,b). A similar, albeit weaker, response was seen for WGA (Fig. 2c). CON A, unlike RCA-I and WGA, also labeled the apical surfaces of saccular hair cells. The latter two lectins labeled only the apical surfaces of supporting cells, leaving unlabeled the apical surfaces of hair cells (Figs. 2b,c). A fourth lectin, VVA, weakly labeled the hair bundles of hair cells but not supporting cells (Fig. 2d). GS-II and UEA-I weakly labeled the apical surfaces, but not the hair bundles, of saccular hair cells.

The binding pattern of GNA, a lectin with a strong affinity for mannose but not glucose residues (Goldstein and Poretz, 1986), was significantly weaker than that of CON A, suggesting that CON A binding was due to the presence of both glucose and mannose residues. Lectin staining produced by WGA was stronger when preceded by neuraminidase treatment, suggesting that sialic residues blocked the access of this lectin to *N*-acetylglucosamine residues (Peters et al., 1979; Monsigny et al., 1980; Debray et al., 1981).

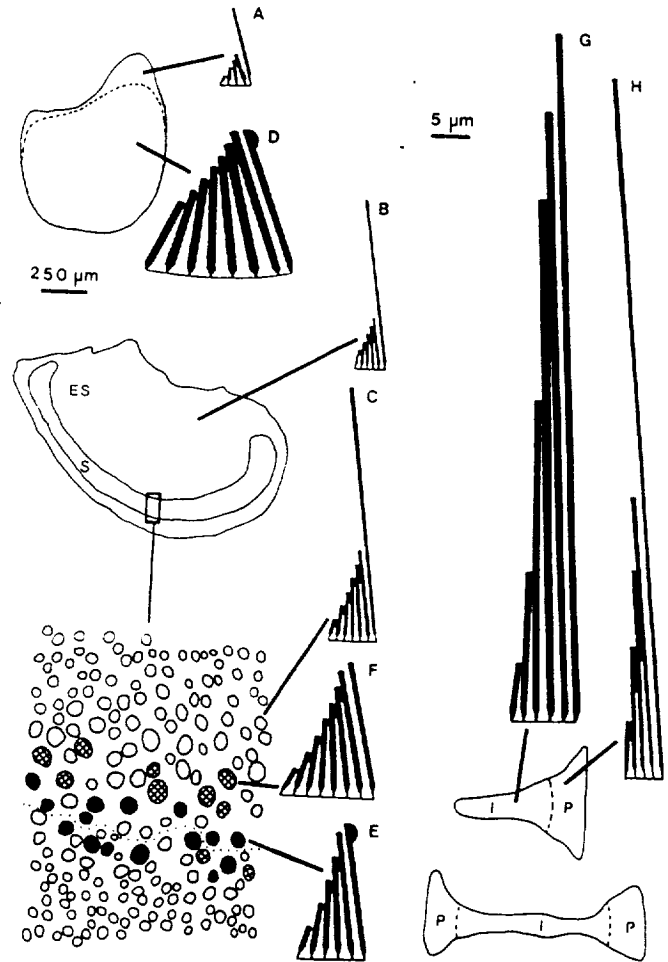


Fig. 1. Surface maps of the sensory surfaces of the bullfrog sacculus (top left), utricle (lower left) and horizontal and anterior vertical semicircular canals (bottom right), showing the distributions of vestibular hair cell types. Idealized cross-sections (drawn to scale) of the hair bundles of vestibular hair cells are shown to the right of each endorgan. S, Striola; ES, Extrastriola; I, Isthmus; P, Planum semilunatum; A–H correspond to the hair type. Scale bar, 250 μ m.

Utricle

The utricular macula in the bullfrog is divided into medial and lateral parts by the striola, a narrow ribbon-shaped zone that runs for the length of the sensory epithelium near its lateral border (Wersall and Bagger-Sjoberg, 1974; Lewis and Li, 1975). Hair cells in the bullfrog utricle differ significantly in hair bundle morphology (Fig. 1). Type B hair cells, the predominant hair cell type in the utricular macula, have uniformly short stereocilia and kinocilia 2–6 \times as long as their longest stereocilia. These cells are found throughout the medial and lateral extrastriola and, more rarely, in the striolar region. Three other hair cell types are confined to the striolar region. Type C hair cells, found throughout the striolar region, resemble an enlarged version of the predominant hair cell type. Moving inward, these cells are gradually replaced by

Type F hair cells, cells with shorter kinocilia and visibly larger hair bundles. Type E hair cells, restricted to the inner striolar rows, have short kinocilia with prominent kinociliary bulbs.

Lectin binding patterns in the bullfrog utricle are illustrated in Fig. 3 and Fig. 4. CON A and RCA-I, as in the sacculus, strongly labeled the hair bundles of all hair cells, regardless of their macular location (Figs. 3a,b;4a,b). By contrast, WGA (Figs. 3c;4c) and, to a lesser extent, VVA (Fig. 4d), labeled the hair bundles of extrastriolar, but not striolar, hair cells. As in the sacculus, CON A strongly labeled the apical surface as well as the hair bundles of hair cells (Fig. 4b). A similar, weaker, response was seen for RCA-I and VVA (Figs. 4a,d). GS-II and UEA, as in the sacculus, weakly labeled the apical surfaces but not the hair bundles of hair cells. Basal staining was not observed

with any lectin except for VVA and, with this lectin, was most pronounced in the striolar region (Figs. 4a-d).

The regional pattern of lectin binding associated with WGA was not correlated with differences in hair bundle morphology. Type B hair cells, for example, although found throughout the utricular macula (Fig. 1), were labeled only in the extrastriolar region (Fig. 4c). Furthermore, striolar hair cells with differing hair bundle morphology did not exhibit different lectin binding patterns (Fig. 3c,4c).

Semicircular canals

The semicircular canals in the bullfrog consist of a central isthmus and one (horizontal canal) or two (vertical canals) planar extensions (Fig. 1). Hair cells in the semicircular canals have significantly longer kinocilia than hair cells in the otolith organs. In the

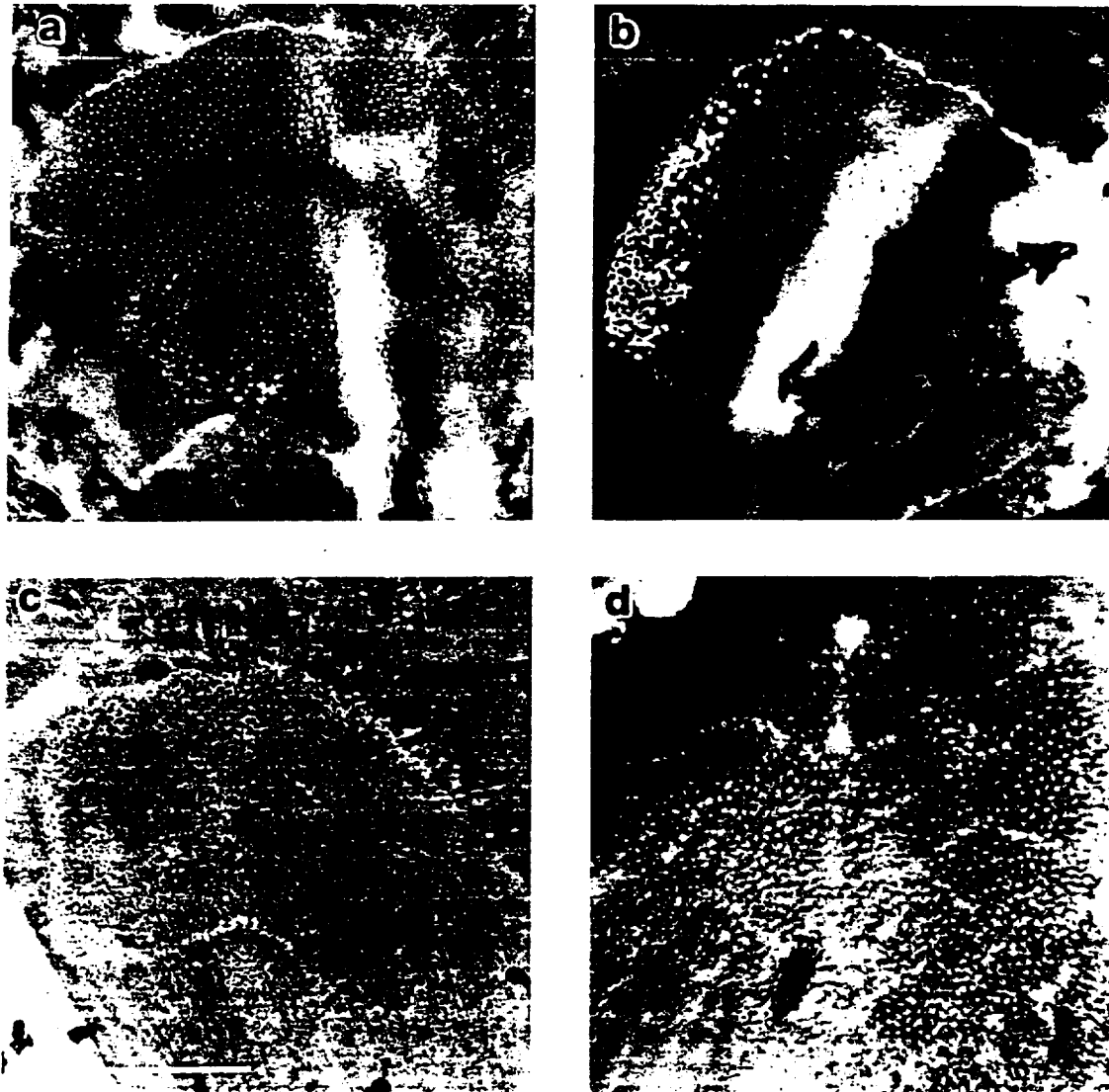


Fig. 2. Lectin binding patterns to CON A (a), RCA-I (b), WGA (c) and VVA (d) in the wholemount bullfrog sacculus. Photomicrographs exposed for 1 s at ASA 400. Scale bar, 250 μ m.

planar extensions, hair cells have short stereocilia (Type H). Hair cells in the central isthmus, on the other hand, have stereocilia only slightly shorter than their kinocilia (Type G).

Lectin binding patterns in the semicircular canals, illustrated in Fig. 5, were similar to those in the utricular macula. RCA-I and CON A, as in the utricle, labeled the hair bundles of all hair cells, regardless of their epithelial location (Fig. 5a). By contrast, WGA labeled the hair bundles of hair cells in the planar extensions but not the central isthmus (Fig. 5b).

Mammalian vestibular endorgans

Lectin binding in the utricle and semicircular canals of the guinea pig was compared to their counterparts in the bullfrog. CON A and RCA-I labeled the hair bundles of both Type I and Type II hair cells, regardless of their epithelial location. WGA labeled the hair bundles of Type I hair cells in all regions. The hair bundles of Type II hair cells, as in the bullfrog, were labeled only in peripheral regions (Fig. 6).

Isolated vestibular hair cells

Lectins were also applied to hair cells isolated from the bullfrog otolith organs and semicircular canals. Basal staining of isolated hair cells (Fig. 7) was more pronounced than in sectioned material (Figs. 4,5). Regional differences in apical staining patterns, however, were preserved in isolated hair cells. CON A and RCA-I, for example, uniformly labeled the hair bundles of all utricular hair cells (Fig. 7, top). WGA, on the other hand, labeled the hair bundles of Type B hair cells isolated from the medial extrastriola (Fig. 7, bottom left) without labeling the hair bundles of hair cells isolated from the utricular striola (Fig. 7, bottom right). Similarly, WGA labeled hair cells isolated from the planar extensions but not the central isthmus of the semicircular canals (not shown).

Discussion

Our results indicate that a number of carbohydrate residues exist on the apical surfaces of hair cells and

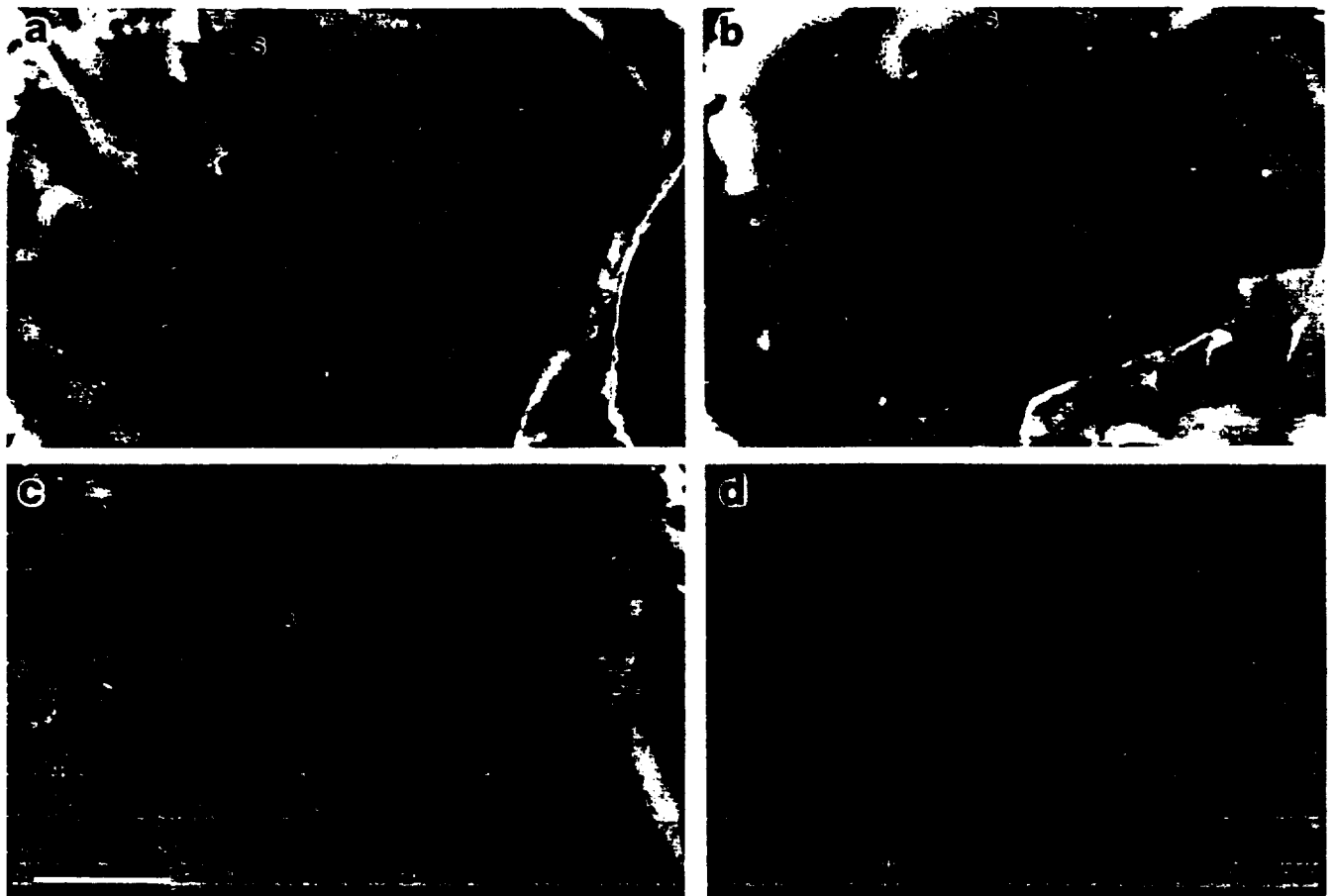


Fig. 3. Lectin binding patterns to CON A (a), RCA-I (b), WGA (c) and WGA pre-incubated with 1 M *N*-acetylglucosamine (d) in the wholemount bullfrog utricle. Photomicrographs exposed for 1 s (a,b) and 30 s (c,d) at ASA 400. S, striola; MES, medial extrastriola; LES, lateral extrastriola. Scale bar, 250 μ m.

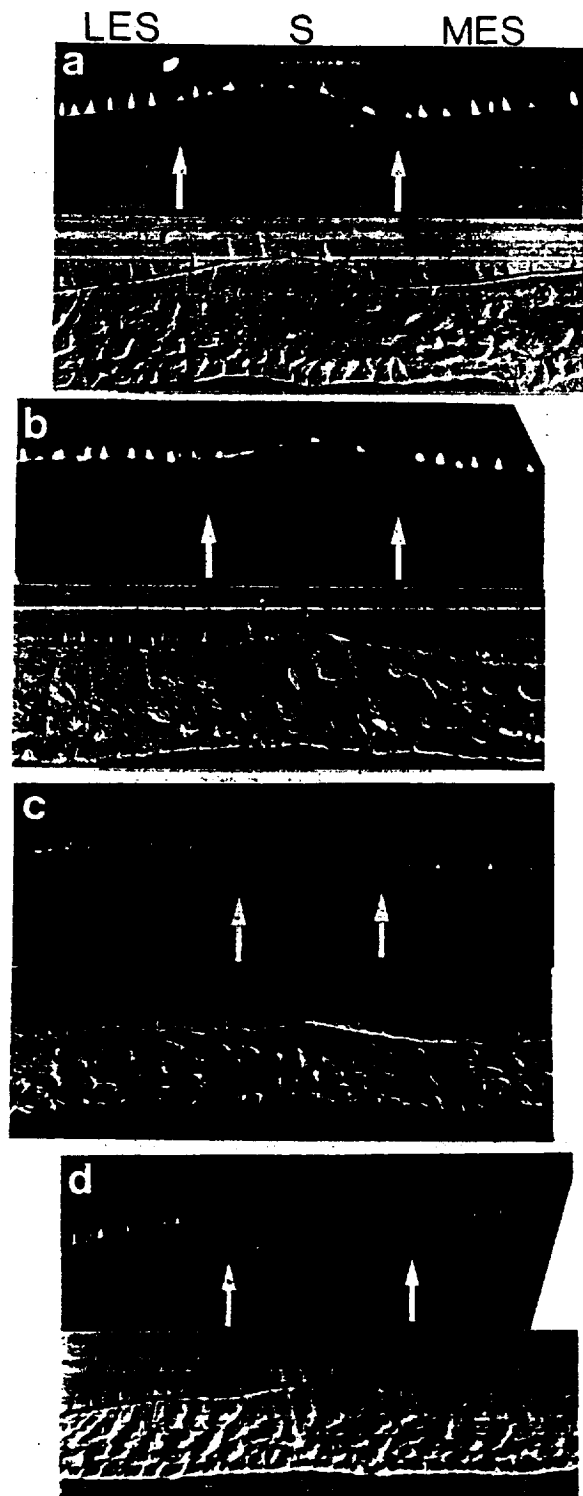


Fig. 4. Photomicrographs of utricular cross-sections viewed with epifluorescent illumination (top) and Nomarski optics (bottom) after incubation with CON A (a), RCA-I (b), WGA (c) and VVA (d). White arrows delineate limits of striolar region. In c, dark arrow indicates striolar Type B hair cell unlabeled by WGA incubation. Fluorescent photomicrographs exposed for 15 s at ASA 400 (a-c) and 4 s at ASA 3200 (d). S, striola; MES, medial extrastrilia; LES, lateral extrastrilia. Scale bar, 50 μ m.

supporting cells in the vestibular endorgans. The amount of lectin binding to these residues could not be quantified with our techniques. The photographic exposure times required to observe fluorescently labeled lectins, however, is inversely correlated with and provides a qualitative measure of lectin binding. In particular, the intense staining produced by CON A is consistent with the presence of a high concentration of mannose and glucose residues on hair cells and supporting cells (Goldstein and Hayes, 1978; Debray et al., 1981). The lesser staining seen with GNA, a lectin with a specific affinity for mannose residues (Goldstein and Poretz, 1986), suggests that CON A staining was due to both glucose and mannose residues. Similarly, the heavy staining produced by RCA-I indicates an abundance of galactose residues on these cells (Hennigar et al., 1978; Baenzinger and Fiete, 1979). The relatively lighter staining seen in endorgans treated with WGA suggests a lower concentration of *N*-acetylglucosamine (GlcNAc) or sialic acid (Peters et al., 1979; Monsigny et al., 1980; Debray et al., 1981). The increase in staining to WGA seen in endorgans pre-treated with neuraminidase suggests that much of this staining was due to contiguous GlcNAc masked by sialic acid residues. This interpretation is supported by the poor staining seen with GS-II, a lectin which does not possess an extended binding site and recognizes only terminal GlcNAc residues (Ebisu et al., 1978; Goldstein et al., 1981). The staining density of VVA was even lower than that of WGA, suggesting that *N*-acetylgalactosamine (GalNAc) residues are relatively rare in the vestibular endorgans (Tollefsen and Kornfeld, 1983; Goldstein and Poretz, 1987). Other lectins, such as UEA-I, bound only weakly to hair cells, indicating a lack of fucose residues (Allen et al., 1977; Periera et al., 1978; Sugii et al., 1982).

Cell surface glycoconjugates include the glycolipids, glycoproteins, and the proteoglycans with their glycosaminoglycan groups (Glick and Flowers, 1978). The carbohydrate residues detected in our experiments are probably attached to glycoproteins since proteoglycans are generally not detected by lectin histochemistry and glycolipids are not well preserved by paraformaldehyde fixation (Spicer and Schulte, 1992). Glycoproteins consist of a protein backbone with oligosaccharide side chains and fall into two main categories according to the attachment of their oligosaccharides to the peptide chain (Kornfeld and Kornfeld, 1985). These include glycoproteins in which a terminal GalNAc is *O*-linked to serine or threonine and those in which a terminal GlcNAc is *N*-linked to asparagine. The intense staining by CON A suggests that most glycoproteins in the vestibular endorgans are of the *N*-linked type. This lectin has its strongest affinity for the core region of high mannose, *N*-linked glycoproteins (Debray et al., 1981) and does not detect *O*-linked glycoproteins, since

O-linked chains generally do not contain the mannose residues on which the lectin affinity depends (Loomis et al., 1987). The intense staining to RCA-I further suggests that these *N*-linked glycoproteins may be of the high *N*-acetyllactosamine (GalNAcb1,4GlcNAc) subtype (Kornfeld and Kornfeld, 1985). The weaker binding produced by WGA is consistent with this interpretation since this lectin does not bind strongly to

lactosamine oligosaccharides (Debray et al., 1981). The presence of VVA staining, however, demonstrates that *O*-linked glycoproteins are also present. This lectin does not detect *N*-linked chains, since these glycoconjugates lack GalNAc (Tollefsen et al., 1983; Kornfeld and Kornfeld, 1985).

With the exception of the bullfrog sacculus (see below), our results are largely in agreement with the

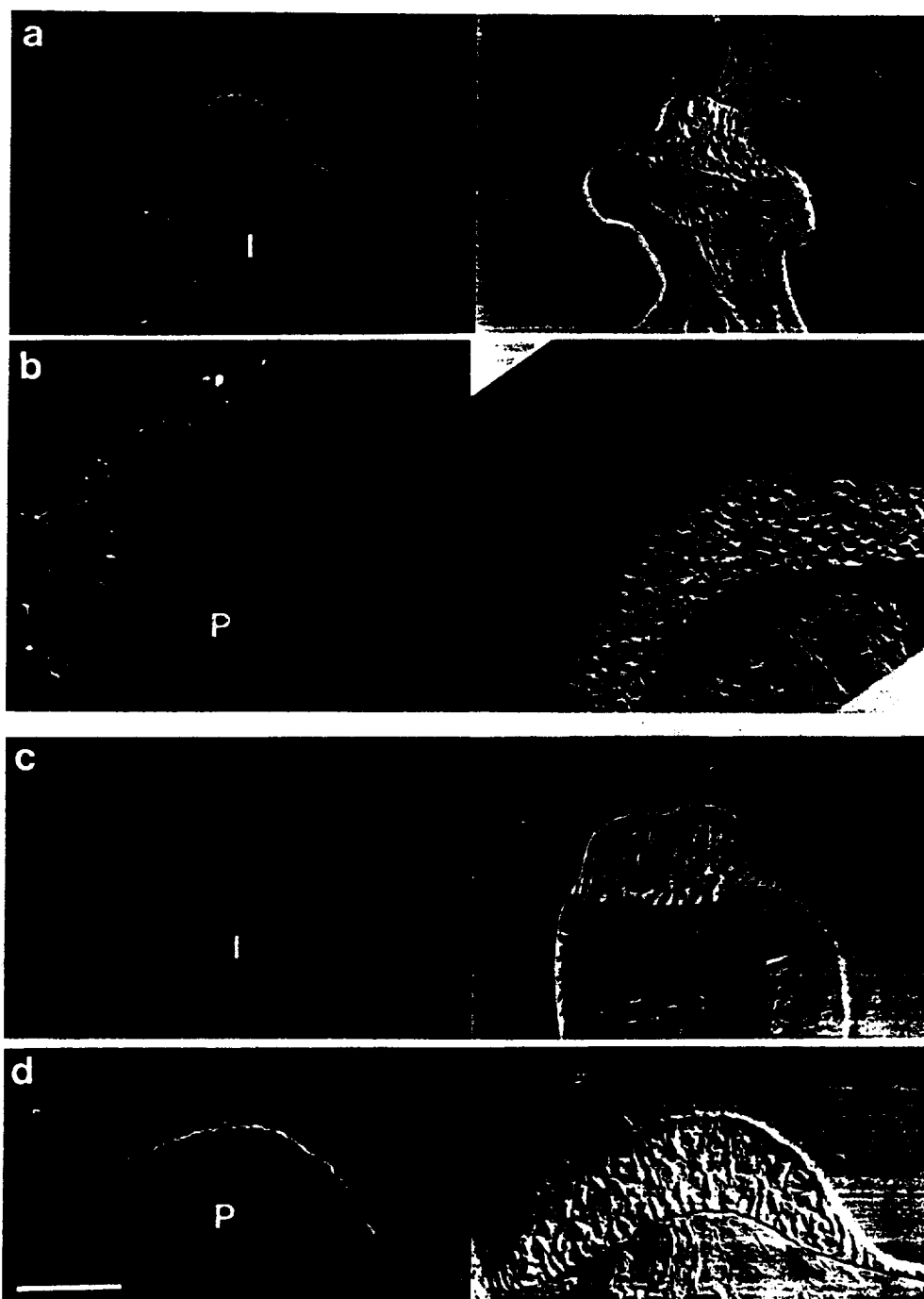


Fig. 5. Photomicrographs of cross-sectioned central isthmus (a,c) and planum semilunatum (b,d) of the bullfrog anterior vertical semicircular canal under epifluorescent illumination (left) and Nomarski optics (right) after incubation with CON A (a,b) and WGA (c,d). Fluorescent photomicrographs exposed for 15 s at ASA 400. I. Isthmus; P. Planum semilunatum. Scale bar, 100 μ m.

results of previous lectin binding studies in fish (Khan et al., 1991), rats (Gil-Loygaza et al., 1985b), and guinea pigs (Tachibana et al., 1987b; Takumida et al., 1989b), suggesting that the glycocalyx of vestibular hair cells is strongly conserved in the lower and higher vertebrates. Similar results have also been obtained in inner hair cells (Gil-Loygaza et al., 1985a; Gil-Loygaza and Brownell, 1988; Khalkhali-Ellis et al., 1987; Tachibana et al., 1987a,c; Lim and Rueda, 1990; Prieto et al., 1990), suggesting that the glycocalyx of auditory and vestibular hair cells is not dissimilar. These studies, using lectin probes, demonstrated the presence of glucose and mannose (CON A), galactose (RCA-I), and GlcNAc (WGA) residues and the absence of GalNAc (VVA) and fucose (UEA-I) residues on hair cells. Unlike previous studies, the staining produced by WGA in our study was significantly weaker than that seen to CON A or RCA-I. The reason for this discrep-

ancy is not clear, but may be age-related since WGA labeling declines progressively during postnatal development (Endo et al., 1991).

Our results also differ from previous histochemical observations (Gil-Loygaza et al., 1985b, Tachibana et al., 1987b; Takumida et al., 1989b) but confirm biochemical data (Khalaki-Ellis et al., 1987) in showing the presence of GalNAc residues on vestibular hair cells. Presumably, this sugar was not detected in earlier studies because these studies used HPA rather than VVA to detect GalNAc residues. Lectins which bind GalNAc differ in their affinity for different oligosaccharides with terminal GalNAc (Debray et al., 1981; Sugiyama et al., 1991). In particular, VVA is specific for terminal α -linked GalNAc and binds preferentially to the disaccharides GalNAc- α 1,3Gal and GalNAc- α 1,6Gal (Kaladas et al., 1981). Negligible staining with HPA in previous experiments suggests the absence of

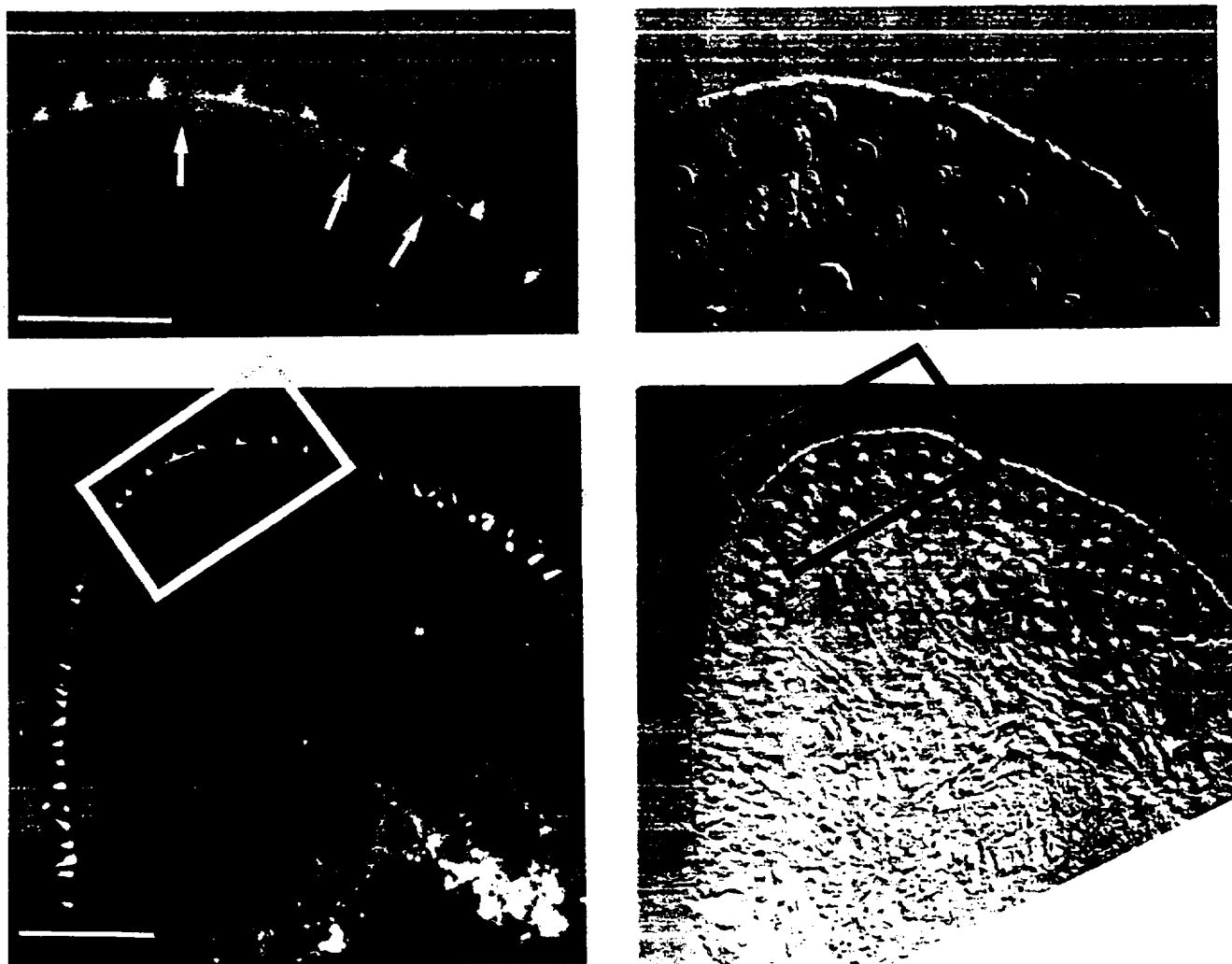


Fig. 6. Photomicrographs of cross-sectioned central isthmus of the guinea pig horizontal semicircular canal under epifluorescent illumination (left) and Nomarski optics (right) after incubation with WGA. Arrows indicate Type II hair cells unlabeled by WGA incubation. Insets of boxed region shown at top left and top right. Fluorescent photomicrographs exposed for 1/2 s at ASA 3200. I, Type I hair cell; II, Type II hair cell. Scale bar, 25 μ m (top), 50 μ m (bottom).

GalNAc- α 1,3GalNAc for which this lectin has a high affinity (Baker et al., 1986). Outer hair cells, unlike inner hair cells and vestibular hair cells, are strongly labeled by HPA (Gil-Loygaza and Brownell, 1988).

Lectin binding patterns in the bullfrog sacculus were distinctly different from those in other vestibular endorgans. Sacculus hair cells, unlike those in the utricle or semicircular canals, were only weakly labeled by lectins and displayed a marked absence of staining to WGA and VVA. Unlike the latter endorgans, the bullfrog sacculus also did not exhibit regional variations in its binding patterns (see below). These differences may be correlated with the distinctive function of this endorgan which, unlike the sacculus of higher vertebrates, is a sensor of substrate-vibration (Koyama et al., 1982; Lewis et al., 1982).

In the utricle and semicircular canals, WGA and, to a lesser extent, VVA, selectively labeled hair cells in different epithelial zones. In particular, these lectins labeled hair cells in peripheral regions but not those

located in more central regions. In mammals, WGA uniformly labeled Type I but not Type II hair cells, demonstrating that this regional variation was confined to Type II hair cells. Among Type II hair cells, this regional variation was not correlated with hair bundle morphology. In the bullfrog utricle, for example, WGA labeled Type B hair cells in the extrastriolar, but not the striolar, regions. Regional variations in WGA staining were also preserved after enzymatic digestion, demonstrating that this lectin can be a useful probe for separating Type I and Type II hair cells from central epithelial regions and for inferring the epithelial origins of isolated Type II hair cells.

In retrospect, it is surprising that regional variations in lectin binding were not recognized in earlier studies. This might be because most previous investigations were made in mammalian tissue. Regional variations in lectin binding, while preserved in mammalian tissue, are more difficult to visualize because they are obscured by differences in the lectin binding of Type I

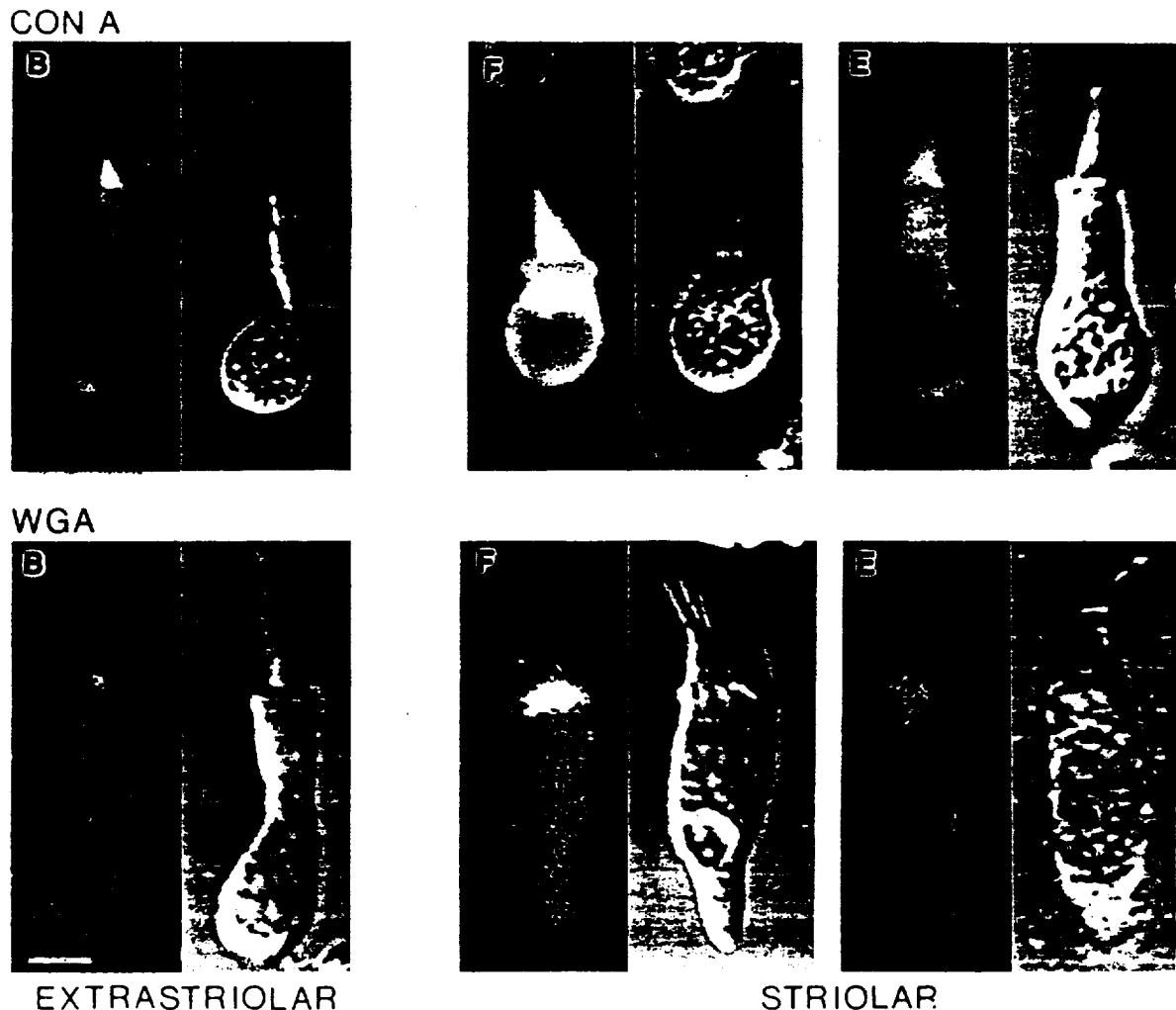


Fig. 7. Lectin binding patterns to CON A (top) and WGA (bottom) in utricular hair cells isolated from the medial extrastriola (left) and the striolar region (right). Fluorescent photomicrographs exposed for 1 s at ASA 3200. B. Type B; E. Type E; F. Type F. Scale bar. 10 μ m.

and Type II hair cells. In addition, most previous studies of lectin binding were carried out in sectioned material rather than wholemount endorgans. Regional variations in lectin binding would be more difficult to observe at this level. Many previous investigations have also used FITC-labeled lectins, resulting in a weaker and less specific staining than that obtained with biotinylated lectins (R. Baird, unpublished observations).

The exact role(s) that glycoconjugates play in inner ear function have not yet been established. Membrane-bound glycoconjugates usually function locally in receptor activity, influencing ion transport across cell membranes (Spicer and Schulte, 1992). In hair cells, it has been suggested that the negative charges on these glycoconjugates, by influencing the surface charge of the plasma membrane, may play a role in sensory transduction by maintaining the integrity of the stereociliary array (Flock et al., 1977; Slepecky and Chamberlain, 1985; Neugebauer and Thurm, 1986; Santi and Anderson, 1987). It has also been suggested that the negative charge of these glycoconjugates may control the microenvironment of the transduction channel (Slepecky and Chamberlain, 1985), sequestering ions such as calcium that are important for maintaining mechanoelectric transduction (Assad et al., 1991; Crawford et al., 1991) and adaptation (Eatock et al., 1985; Crawford et al., 1989). Regional variations in lectin binding may therefore reflect differences in the transduction mechanisms of striolar and extrastriolar hair cells.

Glycoconjugates are also undoubtedly involved in drug-induced ototoxicity processes (Flock et al., 1977). It has been recently speculated (Schacht, 1986) that aminoglycoside antibiotics bind electrostatically with negatively charged components of the hair cell glycocalyx prior to being transported into the hair cell by an energy-dependent transport process (Takada et al., 1985). It has also been suggested that morphological changes observed in gentamicin-treated animals are due to a gradual decrease in the thickness of the glycocalyx (Takumida et al., 1989a) and that, once inside the cell, aminoglycoside antibiotics interfere with glycoconjugate biosynthesis (Schacht, 1986; DeGroot and Veldman, 1988; Takumida et al., 1989c). Thus, the resistance of hair cells to aminoglycoside antibiotics may be correlated with the size and integrity of their glycoconjugate coat. Vestibular hair cells are known to be differentially sensitive to aminoglycoside antibiotics. In the bullfrog, for example, gentamicin is known to damage saccular hair cells more than utricular hair cells (Baird et al., 1993). Moreover, these antibiotics have been shown to selectively affect hair cells in central epithelial regions (Lindeman, 1969b; Yan et al., 1992; Baird et al., 1993). This pattern of selective sensitivity is correlated with the lectin binding pattern of WGA to utricular and semicircular canal hair cells.

It is also possible that glycoconjugates play a role in inner ear development. In other systems, glycoconjugates are known to play important roles in cell recognition and adhesion, serving as recognition markers for specific subsets of sensory cells (Edelman, 1984; Dodd and Jessell, 1986; Peinado et al., 1987). In the inner ear, glycoconjugates are synthesized in different cells at different developmental times (Rueda and Lim, 1988; Lim and Rueda, 1990; Prieto et al., 1990). In a recent study, Endo et al. (1991) have also demonstrated that WGA labeling of the otolith membrane, otoconia, and the sensory epithelium is high in the early embryo and declines progressively during postnatal development. Because differences in WGA binding were correlated with epithelial location and not hair cell type per se, it seems unlikely that glycoconjugates control the differentiation of individual hair cell types in the vestibular endorgans. It is possible, however, that glycoconjugates are used to define the central epithelial regions of vestibular endorgans during development. Glycoconjugates might also be involved in the formation of the cupular or otolith membranes or in determining the relationship between hair cells and these accessory structures. It has previously been suggested that hair cells with differing hair bundle morphology may be coupled to the cupular or otolith membrane in different ways (Lim, 1976; Lim, 1979). Regional differences in staining density might reflect differences in the coupling of hair bundles to the cupular or otolith membranes in central and peripheral regions.

In summary, our results indicate that Type I and Type II vestibular hair cells and Type II hair cells in different epithelial regions differ in their complement of surface glycoconjugates. We conclude that lectin probes are useful for separating and identifying Type I and Type II hair cells and for inferring the epithelial origins of Type II hair cells isolated from central and peripheral regions. Additional biochemical and physiological experiments are needed to identify the surface glycoconjugates of vestibular hair cells and to determine their role(s) in inner ear development and mechanoelectric transduction.

Acknowledgements

We are grateful to Joyce P. Gregory for manuscript preparation. Funding for this research was provided by NIDCD grant DC-00355, NASA grant NCC 2-651, and by the Oregon Lions Sight and Hearing Foundation.

References

- Allen, H.J., Johnson, E.A.Z. and Matta, K.L. (1977) A comparison of the binding specificities of lectins from *Ulex europaeus* and *Lotus tetragonolobus*. *Immunol. Commun.* 6, 585, 585-602.

- Assad, J.A., Shepherd, G.M.G. and Corey, D.A. (1991) Tip-link integrity and mechanical transduction in vertebrate hair cells. *Neuron* 7, 985-994.
- Baenziger, J.U. and Fiete, D. (1979) Structural determinants of *Ricinus communis* agglutinin and toxin specificity for oligosaccharides. *J. Biol. Chem.* 254, 9795-9799.
- Baird, R.A. (1992) Morphophysiological and electrophysiological properties of hair cells in the bullfrog utricle. *Ann. NY Acad. Scis.* 656, 12-26.
- Baird, R.A. (1993a) Comparative transduction properties of hair cells in the bullfrog utricle. I. Responses to intracellular current. *J. Neurophysiol.* (Submitted).
- Baird, R.A. (1993b) Comparative transduction properties of hair cells in the bullfrog utricle. II. Sensitivity and response dynamics to hair bundle displacement. *J. Neurophysiol.* (Submitted).
- Baird, R.A. and Lewis, E.R. (1986) Correspondences between afferent innervation patterns and response dynamics in the bullfrog utricle and lagena. *Brain Res.* 369, 48-64.
- Baird, R.A., Schuff, N.R. and Bancroft, J. (1991) Lectin binding patterns of vestibular hair cells. *Soc. Neurosci. Abstr.* 17, 313.
- Baird, R.A., Torres, M.A. and Schuff, N.R. (1993) Hair cell regeneration in the amphibian vestibular otolith organs following aminoglycoside toxicity. *Hear. Res.* 65, 000-000.
- Baker, D.S., Sugii, S., Kabat, E.A., Ratcliffe, R.M., Hermentin, P. and Lemieux, R.U. (1983) Immunochemical studies on the combining sites of Forssman hapten reactive hemagglutinins from *Dolichos biflorus*, *Helix pomatia*, and *Wistaria floribunda*. *Biochemistry* 22, 2741-2750.
- Correia, M.J., Christensen, B.N., Moore, L.E. and Lang, D.G. (1989) Studies of solitary semicircular canal hair cells in the adult pigeon. I. Frequency- and time-domain analysis of active and passive membrane properties. *J. Neurophysiol.* 62, 924-934.
- Crawford, A.C., Evans, M.G. and Fettiplace, R. (1989) Activation and adaptation of transducer currents in turtle hair cells. *J. Physiol. (Lond.)* 419, 405-434.
- Crawford, A.C., Evans, M.G. and Fettiplace, R. (1991) The actions of calcium on the mechano-electrical transducer current of turtle hair cells. *J. Physiol. (Lond.)* 434, 369-398.
- Debray, H., Decout, D., Strecker, G., Spik, G. and Montreuil, J. (1981) Specificity of twelve lectins towards oligosaccharides and glycopeptides related to *N*-glycosylproteins. *Eur. J. Biochem.* 117, 41-55.
- DeGroot, J.C.M. and Veldman, J.E. (1988) Early effects of gentamicin on inner ear glycocalyx cytochemistry. *Hear. Res.* 35, 39-45.
- Dodd, J. and Jessell, T.M. (1986) Cell surface glycoconjugates and carbohydrate-binding proteins: possible recognition signals in sensory neurone development. *J. Exp. Biol.* 124, 225-238.
- Eatock, R.A., Corey, D.P. and Hudspeth, A.J. (1988) Adaptation of mechanoelectric transduction in hair cells of the bullfrog's sacculus. *J. Neurosci.* 7, 2821-2836.
- Ebisu, S., Shankar-Iyer, P.N. and Goldstein, I.J. (1978) Equilibrium dialysis and carbohydrate-binding studies on the 2-acetomido-2-deoxy-D-glycopyransol-binding lectin from *Bandeiraea simplicifolia* seeds. *Carbohydrate Res.* 61, 129-138.
- Edelman, G.M. (1984) Modulation of cell adhesion during induction, histogenesis, and perinatal development of the nervous system. *Ann. Rev. Neurosci.* 7, 339-377.
- Endo, S., Sekitani, T., Yamashita, H., Kido, T., Masumitsu, Y., Ogata, M. and Miura, M. (1991) Glycoconjugates in the otolith organ of the developing chick embryo. *Acta Otolaryngol. (Stockh.)* 481, 116-120.
- Flock, Å., Flock, B. and Murray, E. (1977) Studies on the sensory hairs of receptor cells in the inner ear. *Acta. Otolaryngol. (Stockh.)* 83, 85-91.
- Gil-Loyzaga, P. and Brownell, W.E. (1988) Wheat germ agglutinin and *Helix pomatia* agglutinin lectin binding on cochlear hair cells. *Hear. Res.* 34, 149-156.
- Gil-Loyzaga, P., Gabrion, J. and Uziel, A. (1985a) Lectins demonstrate the presence of carbohydrates in the tectorial membrane of mammalian cochlea. *Hear. Res.* 20, 1-8.
- Gil-Loyzaga, P., Raymond, J. and Gabrion, J. (1985b) Carbohydrates detected by lectins in the vestibular endorgan. *Hear. Res.* 18, 269-272.
- Glick, M. and Flowers, H. (1978) Surface membranes. In: Horowitz, H. and Pigman, W. (Eds.) *The Glycoconjugates, Vol II, Mammalian Glycoproteins, Glycolipids, and Proteoglycans*. New York, Academic Press, pp. 337-384.
- Goldstein, I.J., Blake, D.A., Ebisu, S., Williams, T.J. and Murphy, L.A. (1981) Carbohydrate binding studies on the *Bandeiraea simplicifolia* isolectins. *J. Biol. Chem.* 256, 3890-3893.
- Goldstein, I.J. and Hayes, C.E. (1978) The lectins: carbohydrate-binding proteins of plants and animals. In: Tipson, R.S. and Horton, D. (Eds.) *Advances in Carbohydrate Chemistry and Biochemistry*. New York, Academic Press, pp. 127-340.
- Goldstein, I.J. and Poretz, R.D. (1986) Isolation, physicochemical characterization, and carbohydrate-binding specificity of lectins. In: Liener, I.E., Sharon, N. and Goldstein, I.J. (Eds.) *The Lectins: Properties, Functions, and Applications in Biology and Medicine*. Orlando, Academic Press, pp. 33-40.
- Hennigar, L.M., Hennigar, R.A., Schulte, B.A. (1987) Histochemical specificity of b-galactose binding lectins from *Arachis hypogaea* (peanut) and *Ricinus communis* (castor bean). *Stain Technol.* 62, 317-325.
- Hirokawa, N. and Tilney, L.G. (1982) Interactions between actin filaments and between actin filaments and membranes in quick-frozen and deeply etched hair cells of the chick ear. *J. Cell. Biol.* 95, 249-261.
- Hook, M., Kjellen, L., Johansson, S. and Robinson, J. (1984) Cell-surface glycosaminoglycans. *Ann. Rev. Biochem.* 53, 847-869.
- Kaladas, P.M., Kabat, E.A., Kimura, A. and Ersson, B. (1981) The specificity of the combining site of the lectin from *Vicia villosa* seeds which reacts with cytotoxic T-lymphoblasts. *Mol. Immunol.* 18, 969-977.
- Khalkhali-Ellis, Z., Hemming, F.W. and Steel, K.P. (1987) Glycoconjugates in the tectorial membrane. *Hear. Res.* 25, 185-191.
- Khan, K.M., Hatfield, J.S. and Drescher, D.G. (1990) The cell coat of the sensory and supporting cells of the rainbow trout saccular macula as demonstrated by reaction with ruthenium red and tannic acid. *J. Histochem. Cytochem.* 38, 1615-1623.
- Khan, K.M., Hatfield, J.S. and Drescher, D.G. (1991) Carbohydrates associated with the cell coat surrounding cells of the rainbow trout saccular macula as revealed by lectin probes. *Hear. Res.* 53, 223-229.
- Kornfeld, R. and Kornfeld, S. (1985) Assembly of asparagine-linked oligosaccharides. *Annu. Rev. Biochem.* 54, 631-664.
- Koyama, H., Lewis, E.R., Leverenz, E.L. and Baird, R.A. (1982) Acute seismic sensitivity in the bullfrog ear. *Brain Res.* 250, 168-172.
- Lewis, E.R., Baird, R.A., Leverenz, E.L. and Koyama, H. (1982) Inner ear: Dye injection reveals peripheral origins of specific sensitivities. *Science* 215, 1641-1643.
- Lewis, E.R. and Li, C.W. (1975) Hair cell types and distributions in the and auditory organs of the bullfrog. *Brain Res.* 83, 35-50.
- Li, C.W. and Lewis, E.R. (1979) Structure and development of vestibular hair cells in the larval bullfrog. *Ann. Otol. Rhinol. Laryngol.* 88, 427-437.
- Lim, D.J. (1976) Morphological and physiological correlates in cochlear and vestibular sensory epithelia. *SEM/1976/II:* 269-276.
- Lim, D.J. (1979) Fine morphology of the otoconial membrane and its relationship to the sensory epithelium. *SEM/1979/III:* 929-938.
- Lim, D. and Rueda, J. (1990) Distribution of glycoconjugates during cochlea development: a histochemical study. *Acta. Otolaryngol. (Stockh.)* 110, 224-233.

- Lindeman, H.H. (1969a) Studies on the morphology of the sensory regions of the vestibular apparatus. *Ergeb. Anat. Entwickl.* 42, 1-113.
- Lindeman, H.H. (1969b) Regional differences in sensitivity of the vestibular sensory epithelia to ototoxic antibiotics. *Acta Otolaryngol.* (Stockh.) 67, 177-189.
- Lis, H. and Sharon, N. (1986) Lectins as molecules and as tools. *Ann. Rev. Biochem.* 55, 35-67.
- Loomis, R.E., Prakobphol, A., Levine, M.J., Reddy, M.S. and Jones, P.C. (1987) Biochemical and biophysical comparison of two mucins from human submandibular-sublingual saliva. *Arch. Biochem. Biophys.* 258, 452-464.
- Luft, J.H. (1976) The structure and properties of the cell surface coat. *Int. Rev. Cytol.* 45, 291-382.
- Monsigny, M., Roche, A.-C., Sene, C., Maget-Dana, R. and Delmotte, F. (1980) Sugar-lectin interactions: how does wheat-germ agglutinin bind sialoglycoconjugates? *Eur. J. Biochem.* 104, 147-153.
- Neugebauer, D.-C. and Thurm, M. (1986) Surface charges influence the distances between vestibular stereocilia. *Naturwissenschaften* 73, 508-509.
- Peinado, A., Macagno, E.R. and Zipser, B. (1987) A group of related surface glycoproteins distinguish sets and subsets of sensory afferents in the leech nervous system. *Brain Res.* 410, 335-339.
- Pereira, M.E.A., Kisailus, E.C., Gruezo, F. and Kabat, E.A. (1978) Immunohistochemical studies on the combining site of the blood group H-specific lectin I from *Ulex europaeus* seeds. *Arch. Biochem. Biophys.* 185, 108-115.
- Peters, B.P., Ebisu, S., Goldstein, I.J. and Flashner, M. (1979) Interaction of wheat germ agglutinin with sialic acid. *Biochemistry* 18, 5505-5511.
- Prieto, J.J. and Merchan, J.A. (1986) Tannic acid staining of the cell coat of the organ of Corti. *Hear. Res.* 24, 237-241.
- Prieto, J.J., Rueda, J., Sala, M.L. and Merchan, J.A. (1990) Lectin staining of saccharides in the normal and hypothyroid developing organ of Corti. *Dev. Brain Res.* 52, 141-149.
- Rennie, K.J. and Ashmore, J.F. (1991) Ionic currents in isolated vestibular hair cells from the guinea-pig crista ampullaris. *Hear. Res.* 51, 279-292.
- Rueda, J. and Lim, D.J. (1988) Possible transient stereociliary adhesion molecules expressed during cochlear development: A preliminary study. In: M. Ohyama and T. Muramatsu (Eds.), *Glycoconjugates in Medicine*. Tokyo, Professional Postgraduate Services, pp. 338-350.
- Santi, P.A. and Anderson, C.B. (1987) A newly identified surface coat on cochlear hair cells. *Hear. Res.* 27, 47-65.
- Schacht, J. (1986) Molecular mechanisms of drug-induced hearing loss. *Hear. Res.* 22, 297-304.
- Sharon, N. and Lis, H. (1982) Lectins as cell recognition molecules. *Science* 231, 227-234.
- Slepecky, N.B. and Chamberlain, S.C. (1985) The cell coat of inner ear sensory and supporting cells as demonstrated by ruthenium red. *Hear. Res.* 17, 281-288.
- Spicer, S.S. and Schulte, B.A. (1992) Diversity of cell glycoconjugates shown histochemically: A perspective. *J. Histochem. and Cytochem.* 40, 1-38.
- Sugii, S., Kabat, E.A. and Baer, H.H. (1982) Further immunochemical studies on the combining sites of *Lotus tetragonolobus* and *Ulex europaeus* I and II lectins. *Carbohydr. Res.* 99, 99-103.
- Sugiyama, S., Spicer, S.S., Munyer, P.D. and Schulte, B.A. (1991) Histochemical analysis of glycoconjugates in gelatinous membranes of the gerbil's inner ear. *Hear. Res.* 55, 263-272.
- Tachibana, M., Morioka, H., Machino, M. and Mizukoshi, O. (1987a) Cytochemical localization of specific carbohydrates in the cochlea using wheat germ agglutinin-gold. *Hear. Res.* 25, 115-119.
- Tachibana, M., Morioka, H., Machino, M., Tanimura, F. and Mizukoshi, O. (1987b) Cupulogenesis and glycoconjugates in the labyrinthine ampulla as revealed by WGA-gold labeling. *Arch. Otorhinolaryngol.* 244, 112-116.
- Tachibana, M., Morioka, H., Machino, M. and Yoshimatsu, M. and Mizukoshi, O. (1987c) Wheat germ agglutinin binding sites in the organ of Corti as revealed by lectin-gold labeling. *Hear. Res.* 27, 239-244.
- Takada, A., Bledsoe, S.C., Jr. and Schacht, J. (1985) An energy-dependent step in aminoglycoside ototoxicity: prevention of gentamicin ototoxicity during reduced endolymphatic potential. *Hear. Res.* 19, 245-251.
- Takumida, M., Bagger-Sjoberg, D., Harada, Y., Lim, D. and Wersall, J. (1989a) Sensory hair fusion and glycocalyx changes following gentamicin exposure in the guinea pig vestibular organs. *Acta Otolaryngol.* (Stockh.) 107, 39-47.
- Takumida, M., Bagger-Sjoberg, D., Wersall, J. and Harada, Y. (1989b) The effect of gentamicin on the glycocalyx and the ciliary interconnections in vestibular sensory cells: a high-resolution scanning electron microscopic investigation. *Hear. Res.* 37, 163-170.
- Takumida, M., Urquiza, R., Bagger-Sjoberg, D. and Wersall, J. (1989c) Effect of gentamicin on the carbohydrates of the vestibular endorgans: an investigation by the use of FITC-lectins. *J. Laryngol. Otol.* 103, 357-362.
- Takumida, M., Wersall, J. and Bagger-Sjoberg, D. (1989d) Initial changes in the sensory hair-cell membrane following aminoglycoside administration in a guinea pig model. *Arch. Otorhinolaryngol.* 246, 26-31.
- Tollefsen, S.E. and Kornfeld, R. (1983) The B₄ lectin from *Vicia villosa* seeds interacts with *N*-acetylgalactosamine residues α -linked to serine or threonine residues in cell surface glycoproteins. *J. Biol. Chem.* 258, 5172-5176.
- Valat, J., Devau, G., Dulon, D. and Sans, A. (1989) Vestibular hair cells isolated from guinea pig labyrinth. *Hear. Res.* 40, 255-264.
- Wersall, J. and Bagger-Sjoberg, D. (1974) Morphology of the vestibular sense organs. In: H.H. Kornhuber (Ed.), *Vestibular System: Basic Mechanisms*. Handbook of Sensory Physiology, Springer-Verlag, New York, pp. 124-170.
- Yan, H.Y., Saidel, W.M., Chang, J.S., Presson, J.C. and Popper, A.N. (1991) Sensory hair cells of a fish ear: evidence of multiple types based on ototoxicity sensitivity. *Proc. R. Soc. Lond. B* 245, 133-138.

Hair cell regeneration in the bullfrog vestibular otolith organs following aminoglycoside toxicity

R.A. Baird, M.A. Torres and N.R. Schuff

R.S. Dow Neurological Sciences Institute, Good Samaritan Hospital and Medical Center, Portland, Oregon, USA

(Received 4 June 1992; Revision received 11 September 1992; Accepted 16 September 1992)

Adult bullfrogs were given single intraotic injections of the aminoglycoside antibiotic gentamicin sulfate and sacrificed at postinjection times ranging from 0.5 to 9 days. The saccular and utricular maculae of normal and injected animals were examined in wholemount and cross-section. Intraotic 200 μ M gentamicin concentrations resulted in the uniform destruction of the hair bundles and, at later times, the cell bodies of saccular hair cells. In the utricle, striolar hair cells were selectively damaged while extrastriolar hair cells were relatively unaffected. Regenerating hair cells, identified in sectioned material by their small cell bodies and short, well-formed hair bundles, were seen in the saccular and utricular maculae as early as 24-48 h postinjection. Immature versions of mature hair cell types in both otolith organs were recognized by the presence or absence of a bulbed kinocilia and the relative lengths of their kinocilia and longest stereocilia. Utricular hair cell types with kinocilia longer than their longest stereocilia were observed at earlier times than hair cell types with shorter kinocilia. In the sacculus, the hair bundles of gentamicin-treated animals, even at 9 days postinjection, were significantly smaller than those of normal animals. The hair bundles of utricular hair cells, on the other hand, reached full maturity within the same time period.

Ototoxicity; Hair cell; Regeneration; Otolith organs; Bullfrog

Introduction

Proliferation and differentiation of sensory hair cells occurs in mammals only during embryonic development. The auditory and vestibular systems of fish (Corwin, 1981, 1985; Popper and Hoxter, 1984), amphibians (Li and Lewis, 1979; Corwin, 1985), and birds (Jorgenson and Matthiesen, 1988; Katayama and Corwin, 1989; Robertson et al., 1992), on the other hand, produce hair cells at a low level throughout life. Newly produced hair cells in fish and amphibians are primarily localized to a distinct peripheral growth zone at the edge of the sensory epithelium. In birds, newly produced hair cells are found in all regions of the sensory epithelium. More importantly, birds and fish retain the capacity to rapidly increase the rate of hair cell regeneration following the elimination of hair cells due to ototoxic drugs (Cruz et al., 1987; Hashino et al., 1991; Lippe et al., 1991; Yan et al., 1991) or noise exposure (Corwin and Cotanche, 1988; Ryals and Rubel, 1988; Girod et al., 1989). In these lower vertebrates, regenerated hair cells develop morphologically normal hair bundles (Cotanche, 1987; Corwin and Cotanche, 1989;

Duckert and Rubel, 1990) which, in both the auditory (Tucci et al., 1990) and vestibular (Jones and Nelson, 1992) organs, appear to be fully functional.

Vestibular and cochlear ototoxicity is a well-known side effect of aminoglycoside antibiotics (Lim, 1986; Schacht, 1986). These drugs reversibly block hair cell transduction channels (Kroese and van den Bercken, 1980; Kroese et al., 1988; Jamarillo and Hudspeth, 1991) and, after longer exposure, irreversibly disrupt hair bundle morphology (Takumida et al., 1989a-c) and cytoplasmic organelles (DeGroot et al., 1990; Hashino et al., 1991), resulting in the degeneration and extrusion of hair cells. Hair cells in the vestibular organs are differentially sensitive to ototoxic drugs, cells in central regions being more sensitive than cells in more peripheral locations (Lindeman, 1969; Yan et al., 1991).

Regeneration of hair cells following exposure to ototoxic drugs has not been previously studied in amphibians. In addition, previous studies of hair cell regeneration have not attempted to examine the development and differentiation of specific hair cell types within individual inner ear endorgans. This is of critical importance in the vestibular organs, where hair cells with differing cell body and hair bundle morphology are located in close proximity to one another (Lindeman, 1969; Wersall and Bagger-Sjoberg, 1974). Varia-

Correspondence to: Richard A. Baird, R.S. Dow Neurological Sciences Institute, 1120 NW 20th Avenue, Portland, OR 97209, USA.



tions in hair bundle morphology are particularly striking in the vestibular organs of the bullfrog, where several hair cell types have previously been described (Lewis and Li, 1975; Baird and Lewis, 1986). These hair cell types have recently been shown to differ dramatically in their physiological response properties (Baird, 1992, 1993a,b).

In the present study, the aminoglycoside antibiotic gentamicin sulfate was used to induce the degeneration of hair cells in the vestibular otolith organs of the bullfrog. The primary aim of this study was to determine whether hair cells in the bullfrog otolith organs would regenerate following exposure to ototoxic drugs. Our results reveal that hair cells in both the saccular and utricular maculae regenerate following ototoxic insult and that immature versions of mature hair cell types in these endorgans are identifiable by their hair bundle morphology.

Preliminary accounts of portions of this data have recently been presented in abstract form (Baird et al., 1993).

Methods

Intraotic injection of gentamicin sulfate

Adult bullfrogs (*Rana catesbeiana*) of either sex weighing 100–200 g were anesthetized by immersion in 0.2% MS-222. Unlike similar experiments in mammals (Takamida et al., 1989a–c), birds (Cruz et al., 1987; Duckert and Rubel, 1990; Lippe et al., 1991) and fish (Yan et al., 1991), systemic injections of gentamicin did not result in the degeneration of vestibular hair cells in amphibians. We therefore used an intraotic approach to administer gentamicin to the inner ear. Using aseptic technique, the right otic capsule was ventrally exposed through a small hole in the roof of the mouth and perforated, using a deburred 25 gauge syringe, at two points immediately above the saccular macula. We then carefully introduced a 10 μ l Hamilton syringe into one of these perforations and slowly injected 9.5 μ l of a 500–2000 μ M gentamicin sulfate solution dissolved in low- Ca^{2+} HEPES-buffered saline into the otic capsule. Mean otic capsule volume, measured in 5 animals, was estimated to be 47.7 ± 3.0 μ l. This volume, which represents an upper limit on the total (endolymphatic and perilymphatic) volume of fluid space encapsulated by the otic capsule, suggests that our injections resulted in 100–400 μ M intraotic gentamicin sulfate concentrations. We believe, although this was not verified histologically, that this injection procedure resulted in a localized rupture of the membranous labyrinth and a mixing of the endolymphatic and perilymphatic fluids. Following intraotic injections, the otic capsule was sealed with bone wax and bullfrogs were allowed to recover from anesthesia.

Removal of the vestibular otolith organs

Bullfrogs injected with gentamicin sulfate were re-anesthetized with 0.2% MS-222 and decapitated 0.5–9 days following gentamicin injection. As in previous studies (Baird, 1992, 1993a,b), saccular and utricular maculae were dissected from the membranous labyrinth in cold, oxygenated HEPES-buffered saline and trimmed of excess nervous and connective tissue to improve the visibility of hair bundles. Otolith membranes were removed with gentle mechanical agitation following a 15–45 min proteolytic digestion in 50 μ g/ml subtiloelptidase BPN^o (Sigma). Excised saccular and utricular maculae were fixed by immersion for 2–4 h in 4% paraformaldehyde in 0.1 M phosphate buffer (pH = 7.25), dehydrated in an ascending series of ethanol solutions, and mounted in depression slides.

Hair cell counts

Measurements of hair cell density were made from the saccular and utricular maculae of 5 normal, 1 saline-injected, and 15 gentamicin-injected animals. These measurements were made by viewing whole-mount maculae under Nomarski illumination with x40/0.9 and x63/1.25 oil immersion objectives and counting the number of hair cells located within a 75×100 μ m rectangle. Hair cells were counted only if they had a clearly recognizable hair bundle and cuticular plate. These counts were made in the central portion of the sacculus and in both the striolar and medial extrastriolar regions of the utriculus. The results of three independent counts were made and averaged for each endorgan.

Hair cell morphology

To examine the cellular and hair bundle morphology of hair cells in more detail, wholemount maculae were embedded in glycol methacrylate (Polysciences, JB-4) and serially sectioned at 8 μ m on a rotary microtome (LKB, Historange). For 10–15 individual sections, the boundaries of the sensory epithelium and, in the utriculus, the striolar region, were traced and stored to hard disk via a video processor board (ITI, FG-100). Hair cell types in normal material were identified, as in previous studies (Baird, 1992, 1993a,b), from their macular location and hair bundle morphology. The macular location of utricular hair cells was determined from their position relative to the striolar border and the reversal of hair bundle polarization. Hair bundle morphology was classified by the size of the hair bundle, the presence or absence of a bulbed kinocilium, and the relative lengths of the kinocilium and longest stereocilia.

Hair cells from gentamicin-treated animals were identified as damaged, undamaged, or regenerating from their cell body and hair bundle morphology. Damaged hair cells had swollen cell bodies, pyknotic

nuclei, and/or fused, splayed, or missing hair bundles. Regenerating hair cells were identified by their small cell bodies, small nuclei, and the presence of short, well-formed hair bundles (see Results). To our surprise, it was possible, based upon the presence or absence of a bulbed kinocilium and the relative lengths of the kinocilium and longest stereocilia, to identify immature versions of mature hair cell types in both the saccular and utricular maculae.

Results

The general appearance of the saccular and utricular maculae from one of 5 uninjected animals is shown in Figs. 1 and 2. From above, both maculae are kidney-shaped. The utricle, unlike the sacculus, is

divided into medial and lateral parts by the striola, a 50–100 μm ribbon-shaped zone, that runs for almost the entire length of the sensory epithelium near its lateral border (Fig. 2A). In cross section, this region is distinguished from flanking extrastriolar regions by the wider spacing of its hair cells and the elevated height of its apical surface (Fig. 2B). Hair cells within the striola reverse their hair bundle polarization near the lateral border of the striola, separating the striola into medial and lateral parts.

The cellular organization of both maculae is similar, consisting of a pseudostratified columnar epithelium of sensory hair cells interspersed with non-sensory supporting cells (Figs. 1A and 2B). Hair cells occupy the upper two-thirds of the sensory epithelium, while supporting cells span its entire distance. The nuclei of hair cells are positioned apical to those of supporting cells.

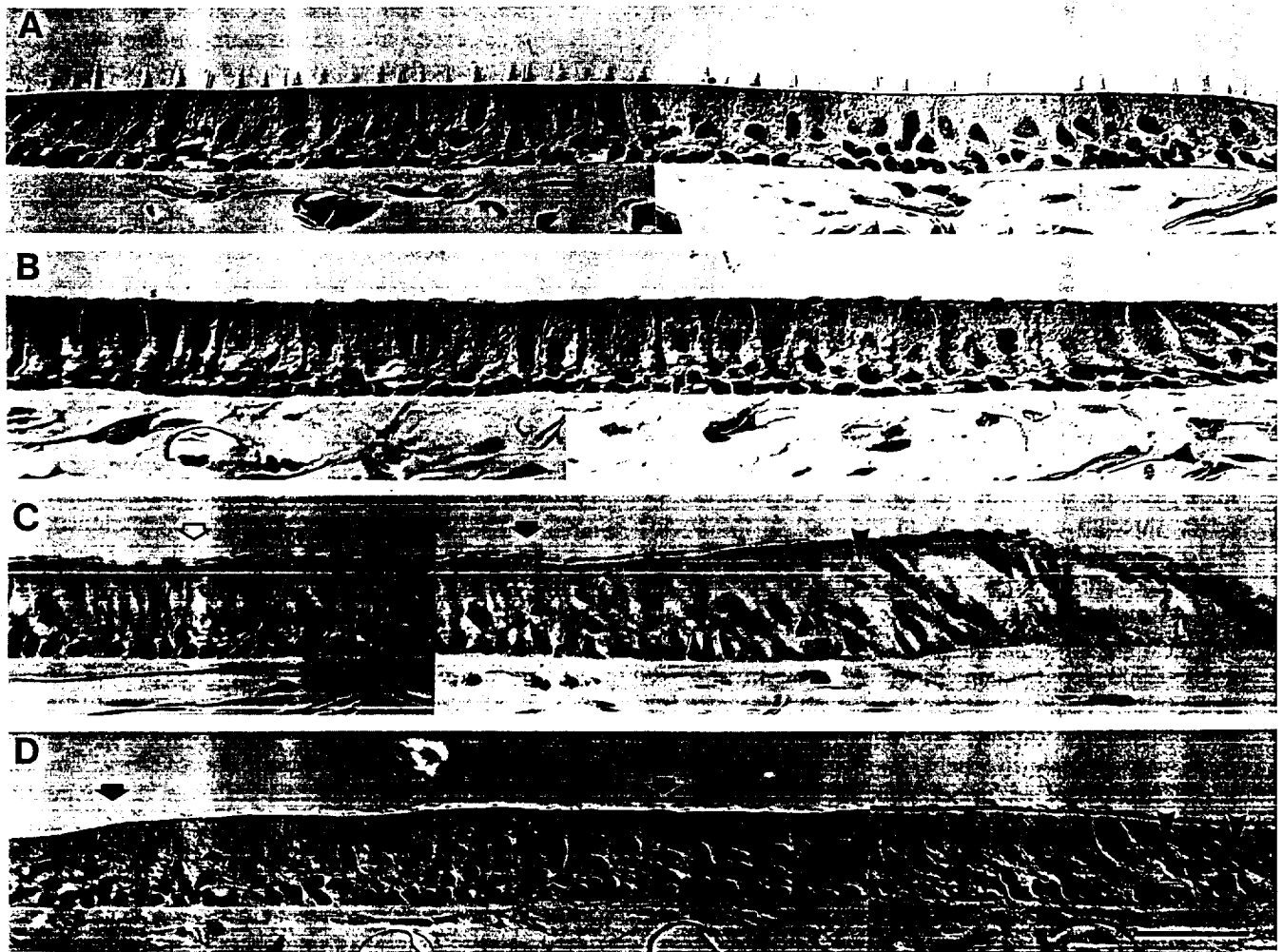


Fig. 1. Nomarski photomicrographs of toluidine-blue stained cross-sections of the right saccular macula from an uninjected animal (A) and animals sacrificed 1 day (B), 2 days (C), and 7 days (D) after 200 μM gentamicin injection. In B, note the universal loss of hair bundles and the beginnings of cellular damage in the peripheral margin (far right). In C, a partially extruded hair cell (solid arrow), regenerating hair cell (solid pointer) and the opening left by an extruded hair cell (open arrow) are shown. Note also the large epithelial holes and apical migration of supporting cell nuclei in the peripheral margin (far right). In D, note regenerating hair cells with no hair bundles (solid pointers) and with long kinocilia (solid arrows). Numerous hair cells with short, bulbed kinocilia are also seen. Scale bar. 50 μm (A–D).

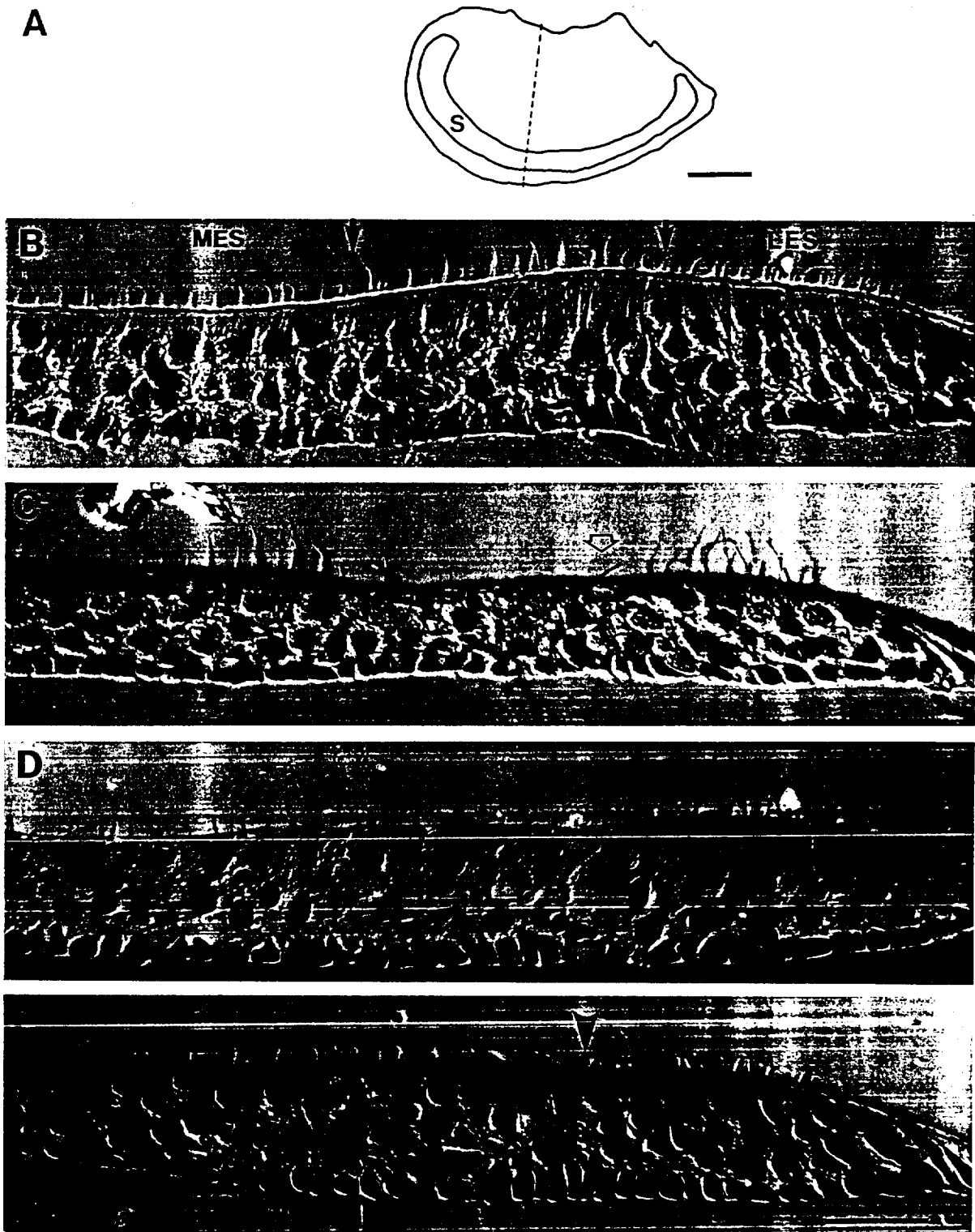


Fig. 2. Surface reconstruction (A) of the wholemount utricular macula. Dashed line $x---x'$ indicates the plane of section seen in subsequent figures. The striola, a ribbon-shaped zone, separates the extrastriola into medial and lateral parts. Nomarski photomicrographs of toluidine-blue stained cross-sections of the right utricular macula from an uninjected animal (B) and animals sacrificed 1 day (C), 3 days (D) and 9 days (E) after $200 \mu\text{M}$ gentamicin injection. In C, open arrow indicates an undamaged striolar hair cell with hair bundle morphology similar to that of extrastriolar hair cells. Pointers in D and E indicate regenerating hair cells. MES, medial extrastriola; S, striola; LES, lateral extrastriola. Scale bars, $250 \mu\text{m}$ (A); $25 \mu\text{m}$ (B-E).

The basal surfaces of supporting cells rest on a basement membrane which separates the sensory epithelium from its afferent and efferent innervation.

The great majority of saccular hair cells have bulbed kinocilia no longer than their longest stereocilia (Fig. 1A). These hair cells occupy the entire central region of the macula. A second type of hair cell, with unbulbed kinocilia longer than its longest stereocilia, is located around the macular perimeter. This hair cell is known from previous studies to be a growth precursor of mature saccular hair cells (Li and Lewis, 1979; Corwin, 1985). Hair cells in the utricle, unlike the sacculus, differ significantly in hair bundle morphology in different membrane regions (Lewis and Li, 1975; Baird and Lewis, 1986). The predominant hair cell type in the utricle has short stereocilia and kinocilia 2–6 times as long as its longest stereocilia. These hair cells are found throughout the medial and lateral extrastriola and, more rarely, in the striolar region. Three other hair cell types, with a variety of hair bundle morphologies, are confined to the striolar region.

Cell body and hair bundle morphology in an animal injected with HEPES-buffer was similar to that of uninjected animals. In gentamicin-treated animals, on the other hand, rapid changes in the cell body and hair bundle morphology of saccular and utricular hair cells were observed following gentamicin injection. The effects of gentamicin treatment were quantified by comparing hair cell density in the saccular and utricular maculae of normal animals with those of animals injected with HEPES-buffer or varying concentrations of gentamicin sulfate (Fig. 3). Hair cell density in the utricular striola and extrastriola of an animal 24 h after

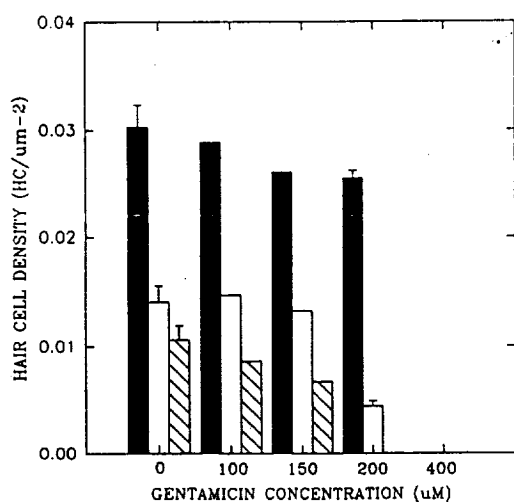


Fig. 3. Scale bar graphs of hair cell density in the sacculus and the striolar and medial extrastriolar regions of the utricle for 5 uninjected animals and 5 animals sacrificed 1 day after receiving injections of varying concentrations of gentamicin sulfate. Values, means \pm standard deviations. Sacculus, (▨); Utricular striola (□); Utricular extrastriola (■).

injection of HEPES-buffer was only slightly less than that in normal animals (0.012 vs. 0.014 and 0.028 vs. 0.030, respectively). This difference was not statistically significant ($P > 0.05$). Injections of gentamicin sulfate, on the other hand, caused large decreases in hair cell density. Hair cell density in the sacculus began to drop for gentamicin concentrations as low as 100 μ M and continued to decrease with increasing gentamicin concentration. Injections of 200 μ M gentamicin sulfate resulted, within 24 h, in the complete degeneration of all saccular hair cells. In the utricle, on the other hand, gentamicin concentrations $< 200 \mu$ M did not significantly decrease striolar or extrastriolar hair cell density below that of normal animals ($P > 0.4$). For 200 μ M concentrations, there was a significant drop in striolar ($P < 0.0005$) but little or no effect on extrastriolar ($P > 0.4$) hair cell density. Animals did not survive 400 μ M gentamicin concentrations. We therefore chose to use 200 μ M intraotic injections for the remainder of these studies.

The first sign of gentamicin toxicity, seen within 12–24 hours following gentamicin injection, was a gradual degeneration of the hair bundle (Figs. 1B and 2C). This degeneration began with a splaying or fusion of individual stereocilia and culminated with the disappearance of the hair bundle. By 24–48 h, further changes were observed in the sensory epithelium of the saccular and utricular maculae. These included hair cells with swollen nuclei and cell bodies, hair cells with absent or pyknotic nuclei, and hair cells with breaks in their plasma membrane (Figs. 1C and 2D). Partially extruded hair cells, particularly in the saccular macula, were often observed (solid arrow, Fig. 1C). Large epithelial holes surrounded on either side by supporting cells were also seen, suggesting the extrusion of many additional hair cells from the sensory epithelium (open arrow, Fig. 1C). These holes were especially prominent in the peripheral margin of the saccular macula (far right, Fig. 1C) and in the striola region of the utricular macula, where they often resulted in a flattening of the apical surface of this region relative to surrounding extrastriolar regions (Fig. 2C). Supporting cells, on the other hand, had normal cellular morphology.

In the sacculus, hair cells were uniformly damaged by gentamicin injection (Figs. 1B and C), although cellular damage was often greater in the peripheral margin than in more central regions (Fig. 1C). Hair cells in the utricular macula, on the other hand, displayed a differential sensitivity to gentamicin (Fig. 2C). Hair cells in the extrastriolar regions of the utricle displayed few, if any, signs of gentamicin toxicity. The great majority of striolar hair cells were severely damaged and degenerated within 12–24 h of gentamicin injection. The hair bundle morphology of undamaged striolar hair cells was similar to that of extrastriolar hair cells (Fig. 2C).

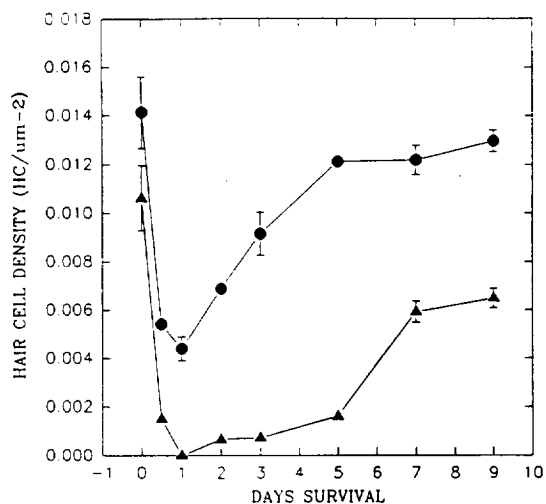


Fig. 4. Hair cell density in the sacculus (▲) and utricular striola (●) plotted against post-injection time for 12 animals receiving 200 μ M gentamicin injections. Values for 5 uninjected animals plotted at 0 days post-injection. Values, means \pm standard deviations.

To test for the possible recovery of hair cells at later postinjection times, we plotted hair cell density in the saccular and utricular maculae versus postinjection time for 12 animals injected with 200 μ M gentamicin sulfate (Fig. 4). The sacculus recovered slowly from gentamicin toxicity, showing little or no recovery for 5 days. At this point, hair cell density increased significantly, restoring half of the normal hair cell density by 9 days. The utricular striola recovered more rapidly, displaying a rapid increase in hair cell density for the first 3 days post-injection and a slower increase from this point up to 9 days post-injection. Hair cell density in the utricular striola of animals sacrificed 9 days postinjection was not significantly different from that in normal animals ($P > 0.10$).

The recovery of hair cell density demonstrated in Fig. 4 suggested that new hair cells were being formed following the degeneration of hair cells damaged by gentamicin toxicity. This conclusion is based upon two assumptions: (1) damaged hair cells rapidly and completely lose their sensory hair bundles, and (2) recovering or regenerating hair cells can be recognized in wholemount preparations by the presence of their sensory hair bundles. To test the latter assumption, we studied sectioned material from animals sacrificed at later postinjection times to more closely examine the cell body and hair bundle morphology of individual hair cells.

By 2–3 days postinjection, obvious signs of repair were evident in the most damaged areas of the saccular and utricular maculae of gentamicin-injected animals. These included the rapid proliferation of supporting cells. In the sacculus, supporting cells at the peripheral margin were seen to migrate from the basement membrane to more apical positions (far right, Fig. 1D), suggesting that these cells might be redifferentiating into hair cells. Similar migrations were observed, although less consistently, in the central sacculus and utricular striola (Figs. 1C and 2D). In addition, newly formed cells, typified by small, narrow cell bodies and small nuclei, were seen in both the saccular and utricular maculae (pointers, Figs. 1C and D; 2D and E). Many of these cells also exhibited mitotic figures (Fig. 5), enabling us to unequivocally identify hair cells undergoing metaphase (Figs. 5A and B), anaphase (Fig. 5C), and telophase (Fig. 5D). Newly formed hair cells were also recognized by their weaker nuclear staining density in toluidine-blue stained material.

Newly formed hair cells, unlike mature hair cells or supporting cells, initially occupied intermediate positions within the sensory epithelium and did not contact the apical surface. Upon contacting this surface, these

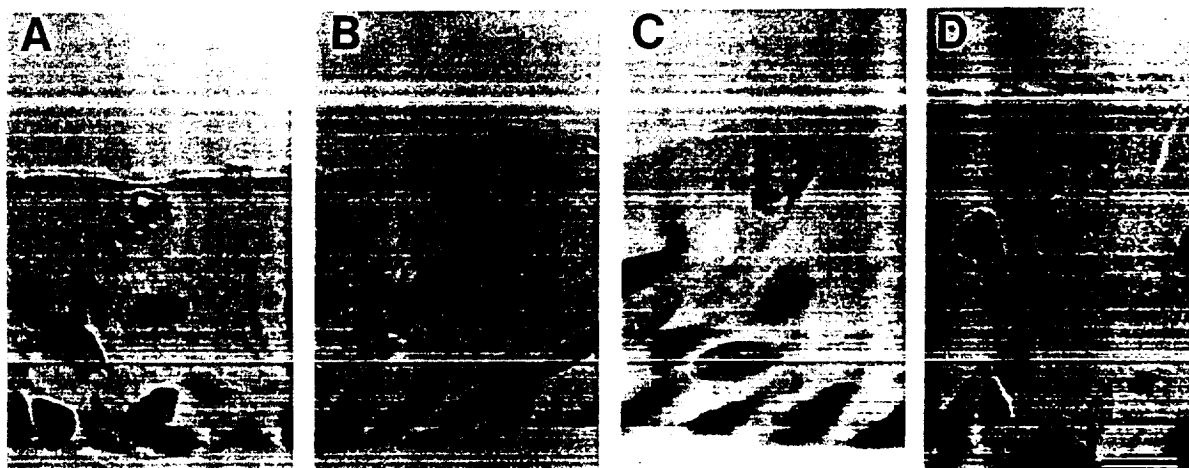


Fig. 5. Nomarski photomicrographs of newly formed hair cells in the saccular macula undergoing metaphase (A,B), anaphase (C) and telophase (D). Scale bar, 10 μ m (A–D).

cells began to acquire the hair bundle characteristic of mature hair cells. Newly formed hair cells were observed as early as 2 days and as late as 9 days postinjec-

tion. By 7–9 days postinjection, the cellular morphology of the saccular and utricular maculae in gentamicin-injected animals more closely resembled that seen

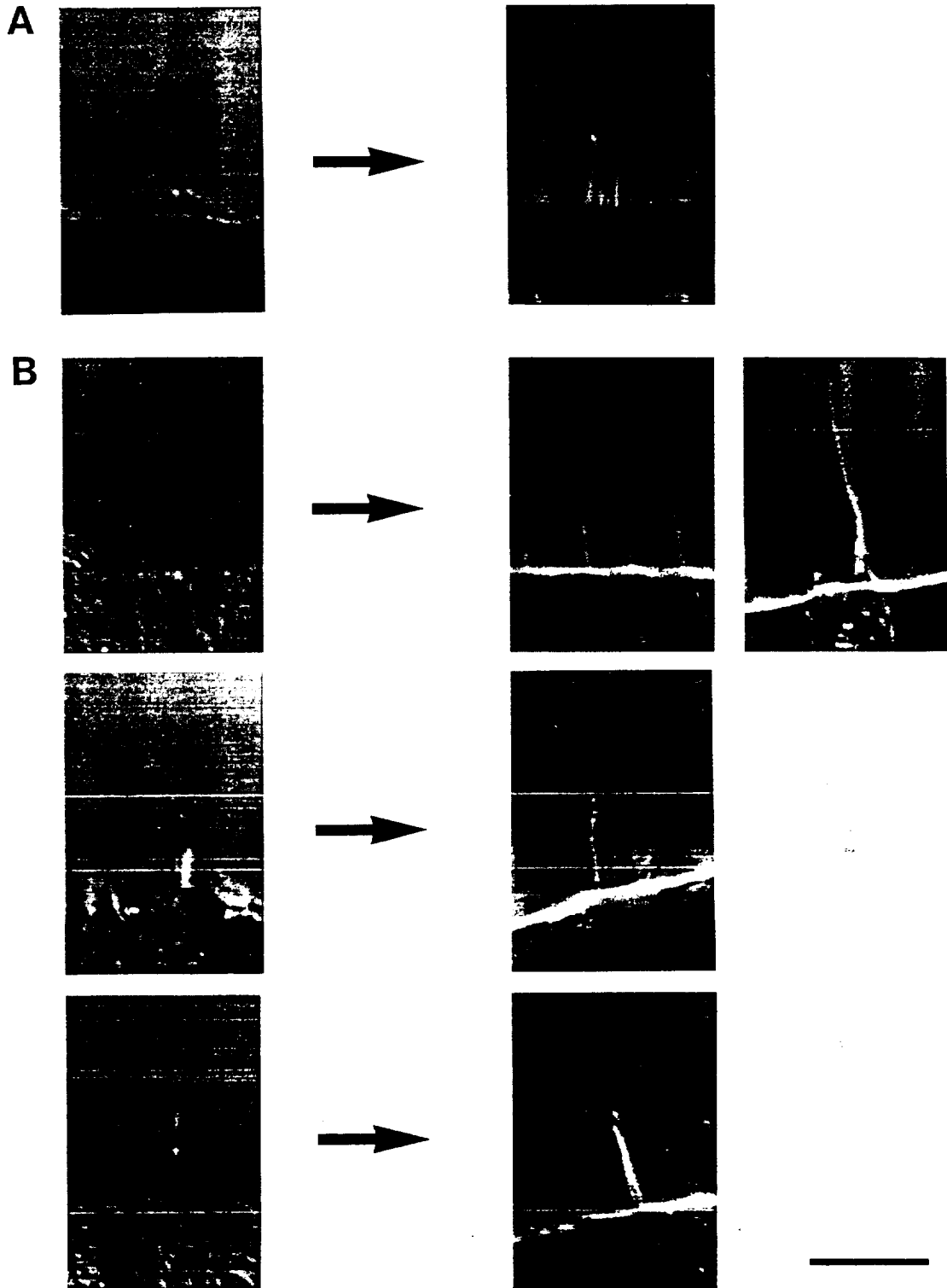


Fig. 6. Nomarski photomicrographs of immature (left) and mature (right) hair cell types in the saccular (A) and utricular (B) maculae. Immature saccular hair cell taken from animal sacrificed 7 days postinjection; immature utricular hair cells taken from animals sacrificed 3–5 days postinjection. Scale bar, 10 μ m.

in normal material (Figs. 1D and 2E). The cell bodies of hair cells and supporting cells were more ordered and normal in appearance. The nuclei of hair cells and supporting cells, as in normal material, were well separated. Epithelial holes in the sensory epithelium, although still apparent (Figs. 1D and 2E), were smaller and less frequent than at earlier postinjection times.

To our surprise, immature versions of most of the mature hair cell types in the bullfrog sacculus and utricle could readily be identified by their distinctive hair bundle morphology (Figs. 6A and B). As in the normal sacculus (Fig. 1A), regenerating hair cells in the peripheral margin and, more rarely, in the central region had unbulbed kinocilia longer than their longest stereocilia (solid arrows, Fig. 1D). Most hair cells in the central region had short, bulbed kinocilia equal in length to their longest stereocilia (Figs. 2E and 6A). In both cases, the hair bundles of newly formed hair cells were significantly shorter than those of mature saccular hair cells, even in animals sacrificed 7–9 days postinjection.

In the utricle, four mature hair cell types have been distinguished by the presence or absence of a bulbed kinocilium and the relative lengths of their kinocilium and longest stereocilia (Lewis and Li, 1975; Baird and Lewis, 1986). Two of these hair cell types have short stereocilia and kinocilia 2–6 times longer than their longest stereocilia, differing only in the absolute lengths of their kinocilia and longest stereocilia. Short hair bundles with similar morphology were often seen in gentamicin-treated animals (Fig. 6B, top). The remaining two types possess bulbed or unbulbed kinocilia approximately equal in length to their longest stereocilia. Immature versions of both of these hair cell types were also observed in gentamicin-injected animals (Fig. 6B, middle and bottom). The hair bundles of newly formed utricular hair cells, unlike saccular hair cells, reached similar lengths as their mature counterparts by 7–9 days postinjection.

Hair cells appeared to repopulate the utricular striola in a fixed order. At 2–5 days postinjection, the great majority of newly formed hair cells had kinocilia longer than their longest stereocilia (Fig. 6B, top). These hair cells, as in normal material, were largely restricted to the outer striolar rows (Fig. 2E). Hair cells with shorter bulbed and unbulbed kinocilia (Fig. 6B, middle and bottom) appeared only at later postinjection times.

Discussion

The results of the present study clearly demonstrate that vestibular hair cells in the bullfrog, like those in birds (Cruz et al., 1987; Hashino et al., 1991; Lippe et al., 1991) and fish (Yan et al., 1991), are sensitive to

aminoglycoside antibiotics. More importantly, our findings demonstrate that vestibular endorgans, like their auditory counterparts (Cruz et al., 1987; Hashino et al., 1991; Lippe et al., 1991), are capable of regenerating new hair cells following aminoglycoside toxicity. Using autoradiography and immunocytochemical labeling, Weisleder and Rubel (1992) have recently shown that vestibular hair cells in the bird also exhibit regeneration following exposure to aminoglycoside antibiotics. Although hair cells in the amphibian vestibular endorgans are known to proliferate at a low level throughout adult life (Li and Lewis, 1979; Corwin, 1985), these findings represent, to our knowledge, the first direct evidence of hair cell regeneration in amphibians.

The degeneration and subsequent regeneration of hair cells seen in this study was more rapid than that seen in other studies. This may be due to the way in which gentamicin was administered to the inner ear. With the exception of one early study (Lindeman, 1969b), most investigators (Cruz et al., 1987; Hashino et al., 1991; Lippe et al., 1991), have administered aminoglycoside antibiotics systemically, resulting in a slow, sustained delivery of these antibiotics to all parts of the body. Our intraotic injection procedure, by contrast, was designed to rapidly deliver a concentrated dose of antibiotic to the inner ear. We are not certain why vestibular hair cells in the bullfrog are not affected by systemic injections of aminoglycoside antibiotics. Our results do, however, emphasize the ability of the vestibular organs to rapidly reproduce new hair cells in response to ototoxic insult. Moreover, they are in good agreement with the results of Yan et al. (1991), who also did not observe hair cell damage in the sacculus after systemic injections of gentamicin in the fish.

It has long been known that aminoglycoside antibiotics can induce cochlear and vestibular ototoxicity. The biochemical mechanism(s) underlying ototoxicity, however, are only poorly understood (Lim, 1986; Schacht, 1986). Schacht and his colleagues (1986) have proposed that aminoglycosides bind electrostatically with negatively charged components of the hair cell plasma membrane. In addition, polycationic aminoglycosides, such as gentamicin and streptomycin, bind to and block negatively charged hair cell transduction channels (Kroese and van den Berken, 1980; Kroese et al., 1988; Jaramillo and Hudspeth, 1991), located at or near the tips of the stereocilia (Hudspeth, 1982; Jaramillo and Hudspeth, 1991). Both of these interactions are believed to be reversible and antagonized by divalent cations. A second, more crucial, interaction is the energy-dependent transport of aminoglycosides into hair cells by endocytosis (Takada et al., 1985; DeGroot et al., 1990) and its subsequent binding to phosphatidylinositol 4,5-bisphosphate (PIP₂) (Schacht, 1986). This binding inhibits the hydrolysis of IP₂, preventing its physiological function (Berridge, 1984; Nishizuka,

1984), and disturbs membrane structure, resulting in non-specific permeabilities of the plasma membrane to external ions.

Hair cells in the vestibular organs were differentially sensitive to gentamicin, saccular hair cells being affected at lower gentamicin concentrations than their utricular counterparts. Within the utricle, hair cells in the striola were affected more than hair cells in extrastriolar regions. Vestibular organs in mammals (Lindeman, 1969b) and fish (Yan et al., 1991) are also known to exhibit such regional sensitivity, hair cells in central regions being more sensitive than hair cells in more peripheral locations. In our study, selective sensitivity to gentamicin was correlated with hair cells with particular hair bundle morphologies. This is the first evidence that such sensitivity is correlated with hair cell type rather than epithelial location *per se*.

The cellular basis for selective gentamicin sensitivity is not well understood. One possibility is that some hair cells are able to slow or prevent the access of aminoglycoside to intracellular compartments, perhaps by varying the level of intracellular calcium at their apical surface. This would be expected to antagonize the electrostatic interaction of aminoglycosides with the transduction channel and plasma membrane, preventing or delaying its intracellular entry and subsequent deleterious effects. A second possibility is that the intracellular effects of aminoglycoside antibiotics are more deleterious in some hair cells than in others. The primary site for these antibiotics appears to be the endoplasmic reticulum and Golgi complex (DeGroot et al., 1990). Hair cells in central regions of the vestibular endorgans possess a more extensive endoplasmic reticulum and larger numbers of mitochondria than hair cells located in more peripheral regions (Yan et al., 1991). Whatever its cellular basis, however, this phenomenon provides investigators with a useful tool to study the degeneration and regeneration of specific hair cell populations in the vestibular organs.

The signals and cellular mechanism(s) which trigger the production of new vestibular hair cells are not known. Hair cell recovery could potentially result from a number of processes, including the migration of undamaged hair cells to damaged regions, the recovery of partially damaged hair cells, the redifferentiation of other cell types into hair cells, and the production of new hair cells by mitosis. Migration of undamaged hair cells cannot contribute to recovery in the sacculus, where a near-complete loss of the existing hair cell population is observed. While migration of undamaged hair cells from extrastriolar regions could contribute to hair cell recovery in the utricular striola, our results suggest that this is unlikely. First, such a migration would be expected to produce a reduction in extrastriolar hair cell density. This was not observed. Secondly, a restoration of the normal distribution of striolar hair

cell types would imply that differentiated extrastriolar hair cells were able to redifferentiate into striolar hair cell types. The existence of distinctive immature versions of mature striolar hair cell types suggests that this does not occur. Our results do not reveal if partially damaged hair cells are able to recover after gentamicin exposure. Two lines of evidence, however, suggest that this is not the case. First, the loss of hair cell nuclei and the creation of large epithelial holes following gentamicin exposure suggests that damaged hair cells are destroyed and extruded from the sensory macula. Studies in the auditory system also suggest that only differentiating hair cells are capable of hair bundle assembly (Corwin and Cotanche, 1989; Tilney, 1986), seemingly ruling out the possibility that mature hair cells can regrow their hair bundles.

The large loss of hair cells in the sacculus and utricular striola argues strongly that recovery must involve the mitotic production of new hair cells. This is supported by the presence of regenerating cells with mitotic figures in gentamicin-treated but not normal animals. These regenerating hair cells were present only in regions of hair cell loss suggesting that, as in the auditory organs, such loss is necessary for mitosis to occur. Mitotic division of a precursor population is also responsible for the restoration of hair cell populations in other lower vertebrates following acoustic trauma (Corwin and Cotanche, 1988; Ryals and Rubel, 1988; Girod et al., 1989; Popper and Hoxter, 1990; Rubel, 1991) and aminoglycoside toxicity (Cruz et al., 1987; Hashino et al., 1991; Lippe et al., 1991). One obvious candidate for this population is some subset of supporting cells (Girod et al., 1989; Popper and Hoxter, 1990; Rubel, 1991). Our results further reveal that supporting cells, following the destruction of existing hair cells, migrated toward the apical surface, leaving no cell nuclei adjacent to the basement membrane. This migration was not necessarily associated with mitotic hair cells, suggesting that supporting cells may also redifferentiate directly into hair cells.

Surprisingly, regenerating hair cells strongly resembled miniature versions of mature hair cells at all stages of their development and could be classified into a number of hair cell types by the same morphological criteria used to identify their mature counterparts. Regenerating hair cells, for example, had kinocilia 2–6 times longer or approximately equal to their longest stereocilia. Similarly, regenerating hair cells with bulbed kinocilia, differing only in absolute kinociliary and stereociliary length, were consistently seen in gentamicin-treated animals. This suggests that the hair bundle morphology of vestibular hair cells, as in auditory hair cells (Corwin and Cotanche, 1989), is location-specific and predetermined early in the regeneration process. Our results do not reveal whether hair cell types transform their hair bundle morphology dur-

ing the regenerative process or if they differentiate from independent precursor cells. In the utricular striola, however, hair cells appeared to regenerate in a fixed order, suggesting that morphologically distinct hair cell types may represent intermediate stages in morphogenic development. In the bullfrog sacculus, moreover, mature hair cells with short, bulbed kinocilia are believed to develop from hair cells with long, unbulbed kinocilia (Li and Lewis, 1979; Corwin, 1985). Regenerating saccular hair cells with both types of hair bundle morphology were seen in our material. However, hair cells with long, unbulbed kinocilia were usually located in the peripheral margin. Moreover, most saccular hair cells, even at early postinjection times, had short, bulbed kinocilia, arguing against a compulsory involvement of hair cells with long, unbulbed kinocilia in the regenerative process. This would seem to contradict the results of Corwin (1985), who argues that developing saccular hair cells initially have long kinocilia which shrink during development to attain the bulbed kinocilium typical of mature saccular hair cells. It is, of course, possible that the processes underlying hair cell regeneration do not mirror those underlying normal development.

Our results emphasize the importance of the vestibular otolith organs as model systems for studies of hair cell regeneration. These organs, particularly the utricular macula, possess a number of hair cell types, which are distinguishable both by their hair bundle morphology (Lewis and Li, 1975; Baird and Lewis, 1986) and their physiological response properties (Baird, 1993a,b). As our results demonstrate, immature versions of these hair cell types can easily be recognized and studied at various stages of development. Studies of the morphological and physiological changes that occur during hair cell regeneration should reveal what signals trigger regeneration in lower vertebrates and hopefully lead to an understanding of the basic mechanisms underlying differentiation and repair in these important receptor cells.

Acknowledgements

We are grateful to Joyce P. Gregory for assistance with manuscript preparation. Funding for this research was provided by NIDCD grant DC-00355, NASA grant NCC 2-651, and by the Oregon Lions Sight and Hearing Foundation.

References

- Baird, R.A. (1992) Morphological and electrophysiological properties of hair cells in the bullfrog utriculus. *Ann. NY Acad. Sci.* 656, 12-26.
- Baird, R.A. (1993a) Comparative transduction and tuning mechanisms of hair cells in the bullfrog utriculus. I. Responses to intracellular current. *J. Neurophysiol.* (Submitted).
- Baird, R.A. (1993b) Comparative transduction and tuning mechanisms of hair cells in the bullfrog utriculus. II. Sensitivity and response dynamics to mechanical stimulation. *J. Neurophysiol.* (Submitted).
- Baird, R.A. and Lewis, E.R. (1986) Correspondences between afferent innervation patterns and response dynamics in the bullfrog utricle and lagena. *Brain Res.* 369, 48-64.
- Baird, R.A., Torres, M.A. and Schuff, N.A. (1993) Hair cell regeneration in the amphibian vestibular otolith organs following gentamicin ototoxicity. *Assoc. Res. Otolaryngol.* 16, (in press).
- Berridge, M.J. and Irvine, R.F. (1989) Inositol phosphates and cell signalling. *Nature* 341, 197-205.
- Corwin, J.T. (1981) Postembryonic production and aging of inner ear hair cells in sharks. *J. Comp. Neurol.* 201, 541-553.
- Corwin, J.T. (1985) Perpetual production of hair cells and maturational changes in hair cell ultrastructure accompany postembryonic growth in an amphibian ear. *Proc. Natl. Acad. Sci. (USA)* 82, 3911-3915.
- Corwin, J.T. and Cotanche, D.A. (1988) Regeneration of sensory hair cells after acoustic trauma. *Science* 240, 1772-1774.
- Corwin, J.T. and Cotanche, D.A. (1989) The development of location-specific hair cell stereocilia in denervated embryonic ears. *J. Comp. Neurol.* 288, 529-537.
- Cotanche, D.A. (1987) Regeneration of hair cell stereociliary bundles in the chick cochlea following severe acoustic trauma. *Hear. Res.* 30, 181-196.
- Cruz, R.M., Lambert, P.R. and Rubel, E.W. (1987) Light microscopic evidence of hair cell regeneration after gentamicin toxicity in chick cochlea. *Arch. Otolaryngol. Head Neck Surg.* 113, 1058-1062.
- DeGroot, J.C.M., Meeuwse, F., Ruizendaal, W.E. and Veldman, J.E. (1990) Ultrastructural localization of gentamicin in the cochlea. *Hear. Res.* 50, 35-42.
- Duckert, L.G. and Rubel, E.W. (1990) Ultrastructural observation on regenerating hair cells in the chick basilar papilla. *Hear. Res.* 48, 161-182.
- Girod, D.A., Duckert, L.G. and Rubel, E.W. (1989) Possible precursors of regenerated hair cells in the avian cochlea following acoustic trauma. *Hear. Res.* 42, 175-194.
- Hashino, E., Tanaka, Y. and Sokabe, M. (1991) Hair cell damage and recovery following chronic application of kanamycin in the chick cochlea. *Hear. Res.* 52, 356-368.
- Hudspeth, A.J. (1982) Extracellular current flow and the site of transduction by vertebrate hair cells. *J. Neurosci.* 2, 1-10.
- Jamarillo, F. and Hudspeth, A.J. (1991) Localization of the hair cell's transduction channels at the hair bundle's top by iontophoretic application of a channel blocker. *Neuron* 7, 409-420.
- Jones, T.A. and Nelson, R.C. (1992) Functional recovery of the peripheral vestibular system following severe streptomycin injury. *Assoc. Res. Otolaryngol.* 15, 161.
- Jorgensen, J.M. and Mathiesen, C. (1988) The avian inner ear: continuous production of hair cells in vestibular sensory organs, but not in the auditory papilla. *Naturwissenschaften* 75, 319-320.
- Katayama, A. and Corwin, J.T. (1989) Cell production in the chicken cochlea. *J. Comp. Neurol.* 281, 129-135.
- Kroese, A.B.A. and Bercken, J. Van Den. (1980) Dual action of ototoxic antibiotics on sensory hair cells. *Nature* 283, 395-397.
- Kroese, A.B.A., Das, A. and Hudspeth, A.J. (1988) Blockage of the transduction channels of hair cells in the bullfrog's sacculus by aminoglycoside antibiotics. *Hear. Res.* 37, 203-218.
- Lewis, E.R. and Li, C.W. (1975) Hair cell types and distributions in the otolithic and auditory organs of the bullfrog. *Brain Res.* 83, 35-50.
- Li, C.W. and Lewis, E.R. (1979) Structure and development of

- vestibular hair cells in the larval bullfrog. *Ann. Otol. Rhinol. and Laryngol.* 88, 427-437.
- Lim, D.J. (1986) Effects of noise and ototoxic drugs at the cellular level in the cochlea: a review. *Am. J. Otolaryngol.* 7, 73-99.
- Lindeman, H.H. (1969a) Studies on the morphology of the sensory regions of the vestibular apparatus. *Ergeb. Anat. Entwickl.* 42, 1-113.
- Lindeman, H.H. (1969b) Regional differences in sensitivity of the vestibular sensory epithelia to ototoxic antibiotics. *Acta. Otolaryngol.* 67, 177-189.
- Lippe, W.R., Westbrook, E.N. and Ryals, B.M. (1991) Hair cell regeneration in the chicken cochlea following aminoglycoside toxicity. *Hear. Res.* 56, 203-210.
- Nishizuka, Y. (1984) Turnover of inositol phospholipids and signal transduction. *Science* 225, 1365-1370.
- Popper, A.N. and Hoxter, B.H. (1984) Growth of a fish ear. I. Quantitative analysis of sensory hair cell and ganglion cell proliferation. *Hear. Res.* 15, 133-142.
- Popper, A.N. and Hoxter, B.H. (1990) Growth of a fish ear. II. Locations of newly proliferated hair cells in the saccular epithelium of *Astronotus ocellatus*. *Hear. Res.* 45, 33-40.
- Roberson, D.F., Weisleder, P., Bohrer, P.S. and Rubel, E.W. (1992) Ongoing production of sensory cells in the vestibular epithelium of the chick. *Hear. Res.* 57, 166-174.
- Rubel, E.W. (1991) Regeneration of hair cells in the avian inner ear. In: A. Dancšár, D. Henderson, R. Salvi and R.P. Hamernik (Eds.), *Noise-Induced Hearing Loss*, St. Louis: Mosby Year Book, pp. 204-227.
- Ryals, B.M. and Rubel, E.W. (1988) Hair cell regeneration after acoustic trauma in adult *Coturnix* quail. *Science* 240, 1774-1776.
- Schacht, J. (1986) Molecular mechanisms of drug-induced hearing loss. *Hear. Res.* 22, 297-304.
- Takada, A., Bledsoe, S.C., Jr. and Schacht, J. (1985) An energy-dependent step in aminoglycoside ototoxicity: prevention of gentamicin ototoxicity during reduced endolymphatic potential. *Hear. Res.* 19, 245-251.
- Takumida, M., Bagger-Sjoberg, D., Wersall, J. and Harada, Y. (1989) The effect of gentamicin on the glycocalyx and the ciliary interconnections in vestibular sensory cells: a high-resolution scanning electron microscopic investigation. *Hear. Res.* 37, 163-170.
- Takumida, M., Bagger-Sjoberg, D., Harada, Y., Lim, D. and Wersall, J. (1989) Sensory hair fusion and glycocalyx changes following gentamicin exposure in the guinea pig vestibular organs. *Acta Otolaryngol.* 107, 39-47.
- Takumida, M., Wersall, J. and Bagger-Sjoberg, D. (1989) Initial changes in the sensory hair-cell membrane following aminoglycoside administration in a guinea pig model. *Arch. Otorhinolaryngol.* 246, 26-31.
- Tilney, L.G., Tilney, M.S., Saunders, J.C. and DeRosier, D.J. (1986) Actin filaments, stereocilia and hair cells of the bird cochlea. III. The development and differentiation of hair cells and stereocilia. *Dev. Biol.* 116, 100-118.
- Tucci, D.L. and Rubel, E.W. (1990) Physiological status of regenerated hair cells in the avian inner ear following aminoglycoside ototoxicity. *Otolaryngol. Head Neck Surg.* 103, 443-450.
- Weisleder, P. and Rubel, E.W. (1992) Hair cell regeneration in the avian vestibular epithelium. *Exp. Neurol.* 115, 2-6.
- Wersall, J. and Bagger-Sjoberg, D. (1974) Morphology of the vestibular sense organs. In: H.H. Kornhuber (Ed.), *Vestibular System: Basic Mechanisms, Handbook of Sensory Physiology*, Springer-Verlag, New York, pp. 124-170.
- Yan, H.Y., Saidel, W.M., Chang, J.S., Presson, J.C. and Popper, A.N. (1991) Sensory hair cells of a fish ear: evidence of multiple types based on ototoxicity sensitivity. *Proc. R. Soc. Lond. B* 245, 133-138.

Peripheral Innervation Patterns of Vestibular Nerve Afferents in the Bullfrog Utriculus

R.A. BAIRD AND N.R. SCHUFF

Department of Neuro-otology and R.S. Dow Neurological Sciences Institute,
Good Samaritan Hospital and Medical Center, Portland, Oregon 97209

ABSTRACT

Vestibular nerve afferents innervating the bullfrog utriculus differ in their response dynamics and sensitivity to natural stimulation. They also supply hair cells that differ markedly in hair bundle morphology. To examine the peripheral innervation patterns of individual utricular afferents more closely, afferent fibers were labeled by the extracellular injection of horseradish peroxidase (HRP) into the vestibular nerve after sectioning the vestibular nerve medial to Scarpa's ganglion to allow the degeneration of sympathetic and efferent fibers. The peripheral arborizations of individual afferents were then correlated with the diameters of their parent axons, the regions of the macula they innervate, and the number and type of hair cells they supply.

The utriculus is divided by the striola, a narrow zone of distinctive morphology, into medial and lateral parts. Utricular afferents were classified as striolar or extrastriolar according to the epithelial entrance of their parent axons and the location of their terminal fields. In general, striolar afferents had thicker parent axons, fewer subepithelial bifurcations, larger terminal fields, and more synaptic endings than afferents in extrastriolar regions. Afferents in a juxtastriolar zone, immediately adjacent to the medial striola, had innervation patterns transitional between those in the striola and more peripheral parts of the medial extrastriola. Most afferents innervated only a single macular zone. The terminal fields of striolar afferents, with the notable exception of a few afferents with thin parent axons, were generally confined to one side of the striola.

Hair cells in the bullfrog utriculus have previously been classified into four types based on hair bundle morphology (Lewis and Li: *Brain Res.* 83:35-50, 1975). Afferents in the extrastriolar and juxtastriolar zones largely or exclusively innervated Type B hair cells, the predominant hair cell type in the utricular macula. Striolar afferents supplied a mixture of four hair cell types, but largely contacted Type B and Type C hair cells, particularly on the outer rows of the medial striola. Afferents supplying more central striolar regions innervated fewer Type B and larger numbers of Type E and Type F hair cells. Striolar afferents with thin parent axons largely supplied Type E hair cells with bulbed kinocilia in the innermost striolar rows. © 1994 Wiley-Liss, Inc.

Key words: inner ear, otolith organ, hair cells, horseradish peroxidase

The peripheral innervation patterns of vestibular nerve afferents were first examined in pioneering silver stain studies (Ramón y Cajal, '08, '09; Lorente de Nó, '26; Poljak, '27). These studies revealed that the vestibular nerve is composed of fibers with a wide range of fiber diameters that supply different regions of the vestibular endorgans. In general, the thickest fibers in the vestibular nerve supply the most central regions of the vestibular endorgans, while more peripheral regions receive afferents with thinner parent diameters. In the vestibular otolith organs, this central region is the striola, a narrow zone of distinctive

morphology that runs the entire length of the sensory epithelium and divides it into medial and lateral parts (Werner, '33; Lindeman, '69; Wersall and Bagger-Sjoberg, '74).

More recently, intracellular and extracellular labelling techniques have been used in both mammals (Fernandez et al., '88, '90) and other vertebrates (O'Leary et al., '76;

Accepted August 4, 1993.

Address reprint requests to Dr. Richard A. Baird, R.S. Dow Neurological Sciences Institute, 1120 NW 20th Avenue, Portland, OR 97209.

Honrubia et al., '81, '89; Schessel and Highstein, '81; Lewis et al., '82; Baird and Lewis, '86; Boyle et al., '91; Myers and Lewis, '91; Schessel et al., '91) to examine afferent innervation patterns in individual vestibular endorgans and to correlate the peripheral innervation patterns of individual afferents with the regions of the endorgan they innervate and the number and types of hair cells they supply. In mammals, these studies have shown that the response dynamics of vestibular afferents are more closely related to their fiber diameter and location in the sensory epithelium than to their terminal morphology (Goldberg et al., '85; Baird et al., '88; Goldberg et al., '90b). Response sensitivity, on the other hand, is related to the number of Type I and Type II hair cells innervated by an afferent fiber.

Studies in lower vertebrates, in preparations in which all hair cells are Type II by cell body and synapse morphology (Wersall and Bagger-Sjoberg, '74), have revealed a similar organizational principle (O'Leary et al., '76; Baird and Lewis, '86; Honrubia et al., '81, '89; Boyle et al., '91; Myers and Lewis, '91). These results suggest that differences in afferent sensitivity and response dynamics are the result of regional variations in presynaptic transduction mechanisms. In the semicircular canals, these differences may reflect regional variations in cupular membrane dynamics (Hillman and McLaren, '79; McLaren and Hillman, '79; Boyle et al., '91) or the coupling of the cupular membrane to hair cells in different epithelial locations (Lim, '76; Honrubia et al., '81, '89). In the otolith organs, on the other hand, differences in afferent sensitivity may be determined by transduction mechanisms within individual hair cells. In the bullfrog utricle, a number of subtypes of the Type II hair cell have been defined based on hair bundle morphology (Lewis and Li, '75). Morphophysiological studies in this endorgan have shown that the sensitivity of an afferent is correlated with both the macular location and the hair bundle morphology of its innervated hair cells (Baird and Lewis, '86; Myers and Lewis, '91).

The present study is part of a larger project in which intracellular recording techniques were used to characterize the physiological response properties of hair cells in the bullfrog utricular macula (Baird, '92, '93a,b). In this paper, afferent fibers supplying the utricular macula of the bullfrog were labeled by extracellular injections of HRP into the vestibular nerve after previously sectioning the nerve medial to Scarpa's ganglion to allow the degeneration of sympathetic and efferent fibers. The aim of these studies was to correlate the peripheral innervation patterns of individual afferents with the sizes of their parent axons, the regions of the endorgan they innervate, and the number and types of hair cells they supply.

Our results provide a context for recent companion studies (Baird, '92, '93a,b), in which we demonstrate that utricular hair cells differ in their voltage responses to intracellular current and hair bundle displacement. By revealing the relation between individual afferents and the number and types of hair cells they supply, they also suggest how differences in the transduction mechanisms of different hair cell types in the utricular macula might contribute to differences in sensitivity and response dynamics among vestibular afferents. Finally, our results extend the results of previously published morphophysiological studies (Baird and Lewis, '86; Myers and Lewis, '91). In these studies, intra-axonal labeling techniques were used to correlate the morphology and physiology of individual vestibular nerve afferents. Unfortunately, such studies are

only able to record from small samples of fibers and are highly biased towards sampling from large-diameter fibers. Using extracellular HRP techniques, we were able to label a larger, more representative sample of afferent fibers. In addition, afferents in earlier studies were labeled with the fluorescent dye Lucifer Yellow and their terminal arborizations reconstructed in wholemount preparations. It is difficult to identify hair cell types and to assess fully the terminal arbors of afferents under these conditions. These problems were circumvented in the present study by observing labeled afferents and unlabeled hair cells with Nomarski optics in both wholemount and sectioned material.

Preliminary accounts of portions of this data have been presented in abstract form (Baird, '91).

MATERIALS AND METHODS

Sectioning of the vestibular nerve

Eight bullfrogs (*Rana catesbeiana*), weighing 90–160 g, were anesthetized by immersion in 0.2% MS-222 (Sigma). With sterile technique, the right vestibular nerve was exposed intracranially through a small hole in the parasphenoidal bone and sectioned medial to Scarpa's ganglion to allow the degeneration of sympathetic and efferent fibers (Robbins et al., '67). Great care was taken during this procedure to avoid disturbance of the vasculature surrounding the vestibular nerve. Following surgery, the hole was packed with sterile Gelfoam. We then sutured the incision through the overlying muscle, applied topical anesthetic to the wound, and allowed bullfrogs to recover from the effects of the anesthetic. Upon recovering from anesthesia, bullfrogs initially displayed a tilting of the head toward the side of the lesion, an asymmetrical pose typical after unilateral labyrinthectomy, and made little or no active movements. Bullfrogs were placed in recirculating aquaria in a quiet, darkened room until they exhibited normal postural reflexes (normally 1–2 days) and then returned to normal lighting conditions.

Injection of horseradish peroxidase

After 10–14 days, a length of time sufficient to guarantee the degeneration of efferent vestibular fibers (Robbins et al., '67), bullfrogs were reanesthetized with 0.2% MS-222. The right vestibular nerve was reexposed and injected extracellularly with a solution of HRP. Dimethyl sulfoxide (DMSO) was added to the injection solution to facilitate the labeling of the terminal arbors of labeled afferent fibers (Keefer et al., '76; West and Black, '79). Thin-walled borosilicate micropipettes, broken to tip diameters of 30–50 μm , were filled with a solution of 20% HRP (Sigma, type VI) and 2% DMSO (Sigma) in 0.1 M phosphate buffer (pH 7.25). Typically, HRP was pressure injected at three sites across the anterior-posterior extent of the anterior branch of the right vestibular nerve. Following HRP injections, bullfrogs were repacked with Gelfoam, resutured, and allowed to recover from anesthesia.

Removal of the vestibular endorgans

Three days after HRP injection, animals were again reanesthetized with 0.2% MS-222, decapitated, and the anterior vestibular nerve and utricular macula from the injected side dissected from the membranous labyrinth in cold, oxygenated physiological saline. We then fixed the vestibular nerve and utricular macula overnight in 4.0% paraformaldehyde in 0.1 M phosphate buffer (pH 7.25).

After rinsing in fresh phosphate buffer, utricular maculae were separated from the vestibular nerve. The vestibular nerve was then embedded in glycol methacrylate (Polysciences, JB-4), serially cross-sectioned at 1 μm with a sliding microtome (LKB, Historange), and counterstained for 1 minute in 1% Toluidine Blue.

The otolith membranes of utricular maculae were removed by gentle mechanical agitation after a brief (30–45 minute) enzymatic digestion in 30 $\mu\text{g}/\text{ml}$ subtiloelptidase BPN' (Sigma). A cobalt modification of the diaminobenzidine (DAB) procedure was then used to visualize HRP reaction product in the utricular macula (Adams, '77). To ensure penetration of reagents, maculae were preincubated for 30 minutes in 1% DMSO and an additional 30 minutes in 0.05% DAB, both in 0.1 M phosphate buffer. HRP reaction product was visualized by adding 0.015% cobalt chloride and 0.015% hydrogen peroxide to the above solution for an additional 10–20 minutes. Maculae were then dehydrated in an ethanol series, cleared briefly in xylene, and mounted in Eukit (Calibrated Instr.) on clean glass slides.

Morphological analyses

Material was examined with Nomarski optics with $\times 63$ and $\times 100$ oil-immersion objectives (Zeiss). We first compared Toluidine Blue-stained cross sections of the anterior vestibular nerve branchlet immediately proximal to the utricular macula in normal and nerve-sectioned animals. Myelinated axon profiles were divided into one of two classes: 1) normal axons; and 2) degenerated axons, defined as those axons whose volume of cytoplasmic material was <25% of their interior volume. Axons in the first group were assumed to be the axons of vestibular afferents; axons in the second group were assumed to be the remnants of vestibular efferents (Robbins et al., '67; Dunn, '78; Gacek, '84).

The possibility for direct counts or measurements of axon diameter for fibers supplying the utricular macula was precluded since no single plane contained all of these fibers in cross section. We therefore determined, in two normal and two nerve-sectioned animals, the number and axon diameter of the above two fiber classes in the anterior vestibular nerve and the horizontal and anterior vertical ampullary nerve branchlets by using a computerized image analysis program (Bioquant, System IV). For each fiber class, we estimated figures for the utricular macula by subtracting the number of ampullary nerve fibers from the number of fibers in the anterior vestibular nerve. Individual axon diameters were multiplied by a normalization factor (see below), averaged to obtain mean values, and sorted into 0.05 μm bins.

Using the Bioquant image analysis system, we drew the macular outline and the borders of the striolar region for each wholemount macula. The entrance of each labeled axon into the sensory epithelium was indicated on a standard surface map of the utricular macula determined by overlaying the striolar regions of the utricular maculae in four nerve-sectioned animals. The size of each parent axon was obtained by averaging its axolemmal diameter, measured every 10 μm , starting from the basement membrane and continuing proximally for 100 μm or as far as the axon could be traced. For afferents that bifurcated below the sensory epithelium, the entrance of the thickest branch was used to define the unit's epithelial location and measurements of axolemmal diameter began proximal to the first

branch point. The terminal field of an afferent was defined by the total extent of its peripheral arborization in the horizontal plane. The surface area of the sensory macula was used to normalize for differential shrinkage between specimens. For each macula, axon diameters and terminal-field dimensions were multiplied by a normalization factor, $(A_m/A_i)^{1/2}$, where A_i is the area of a particular epithelium and A_m is the mean area of $0.554 \pm 0.003 \text{ mm}^2$ (mean \pm SEM) for a sample that included four maculae from normal animals and four maculae from nerve-sectioned animals.

To examine terminal morphology and the intraepithelial distribution of synaptic endings more closely, wholemount utricular maculae were embedded in glycol methacrylate (Polysciences, JB-4) and serially sectioned at 10–20 μm in a coronal plane. The plane of section is shown in Figure 1a. The size of the parent axons and the terminal fields of labeled afferents were confirmed in sectioned material. The complete peripheral arborizations of well-isolated afferents were then reconstructed in their entirety from serial sections and drawn with a camera lucida (total magnification $\times 1,800$). With Nomarski optics, the number and type of hair cells contacted by well-labeled afferents were determined by examining the relationship between their terminal endings and individual hair cells.

Utriclar hair cells, following the original scheme of Lewis and Li ('75), were classified into four types according to the size of their hair bundles, the absence or presence of a bulbed kinocilium, and the relative lengths of their kinocilium and tallest stereocilia (Fig. 1b,c). Type B cells, the predominant hair cell type in the utricular macula, had small hair bundles and short stereocilia, with kinocilia 2–6 times as long as their tallest stereocilia. These cells were found throughout the medial and lateral extrastriolar and, more rarely, in the striolar region. Three other hair cell types, with stereocilia markedly longer than those of Type B cells, were confined to the striolar region. Type C cells, concentrated in the outer striolar rows, resembled enlarged Type B cells, having kinocilia and stereocilia approximately twice as long as the latter hair cell type. Moving inward, these cells were gradually replaced by two hair cell types with kinocilia approximately equal in length to their tallest stereocilia, significantly shorter than the kinocilia of Type B and Type C cells. Type F cells had visibly larger hair bundles than other utricular hair cells. Type E cells, restricted to the innermost striolar rows, had somewhat smaller hair bundles and, unlike Type F cells, possessed prominent kinociliary bulbs.

Unless otherwise stated, statistical comparisons of morphometric data were based on a one-way analysis of variance (ANOVA). When appropriate, post hoc pairwise multiple comparisons were performed using the Tukey multiple comparison test adjusting, when necessary, for unequal group sizes (Miller, '77).

RESULTS

Organization of the vestibular nerve

A Toluidine Blue-stained cross section of the anterior vestibular nerve branchlet immediately medial to the utricular macula in a normal animal is illustrated in Figure 2a. The stained nuclei of Schwann cells (black profiles) and the myelin sheath and interior cytoplasm of myelinated fibers are clearly seen. Myelinated fibers in the nerve branchlet had a wide variety of axolemmal diameters, ranging from

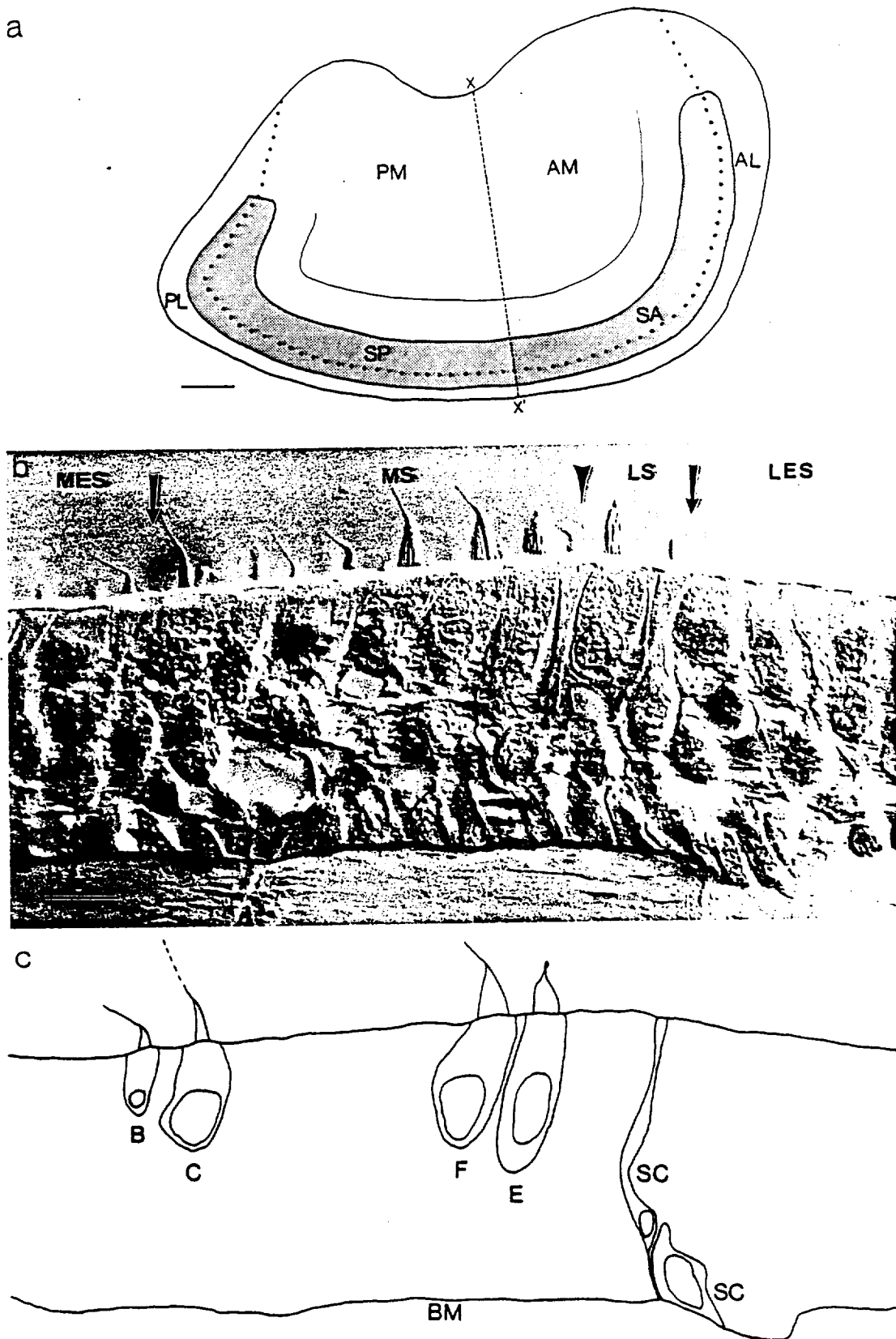


Fig. 1. a: Standard surface map of the utricular macula based on 8 maculae. The striola (shown shaded), a thin ribbon-shaped area, and its anterior and posterior extensions (dotted lines) separate the extrastriola into a larger medial and a smaller lateral zone. Thin solid line indicates the border of the juxtastriolar region. A dashed line (x---x') divides the macula into anterior and posterior halves and indicates the plane of section seen below and in Figure 3. AL, anterolateral extrastriola; AM, anteromedial extrastriola; PL, posterolateral extrastriola; PM, posteromedial extrastriola; SA, anterior striola; SP, posterior striola.

b: Photomicrograph of Toluidine Blue-stained cross section of the utricular striola and surrounding extrastriolar regions. Arrows denote the medial (left) and lateral (right) borders of the striolar region; arrowhead indicates the reversal of hair cell polarization. MES, medial extrastriola; MS, medial striola; LS, lateral striola; LES, lateral extrastriola. c: Schematic sketch of section in b, indicating the intraepithelial location and cellular morphology of representative hair cells and supporting cells in the utricular macula. B, Type B; C, Type C; E, Type E; F, Type F; SC, supporting cell; BM, basement membrane. Bars = 100 μ m in A, 25 μ m in B.

0.2 to $> 5 \mu\text{m}$. The great majority of fibers innervating the utricular macula had axolemmal diameters lying between 0.3 and $0.5 \mu\text{m}$ (Fig. 2c). Two degenerated myelinated fibers (not shown in Fig. 2) were recognizable by their lack of cytoplasmic material. A substantial number of unmyelinated fibers, primarily in the central portion of the nerve branchlet, were also observed. The axolemmal diameters of these fibers were invariably smaller than those of myelinated axons and could not be reliably measured in the light microscope. Large numbers of these fibers were also seen outside the lateral macular margins in wholemount utriculus preparations. These fibers did not enter the sensory epithelium and were observed in close proximity to blood vessels. They were therefore assumed to be the axons of sympathetic fibers (Lindeman, '69; Dunn, '78).

The anterior vestibular nerve branchlets of nerve-sectioned animals, as in normal animals, were composed of myelinated fibers with widely varying axolemmal diameters (Fig. 2b). The interior cytoplasm of many afferents in nerve-sectioned animals were dark in appearance, indicating that they were labeled with horseradish peroxidase (pointers, Fig. 2b). The axolemmal diameters of myelinated fibers were similar in normal (Fig. 2c) and nerve-sectioned (Fig. 2d) animals. In two other respects, the nerve branchlets of nerve-sectioned animals differed from those of normal animals. First, we did not observe unmyelinated fibers in either the vestibular nerve or the utricular macula of nerve-sectioned animals. Second, degenerated myelinated fibers were seen in large numbers in nerve-sectioned animals (arrows, Fig. 2b). These fibers, whose axolemmal diameters were distributed similarly to those of normal fibers (Fig. 2d), were assumed to be the degenerated remnants of vestibular efferent fibers (Robbins et al., '67; Dunn, '78; Gacek, '84).

The number and axolemmal diameter of myelinated fibers innervating the utricular macula, estimated by subtracting the number of ampullary nerve fibers from the number of fibers in the anterior vestibular nerve, are summarized in Table 1. In two normal animals, this calculation resulted in an estimate of $2,315 \pm 267$ myelinated fibers innervating the utricular macula. Similar calculations in two nerve-sectioned animals resulted in a total of $2,024 \pm 269$ myelinated fibers, of which $1,775 \pm 132$ were normal fibers and 249 ± 137 were degenerated fibers. Assuming that these degenerated myelinated fibers represent the remnants of vestibular efferent fibers, our analysis suggests that efferent neurons represent 10–15% of the normal utricular innervation.

Organization of the utricular macula

The utricular macula of the bullfrog is a kidney-shaped epithelium whose long and short axes, measured in eight dissected specimens, had mean values of 1.15 and 0.58 mm, respectively. The posterior part of the macula, as in mammals (Lindeman, '69; Wersall and Bagger-Sjoberg, '74; Fernandez et al., '90), lies in a nearly horizontal plane. Its anterior part is curved upwards. The utricular macula in the bullfrog is divided into a large medial zone and a smaller lateral zone by the striola, a 75–100 μm ribbon-shaped zone that runs for almost the entire length of the sensory epithelium near its lateral border (Fig. 1).

The plane of section is shown in Figure 1a and illustrated in Figure 1b. The cellular organization of the utricular macula is a pseudostratified columnar epithelium of sensory hair cells interspersed with nonsensory supporting

cells (Fig. 1b,c). Hair cells occupy the upper two-thirds of the sensory epithelium, while supporting cells span its entire distance. The nuclei of hair cells are positioned apical to those of supporting cells. The basal surfaces of supporting cells rest on or near a basement membrane that separates the sensory epithelium from its afferent and efferent innervation.

The striola differed in several respects from flanking extrastriolar regions. Hair cells in the striola tended to be larger in size and more widely spaced than hair cells located in the medial or lateral extrastriola (Fig. 1b). Hair cells in the utricular macula also differed markedly in their hair bundle morphology (Fig. 1b,c). In sectioned material, the apical surface of the striola was higher in elevation than the medial or lateral extrastriola, giving the striola a hill-like appearance (Figs. 1b, 3a,b). In either extrastriolar region, the orientation of hair cells was directed toward the striolar region. Hair cells within the striola were oriented in the same direction as adjacent extrastriolar cells. This orientation reversed within the striola, the line of reversal occurring lateral to the striolar midline. On average, the striola consisted of five to seven medial rows and two to three lateral rows of hair cells.

The boundaries between the striola and the medial and lateral extrastriola were easily recognized in both wholemount and sectioned material. Relative areas of these macular regions were determined in the four nerve-sectioned maculae that produced useful data. The striola made up $20.4 \pm 1.8\%$ of the sensory macula; the medial extrastriola, $64.7 \pm 2.5\%$; and the lateral extrastriola, $15.0 \pm 0.9\%$. Within the striola, the medial and lateral rows made up $16.3 \pm 2.2\%$ and $4.0 \pm 0.6\%$ of the macular area, respectively. To analyze regional variations in the utricular macula, a straight line was drawn across the endorgan to divide the striola and two extrastriolar regions into anterior and posterior halves (dashed line, Fig. 1). In the remainder of the paper, we shall refer to the anterior (SA) and posterior (SP) striola. The extrastriolar region is similarly divided into four quarters, designated as anterolateral (AL), anteromedial (AM), posterolateral (PL), and posteromedial (PM).

Peripheral innervation patterns

In nerve-sectioned animals, cell bodies and proximal axons in the vestibular nerve were, at best, only lightly labeled. The terminal axons and dendritic arbors of labeled afferents within the utricular macula, on the other hand, were darkly stained (Figs. 3a,b, 6a–f). The conclusions that follow are based on 333 labeled afferents obtained from the utricular maculae of four nerve-sectioned animals. Each labeled afferent was characterized by the diameter of its parent axon and the macular location at which it entered the sensory epithelium. The terminal fields of 144 afferents were sufficiently well isolated from other labeled fibers that they could be reconstructed in their entirety. For 56 of these afferents, we determined the number of synaptic endings and the number and type of hair cells innervated by the afferent fiber. We also qualitatively examined the terminal arbors of several dozen labeled afferents in four additional animals in which the vestibular nerve was not sectioned. This qualitative examination confirmed that the axon diameters, terminal fields, and synaptic morphology of labeled afferents were not obviously different in normal and nerve-sectioned animals, suggesting that cutting the cen-

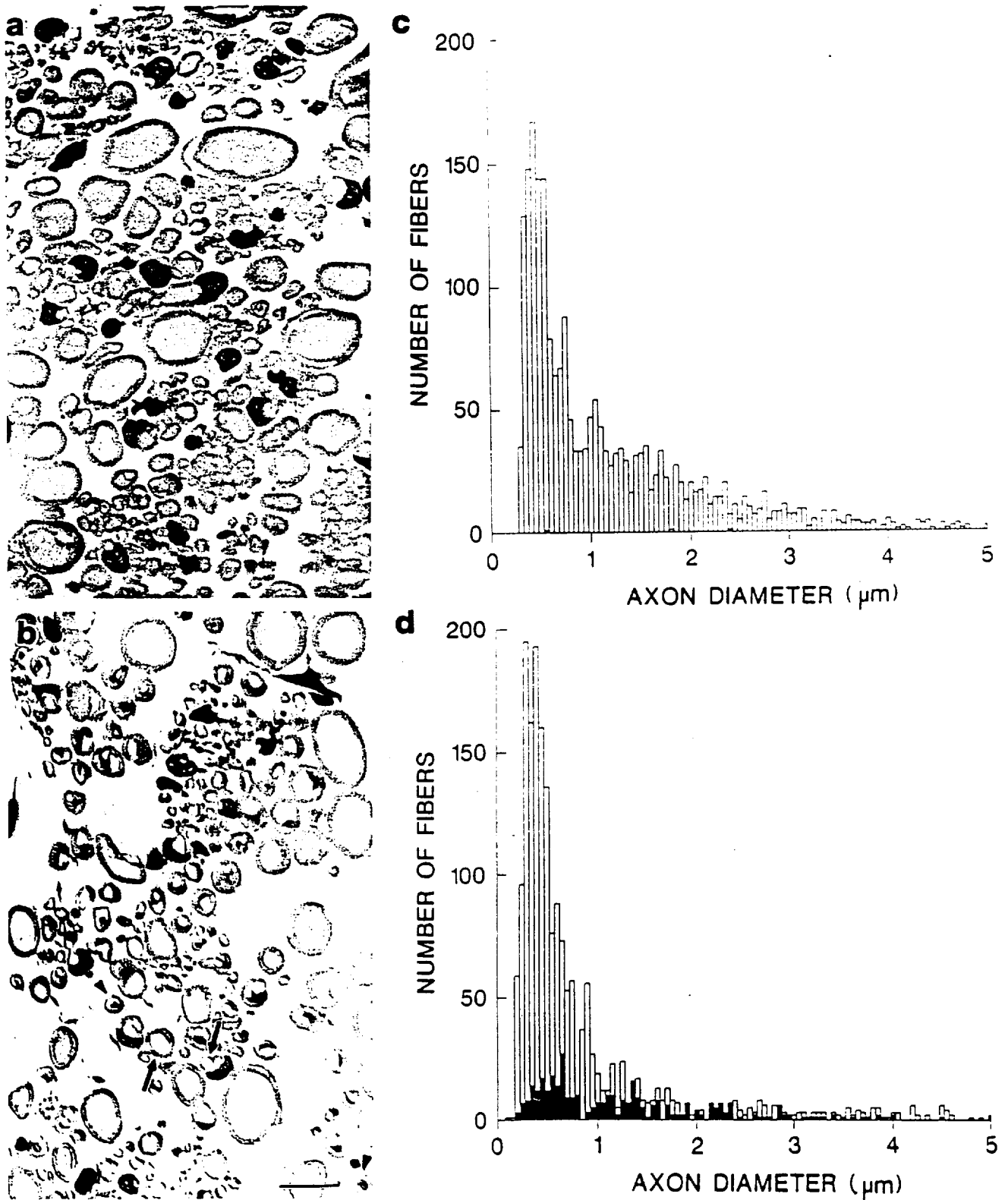


Fig. 2. Photomicrographs of Toluidine Blue-stained cross sections of the anterior vestibular nerve immediately medial to the utricular macula in a typical normal animal (a) and an animal sacrificed 14 days after sectioning of the eighth nerve medial to Scarpa's ganglion (b). Dark profiles in a and b represent the nuclei of Toluidine Blue-stained

Schwann cells. In b, arrows indicate representative degenerated axons lacking cytoplasmic material. Pointers indicate representative axons labeled with horseradish peroxidase. c,d: Histograms of axolemmal diameter of normal (open) and degenerated (solid) myelinated fibers in a normal (a) and a nerve-sectioned (b) animal. Bar = 10 μm.

TABLE 1. Counts of Myelinated, Degenerated, and Unmyelinated Fibers¹

Nerve branchlet	Normal animals				Nerve-sectioned animals			
	No.	Fiber type		No.	Fiber type			
		Normal	Degenerated		Normal	Degenerated		
AN	8,027	4012.0 ± 28.3	1.5 ± 0.7	7,598	3297.5 ± 87.0	501.5 ± 212.3		
HC	1,767	803.5 ± 145.0	0	1,768	735.0 ± 132.9	149.0 ± 76.4		
AVC	1,627	813.5 ± 94.0	0	1,782	787.5 ± 88.4	103.5 ± 0.7		
UN	4,633	2315.0 ± 267.3	1.5 ± 0.7	4,048	1775.0 ± 131.5	249.0 ± 137.2		

¹Values are means ± SD; No., total number of axon profiles from two normal animals and two nerve-sectioned animals. Axon diameters are corrected for differential shrinkage (see Materials and Methods). Axon profiles are obtained from the anterior nerve (AN), horizontal semicircular canal (HC), and anterior vertical semicircular canal (AVC). Values for the utricular branchlet (UN) are estimated from the formula UN = AN - HC - AVC.

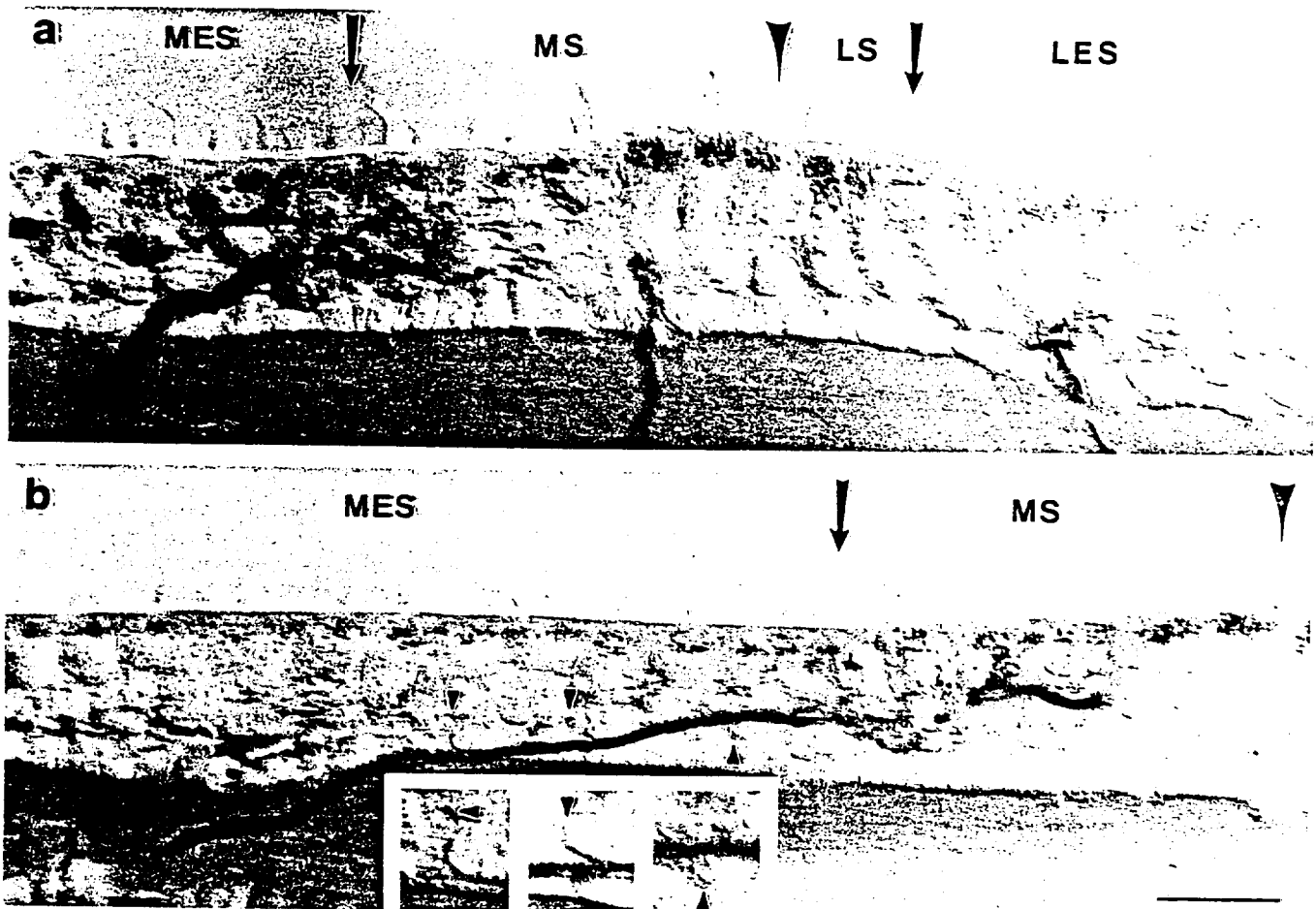


Fig. 3. Photomicrographs of the cross-sectioned striola (a) and medial extrastriola (b) of the utricular macula. The small dark particles near the apical surfaces of hair cells are peroxidase-containing organelles (probably mitochondria) labeled by the histological procedure used to visualize horseradish peroxidase. Three horseradish peroxidase-labeled afferents, located in the medial striola (left), central striola (middle), and lateral extrastriola (right) are seen in a. In b, one branch of a bifurcating juxtastriolar afferent is seen. Small collateral branches,

indicated by small arrowheads in the main figure and in the insets below, terminate in bouton-like endings. A second horseradish peroxidase-labeled afferent (right), located in the medial striola, is also seen. In a, arrows denote the medial (left) and lateral (right) striolar borders; in b, a single arrow indicates the medial striolar border. Large arrowhead indicates the reversal of hair cell polarization. MES, medial extrastriola; MS, medial striola; LS, lateral striola; LES, lateral extrastriola. Bars = 250 μm in a, 25 μm in b.

tral processes of vestibular afferents did not alter the normal morphology of their peripheral processes.

The utricular nerve branchlet separates from the anterior branch of the vestibular nerve. As in mammals (Fernandez et al., '90), some fibers run immediately under the connective tissue stroma and pass through it to reach the curved anterior portion of the macula. Afferent fibers supplying more posterior regions first entered a fiber layer

located at the bottom of the stroma. The latter fibers, upon reaching their destinations, bend sharply upwards and take a direct course through the stroma and into the sensory epithelium. Fibers supplying the lateral macula often run past the edge of the macula before returning medially and bending sharply upwards through the sensory epithelium.

A small (43/333 = 12.9%) proportion of utricular afferents bifurcated below the sensory epithelium, typically

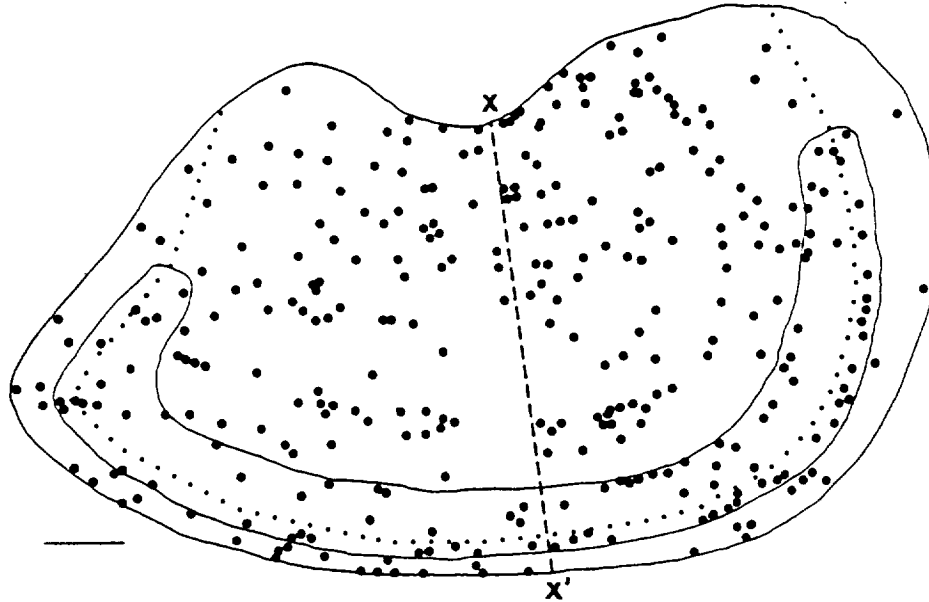


Fig. 4. Distribution of 92 striolar and 241 extrastriolar afferents indicated on a standard surface map of the utricular macula. The striola, a thin ribbon-shaped area, and its anterior and posterior

extensions (dotted lines) separate the extrastriola into a larger medial and a smaller lateral zone. A dashed line (x---x') divides the macula into anterior and posterior halves. Bar = 100 μ m.

within 10–30 μ m of the basement membrane. Bifurcations were found in axons destined for both the striolar (9/92 = 9.8%) and extrastriolar (34/241 = 14.1%) regions. More than three-quarters of these fibers had single branch points (Figs. 7b, 8a). In a few units, one or both primary branches divided a second time (Fig. 7a). The branches of bifurcating afferents were usually similar in diameter and innervated contiguous or closely adjacent groups of hair cells in the same part of the sensory epithelium.

The branches of bifurcating fibers as well as the parent axons of nonbifurcating fibers typically began dividing into their terminal arborizations within 10–20 μ m after crossing the basement membrane. Some axons in the medial extrastriola were exceptional in this regard. For these fibers, the axon ran unbranched in the lower part of the epithelium without giving rise to synaptic endings (right branch, Fig. 8a) or giving rise to only a small number of thin collateral branches (insets, Fig. 3b; left branch, Fig. 8a,b–d) for up to 50 μ m before dividing into their terminal arborizations. The arborizations of utricular afferents were compact, seldom extending more than 50–75 μ m in any direction from the parent axon.

Utriclar afferents were classified as striolar or extrastriolar according to the epithelial entrance of their parent axons and the macular location of their terminal fields. The parent axons of two striolar afferents, one innervating the outer rows (left) and one supplying the inner rows (middle) of the medial striola, are shown in Figure 3a. A third afferent, innervating the lateral extrastriola, is shown to the far right. The epithelial entrances of all 333 labeled afferents are indicated with dots on a standard surface map of the utricular macula in Figure 4. In this figure, the striola, a thin ribbon-shaped area, and its anterior and posterior extensions (dotted lines) separate the extrastriolar region into a larger medial and a smaller lateral zone. A dashed line (x---x') divides the macula into anterior and posterior halves.

The percentages of afferents in the anterior and posterior striola and in the four quarters of the extrastriola are shown in Table 2. The proportions are close to those expected on an areal basis. Thus, the division of afferents between the striola (27.6%) and the extrastriola (72.4%) is similar to the 20.4–79.6% split expected from the relative areas of these two zones. The major discrepancy is the presence of a larger number of afferents in the anterior striola than would be expected on an areal basis (16.2% vs. 10.2%, respectively). With two exceptions, the proportion of afferents in the extrastriola also parallels the relative areas of the four extrastriolar zones: 1) there were slightly more afferents in the anteromedial region than in the posteromedial region; and 2) there were fewer afferents in the anterolateral region than expected on an areal basis.

Table 2 also compares the morphological characteristics of striolar and extrastriolar afferents innervating different regions of the utricular macula. The legend to Table 2 summarizes the results of statistical tests. When striolar and extrastriolar afferents are compared, the former have thicker parent axons, fewer subepithelial bifurcations, and larger terminal fields than the latter. There were also regional differences among both striolar and extrastriolar afferents. Afferents in the posterior striola had more frequent subepithelial bifurcations and larger terminal fields than afferents in the anterior striola. Among extrastriolar afferents, afferents in the lateral zone had larger parent axons and larger terminal fields than afferents in the medial zone. Afferents in the anterolateral extrastriola also had more frequent subepithelial bifurcations than afferents in other extrastriolar regions. Other regional differences among striolar and extrastriolar afferents were small and statistically insignificant.

Afferents in a juxtastricular zone, immediately adjacent to the medial striola, had innervation patterns that were transitional between those in the striola and more peripheral parts of the medial extrastriola. Afferents supplying

TABLE 2. Regional Characteristics of Labeled Afferents¹

Fiber type	All fibers				Reconstructed fibers				
	No.	Percent (%)	Axon (μm)	Bifurcations (%)	No.	Long axis (μm)	Short axis (μm)	Terminal area (μm ²) (C _T)	
Striola	92	27.6	2.17 ± 0.92	9.8	35	64.2 ± 17.4	38.2 ± 9.7	1,383 ± 550	0.25 ± 0.10
SA	54	16.2	2.18 ± 0.94	0	21	61.5 ± 18.3	35.6 ± 7.5	1,124 ± 304	0.20 ± 0.06
SP	38	11.4	2.16 ± 0.88	23.7	14	68.9 ± 14.0	42.4 ± 10.9	1,771 ± 588	0.32 ± 0.11
Extrastriola	241	72.4	1.06 ± 0.52	14.1	107	46.8 ± 23.0	26.2 ± 12.3	746 ± 594	0.14 ± 0.11
AM	105	31.5	0.98 ± 0.43	11.4	54	42.3 ± 19.2	24.6 ± 12.7	634 ± 563	0.11 ± 0.10
PM	93	27.9	0.96 ± 0.46	15.0	43	45.5 ± 18.9	26.9 ± 12.1	747 ± 566	0.14 ± 0.10
AL	14	4.2	1.32 ± 0.57	28.6	2	62.8 ± 9.2	42.8 ± 5.2	1,544 ± 291	0.28 ± 0.05
PL	29	8.7	1.52 ± 0.68	13.8	8	80.2 ± 38.8	28.6 ± 8.4	1,346 ± 532	0.24 ± 0.10

¹Values are means ± SD; No., number of afferents. Percent of total is percentage of all labeled afferents. Axon diameters are corrected for differential shrinkage (see Materials and Methods). Bifurcations (%) is the percentage of axons in each category that branched below the basement membrane. Terminal-field areas are expressed in μm² and as a percentage of macular surface area. Striolar afferents supply the anterior (SA) or posterior (SP) striola. Extrastriolar afferents supply the anteromedial (AM), anterolateral (AL), posteromedial (PM), or posterolateral (PL) macula. The following differences were statistically significant. Axon diameter: SA + SP vs. AM + PM, SA vs. AL + PL, P < 0.0001 in all cases; SP vs. AL, P < 0.0005; SP vs. PL, PL vs. AM + PM, P < 0.001 in all cases. Long axis: PL vs. AM + PM, P < 0.0001 in all cases; SP vs. AM, P < 0.0005; SA vs. AM, SP vs. PM, P < 0.005; SA vs. PM, P < 0.05. Short axis: SP vs. AM, P < 0.0001; SP vs. PM, P < 0.0005; SA vs. AM, P < 0.005; SA vs. PM, P < 0.05. Terminal area: SP vs. AM + PM, P < 0.0001 in all cases; SA vs. AM, P < 0.005; SP vs. SA, PL vs. AM, P, 0.01; PL vs. PM, P < 0.05.

TABLE 3. Zonal Characteristics of Labeled Afferents¹

Fiber type	All fibers				Reconstructed fibers				
	No.	Percent (%)	Axon (μm)	Bifurcations (%)	No.	Long axis (μm)	Short axis (μm)	Terminal area (μm ²) (C _T)	
Striola	92	27.6	2.17 ± 0.92	9.8	35	64.2 ± 17.4	38.2 ± 9.7	1,383 ± 550	0.25 ± 0.10
MS	51	15.3	2.15 ± 0.93	5.9	26	63.8 ± 19.9	39.4 ± 10.0	1,423 ± 605	0.26 ± 0.11
LS	41	12.3	2.20 ± 0.93	14.6	9	65.9 ± 9.5	34.8 ± 8.5	1,267 ± 349	0.23 ± 0.06
Juxtastriola	65	19.5	1.35 ± 0.51	7.7	17	67.2 ± 13.1	42.6 ± 12.1	1,505 ± 620	0.27 ± 0.11
Extrastriola	17	52.8	0.95 ± 0.48	16.5	92	42.3 ± 23.3	23.5 ± 10.1	609 ± 476	0.11 ± 0.09
MES	13	39.9	0.79 ± 0.25	15.8	82	39.4 ± 16.9	22.5 ± 9.8	516 ± 383	0.09 ± 0.07
LES	43	12.9	1.45 ± 0.64	18.6	10	76.8 ± 35.1	31.4 ± 9.7	1,386 ± 486	0.25 ± 0.09

¹Values are means ± SD; No., number of afferents. Percent of total is percentage of all labeled afferents. Axon diameters are corrected for differential shrinkage (see Materials and Methods). Bifurcations (%) is the percentage of axons in each category that branched below the basement membrane. Terminal areas are expressed in μm² and as a percentage of macular surface area. Striolar afferents supply the medial (MS) or lateral (LS) striola; extrastriolar afferents supply the medial (MES) or lateral (LES) extrastriola. The following differences were statistically significant. Axon diameter: juxtastriola + LES vs. LS + MS + MES; LS + MS vs. MES, P < 0.0001 in all cases. Long axis: juxtastriola + MS vs. MES, P < 0.0001 in all cases; LS vs. MES, P < 0.0005. Short axis: juxtastriola + MS vs. MES, P < 0.0001 in all cases; LS vs. MES, P < 0.005; juxtastriola vs. LES, P < 0.05. Terminal area: LS + LES + juxtastriola vs. MES; MS vs. MES, P < 0.0001 in all cases.

this zone tended to enter the sensory epithelium approximately 100 μm from the medial striolar border (Fig. 4). They then traveled laterally perpendicular to the striola giving rise to few, if any, synaptic endings for relatively long distances (Figs. 3b, 8a-d). Relatively few afferents entered the sensory epithelium within 100-200 μm of the medial striolar border (Fig. 4).

The morphological characteristics of striolar, juxtastriolar, and extrastriolar afferents are compared in Table 3. The legend to Table 3 also summarizes the results of statistical tests. Juxtastriolar afferents resembled striolar afferents, tending to have thicker parent axons, fewer subepithelial bifurcations, and larger terminal fields than afferents supplying more peripheral regions of the medial extrastriola. There were also regional differences between afferents supplying the medial and lateral extrastriolar zones. Afferents in the lateral extrastriola, for example, had larger parent axons and larger terminal fields than afferents in the medial extrastriola. By contrast, afferents in the lateral striola had more frequent subepithelial bifurcations and smaller terminal fields than afferents in the medial striola. The morphological characteristics of juxtastriolar afferents closely resembled those of lateral extrastriolar afferents, suggesting that many of the properties of utricular afferents were a function of their relative proximity to the striolar region.

Striolar, juxtastriolar, and extrastriolar afferents also differed in the size and orientation of their terminal fields. This can best be appreciated from Figure 5a, which illustrates the terminal fields of 33 fully reconstructed afferents.

The long and short axes of terminal fields in the peripheral margins of the medial extrastriola were short and similar in size. These fields were small, representing on average 0.09% of the total macular area. The terminal fields of medial extrastriolar afferents closer to the striolar region were larger and more elongate. In the juxtastriola, for example, the long axes of terminal fields were significantly larger than their short axes, increasing their area on average to 0.27% of the total macular area. The long axes of these afferents were oriented parallel to the direction of hair cell morphological polarization, which was generally perpendicular to the striolar border (Fig. 5b). In contrast, terminal fields within the striola were largely oriented parallel to the striolar border, at right angles to the direction of hair cell morphological polarization. This was particularly true of afferents supplying the central and lateral striola and was also true of afferents supplying the lateral extrastriolar region. On average, terminal fields in the striola and lateral extrastriola represented 0.25% of the total macular area.

Labeled afferents in the utricular macula possessed several types of specialized endings. These endings, which were observed in close proximity to hair cells, may represent points of synaptic contact between hair cells and utricular nerve afferents. Afferents in both the striolar and extrastriolar regions commonly possessed dendritic swellings that resembled en passant (left arrow, Fig. 6a) and terminal (right arrow, Fig. 6a; arrows, Fig. 6b) bouton endings. The size and shape of these endings varied considerably. The smallest endings were round, with diameters of 0.5 μm

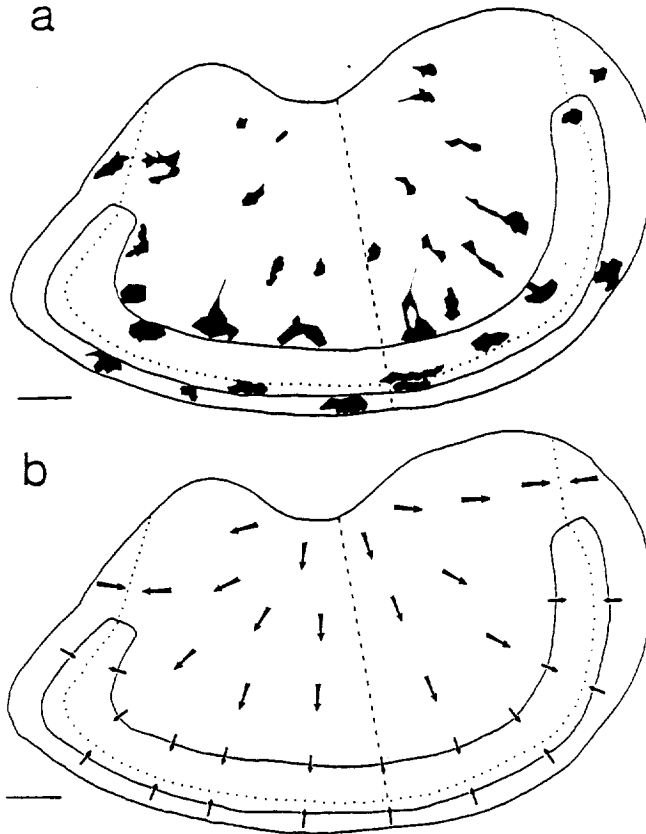


Fig. 5. a: Orientation of the terminal arbors of 7 striolar and 26 extrastriolar afferents indicated on a standard surface map of the utricular macula. b: Map of hair cell morphological polarization (adapted from Lewis and Li, '75). The striola, a thin ribbon-shaped area, and its anterior and posterior extensions (dotted lines) separate the extrastriola into a larger medial and a smaller lateral zone. A dashed line (x--x') divides the macula into anterior and posterior halves. Bars = 100 μm .

(arrows, Fig. 6a). Larger endings were ovoid in appearance, with widths and lengths up to 3 μm and 5 μm , respectively (arrows, Fig. 6b). Bouton-like endings were also infrequently observed in close proximity to the basement membrane, suggesting that they might be contacting the cell bodies of supporting cells (compare Figs. 1b and 6c). Bouton-like endings, whether en passant or terminal, were typically located on thin branches <1 μm in diameter. Other labeled afferents, especially in the striolar region, possessed other types of specialized endings. These included club endings, large (2–3 μm) rounded terminals (arrow, Fig. 6d), and fine (<0.5 μm) dendritic spines (arrow, Fig. 6e), both of which emerged directly from thick dendritic branches. Hair cells in both striolar and extrastriolar regions were also contacted by claw-like endings that partially enveloped their basolateral surfaces (arrow, Fig. 6f). The branching patterns and synaptic morphology of striolar, juxtastricular, and extrastriolar afferents differed and will be described separately.

Extrastriolar afferents

There were 80 fully reconstructed afferents in the medial extrastriola. These afferents had thin (<1 μm) parent axons, which, upon entering the sensory epithelium, rap-

idly bifurcated into numerous smaller branches. These branches arose as collaterals from the parent axon (Fig. 7a,b,d–f) or one of its thick branches (Fig. 7b,f). Arborizations were compact, seldom extending >50 μm in any direction from the parent axon. Medial extrastriolar afferents varied in complexity from those with <15 bouton-like endings (Fig. 7d,e) to those with >50 bouton-like endings (Fig. 7b). These endings varied tremendously in size (Fig. 6a,b).

Afferents supplying the peripheral margin of the medial extrastriola differed in several respects from afferents innervating more central portions of the medial extrastriola. Unlike more centrally located afferents, afferents on the medial margin had thinner parent axons, more subepithelial bifurcations, and larger numbers of apparent synaptic endings. Afferents supplying the peripheral margin also appeared to contact cells without hair bundles located outside the sensory macula and hair cells with immature hair bundles located on the macular border (Fig. 7a). Marginal afferents, unlike other medial extrastriolar afferents, often contacted hair cells with large claw-like endings (arrow, Fig. 6f; asterisk, Fig. 7a).

The terminal arbors of ten fully reconstructed afferents in the lateral extrastriola were significantly larger than those of medial extrastriolar afferents. These arbors arose from thicker parent axons than those of medial extrastriolar afferents and branched profusely, producing >150 bouton-like endings (Fig. 7c,g). The bouton-like endings of afferents in the lateral extrastriola, unlike those of medial extrastriolar afferents, were uniformly small (Fig. 6a). More specialized types of endings were not observed in lateral extrastriolar afferents.

The terminal fields of lateral extrastriolar afferents were usually confined to the extrastriolar zone (right, Fig. 3a). A typical example of such an afferent, which extends medially but stays within the lateral extrastriola, is shown in Figure 7g. Only three of ten lateral extrastriolar afferents were observed to cross the lateral striolar border. None of these afferents had similar numbers of endings or contacted similar numbers of hair cells in the striolar and extrastriolar zones. Rather, they typically extended a single branch or a small number of branches over the striolar border, contacting one to four striolar hair cells (Fig. 7c).

Juxtastricular afferents

There were 17 afferents assigned to the juxtastricular region. Juxtastricular afferents typically had medium-sized parent axons that entered the sensory epithelium medial to the striola and ran laterally in the lower part of the sensory epithelium for 25–50 μm , giving rise to few, if any, apparent synaptic endings (insets, Fig. 3b). In a few cases, the parent axons of juxtastricular afferents were bifurcated, both branches running laterally in the lower part of the sensory epithelium (Fig. 8a). They then intermittently gave rise to small collateral branches that contacted single hair cells or small clusters of hair cells (Fig. 8b–d) with bouton-like endings. At their most lateral extent, the parent axons of juxtastricular afferents bifurcated into numerous smaller branches that terminated in bouton-like endings (Fig. 8a–d). The terminal arbors of juxtastricular afferents were the largest in the utricular macula, often extending laterally >100 μm from their entrance into the sensory epithelium. These afferents typically had >150 bouton-like endings, which, with few exceptions (Fig. 8b), were uniformly small in size. Juxtastricular afferents that terminated near

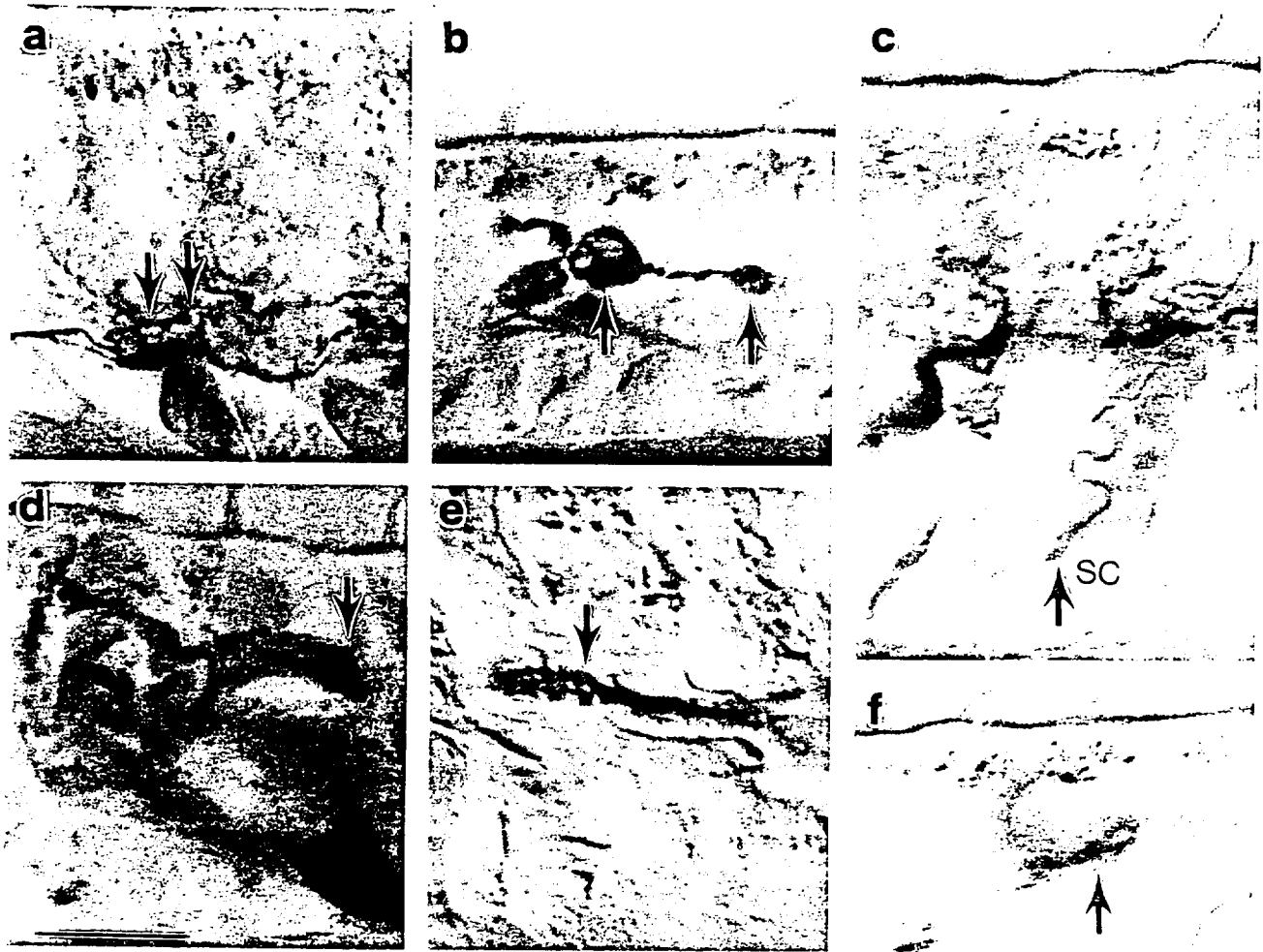


Fig. 6. a,b: Photomicrographs of small (a) and large (b) bouton-like endings in afferents labeled by horseradish peroxidase. Arrows indicate en passant (left) and terminal (right) bouton-like endings. c: Photomicrograph of a terminal bouton-like ending contacting a cell located immediately adjacent to the basement membrane, suggesting that

supporting cells (SC) as well as hair cells are innervated by vestibular afferents. d-f: Photomicrographs of other putative synaptic endings, including club endings (d), dendritic spines (e), and claw-like synaptic endings (f). In each case, arrows mark the location of the appropriate ending. Bar = 10 μ m.

the striola border (Fig. 8a,b,d) tended to have more extensive arbors than those located further away (Fig. 8c).

The terminal fields of juxtastricular afferents were usually confined to the medial extrastricola. Of 7/17 (41.2%) afferents that crossed the striolar border, none had similar numbers of synaptic endings or was contacted by similar numbers of hair cells in the two zones. Rather, they typically extended a single branch or a few branches over the striolar border, innervating from two to ten striolar hair cells (Fig. 8a,b). On average, this represented 10.3% of the total innervation of these afferents. A more extreme situation is illustrated in Figure 8d, in which a juxtastricular afferent that straddled the striolar region extended into the middle striolar rows, innervating 20 striolar hair cells.

Striolar afferents

Within the striolar region, 32 afferents, including 24 in the medial and 8 in the lateral striola, were fully reconstructed. Striolar afferents typically had thick (> 2 μ m) parent axons that did not bifurcate below the sensory epithelium (left, Fig. 3a). Many (16/32) of these afferents

entered the sensory epithelium within 10–20 μ m of the medial (Fig. 9a–d) or lateral (Fig. 9g) striolar border. Other striolar afferents (10/32), particularly in the medial striola, entered the sensory epithelium somewhat more centrally (Fig. 9e). In both cases, the parent axons of these afferents began bifurcating immediately into many large collateral branches, tapering in diameter and dividing into numerous smaller processes. A small (6/32) number of striolar afferents with thin parent axons innervated the innermost rows of the striolar region (middle, Fig. 3a). These axons, upon entering the sensory epithelium, ran anteriorly and/or posteriorly for long distances, intermittently giving rise to short, thin collateral branches that contacted small clusters of hair cells with bouton-like endings (Fig. 9f). These afferents, unlike other striolar afferents, had long, narrow terminal fields oriented parallel to the striolar border.

Striolar afferents varied in complexity from those with < 100 endings (Fig. 9c) to those with > 350 endings (Fig. 9e). As in other macular regions, striolar afferents largely contacted hair cells with bouton-like endings. In addition, striolar afferents possessed club endings, large (2–3 μ m)

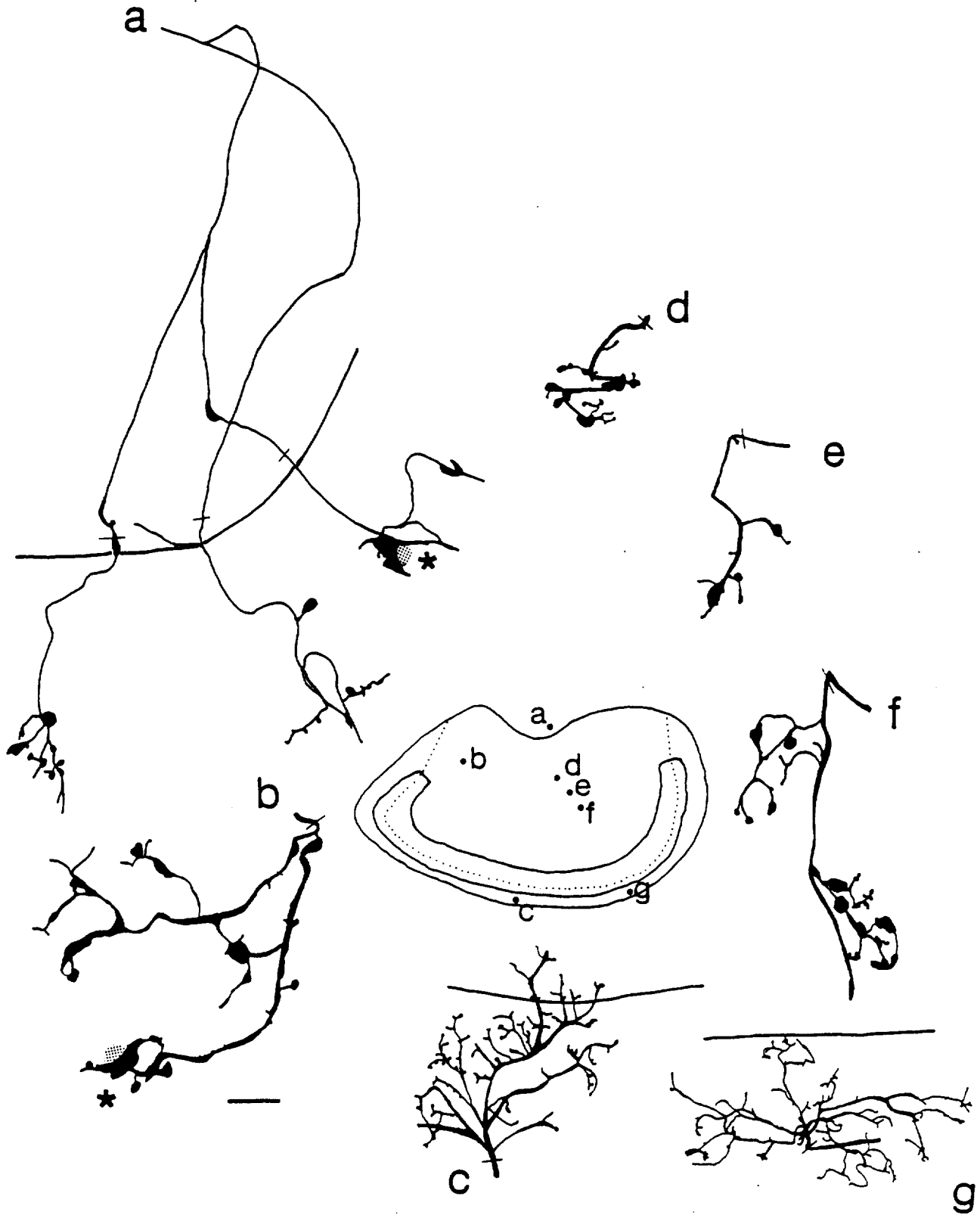


Fig. 7. Reconstructions of seven afferents located in the medial (a, b, d-f) and lateral (c, g) extrastria, with macular locations indicated on a standard surface map of the utricular macula (inset). In this and following figures, thin line segments in each drawing indicate the entrance point of the parent axon or its bifurcating branch(es) into the

sensory epithelium. In a and b, asterisks indicate claw-like endings that partially surround the basal surface of innervated hair cells. Solid line in a indicates the macular border; similar lines in f and g indicate the lateral striolar border. Bar = 10 μ m.

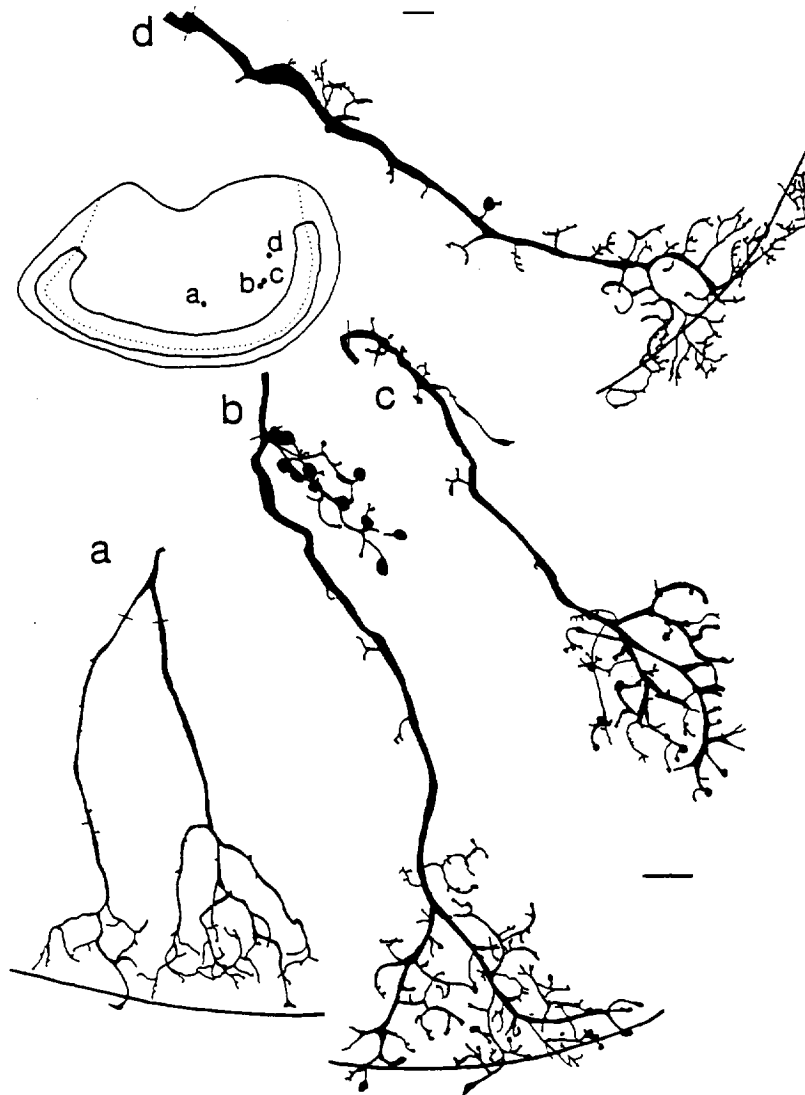


Fig. 8. Reconstructions of four afferents located in the juxtastriola (a-d), with macular locations indicated on a standard surface map of the utricular macula (inset). Thin line segments in each drawing indicate the entrance point of the parent axon or its bifurcating branch(es) into the sensory epithelium. Solid lines in selected drawings indicate the medial striolar border. Bar = 10 μ m.

rounded terminals that emanated directly from thick dendritic branches to contact single hair cells (Figs. 6e, 9g). Striolar afferents were also observed to contact hair cells with dendritic spines, small (<0.5 μ m) endings that, like club endings, emerged directly from thick dendritic processes (Figs. 6e, 9e).

The terminal fields of striolar afferents were relatively compact in two respects. First, they were generally confined to the medial or lateral side of the striolar region. This was true of 19/24 afferents in the medial striola and 3/8 afferents in the lateral striola. Striolar afferents with thick (>2 μ m) parent axons were also more likely to have terminal fields restricted to one side of the striolar region than striolar afferents with thin (<2 μ m) parent axons, regardless of whether they entered the sensory epithelium in the outer or inner striolar rows. The terminal fields of 20/26 striolar afferents with thick parent axons, for example, were confined to either the medial or lateral side of

the striolar region. An example of a medial striolar afferent, which extended laterally but stayed within the medial striola, is shown in Figure 9e. Of the six remaining striolar afferents with thick parent axons, none had similar numbers of endings or contacted similar numbers of hair cells in the medial and lateral striola. Rather, they typically extended a single branch over the striolar border, contacting one to four hair cells in the opposing striolar region. One such afferent, originating in the lateral striola, is shown in Figure 9g. A majority (4/6) of striolar afferents with thin parent axons, on the other hand, often encompassed both sides of the striolar region (Figs. 9f, 10d). It was not uncommon for these afferents to have similar numbers of synaptic endings or to contact similar numbers of hair cells on the two sides of the striolar zone. This organization has a functional implication. Since hair cells in the medial and lateral parts of the striola have opposed morphological polarizations (Lindeman, '69; Wersall and Bagger-Sjoberg,

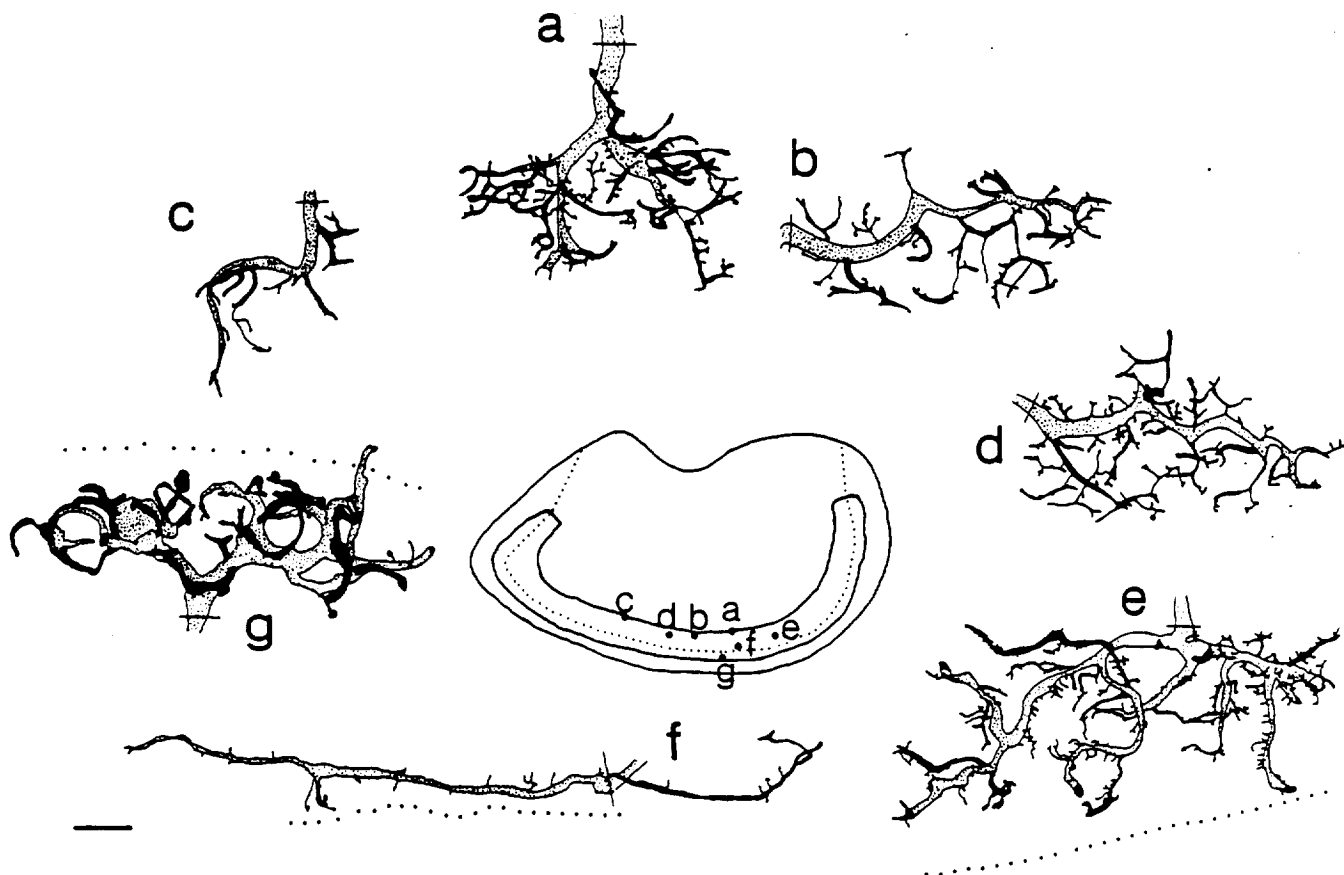


Fig. 9. Reconstructions of seven afferents located in the medial (a–e), central (f), and lateral (g) striola, with macular locations indicated on a standard surface map of the utricular macula (inset). The parent axons and larger collateral branches of afferents have been stippled and the thinner collateral branches blackened for graphical

clarity. Thin line segments in each drawing indicate the entrance point of the parent axon or its bifurcating branch(es) into the sensory epithelium. Dotted lines in selected drawings indicate the reversal of hair cell polarization. Bar = 10 μ m.

'74), restricting their terminal fields to one side of the striolar region ensures that an afferent will only contact hair cells with similar directional properties.

Second, the terminal fields of striolar afferents did not extend beyond the medial or lateral striolar border. This was true of 19/24 afferents in the medial striola and 7/8 afferents in the lateral striola. This arrangement suggests that the innervation of the striolar and the extrastriolar regions is relatively independent. This is confirmed by the observation that 43/56 reconstructed afferents (26/32 striolar, 10/17 juxtastriolar, and 7/10 lateral extrastriolar) were restricted to their zones of origin. No juxtastriolar or lateral extrastriolar afferent that crossed the striolar border had similar numbers of synaptic endings or contacted similar numbers of hair cells in the striolar and extrastriolar zones.

Synaptic endings and hair cell types

The numbers of synaptic endings and hair cells supplied by 139 reconstructed afferents are compared in Table 4. The legend to Table 4 also summarizes the results of statistical tests. Among 39 extrastriolar and juxtastriolar afferents on which synaptic counts were performed, it was observed that an individual hair cell could receive from one to four synaptic endings from a given afferent. This resulted in an average number of 1.9 ± 0.7 synaptic endings/

hair cell. This ratio rose sharply to 5.0 ± 1.6 for 17 afferents in the striolar region, where individual hair cells could receive as many as 15 synaptic endings. The average number of synaptic endings per hair cell in striolar afferents with thick parent axons was similar for all hair cell types. In striolar afferents with thin parent axons, Type B hair cells received significantly fewer synaptic contacts than other hair cell types.

Afferents in the medial extrastriola were the only afferents to innervate uniformly a single hair cell type, contacting 15.4 ± 10.6 Type B hair cells (Table 4). Juxtastriolar and lateral extrastriolar afferents, with the exception of ten afferents that supplied both the striolar and extrastriolar zones, also exclusively innervated Type B hair cells. The mean number of Type B hair cells contacted by medial extrastriolar afferents was significantly lower than that contacted by juxtastriolar or lateral extrastriolar afferents. Juxtastriolar and lateral extrastriolar afferents contacted similar numbers of Type B hair cells, lending further support to the suggestion that the morphological characteristics of utricular afferents were largely determined by their proximity to the striolar region.

The distribution of hair cell types innervated by a striolar afferent was a function of the macular entrance of its parent axon. The distribution of hair cell types contacted by

TABLE 4. Hair Cells, Synaptic Endings, and Afferent Nerve Fibers¹

Fiber type	No.	Number of hair cells					No.	Synaptic endings n _s	Endings hair cell n _s , n _T
		Type B n _B	Type C n _C	Type F n _F	Type E n _E	Total n _T			
Striola	32	11.9 ± 7.0	21.9 ± 11.9	3.0 ± 3.3	5.3 ± 6.3	42.1 ± 14.5	17	178.9 ± 72.0	5.02 ± 1.60
MS	24	13.1 ± 7.6	20.0 ± 10.6	2.7 ± 3.4	4.3 ± 6.4	40.1 ± 12.7	14	184.1 ± 78.7	5.02 ± 1.75
LS	8	8.1 ± 2.1	27.6 ± 14.5	3.9 ± 3.1	8.3 ± 5.1	47.9 ± 18.6	3	154.7 ± 11.6	4.98 ± 0.76
Juxtastriola	17	57.6 ± 22.1	3.1 ± 4.9	0.3 ± 0.8	0	61.4 ± 21.8	5	128.4 ± 37.9	1.82 ± 0.36
Extrastriola	90	21.1 ± 20.9	0.1 ± 0.4	0	0	21.2 ± 21.1	34	29.2 ± 31.9	2.09 ± 0.87
MES	80	15.4 ± 10.6	0	0	0	15.4 ± 10.6	32	23.0 ± 13.5	2.07 ± 0.86
LES	10	67.0 ± 26.7	0.6 ± 1.3	0	0	67.6 ± 26.6	2	138.5 ± 71.4	2.38 ± 1.32

¹Values are means ± SD; No., number of afferents. Table indicates number of synaptic endings (n_s) and the number of Type B (n_B), Type C (n_C), Type E (n_E), Type F (n_F), and total number (n_T) of hair cells innervated by afferents in each category. The following differences were statistically significant. Type B cells: LES vs. MES + MS + LS; juxtastriola vs. MES + MS + LS, P < 0.0001 in all cases. Type C cells: LS vs. MES; MS vs. juxtastriola + LES; LS vs. juxtastriola + LES, P < 0.0001 in all cases. Type F cells: LS vs. juxtastriola + MES - LES; MS vs. juxtastriola + MES + LES, P < 0.0001 in all cases. Type E cells: LS vs. juxtastriola + MES + LES; MS vs. juxtastriola + MES, P < 0.0001 in all cases. MS vs. LS + LES, P < 0.001. Total cells: LES vs. MS + MES; juxtastriola vs. MS + MES; MES vs. MS + LS, P < 0.0001 in all cases. LES vs. LS, P < 0.05. Synaptic endings: MS vs. MES, P < 0.0001. MES vs. juxtastriola + LS, P < 0.0005 in all cases. LES vs. MES, P < 0.005. Endings/hair cell: MS vs. MES, P < 0.001. MS vs. juxtastriola, P < 0.0005. LS vs. MES, P < 0.001. LS vs. juxtastriola, P < 0.005. MS vs. LES, P < 0.05.

four typical striolar afferents (Fig. 9a,b,e,f) is shown in Figure 10. Striolar afferents supplying the outer rows of the medial striola largely or exclusively contacted Type B and Type C hair cells. For any single afferent, the numbers of these hair cell types were inversely correlated, with some afferents innervating large numbers of Type C (Fig. 10a) and others large numbers of Type B hair cells (Fig. 10b). Afferents innervating the central or lateral striola innervated a complex mixture of all four hair cell types (Fig. 10c). Striolar afferents with thin parent axons innervated the central portion of the striolar region and contacted relatively large numbers of Type E hair cells, often of opposing morphological polarities (Fig. 10d).

The relative percentage of each hair cell type innervated by all 32 fully reconstructed striolar afferents is illustrated in Figure 11. The afferents are ordered by macular location, with afferents to the left and right of the figure supplying the medial and lateral striolar region, respectively. Several important points are evident from this figure. First, with the exception of afferents supplying the central striola, striolar afferents largely innervated Type B and Type C hair cells. This was especially true for the 16/32 afferents that supplied the outer rows of the medial and lateral striola, in which Type B and Type C hair cells made up 70 to 100% of the total innervation. Second, afferents supplying other regions of the medial and lateral striola innervated fewer Type B and larger numbers of Type E and Type F hair cells. Even in these afferents, however, Type C cells made up the majority of innervated hair cells. This was true for all but three afferents supplying the most central region of the striola. These three afferents innervated more Type E hair cells than any other hair cell type. Finally, the number of Type F hair cells contacted by a striolar afferent was small, seldom exceeding 10% of its total innervation.

DISCUSSION

Nature of labeled processes

The HRP techniques used here can potentially label sympathetic and efferent axons as well as afferent axons. We therefore sectioned the central processes of the former axons medial to their cell bodies to allow the peripheral processes of these fibers to degenerate before labeling the peripheral terminations of vestibular afferents with HRP. Two observations indicate that this procedure was successful. First, fine (< 0.5 μm) unmyelinated fibers were consistently seen in normal but not nerve-sectioned animals. These fibers, which innervate large numbers of capillaries

outside the boundaries of the sensory macula, are assumed to be sympathetic neurons (Lindeman, '69; Dunn, '76). Second, degenerated axon profiles, assumed to be the remnants of myelinated efferent neurons, were seen in nerve-sectioned but not normal animals. Somewhat surprisingly, the axon diameter of degenerated fibers was not significantly different from that of normal myelinated fibers. In previous studies, the fiber diameters of efferent neurons have been reported to be thinner than those of afferent neurons (Robbins et al., '67; Gacek, '84). The number of degenerated fibers in the anterior nerve was also somewhat higher than expected, being similar to the number of brainstem efferent neurons reported to innervate each vestibular labyrinth (Will, '82). This disparity probably reflects the collateralization of efferent neurons within the vestibular nerve.

Afferent classes

Vestibular afferents in the chinchilla and squirrel monkey have previously been classified into calyx, bouton, and dimorphic classes depending upon whether they terminate in calyx endings, bouton endings, or a mixture of both types of endings (Fernandez et al., '88, '90, '91). Vestibular afferents in lower vertebrates, unlike those of mammals, terminate only in noncalyceal endings and innervate only Type II hair cells (Honrubia et al., '81, '89; Baird and Lewis, '86; Boyle et al., '91; Myers and Lewis, '91). Like afferents in mammalian preparations, however, afferents in central and peripheral epithelial regions differ in the diameter of their parent axons, the size of their terminal fields, the number of their synaptic endings, and the number of hair cells that they innervate. In the utricle, these differences are associated with the striola, a circumscribed central region, and a broader peripheral or extrastriolar zone. Afferents in close proximity to the striola, including those in both the medial juxtastriola and the lateral extrastriola, are transitional in their properties.

The number of striolar afferents was significantly larger and the number of extrastriolar and juxtastricular afferents significantly smaller than that expected on an areal basis. Because the latter afferents are thin, they may be more difficult to label. To investigate the role of axon diameter, we sorted labeled afferents on the basis of size into 0.5 μm bins, starting at the thin end of the spectrum. For each bin, we determined the proportions of labeled afferents that were striolar (p_S), juxtastricular (p_J), medial (p_{MES}), and lateral extrastriolar (p_{LES}). The proportion of all afferents (p_T) whose size fell within the same bin was obtained from

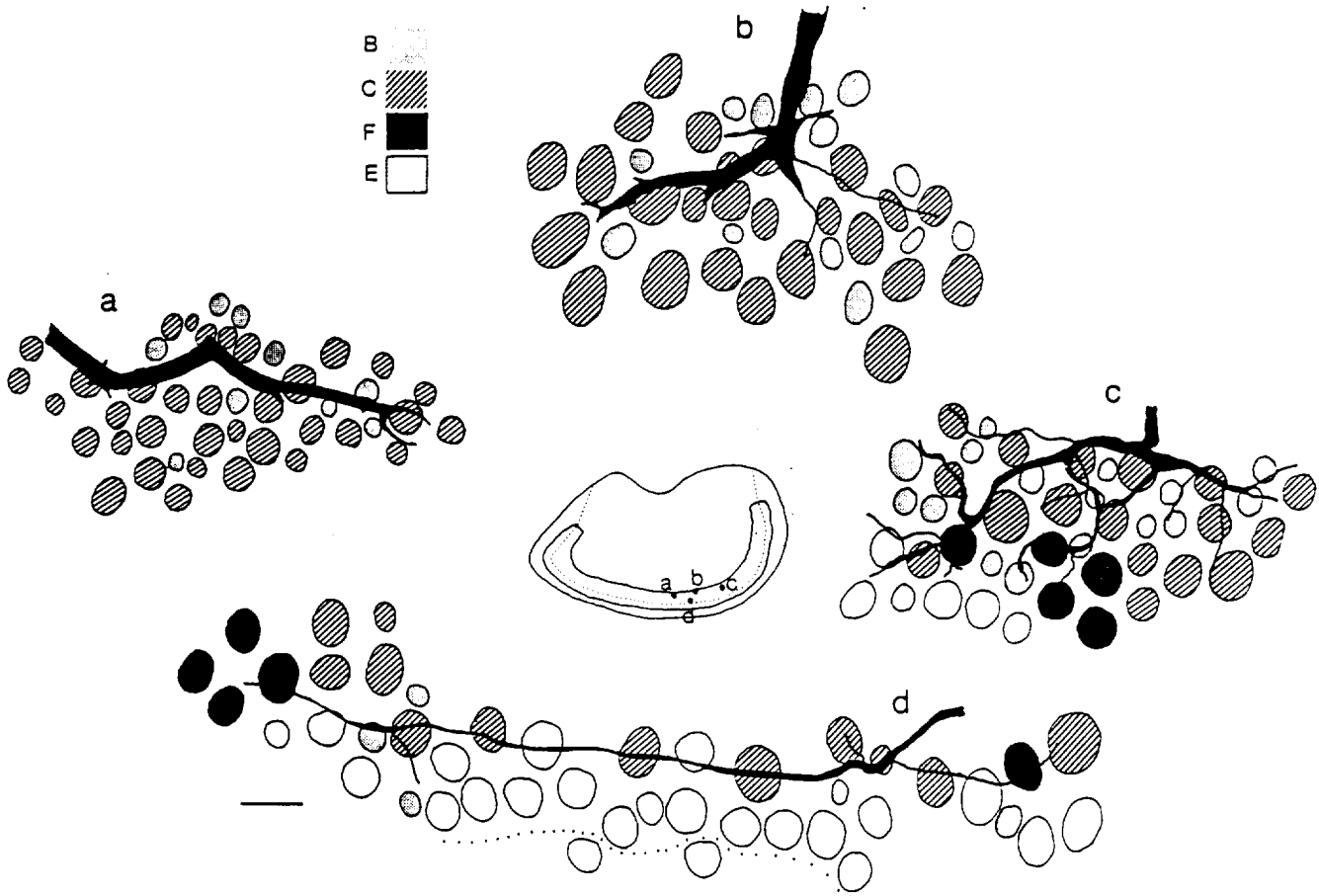


Fig. 10. a-d: Distribution of innervated hair cell types for four afferents illustrated in the previous figure, with macular locations indicated on a standard surface map of the utricular macula (inset). Dotted line in drawing d indicates the reversal of hair cell polarization. B, Type B; C, Type C; E, Type E; F, Type F. Bar = 10 μ m.

our histogram of axon diameter in normal material, correcting for the presence of efferent fibers. The individual proportions (p_s , p_j , p_{MES} , and p_{LES}) were then multiplied by the overall proportion p_T . By summing each of the three products over all bins, we obtained estimates of the proportions of the three afferent classes corrected for differences in their axon diameters. The corrected proportions were striolar units, 12.5%; juxtastricular units, 8.6%; medial extrastricular, 72.8%; and lateral extrastricular units, 5.8%. As expected, the correction results in an increase in the relative proportion of thin afferents. The result is a large increase in the percentage of medial extrastricular and smaller decreases in the percentage of striolar, juxtastricular, and lateral extrastricular afferents (see Table 3).

Regional organization of the utricular macula

As in the chinchilla (Fernandez et al., '90), the utricular macula of the bullfrog can be divided into three zones: the striola, the juxtastricular, and extrastricular. In both species, the striola is characterized by the presence of widely spaced hair cells. In addition, hair cells in the amphibian striola possess distinctive hair bundle morphology (Lewis and Li, '75) and have unique macular distributions (Baird, '92, '93a). There is an abrupt transition in morphology between the striola and juxtastricular, and few afferents innervate

both zones. In contrast, no morphological boundary exists between the juxtastricular and the extrastricular. Rather, the distinction between the latter two zones is based solely on differences in their afferent innervation patterns. It is probably for this reason that a separate juxtastricular zone in the utricle has only recently been recognized (Fernandez et al., '90).

The three macular zones in the utricle differ in the kinds of afferents they receive. When striolar and medial extrastricular afferents are compared, the former have thicker axons, larger terminal fields, more synaptic endings, and innervate larger numbers of hair cells. Afferent morphology in the juxtastricular is transitional between that of the other two zones and strongly resembles that seen in the lateral extrastricular, suggesting that the morphological characteristics of afferents is correlated with their relative proximity to the striolar region. Juxtastricular afferents are similar to striolar afferents in having few subepithelial bifurcations, large terminal fields oriented parallel to the striola, and contacting many hair cells. Unlike striolar afferents, they have thin parent axons, lack specialized synaptic endings, and possess fewer synaptic endings per hair cell. In the latter respects, juxtastricular afferents resemble afferents in the medial extrastricular. Juxtastricular afferents are also unique in that they enter the sensory epithelium and travel

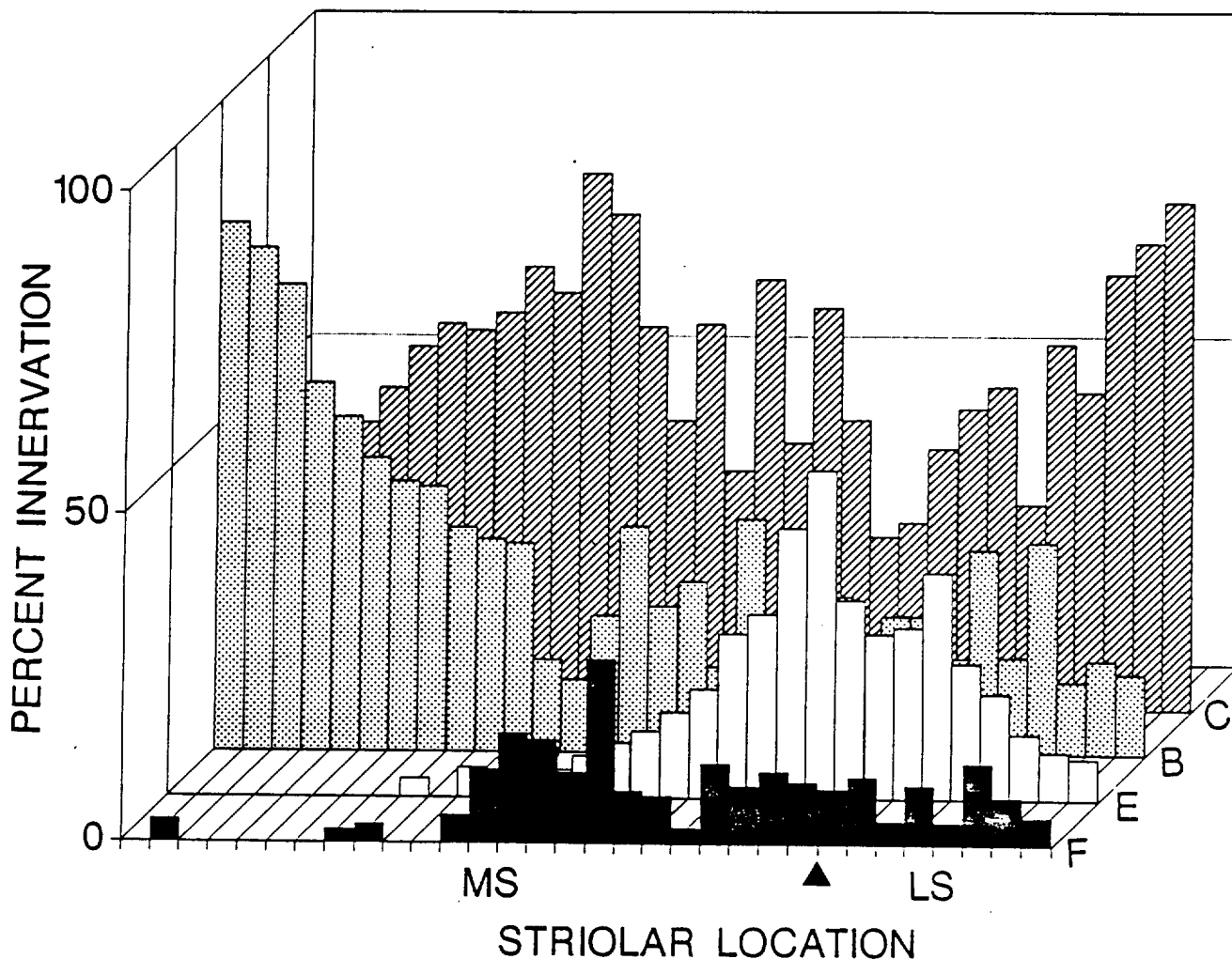


Fig. 11. Bar graph of relative percentage of each hair cell type innervated by 32 fully reconstructed striolar afferents. Afferents are ordered by macular location, with afferents to the left and right of the pointer supplying the medial and lateral striola, respectively. MS, medial striola; LS, lateral striola. B, Type B; C, Type C; E, Type E; F, Type F.

for relatively long distances without making synaptic contact with hair cells.

The striola and extrastriola can be divided into four topographic areas whose hair cells differ in the morphological polarization of their hair bundles (Lindeman, '67; Wersall and Bagger-Sjoberg, '74). By and large, regional differences among striolar afferents in the four quadrants of the macula are small. In particular, afferents in anteromedial and anterolateral regions did not differ in axon size and terminal morphology from afferents in other macular regions. This finding is in contrast to the results of Fernandez et al. ('90) in the chinchilla. The significance of this difference is unclear. As Goldberg et al. ('90b) point out, the discharge properties of afferents destined for the anterior curvature are not significantly different from afferents destined for more posterior locations.

While there are obvious parallels in the organization of the utricular macula in amphibians and mammals, there are also some significant differences. The most obvious of these is the fact that the striolar region in the bullfrog, unlike that of mammals (Lindeman, '69; Wersall and

Bagger-Sjoberg, '74; Fernandez et al., '90), is located asymmetrically. This region also occupies a significantly larger fraction of the sensory epithelium, both by area and percentage of innervation, than in the mammal (20% and 8%, respectively). As afferents excited by ipsilateral head tilts innervate the medial portions of the utricular macula whereas those excited by contralateral head tilts supply more lateral regions, this would suggest that most afferents in the bullfrog utriculus should be excited by ipsilateral, as compared with contralateral, head tilts. A similar predominance is seen in the cat (Loe et al., '73) and monkey (Fernandez et al., '72; Fernandez and Goldberg, '76a). In the chinchilla, however, afferents excited by ipsilateral and contralateral head tilts are observed with approximately equal frequency (Goldberg et al., '90b).

Several other differences between amphibians and mammals are also evident. Subepithelial bifurcations of utricular afferents are more common in the chinchilla, while regional differences in the innervation patterns of utricular afferents are more striking in the bullfrog, particularly in the juxta-striolar zone. In addition, there is more cross-

over between macular zones in the bullfrog than in the chinchilla. This is particularly true for juxtastricular and lateral striolar afferents. Hair cell density, while similar in the amphibian and mammalian striola, is significantly higher in the lateral extrastricular region of the bullfrog utriculus. This may partially compensate for the relatively small area of this region relative to the medial extrastricular.

Afferent branching patterns

The terminal fields of afferents in the utricular macula are extremely compact. Afferents destined for the medial extrastricular seldom bifurcate below the sensory epithelium and, if so, contact contiguous or closely adjacent groups of hair cells. Moreover, the terminal field areas of these afferents show little regional variation, and their most distal synaptic endings are seldom $> 25 \mu\text{m}$ from their parent axons. Terminal fields in the juxtastricular and striolar regions are significantly larger than those in medial extrastricular regions. The terminal fields of these afferents, however, are still relatively compact, never extending $> 75 \mu\text{m}$ from their parent axons. These circumscribed terminal fields suggest that utricular afferents have a single site of spike initiation (Goldberg et al., '84).

The size and orientation of terminal fields help to ensure that most utricular afferents contact hair cells with similar morphological polarization vectors. In the medial extrastricular and juxtastricular, for example, the long axes of the terminal fields of most utricular afferents are oriented toward the striola, ensuring that they contact hair cells with nearly identical morphological polarization vectors. Afferents destined for the striolar region have terminal fields oriented parallel with the striola. The relatively large size of these fields makes it likely that individual striolar afferents supply hair cells with slightly different hair bundle orientations. As has been shown previously (Fernandez et al., '72), however, such an arrangement should have only a small influence on an afferent's sensitivity or directional properties. Obviously, an afferent's sensitivity would be reduced if it were to innervate oppositely polarized hair cells. This can only occur within the striola, which contains the boundary separating hair cells of opposing polarities (Lindeman, '67; Wersall and Bagger-Sjoberg, '74). Because extrastricular and juxtastricular afferents do not cross the striola, there is no possibility that they can contact functionally opposed hair cells. Within the striola, the terminal fields of afferents are largely restricted in their innervation to the medial or the lateral side of the striolar zone, preventing this from occurring for these afferents as well.

The degree of complexity of striolar and extrastricular afferents in the bullfrog is exactly opposite to that observed in mammals, in which central fields are simple and peripheral fields are complex (Fernandez et al., '90). Our results are, however, in good agreement with the results of morphophysiological studies in the bullfrog (Myers and Lewis, '91) and toadfish (Boyle et al., '91) semicircular canals. The reason for this discrepancy is obscure. Interestingly, the regional organization of the vestibular endorgans in lower and higher vertebrates is similar, with afferents innervating the central zone having higher gains and more phasic response dynamics than those supplying more peripheral regions. This suggests that sensitivity and response dynamics of vestibular afferents are determined not by differences in terminal morphology but rather are determined by other presynaptic (Goldberg et al., '85, '90b; Baird et al., '88) and postsynaptic (Goldberg et al., '84) transduction mecha-

nisms that vary as one proceeds from central to peripheral zones. These properties may be determined, at least in the otolith organs, by differences in the comparative transduction mechanisms of hair cell types with unique macular distributions (see below).

Synaptic morphology

The great majority ($> 98\%$) of afferents in the mammalian utriculus possess calyceal endings (Goldberg et al., '90b). By contrast, afferents in the bullfrog utriculus uniformly possess noncalyceal endings. The great majority of these endings are en passant or terminal bouton-like endings. However, many afferents, especially in the striolar region, had club-like or claw-like synaptic endings. These endings are similar in morphology to those reported by Honrubia et al. ('89) and Boyle et al. ('91) in the bullfrog and toadfish semicircular canals. These endings, unlike calyceal endings, did not completely surround the basolateral surface of hair cells. Moreover, they were always associated with bouton-like endings and were largely restricted to the central, or striolar, region. They are, however, reminiscent of the calyceal endings seen in higher vertebrates in one major respect. Like calyceal endings, they were always found at the end of relatively thick branches, whereas bouton-like endings were located on thinner collaterals. The precise significance of this arrangement is unclear.

Relationship of afferent innervation patterns to hair cell types

The bullfrog, unlike the mammal, possesses only Type II hair cells. These hair cells have, however, a number of distinctive hair bundle morphologies (Lewis and Li, '75). Moreover, they have recently been shown to differ markedly in their responses to intracellular current and hair bundle displacement (Baird, '92, '93a,b). Recent studies have shown that the tallest stereocilia of Type I and Type II hair cells in mammals also display regional variations in morphology (Lapeyre et al., '92). It is not yet known whether these regional variations are associated with differences in hair bundle physiology. Studies have shown, however, that Type II hair cells in different regions of the guinea pig utriculus and semicircular canals also differ in their lectin binding properties (Baird et al., '93).

The terminal fields of afferents are largely restricted to distinct macular zones. One consequence of this is that extrastricular and juxtastricular afferents largely or exclusively innervate Type B hair cells. These are the only afferents to innervate a single hair cell type. By contrast, striolar afferents innervate a complex mixture of four hair cell types. The type of hair cells innervated by striolar afferents is correlated with the macular entrance of their parent axons. This is a consequence of the restricted terminal fields of these afferents and the restricted macular distributions of hair cell types (Baird, '92, '93a). Afferents supplying the outer rows of the striola innervate large numbers of Type B and Type C hair cells. Afferents innervating more central striolar rows, on the other hand, contact a complex mixture of four hair cell types. A small number of striolar afferents, with thin parent axons, supplies only the innermost rows of the striola, contacting relatively large numbers of Type E and Type F hair cells. This segregation of input to different afferent classes lends support to the idea that differences in afferent sensitivities and response dynamics may largely be determined by

differences in the transduction mechanisms of their innervated hair cells (Baird, '92, '93a,b).

Relation to morphophysiological studies of otolith afferents

An attempt was made to correlate the results of this study with the results of previous physiological (Loe et al., '73; Macadar et al., '75; Blanks and Precht, '76; Fernandez and Goldberg, '76a,b; Caston et al., '77; Goldberg et al., '90a) and morphophysiological (Goldberg et al., '85; Baird and Lewis, '86; Goldberg et al., '90b; Myers and Lewis, '91) studies of otolith afferents. In lower vertebrates, afferents supplying the vestibular otolith organs have been shown to possess either gravitational or vibration sensitivity (Macadar et al., '75; Blanks and Precht, '76; Caston et al., '77; Baird and Lewis, '86). Afferents with gravitational sensitivity have been further classified into three classes according to their responses to head tilt. Tonic gravity afferents respond to head position, *phasic gravity* afferents respond to head velocity, and phasic-tonic afferents respond to both head position and velocity. In mammals, otolith afferents do not exhibit purely phasic behavior and do not possess sensitivity to substrate-borne vibration (Loe et al., '73; Fernandez and Goldberg, '76a; Anderson et al., '78).

Morphophysiological studies in the bullfrog have shown that the response dynamics of utricular afferents are correlated with the macular location and hair bundle morphology of their innervated hair cells (Baird and Lewis, '86; Myers and Lewis, '91). Tonic gravity afferents, for example, contact hair cells in the extrastriolar and juxtastriolar regions. These hair cells are known from previous studies to be Type B (Lewis and Li, '75). The remaining afferents contact hair cells in the striolar region. Afferents with phasic and phasic-tonic gravity sensitivity have thick parent axons. They also tend to innervate more hair cells in the inner striolar rows than afferents with phasic-tonic sensitivity, suggesting that phasic-tonic afferents owned their head position sensitivity to Type C hair cells and their head velocity sensitivity to Type F hair cells (Baird and Lewis, '86). Our present results suggest that this is unlikely. Type F hair cells, for example, represent only a small percentage of the total innervation of striolar afferents. Striolar afferents largely innervate Type B and Type C hair cells, particularly on the outer striolar rows. Moreover, the number of Type B and Type C hair cells innervated by striolar afferents is inversely correlated. This finding suggests that striolar afferents with varying degrees of tonic and phasic gravity sensitivity differ in the number of Type B and Type C hair cells they contact. This hypothesis is supported by the results of our recent hair cell studies, which indicate that Type B cells, whether located in the striolar or extrastriolar region, are sensitive only to low frequencies and exhibit tonic response dynamics to hair bundle displacement (Baird, '92, '93a,b). Type C hair cells, on the other hand, adapt rapidly to hair bundle displacement, suggesting that they encode head velocity rather than head position. Under this hypothesis, tonic and phasic gravity sensitivity would be conferred by nonadapting Type B and adapting Type C hair cells, respectively.

Striolar afferents with vibratory sensitivity have thin parent axons and innervate large numbers of hair cells in the innermost striolar rows (Baird and Lewis, '86). Hair cells in these rows are known from previous studies to be Type E (Lewis and Li, '75). More recent studies have shown that these hair cells are the only hair cell type in the

bullfrog utricle to exhibit electrical resonance (Baird et al., '92, '93a). We therefore hypothesize that vibratory afferents owe their response properties to the electrical response properties of Type E hair cells. These afferents, unlike other striolar afferents, often innervate hair cells of opposing polarities and are presumably more interested in encoding stimulus frequency than in encoding stimulus amplitude and direction.

Our results do not indicate a clear physiological role for Type F hair cells. One possibility is indicated by physiological (Macadar et al., '75) and morphophysiological (Baird and Lewis, '86) studies indicating that phasic gravity afferents in the utricle can be further divided into slow and fast varieties. The responses of slow phasic afferents initially resemble phasic-tonic afferents, exhibiting tonic responses to head position that eventually revert to prestimulus levels. It is possible that input from Type F hair cells may subtly modify the response dynamics of phasic gravity afferents. This is supported by our recent hair cell studies, which indicate that Type F hair cells possess high frequency sensitivity but, like Type B hair cells, are slowly adapting. The ratio of Type C and Type F cells may therefore be important for determining the response dynamics of phasic gravity afferents, i.e., the response dynamics of phasic gravity afferents may be determined by the adaptation kinetics of their innervated hair cells. Because Type F hair cells tend to be innervated by afferents that also innervate large numbers of Type E hair cells, they may also confer gravitational sensitivity upon vibratory afferents. Afferents with both gravitational and vibrational sensitivity have been shown to exist in previous morphophysiological studies (Baird and Lewis, '86).

ACKNOWLEDGMENTS

We are indebted to Ms. Beverly Smith for manuscript preparation. Funding for this work was provided by National Institute of Deafness and Communicative Disorders grant DC-00355, by National Aeronautics and Space Administration grant NCC 2-651, and by grants from the Oregon Lions Sight and Hearing Foundation.

LITERATURE CITED

- Adams, J.C. (1977) Technical considerations on the use of horseradish peroxidase as a neuronal marker. *J. Neurosci.* 2:141-145.
- Anderson, J.H., R.H.I. Blanks, and W. Precht (1978) Response characteristics of semicircular canal and otolith systems in cat. I. Dynamic responses of primary vestibular fibers. *Exp. Brain Res.* 32:491-507.
- Baird, R.A. (1992) Morphological and electrophysiological properties of hair cells in the bullfrog utricle. *Ann. NY Acad. Sci.* 656:12-26.
- Baird, R.A. (1993a) Comparative transduction and tuning mechanisms of hair cells in the bullfrog utricle. I. Responses to intracellular current. *J. Neurophysiol.* (in press).
- Baird, R.A. (1993b) Comparative transduction and tuning mechanisms of hair cells in the bullfrog utricle. II. Sensitivity and response dynamics to mechanical displacement. *J. Neurophysiol.* (in press).
- Baird, R.A., and E.R. Lewis (1986) Correspondences between afferent innervation patterns and response dynamics in the bullfrog utricle and lagena. *Brain Res.* 369:48-64.
- Baird, R.A., and N.R. Schuff (1991) Transduction mechanisms of hair cells in the bullfrog utricle. *Assoc. Res. Otolaryngol. Abstr.* 14:38.
- Baird, R.A., G. Desmadryl, C. Fernandez, and J.M. Goldberg (1988) The vestibular nerve of the chinchilla. II. Relation between afferent response properties and peripheral innervation patterns in the semicircular canals. *J. Neurophysiol.* 60:182-203.
- Baird, R.A., N.A. Schuff, and J. Bancroft (1993) Lectin binding patterns of vestibular hair cells. *Hear. Res.* 65:151-153.

- Blanks, R.H.I., and W. Precht (1976) Functional characterization of primary vestibular afferents in the frog. *Exp. Brain Res.* 25:369-390.
- Boyle, R., J.P. Carey, and S.M. Highstein (1991) Morphological correlates of response dynamics and efferent stimulation in horizontal semicircular canal afferents of the toadfish, *Opsanus tau*. *J. Neurophysiol.* 66:1504-1521.
- Caston, J., W. Precht, and R.H.I. Blanks (1977) Response characteristics of frog's lagenar afferents to natural stimulation. *J. Comp. Physiol.* 118:273-289.
- Dunn, R.F. (1978) Nerve fibers of the eighth nerve and their distribution to the sensory nerves of the inner ear in the bullfrog. *J. Comp. Neurol.* 182:621-636.
- Fernandez, C., and J.M. Goldberg (1976a) Physiology of peripheral neurons innervating otolith organs of the squirrel monkey. I. Response to static tilts and to long-duration centrifugal force. *J. Neurophysiol.* 39:970-984.
- Fernandez, C., and J.M. Goldberg (1976b) Physiology of peripheral neurons innervating otolith organs of the squirrel monkey. III. Response dynamics. *J. Neurophysiol.* 39:995-1008.
- Fernandez, C., J.M. Goldberg, and W.K. Abend (1972) Response to static tilts of peripheral neurons innervating otolith organs of the squirrel monkey. *J. Neurophysiol.* 35:978-997.
- Fernandez, C., R.A. Baird, and J.M. Goldberg (1988) The vestibular nerve of the chinchilla. I. Peripheral innervation patterns in the horizontal and superior semicircular canals. *J. Neurophysiol.* 60:167-181.
- Fernandez, C., J.M. Goldberg, and R.A. Baird (1990) The vestibular nerve of the chinchilla. III. Peripheral innervation patterns in the utricular macula. *J. Neurophysiol.* 63:767-780.
- Gacek, R.R. (1984) Efferent innervation of the labyrinth. *Am. J. Otolaryngol.* 5:206-224.
- Goldberg, J.M., C.E. Smith, and C. Fernandez (1984) The relation between discharge regularity and responses to externally applied galvanic currents in vestibular-nerve afferents of the squirrel monkey. *J. Neurophysiol.* 51:1236-1256.
- Goldberg, J.M., R.A. Baird, and C. Fernandez (1985) Morphophysiological studies of the mammalian vestibular labyrinth. In M.J. Correia and A.A. Perachio (eds): *Progress in Clinical and Basic Research*. Vol. 176: Contemporary Sensory Neurobiology. New York: Alan R. Liss, pp. 231-245.
- Goldberg, J.M., G. Desmadryl, R.A. Baird, and C. Fernandez (1990a) The vestibular nerve in the chinchilla. IV. Discharge properties of utricular afferents. *J. Neurophysiol.* 63:781-790.
- Goldberg, J.M., G. Desmadryl, R.A. Baird, and C. Fernandez (1990b) The vestibular nerve in the chinchilla. V. Relation between afferent response properties and peripheral innervation patterns in the utricular macula. *J. Neurophysiol.* 63:791-804.
- Hillman, D.E., and J.W. McLaren (1979) Displacement configuration of semicircular canal cupulae. *Neuroscience* 4:1989-2000.
- Honrubia, V., S.T. Sitko, J. Kimm, W. Betts, and I.R. Schwartz (1981) Physiological and anatomical characteristics of primary vestibular afferent neurons in the bullfrog. *Int. J. Neurosci.* 15:197-206.
- Honrubia, V., L.F. Hoffman, S.T. Sitko, and I.R. Schwartz (1989) Anatomic and physiological correlates in bullfrog vestibular nerve. *J. Neurophysiol.* 61:688-701.
- Keefer, D.A., W.B. Spatz, and U. Misgeld (1976) Golgi-like staining of neocortical neurons using retrogradely transported horseradish peroxidase. *Neurosci. Lett.* 3:233-237.
- Lapeyre, P., A. Guilhaume, and Y. Cazals (1992) Differences in hair bundles associated with type I and type II vestibular hair cells of the guinea pig saccule. *Acta Otolaryngol. (Stockh.)* 112:635-642.
- Lewis, E.R., and C.W. Li (1975) Hair cell types and distributions in the otolithic and auditory organs of the bullfrog. *Brain Res.* 33:35-50.
- Lewis, E.R., R.A. Baird, E.L. Leverenz, and H. Koyama (1982) Inner ear: Dye injection reveals peripheral origins of specific sensitivities. *Science* 215:1641-1643.
- Lim, D.J. (1976) Morphological and physiological correlates in cochlear and vestibular sensory epithelia. In O. Jahari and R.P. Becker (eds): *Scanning Electron Microscopy/1976/V*. Chicago: IIT Research Institute, pp. 269-276.
- Lindeman, H.H. (1969) Studies on the morphology of the sensory regions of the vestibular apparatus. *Ergeb. Anat. Entwicklungsgesch.* 42:1-113.
- Loe, P.R., D.L. Tomko, and G. Werner (1973) The neural signal of angular head position in primary afferent vestibular nerve axons. *J. Physiol. (Lond.)* 230:29-50.
- Lorente de Nó, R. (1926) Études sur l'anatomie et la physiologie du labyrinthe de l'oreille et du VIII^e nerf. Deuxième partie. Quelques données au sujet de l'anatomie des organes sensoriels du labyrinthe. *Trab. Lab. Invest. Biol. Univ. Madrid.* 24:53-153.
- Macadar, O., G.E. Wolfe, D.P. O'Leary, and J.P. Segundo (1975) Response of the elasmobranch utricle to maintained spatial orientation, transitions, and jitter. *Exp. Brain Res.* 22:1-22.
- McLaren, J.W., and D.E. Hillman (1979) Displacement of the semicircular canal cupula during sinusoidal rotation. *Neuroscience* 4:2001-200.
- Miller, R.G. Jr. (1977) Developments in multiple comparisons, 1966-1977. *J. Am. Stat. Assoc.* 72:779-788.
- Myers, S.F., and E.R. Lewis (1991) Vestibular afferent responses to microrotational stimuli. *Brain Res.* 543:36-44.
- O'Leary, D.P., R.F. Dunn, and V. Honrubia (1976) Analysis of afferent responses from isolated semicircular canal of the guitarfish using rotational acceleration white-noise inputs. I. Correlation of response dynamics with receptor innervation. *J. Neurophysiol.* 39:631-644.
- Poljak, S. (1927) Über die Nervenendigungen in den vestibulären Sinnesendstellen bei den Säugetieren. *Z. Anat. Entwicklungsgesch.* 84:131-144.
- Ramón y Cajal, S. (1908) Terminación periférica del nervio acústico del las aves. *Trab. Lab. Invest. Biol. Univ. Madrid* 6:161-176.
- Ramón y Cajal, S. (1909) *Histologie du Système Nerveux de l'Homme et des Vertébrés*, Vol. I. Paris: Maloine.
- Robbins, R.G., R.S. Bauknight, and V. Honrubia (1967) Anatomical distribution of efferent fibers in the VIIIth cranial nerve of the bullfrog (*Rana catesbeiana*). *Acta Otolaryngol. (Stockh.)* 64:436-448.
- Schessel, D.A., and S.M. Highstein (1981) Is transmission between the vestibular type I hair cell and its primary afferent chemical? *Ann. NY Acad. Sci.* 374:210-214.
- Schessel, D.A., R. Ginsberg, and S.M. Highstein (1991) Morphophysiology of synaptic transmission between type I hair cells and vestibular primary afferents. An intracellular study employing horseradish peroxidase in the lizard, *Calotes versicolor*. *Brain Res.* 544:1-16.
- Werner, C.F. (1933) Die Differenzierung der Maculae in Labyrinth, insbesondere bei Säugetieren. *Z. Anat. Entwicklungsgesch.* 99:696-709.
- Wersall, J., and D. Bagger-Sjoberg (1974) Morphology of the vestibular sense organs. In H.H. Kornhuber (ed): *Handbook of Sensory Physiology. Vestibular System: Basic Mechanisms*. New York: Springer-Verlag, pp. 124-170.
- West, J.R., and A.C. Black, Jr. (1979) Enhancing the anterograde movement of HRP to label sparse neuronal projections. *Neurosci. Lett.* 12:159-182.
- Will, U. (1982) Efferent neurons of the lateral-line system and the VIIIth cranial nerve in the brainstem of anurans. A comparative study using retrograde tracer methods. *Cell Tissue Res.* 225:673-685.

R-19

Comparative Transduction Mechanisms of Hair Cells in the Bullfrog Utriculus. I. Responses to Intracellular Current

RICHARD A. BAIRD

Department of Neuro-otology and R. S. Dow Neurological Sciences Institute, Good Samaritan Hospital and Medical Center, Portland, Oregon 97209

SUMMARY AND CONCLUSIONS

1. Hair cells in whole-mount *in vitro* preparations of the utricular macula of the bullfrog (*Rana catesbeiana*) were selected according to their macular location and hair bundle morphology. The voltage responses of selected hair cells to intracellular current steps and sinusoids in the frequency range of 0.5–200 Hz were studied with conventional intracellular recordings.

2. The utricular macula is divided into medial and lateral parts by the striola, a 75- to 100- μm zone that runs for nearly the entire length of the sensory macula near its lateral border. The striola is distinguished from flanking extrastriolar regions by the elevated height of its apical surface and the wider spacing of its hair cells. A line dividing hair cells of opposing polarities, located near the lateral border of the striola, separates it into medial and lateral parts. On average, the striola consists of five to seven medial and two to three lateral rows of hair cells.

3. Utricular hair cells were classified into four types on the basis of hair bundle morphology. Type B cells, the predominant hair cell type in the utricular macula, are small cells with short stereocilia and kinocilia 2–6 times as long as their longest stereocilia. These hair cells were found throughout the extrastriolar and, more rarely, in the striolar region. Three other hair cell types were restricted to the striolar region. Type C cells, found primarily in the outer striolar rows, resemble enlarged versions of Type B hair cells. Type F cells have kinocilia approximately equal in length to their longest stereocilia and are restricted to the middle striolar rows. Type E cells, found only in the innermost striolar rows, have short kinocilia with prominent kinociliary bulbs.

4. The resting potential of 99 hair cells was -58.0 ± 7.6 (SD) mV and did not vary significantly for hair cells in differing macular locations or with differing hair bundle morphology. The R_N of hair cells, measured from the voltage response to current steps, varied from 200 to $>2,000$ M Ω and was not well correlated with cell size. On average, Type B cells had the highest R_N , followed by Type F, Type E, and Type C cells. When normalized to their surface area, the membrane resistance of hair cells ranged from $<1,000$ to $>10,000$ k $\Omega \cdot \text{cm}^2$. The input capacitance of hair cells ranged from <3 to >15 pA, corresponding on average to a membrane capacitance of 0.8 ± 0.2 pA/cm 2 .

5. The current-voltage (I - V) relations of utricular hair cells were correlated with their hair bundle morphology. Type B cells, in both the striolar ($n = 4$) and extrastriolar ($n = 3$) regions, had slightly outwardly rectifying I - V relations. The I - V relations of Type C cells ($n = 15$) were nearly linear for both depolarizing and hyperpolarizing currents. Type F cells ($n = 19$) had sigmoidal I - V relations that saturated for larger depolarizing and hyperpolarizing currents. Type E cells ($n = 14$), in addition to being outwardly rectifying at depolarizing currents, had a pronounced inward (anomalous) rectification for voltages more negative than -100 mV.

6. The voltage responses of Type B cells to intracellular current were largely passive. Hair cells restricted to the striolar region, on the other hand, exhibited active voltage responses at the onset and

termination of depolarizing currents. The voltage responses of Type C cells were fast, peaking in 10–15 ms, and did not vary with current amplitude. Type F cells had slower responses, peaking in 25–50 ms. Most Type E cells, unlike other utricular hair cells, were electrically resonant, exhibiting one to three cycles of highly damped oscillations at the onset of depolarizing and the termination of hyperpolarizing current steps. A few Type E cells displayed spikelike responses.

7. To simulate the *in vivo* situation during hair bundle stimulation I examined the voltage responses of utricular hair cells to sinusoidal currents in the frequency range of 0.5–200 Hz. Type B and Type C cells had nearly linear responses for a wide range of stimulus amplitudes. Type E and, to a lesser extent, Type F cells displayed large nonlinear deviations during the depolarizing portion of their response. These deviations were most evident at low stimulus frequencies and their peak shifted with increasing frequency in individual cells.

8. My results suggest that utricular hair cells differ in their complements of basolateral membrane conductances. These conductances modify the sensitivity and response dynamics of hair cells to natural stimulation. Type B and Type F cells, for example, have high R_N and are dominated by slow potassium currents, suggesting that they encode tonic head movement. Type C cells, on the other hand, have low R_N and faster membrane currents, enabling them to encode phasic head movements over a wide range of amplitudes and frequencies. Type E cells are electrically resonating and presumably enable the bullfrog utriculus, to encode substrate-borne vibration.

9. The utricular macula is organized to encode both tonic and dynamic displacement. Hair cells in extrastriolar regions possess only low-frequency sensitivity and presumably encode static gravity and tonic head movements. Hair cell types restricted to the striola, on the other hand, are adapted to encode high-frequency information. Within this dynamic zone there is a segregation of function, with Type C cells in the outer striolar rows providing dynamic gravity sensitivity and Type E cells in the innermost rows supplying vibratory sensitivity.

INTRODUCTION

Hair cells, the receptor cells of the vestibular otolith organs, encode information about the amplitude, frequency, and direction of static gravity and dynamic linear accelerations, including sound, substrate-borne vibration, and head and body movement (Hudspeth 1986). Receptor potentials from auditory (Crawford and Fettiplace 1981; Dallos 1986; Nutall 1985; Russell et al. 1986) and vestibular (Corey and Hudspeth 1979, 1983; Hudspeth and Corey 1977; Ohmori 1984) hair cells have provided important information concerning the first stages of sensory processing in these important cells. With few exceptions, however,



previous studies of mechanoelectric transduction in otolith hair cells have been confined to the bullfrog sacculus (for reviews, see Howard et al. 1988; Hudspeth 1986; Roberts et al. 1988). In the bullfrog this endorgan is a sensor of substrate-borne vibration (Koyama et al. 1982; Lewis et al. 1982). Little is known about comparative hair cell transduction mechanisms in other otolith endorgans, particularly those that possess static gravity sensitivity.

Hair cells in the bullfrog sacculus are specifically adapted to sense small-amplitude, high-frequency linear accelerations. Not surprisingly, these hair cells display many properties that are undesirable or inappropriate for hair cells that must provide static gravity sensitivity. The receptor currents of saccular hair cells, for example, adapt to maintained displacements of their hair bundles, sharply limiting their low-frequency sensitivity (Eatock et al. 1987). Saccular hair cells also exhibit an electrical resonance to intracellular current or hair bundle displacement (Ashmore 1983; Hudspeth and Lewis 1988a; Lewis and Hudspeth 1983). This phenomenon, determined by the interplay of basolateral calcium and calcium-activated potassium conductances (Hudspeth and Lewis 1988b), further sharpens the response of saccular hair cells to high frequencies.

I was interested in seeing how the transduction mechanisms of hair cells in a gravity-sensing otolith endorgan would differ from those in the bullfrog sacculus. The bullfrog utricle is an appropriate model for these studies, because its structure is representative of higher vertebrates in general (Lindeman 1969; Wersall and Bagger-Sjoberg 1974) and its function as a sensor of static gravity and dynamic linear acceleration is well known (Baird and Lewis 1986; Lewis et al. 1982). Hair cells in the bullfrog utricle, classifiable as Type II by cell body and synapse morphology, differ markedly in hair bundle morphology from those in the bullfrog sacculus (Baird and Lewis 1986; Lewis and Li 1975). Moreover, the hair bundle morphologies of utricular hair cells, unlike those in the sacculus, differ in different membrane regions.

Recent studies in both the semicircular canals (Baird et al. 1988; Boyle et al. 1991; Goldberg et al. 1985; Honrubia et al. 1981, 1989) and the otolith endorgans (Goldberg et al. 1990) in a wide variety of vertebrate species have used morphophysiological techniques to relate the response properties of vestibular nerve afferents to their terminal morphology. These studies have shown that many of the discharge properties of vestibular afferents, including their sensitivity and response dynamics to natural stimulation, are correlated with their epithelial location. In particular, the vestibular endorgans are regionally organized, with afferents innervating the central zones of these endorgans having higher sensitivities and more phasic response dynamics than afferents supplying their peripheral zone. In mammals the sensitivities of vestibular afferents are determined by both their terminal morphology (Baird et al. 1988; Goldberg et al. 1985, 1990) and their postsynaptic recovery processes (Goldberg et al. 1984). Differences in response dynamics, on the other hand, appear to be solely determined by regional variations in presynaptic transduction mechanisms (Baird et al. 1988; Goldberg et al. 1985, 1990). In the semicircular canal, regional variations in cupular dynamics (Boyle et al. 1991; Hillman and McLaren

1979; Honrubia et al. 1981, 1989; McLaren and Hillman 1979) or the coupling of the cupula to the sensory hair bundles of hair cells (Honrubia et al. 1981, 1989; Lim 1976) may underlie the diversity in response dynamics. In the otolith organs, on the other hand, differences in afferent response dynamics may be determined by differences in the transduction properties of different hair cell types. In the bullfrog utricle the response dynamics of utricular afferents are correlated with the hair bundle morphology of their innervated hair cells (Baird and Lewis 1986), suggesting that hair cells with differing hair bundle morphology may represent independent hair cell types with distinctive physiological response properties.

To test this hypothesis I selected utricular hair cells according to their macular location and hair bundle morphology and recorded their sensitivity and response dynamics to intracellular current and, in a companion study (Baird 1994), to hair bundle displacement. These recordings were made in whole-mount *in vitro* preparations of the bullfrog utricle to preserve the macular location of utricular hair cells. Intracellular recordings were made with conventional microelectrodes because whole-cell patch-clamp recordings of hair cells are extremely difficult from the apical surface (Holton and Hudspeth 1986). The primary aim of this study was to see whether hair cells differing in their macular location or hair bundle morphology differed in their membrane properties or voltage responses to intracellular current. I was particularly interested in assessing, as in recent studies of auditory and vibratory hair cells (Art et al. 1986; Ashmore 1983; Crawford and Fettiplace 1981; Fuchs et al. 1988; Lewis and Hudspeth 1983; Pitchford and Ashmore 1987), whether electrical resonance contributed to frequency tuning in utricular hair cells and, if so, whether such resonance was restricted to hair cells located in particular macular regions (Art and Fettiplace 1987; Roberts et al. 1986) or possessing specific hair bundle morphologies (Fuchs et al. 1988; Sugihara and Furukawa 1989). I also hoped to determine how the transduction mechanisms of different hair cell types might contribute to differences in sensitivity and response dynamics among vestibular afferents.

My results reveal that the utricle is highly organized, with utricular hair cells in different macular regions varying markedly in their voltage responses to intracellular current. In particular, hair cells in the central, or striolar, region of the utricle have faster membrane currents than hair cells supplying the peripheral zone. Hair cells that differ in hair bundle morphology also differ in their passive and active membrane properties, suggesting that these cells differ in their complement of basolateral membrane conductances. One hair cell type, restricted to the innermost striola, displays electrical resonance. This resonance, unlike that seen in saccular hair cells (Ashmore 1983; Hudspeth and Lewis 1988a; Lewis and Hudspeth 1983), is highly damped and is similar in many ways to that observed in pigeon semicircular canal hair cells (Correia et al. 1989) and the toadfish sacculus (Steinacker and Romero 1992).

Preliminary accounts of portions of this data have been presented in abstract (Baird and Schuff 1990, 1991) and short manuscript form (Baird 1992).

METHODS

Isolation of the utricular macula

Adult bullfrogs (*Rana catesbeiana*), weighing 100–150 g, were anesthetized with 0.2% MS-222 (Sigma) and decapitated. The decapitated head was placed in cold, oxygenated artificial saline containing (in mM) 110 Na⁺, 2 K⁺, 4 Ca²⁺, 120 Cl⁻, 3 D-Glucose and 5 N-2-hydroxyethylpiperazine-N'-2-ethanesulfonic acid, pH 7.25. The osmotic strength of this solution, measured with a freezing-point osmometer (Fiske), was 220–240 mOsm. While in the above solution the membranous labyrinth was exposed and the utricular maculae were dissected free of the vestibular nerves and the horizontal and anterior vertical semicircular canals. Utricular maculae were stored in cold, oxygenated artificial saline for ≤ 8 h. Immediately before intracellular recordings the otolith membrane was removed by gentle mechanical agitation after enzymatically digesting the utricular macula for 30–45 min in 50 μ g/ml subtilisin BPN' (Sigma). Excised maculae were trimmed of excess nerve to improve the visibility of hair bundles and bisected perpendicularly to the striola with a Teflon-coated double-edged razor blade. Macular pieces were then mounted flat, hair cells uppermost, in a small chamber on the fixed stage of an upright microscope (Zeiss, model 16) and perfused at a rate of 0.2–0.5 ml/min with oxygenated saline maintained at room temperature (20–22°C). The preparation was protected from radiant heating with an infrared filter in the microscope illumination system.

Identification of utricular hair cells

Before attempting intracellular recordings I visualized the apical surface of the utricular macula with a $\times 40$ water-immersion objective (Zeiss). The striolar region was identified from its characteristic ribbon-shaped appearance (Fig. 1, A and B) and divided, by the polarization of its constituent hair cells, into medial and lateral parts. Using Nomarski optics and a contrast-enhancement video camera (Hamamatsu, C2400), utricular hair cells were viewed from above and recorded on videotape with an S-VHS videocassette recorder (Panasonic, PV-S4864).

Hair cells were identified by macular location and hair bundle morphology. Hair cells were first assigned to the medial or lateral side of the striolar or extrastriolar region. The position of hair cells within the extrastriolar regions was measured from the medial or lateral striolar border. Striolar hair cells, depending on their relative distance from the line dividing hair cells of opposing polarities, were placed into one of three categories. Hair cells immediately adjacent to this line were assigned to the inner striolar rows. Hair cells adjacent to the medial and lateral extrastriolar region were described as being in the outer striolar rows. The remaining striolar hair cells were assigned to the middle striolar rows. I did not measure the position of hair cells parallel to the long axis of the striola. Selected hair cells were generally located in the broad central region of the macula (Fig. 1A).

With my optics I could just resolve the component kinocilia and stereocilia of striolar hair cells (Fig. 1B). Hair bundle morphology was characterized by the size of the hair bundle, the presence or absence of a bulbed kinocilium, and the relative lengths of the kinocilium and longest stereocilia. The latter two discriminations were made by gently separating the kinocilium from the stereociliary array with a fine glass probe. In pilot experiments, my on-line identification of hair cell morphology was verified by labeling selected hair cells with Lucifer yellow (Stewart 1978) or biocytin (Honikawa and Armstrong 1988) microelectrodes and corroborating their hair bundle morphology in sectioned material. Dye-filled microelectrodes were not routinely used because of the capriciousness of dye ejection from high-resistance microelectrodes.

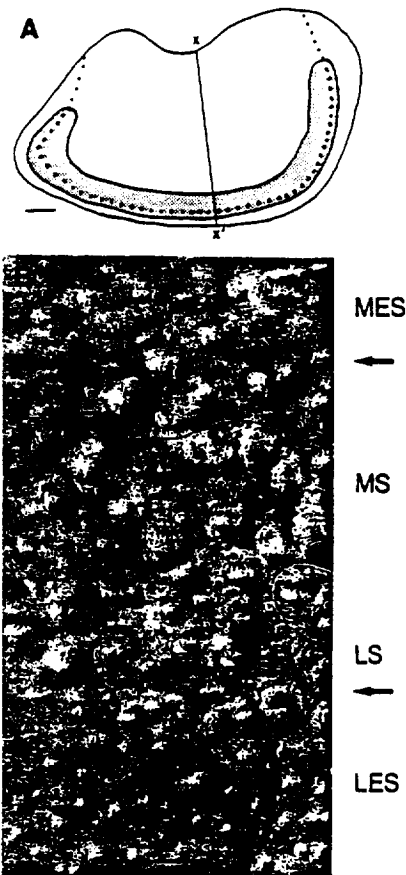


FIG. 1. A: surface reconstruction of the whole-mount utricular macula. Crosses with solid line: plane of section seen in Fig. 2. The striola (shaded area), a narrow ribbon-shaped zone, and its anterior and posterior extensions (dotted lines) separate the extrastriola into medial and lateral parts. Bar: 100 μ m. B: Nomarski photomicrograph of the utricular striola and surrounding extrastriolar regions. Arrows: medial (*top*) and lateral (*bottom*) borders of the striolar region. Dotted line: reversal of hair cell polarization. MES, medial extra-striolar; MS, medial striolar; LS, lateral striolar; LES, lateral extra-striolar. Bar: 25 μ m.

Intracellular recordings

Intracellular recordings were performed with glass microelectrodes pulled from thin-walled aluminosilicate glass (A-M Systems) and bent at 45–90° angles 200–250 μ m from their tips to allow nearly vertical penetrations of the apical surfaces of hair cells (Hudspeth and Corey 1977). The shanks of microelectrodes were coated with silicone plastic (Dow Corning, Sylgard 184) to increase mechanical strength and reduce capacitance. In some experiments microelectrode tips were dipped briefly in 100 μ g/ml streptomycin sulfate (Sigma) immediately before use to improve the quality of intracellular recordings (Holton and Hudspeth 1986). Recording microelectrodes were filled with 3 M KCl and had resistances between 150 and 300 M Ω . Microelectrodes with time constants > 250 μ s were discarded. The remaining microelectrodes were checked for their ability to pass depolarizing and hyperpolarizing currents in the range of ± 1 nA in a linear manner. Responses to larger currents were corrected for microelectrode characteristics.

Intracellular voltage responses were recorded with an Axoclamp-2A amplifier (Axon Instruments) operating in continuous bridge mode. Voltage outputs from the Axoclamp-2A amplifier, stimulus waveforms, and internal sync marks were recorded and stored on videotape (Instrutech). These waveforms were also digi-

tally sampled at 10 kHz, stored on hard disk, and analyzed on- and off-line with a DEC LSI 11/73 microcomputer.

The responses of hair cells to intracellular current were first determined from their steady-state and dynamic voltage responses to 100-ms depolarizing and hyperpolarizing current steps. Microelectrodes were balanced in the saline bath before impaling and immediately after withdrawing from hair cells. On some occasions it was necessary to readjust the bridge balance intracellularly to cancel a fast component in the voltage responses. This fast component, which had a fast (< 1 ms) time constant and a symmetrical response to depolarizing and hyperpolarizing current steps, was attributed to the electrode resistance. The slower components of voltage responses were attributed to the hair cell membrane.

The responses of hair cells to intracellular current were averages of results obtained in response to 16 stimulus presentations. Current steps were usually alternated between hyperpolarizing and depolarizing values, starting at -10 to -40 pA and increasing current amplitude by 10 or 20 pA at each iteration. In a few experiments hair cells were depolarized or hyperpolarized with constant current before the presentation of current steps. Steady-state voltage responses were measured 50–100 ms from the onset of current steps and used to calculate the steady-state current-voltage (I - V) relations of utricular hair cells. R_N was measured with small (-10 to -40 pA) hyperpolarizing current steps and determined from the slope of the best-fitting regression line through the linear portion of the I - V relation. Steady-state slope conductances were determined over a 40-mV range depolarizing and hyperpolarizing to resting membrane potential. The membrane time constant (t_m) was estimated from the slowest component of the voltage response to a hyperpolarizing current step. Voltage responses were rejected for this purpose if 1) they did not fall in the linear portion of the I - V relation, 2) they displayed a significant sag after their initial hyperpolarizing response, or 3) time constants for the response at the onset and offset of the current step were significantly different. Input capacitance (C_N) was calculated from the relation $C_N = t_m/R_N$.

Sinusoidal stimuli were superimposed with small (10–40 pA) depolarizing bias currents and delivered to the recording microelectrode by a function generator (Wavetek, model 185). I then examined the voltage responses of hair cells to sinusoidal current using individual sinusoids and logarithmic frequency sweeps. In the latter case hair cells were stimulated at a start frequency (0.5 or 5.0 Hz) for several cycles. Sinusoidal current was then logarithmically swept over a low (0.5–20) or high (5.0–200 Hz) frequency range, during which frequency was increased between the start and end frequencies in 10 equally spaced discrete steps. For individual sinusoids the number of rotation cycles was matched to the frequency of oscillation to maintain an equal duration of stimulation for each experimental condition. Responses to successive sine wave cycles were averaged; the number of cycles was matched to stimulus frequency, varying from 2 at 0.5 Hz to 16 at 200 Hz. Cycle histograms were created by plotting for discrete frequencies the averaged voltage responses versus the stimulus cycle. The peak-to-peak amplitude of sinusoidal currents was varied from 10 to 100 pA, producing a maximum voltage response of ~ 5 –20 mV.

Morphological analyses

Four utricular maculae were fixed for 2 h in 4.0% paraformaldehyde in 0.1 M phosphate buffer, rinsed in 0.1 M phosphate buffer, dehydrated in a series of ethanol solutions, and mounted in depression slides. Under low magnification the boundaries of the sensory macula and the striolar region were input to a computerized image analysis system (Bioquant, system IV). At higher magnification hair cell density in representative macular areas was determined by counting the number of hair cells within a 100×75 μm rectangle. Within each endorgan four measurements were

made across the anterior-to-posterior extent of the macula and averaged to obtain a mean value for hair cell density in the striolar and medial and lateral extrastriolar zones. I then averaged these measures across animals for each macular zone. In the striolar region the outlines of individual hair cells were traced. Whole-mount maculae were then rinsed briefly in xylene and absolute ethanol, embedded in glycol methacrylate (Polysciences, JB-4), and serially sectioned at 8 μm in a coronal plane.

Sectioned material was examined with $\times 40$ and $\times 63$ oil immersion objectives under bright-field illumination. Individual hair cells in the striolar and extrastriolar regions were classified according to their hair bundle morphology. For each hair cell measurements were made of hair bundle diameter and the lengths of the kinocilium and shortest and longest stereocilia. Estimates of the total surface area of hair cells were made by modeling hair cells as idealized spheres and/or cylinders (Fig. 2, middle). The diameter of spherical cells was measured and the surface area calculated as $A = 4\pi r^2$. For cylindrical hair cells the longitudinal axis was measured and measurements of the horizontal axis at 2 to 5- μm intervals from the apical surface were averaged to calculate hair cell diameter. The surface area of cylindrical hair cells was then calculated as $A = 2\pi r(r + h)$. In a few cases the apical and basal portions of hair cells were modeled using a combined cylinder-sphere model. The surface area of these cells was approximated by the formula $A = 2\pi(r_1 h + 2r_2^2)$, where r_1 and r_2 were the radii of the cylindrical and spherical portions of the cell, respectively. For each hair cell type the average contribution of the stereociliary membrane to total surface area was calculated using a cylindrical model and mean values of stereocilia number, diameter, and length obtained from a separate population of hair cells (see Table 1, Baird 1994).

Statistical procedures

Unless otherwise stated statistical comparisons of morphometric data were based on a one-way analysis of variance. Where appropriate, post hoc pairwise multiple comparisons were performed using the Tukey multiple comparison test adjusting, when necessary, for unequal group sizes (Miller 1977).

RESULTS

Organization of the utricular macula

The utricular macula of the bullfrog, as in other vertebrates, is a kidney-shaped structure (Fernandez et al. 1990; Lindeman 1969; Wersall and Bagger-Sjoberg 1974). The posterior part of the sensory epithelium lies in a horizontal plane. Its anterior part, as in mammals, is curved upward. The utricular macula in the bullfrog is divided into a large medial and a smaller lateral region by the striola, a narrow zone of distinctive morphology that runs for most of the length of the sensory epithelium near its lateral border (Fig. 1A).

The striola, a 75- to 100- μm -wide ribbon-shaped zone, differed in several respects from flanking extrastriolar regions. Some of these differences can be appreciated from the photomicrographs of Figs. 1 and 2. Hair cells in the striola tended to be larger and more widely spaced than hair cells in the medial or lateral extrastriola (Fig. 1B). The density of hair cells in the striolar region of four animals was 0.018 ± 0.002 (SD) hair cells per μm^2 . Hair cell density in the medial and lateral extrastriola was significantly

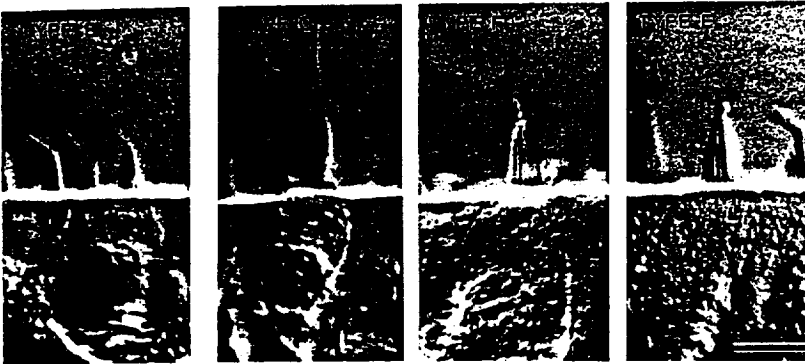
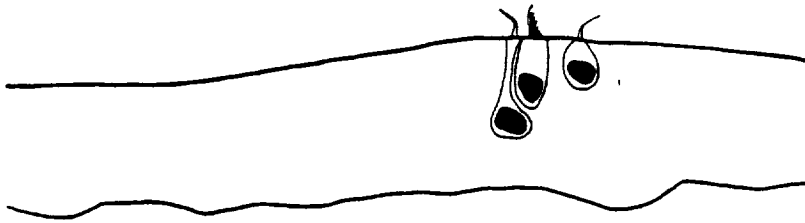
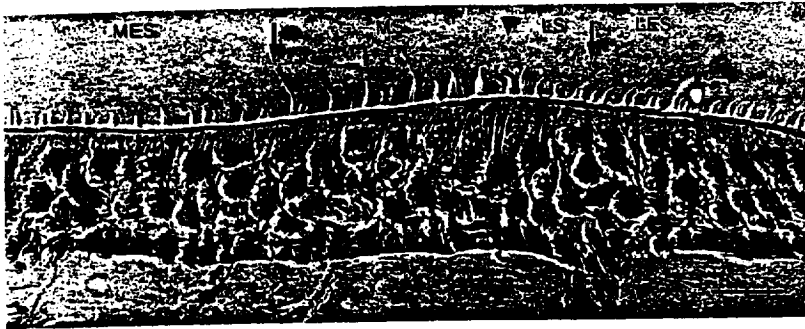


FIG. 2. Nomarski photomicrograph (*top*) and schematic sketch (*middle*) of toluidine-blue stained cross-section of the utricular macula, indicating the cellular morphology of representative hair cells in the utricular macula. Outer arrows: medial (*left*) and lateral (*right*) borders of the striolar region. Pointer: reversal of hair cell polarization. *Bottom*: Nomarski photomicrographs of the hair bundles of individual hair cells in the extrastriolar (*left*) and striolar (*right*) regions. Bars: 25 μm (*top* and *middle*); 10 μm (*bottom*).

higher, averaging 0.030 ± 0.002 and 0.047 ± 0.005 , respectively. In sectioned material the apical surface of the striola was higher in elevation than that of the surrounding extrastriolar regions, giving the striola a hill-like appearance (Fig. 2, *top*). Finally, most hair cells in the striolar region (Fig. 2, *bottom right*) were larger and had different hair bundle morphologies than hair cells located in the extrastriolar regions (Fig. 2, *bottom left*).

The boundaries between the striolar region and the medial and lateral extrasriola were easily recognized in whole-mount (Fig. 1*B*) and sectioned (Fig. 2, *top*) material. In either extrastriolar region the orientation of hair cells was directed toward the striolar region. Hair cells in the striolar region were oriented in the same direction as adjacent extrastriolar cells. A line dividing hair cells of opposing polarities, located near the lateral border of the striola, further separated the striola into medial and lateral rows (dotted line, Fig. 1, *A* and *B*; pointer, Fig. 2, *top*). On average, the striola consisted of five to seven medial rows and two to three lateral rows of hair cells (Figs. 1*B* and 2, *top*). For the remainder of this paper I will refer to the portion of the striola bordering the line dividing hair cells of opposing polarities as the inner rows, that adjacent to the medial or lateral extrasriola as the outer rows, and the remainder of the striola as the middle rows.

Morphological characteristics of utricular hair cells

Utriclar hair cells, following the original scheme of Lewis and Li (1975), were classified into four types by hair bundle morphology (Fig. 2, *bottom*). Type B cells, the predominant hair cell type in the utricular macula, had small apical surfaces and short stereocilia, with kinocilia 2–6 times as long as their longest stereocilia (Fig. 2, *bottom left*). Three other hair cell types had a variety of surface morphologies, with stereocilia markedly longer than those of Type B cells (Fig. 2, *bottom right*). Type C cells resembled an enlarged version of Type B cells, having kinocilia and stereocilia approximately twice as large as the latter hair cell type. The remaining two hair cell types had kinocilia equal or slightly longer in length than their longest stereocilia, significantly shorter than the kinocilia of Type B and Type C cells. Type F cells had visibly larger hair bundles than other utricular hair cells. Type E cells had smaller hair bundles and, unlike Type F cells, prominent kinociliary bulbs.

With the exception of Type F cells the great majority of utricular hair cells had cylindrical cell bodies. This was particularly true of Type E cells, which uniformly had cylindrical cell bodies. The majority ($14/23 = 60.9\%$) of Type F cells, by contrast, had spherical cell bodies. The cell bodies of Type B and Type C cells were a function of their macular

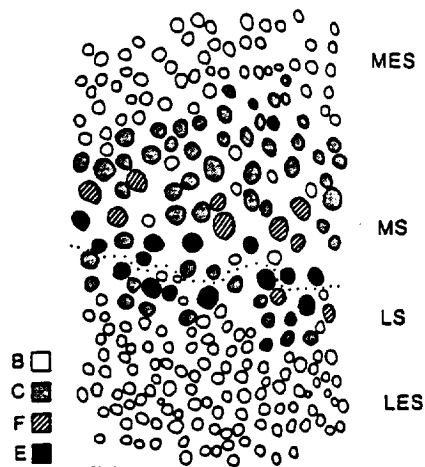


FIG. 3. Macular distribution of hair cell types in the utricular macula. Dotted line: reversal of hair cell polarization. Bar: 25 μm .

location. Type B cells in extrastrial regions, including 22 of 30 in the medial extrastrial and 16 of 19 in the lateral extrastrial, had cylindrical cell bodies. The cell bodies of 5 of 6 striolar Type B cells, on the other hand, were best described by a cylinder-sphere model. Type C cells had cylindrical (22/41 = 53.7%) or spherical (11/41 = 26.8%) cell bodies, depending on whether they were located in the outer or inner striolar rows.

The macular distribution of the above hair cell types in a typical utricular macula is depicted in Fig. 3. Type B cells were found throughout the medial and lateral extrastrial and, more rarely, in the striolar region. The remaining three hair cell types were confined to the striolar region. Type C cells were found throughout the striola but were particularly numerous in the outer striolar rows. Moving inward, these hair cells were gradually replaced by Type F cells. The latter hair cells, unlike Type C cells, were restricted to the middle striolar rows. Type E cells were seen only in the innermost striolar rows, lying astride both sides of the line dividing hair cells of opposing polarities. In four animals extrastrial Type B cells were estimated to make up $87.8 \pm 3.4\%$ of utricular hair cells. Of 365 striolar hair cells identified in my morphological studies, 54 (20.4%) were Type B, 132 (49.8%) were Type C, 24 (9.0%) were Type F, and 55 (20.8%) were Type E.

The morphological characteristics of 135 utricular hair cells and regional variations among the hair cell types are summarized in Table 1. The legend to Table 1 also summarizes the results of statistical tests. Hair cells in the utriculus differed markedly in their lengths and apical diameters. As a group Type B hair cells had the smallest apical diameters of utricular hair cells. Type B cells in the striolar and lateral extrastrial regions had significantly smaller apical diameters and longer lengths than Type B cells in the medial extrastrial region. There was, however, no significant difference in surface area between Type B cells in different macular regions ($P > 0.5$). With the exception of Type B cells, hair cells in the striolar region were larger in diameter and surface area than hair cells in the medial extrastrial. Among both Type C and Type F cells, hair cells in the inner striolar rows tended to be smaller in diameter and longer in length than their counterparts in the outer striolar rows.

Type B and Type E hair cells, both of which were largely restricted to the inner rows, were also significantly longer in length than other utricular hair cells.

Hair cell types in the utriculus also differed dramatically in the lengths of their constituent kinocilia and stereocilia. The shortest and longest stereocilia of Type B and Type C cells were shorter than those of Type F and Type E cells. The kinocilia and the longest, but not the shortest, stereocilia of Type C cells were also significantly longer than those of Type B cells. Among Type B cells, hair cells in the striola had somewhat shorter kinocilia and stereocilia than those in the medial and lateral extrastrial. With the exception of Type B cells, regional differences among hair cell types were small and statistically insignificant.

Passive membrane properties of utricular hair cells

The responses of 99 utricular hair cells were examined with intracellular current steps. Of this total 8 (8.1%) were Type B cells located in the medial ($n = 7$) or lateral ($n = 1$) extrastrial within 100 μm of the striolar region. The remaining 91 (91.9%) hair cells were located within the striolar region. Of these 6 (6.6%) were Type B, 28 (30.8%) were Type C, 35 (38.4%) were Type F, and 22 (24.2%) were Type E. Not surprisingly, my intracellular recordings were biased toward sampling from hair cells with larger apical surfaces. Thus Type F cells, the largest utricular hair cells, were overrepresented and Type B cells, the smallest utricular hair cells, were underrepresented in my physiological sample. This was particularly true for Type B cells from the striola and lateral extrastrial.

The passive membrane properties of utricular hair cells are summarized in Table 2. The resting membrane potentials of all 99 hair cells ranged from -40 to -75 mV (-58.0 ± 7.6 mV, mean \pm SD). There was no significant difference in the resting membrane potential of hair cells located in different macular zones. The resting membrane potentials of hair cells in the striolar region, for example, were similar to those of hair cells in the medial and lateral extrastrial regions ($P > 0.2$). There was also no significant difference in the resting membrane potentials of different hair cell types ($P > 0.2$). By contrast, the R_N and t_m of hair cells varied markedly for different hair cell types. Type C cells had the lowest R_N (236 ± 40 M Ω) and time constants (2.7 ± 1.1 ms) of all utricular hair cells. Type B cells, whether in the striola or extrastrial, had R_N (1764 ± 768 M Ω) and time constants (8.2 ± 3.0 ms) consistently higher than those of other hair cells. The C_N of utricular hair cells was calculated from the relation $C_N = t_m/R_N$ and varied from <2 to >20 pF.

The specific membrane resistance and capacitance of utricular hair cells were estimated by normalizing the R_N and capacitance of individual cells to the mean surface areas of hair cell types (Table 2). Because hair cell types also differed in the number and size of their stereocilia, the contribution of the stereociliary array to membrane surface area was included in this calculation (Table 1, Baird 1994). When normalized to their surface area the r_m of utricular hair cells ranged from $<1,500$ to $>15,000$ k $\Omega \cdot \text{cm}^2$ and was lowest for Type C cells and highest for Type F cells. Mean

TABLE 1. Morphological properties of utricular hair cells

Cell Type	n	Hair Cell			Stereociliary Length		Kinociliary Length, μm
		Diameter, μm	Length, μm	Surface Area, μm^2	Shortest, μm	Longest, μm	
Type B	55	4.5 \pm 1.1	13.6 \pm 4.1	383.1 \pm 70.3	1.1 \pm 0.5	3.8 \pm 1.0	12.2 \pm 1.9
MES	30	5.2 \pm 0.9	11.5 \pm 3.0	385.3 \pm 64.8	1.2 \pm 0.5	4.0 \pm 0.9	12.6 \pm 1.6
MS/LS	6	3.4 \pm 0.3	20.0 \pm 5.1	373.5 \pm 68.0	0.7 \pm 0.4	2.8 \pm 0.4	10.3 \pm 1.9
LES	19	3.9 \pm 0.8	15.0 \pm 2.4	382.6 \pm 82.1	1.1 \pm 0.4	3.9 \pm 1.0	12.1 \pm 2.0
Type C	41	5.1 \pm 0.8	12.4 \pm 3.8	556.9 \pm 113.5	1.3 \pm 0.6	6.3 \pm 1.2	16.6 \pm 2.3
Type F	23	7.0 \pm 1.4	13.1 \pm 3.7	1106.3 \pm 181.9	1.9 \pm 0.9	8.2 \pm 1.3	9.3 \pm 1.2
Type E	16	6.3 \pm 1.6	21.9 \pm 3.5	805.0 \pm 111.2	2.1 \pm 0.7	8.9 \pm 1.1	9.8 \pm 1.1

Values are means \pm SD; n is number of hair cells. Surface area calculated using a cylinder ($SA = 2\pi r(h + 2r)$), sphere ($SA = 4\pi r^2$), or cylinder and sphere ($SA = 2\pi(r_1h + 2r_1^2)$) model, as appropriate, and includes the mean contribution of the stereociliary membrane. The following differences were statistically significant. Hair cell diameter: Type F vs. Types C and B, Type E vs. Type B, MES Type B vs. LES Type B, $P < 0.001$; MES Type B vs. striolar Type B, $P < 0.005$; Type E vs. Type C, $P < 0.05$. Hair cell length: Type E vs. Types F, B, and C, Striolar Type B vs. MES Type B, $P < 0.001$; LES Type B vs. MES Type B, $P < 0.01$; striolar Type B vs. LES Type B, $P < 0.05$. Surface area: Types F and E vs. Types C and B, MES Type B vs. LES Type B, $P < 0.001$ in all cases; Type F vs. Type E, Type C vs. Type B, $P < 0.005$. Shortest stereociliary length: Type E vs. Types C and B, Type F vs. Type B, $P < 0.001$; Type F vs. Type C, $P < 0.005$. Longest stereociliary length: Types E and F vs. Types C and B, Type C vs. Type B, $P < 0.001$ in all cases. Kinociliary length: Types C and B vs. Types E and F, Type C vs. Type B, $P < 0.001$ in all cases. MES, medial extrastriola; MS, medial striola; LS, lateral striola; LES, lateral extrastriola.

membrane capacitance varied from 0.6 $\mu\text{F}/\text{cm}^2$ for Type F cells to 2.1 $\mu\text{F}/\text{cm}^2$ for Type C cells.

Voltage responses to intracellular current steps

RESPONSES TO DEPOLARIZING CURRENTS. The voltage responses of all utricular hair cells were similar for small depolarizing currents. There were marked differences, however, in the voltage responses of hair cells to larger depolarizing currents. These differences were not strongly correlated with macular location. Hair cells with similar hair bundle morphology, on the other hand, had similar voltage responses regardless of their macular location. This is clearly seen in Fig. 4, which illustrates the voltage responses of typical Type B, Type C, and Type F cells to intracellular current steps. In Type B cells depolarizing currents largely produced passive exponential changes in membrane potential, although some evidence of active potential changes were seen for large depolarizing currents (Fig. 4, top left). Active potential changes were more commonly seen in Type C (Fig. 4, top right) and Type F (Fig. 4,

bottom left) cells, resulting in depolarizing peaks with associated decreases in slope resistance. These peaks were evoked from resting membrane potential by depolarizing current steps and their size was graded with current amplitude. Active potential changes in Type C cells were uniformly small (Fig. 4, top right). These changes had rapid onsets, with time-to-peak values < 10 ms, and slightly slower decay times. The size of these peaks did not decrease at large positive potentials. Type F cells typically exhibited larger and slower (> 25 ms) potential changes, which decayed more slowly to steady-state values (Fig. 4, bottom left). Unlike Type C cells, the peaks of Type F decreased in size for voltages more positive than -10 mV. Type F cells also displayed a small hyperpolarizing undershoot at the termination of depolarizing current steps. Five Type F cells, with more outwardly rectifying $I-V$ relations (open circles and open squares, Fig. 6), had more rapid onsets and decays than typical Type F cells. Three of these cells (Fig. 4, bottom middle), all located in the outer striolar rows, had voltage responses to depolarizing current resembling those of Type C cells. These cells had smaller, more rapid onsets

TABLE 2. Passive membrane properties of utricular hair cells

Cell Type	n	Membrane Potential, mV	n	Resistance		Time Constant, ms	Capacitance	
				Input, $\text{M}\Omega$	Membrane, $\text{k}\Omega/\text{cm}^2$		Input, pF	Membrane, $\mu\text{F}/\text{cm}^2$
Type B	14	-59.3 \pm 7.7	8	1764 \pm 768	6690 \pm 2924	8.17 \pm 3.00	4.86 \pm 2.20	1.29 \pm 0.59
MES	7	-60.1 \pm 7.7	3	1960 \pm 648	7552 \pm 2497	6.66 \pm 3.38	3.72 \pm 1.14	0.96 \pm 0.30
MS/LS	6	-58.8 \pm 8.8	5	1606 \pm 890	6000 \pm 3330	9.30 \pm 2.43	5.71 \pm 2.55	1.53 \pm 0.68
LES	1	-55.9	0	—	—	—	—	—
Type C	28	-58.7 \pm 8.1	18	236 \pm 40	1313 \pm 225	2.70 \pm 1.08	11.61 \pm 4.69	2.08 \pm 0.84
Type F	35	-57.8 \pm 7.2	22	908 \pm 417	10043 \pm 4609	5.44 \pm 1.79	6.91 \pm 3.18	0.62 \pm 0.29
Type E	22	-56.7 \pm 7.7	18	366 \pm 143	4011 \pm 1626	5.18 \pm 2.76	14.73 \pm 6.63	1.83 \pm 0.82

Values are means \pm SD; n is number of hair cells. Input resistance (R_N) is average resistance over the range of -100 to -60 mV. Membrane time constant is determined from the voltage response to a hyperpolarizing current step (-10 to -40 pA, 100 ms duration). Input capacitance (C_N) is calculated by dividing the membrane time constant by the input resistance. Specific membrane resistance (r_m) and specific membrane capacitance (c_m) calculated from $r_m = R_N \cdot SA$ and $c_m = C_N/SA$, where SA is mean surface area. The following differences were statistically significant. Input resistance: Type B vs. Types F, E, and C, Type F vs. Types E and C, $P < 0.001$. Membrane resistance: Type F vs. Types E and C, Type B vs. Type C, $P < 0.001$; Type F vs. Type B, Type E vs. Type C, $P < 0.05$. Input capacitance: Type E vs. Types F and B, $P < 0.001$; Type C vs. Types F and B, $P < 0.05$. Membrane capacitance: Types C and E vs. Type F, $P < 0.001$; Type C vs. Type B, $P < 0.05$. For abbreviations, see Table 1.

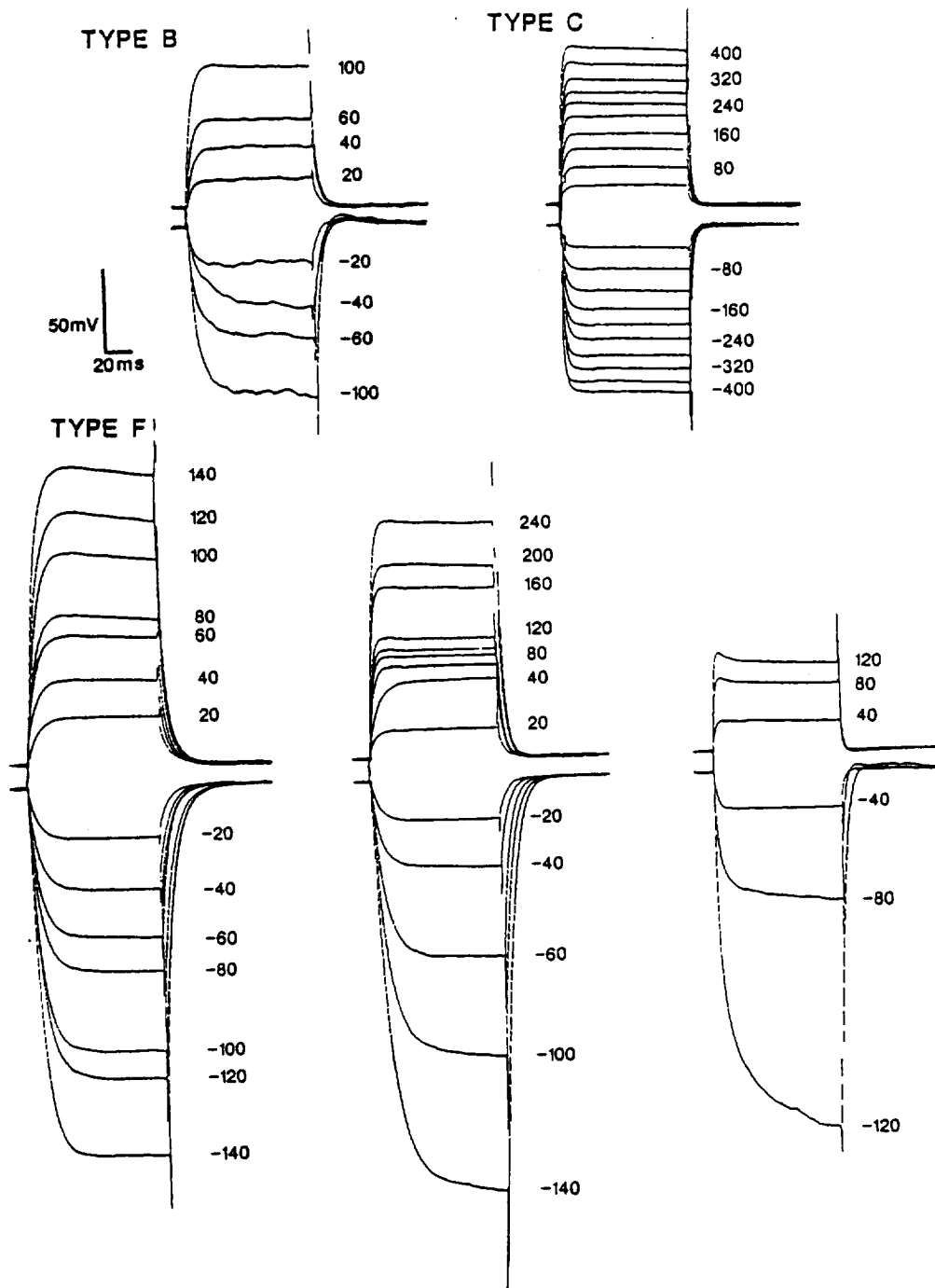


FIG. 4. Voltage responses of Type B (top left), Type C (top right), and Type F (bottom left) hair cells to 100-ms depolarizing and hyperpolarizing current steps of varying amplitude. Also shown are the voltage responses of 2 transitional Type F hair cells (bottom middle and bottom right). Numbers to the right of each trace are the amplitude of the step stimulus (picoamperes).

and a smaller hyperpolarizing undershoot at the termination of depolarizing steps than most Type F cells. Two other Type F cells (Fig. 4, bottom right) had voltage responses resembling those of Type E cells, with large, rapid onsets and a large hyperpolarizing undershoot at the termination of depolarizing steps. These cells were both located in the inner striolar rows.

Termination of the depolarizing peaks of Type C and Type F cells could result from the inactivation of a transient

membrane conductance, the delayed activation of an inactivating membrane conductance, or both. The linearity of the $I-V$ relation for long times and the lack of a substantial hyperpolarizing undershoot at the end of depolarizing current steps suggests that the termination of the depolarizing peak was the result of a transient conductance change. This suggestion is supported by the results of experiments in which hair cells were held at depolarized or hyperpolarized membrane potentials by the injection of constant

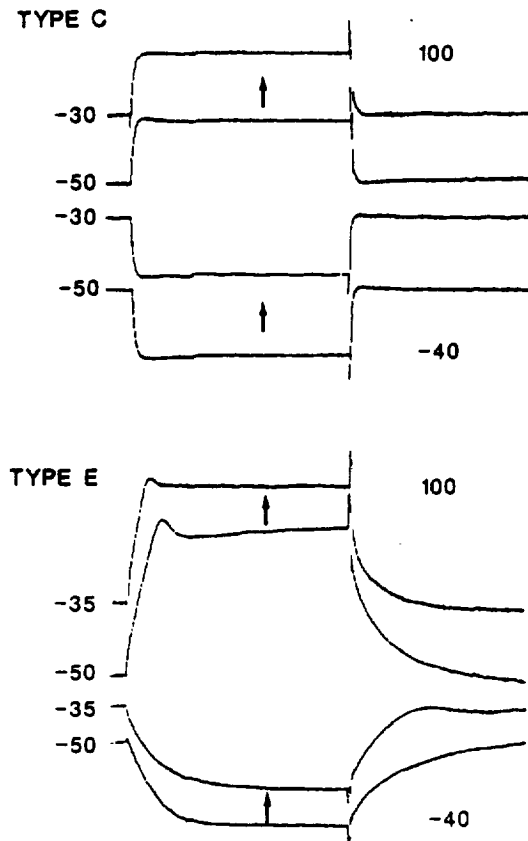


FIG. 5. Voltage responses of a Type C (*top*) and Type E (*bottom*) hair cell held at depolarizing membrane potentials to depolarizing and hyperpolarizing current steps. Numbers to the *left* of each trace indicate resting membrane potential (millivolts); numbers to the *right* are the amplitude of the step stimulus (picoamperes).

current (Fig. 5). In these experiments the depolarizing peaks of Type C cells were reduced in response to depolarizing current steps (Fig. 5, *top*). Similarly, these peaks were increased when cells were held at hyperpolarizing membrane potentials (data not shown), suggesting that the time course of the depolarizing peak largely results from inactivation of membrane current at depolarized membrane potentials.

RESPONSES TO HYPERPOLARIZING CURRENTS. The responses of Type B cells to hyperpolarizing currents differed in two ways from those to depolarizing currents. One, hyperpolarizing currents produced slightly larger responses than depolarizing currents. Two, a rebound depolarization was observed at the termination of the current step. In response to similar currents, Type C cells displayed both a small sag in membrane potential from an initial maximum and a rebound depolarization at the termination of the current step. This rebound depolarization and, to a lesser extent, the sag were smaller in Type C cells with more depolarized resting membrane potentials and were decreased in amplitude by direct current depolarization (Fig. 5, *top*). Type F cells, unlike Type C cells, did not display sags or rebound depolarizations at the end of a hyperpolarizing current step. Rather, hyperpolarizing current steps caused large, slow potential changes in these hair cells, suggesting a strongly rectifying $I-V$ relationship.

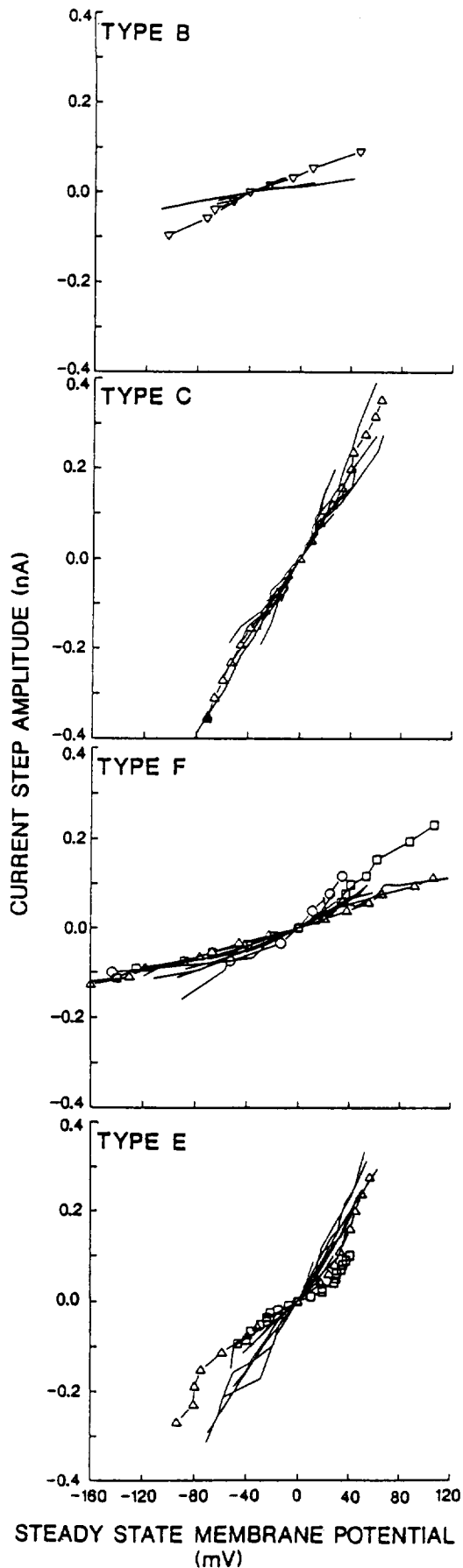
Steady-state $I-V$ relations

The steady-state $I-V$ relations of all utricular hair cells were relatively linear near resting potential. There were marked differences, however, in the voltage responses of hair cells at large depolarizing and hyperpolarizing currents. This is clearly seen in Fig. 6, which shows the steady-state $I-V$ relations of 55 hair cells that were recorded at four or more values of intracellular current. Type B cells, in both the striola ($n = 4$) and medial extrastriola ($n = 3$), had slightly outwardly rectifying $I-V$ relations, with slope conductances varying from 0.59 ± 0.39 nS for hyperpolarizing currents to 0.81 ± 0.42 nS for depolarizing currents (Fig. 6, *top*). I was unable to obtain the $I-V$ relations of Type B cells in the lateral extrastriola. Type C cells ($n = 15$) had nearly linear $I-V$ relations and higher slope conductances (Fig. 6, *top middle*). As expected, the conductances of these cells to depolarizing currents were only slightly different from those to hyperpolarizing currents (5.06 ± 1.10 and 4.49 ± 0.86 nS, respectively). Type F cells ($n = 19$), on the other hand, had strongly outwardly rectifying $I-V$ relations, with slope conductances of 1.33 ± 0.52 nS for hyperpolarizing currents and 1.94 ± 0.84 nS for depolarizing currents (Fig. 6, *bottom middle*). Most Type F cells had sigmoidal $I-V$ relations that saturated for large depolarizing currents (open triangles). Other Type F cells, located in the outer (open squares) or inner (open circles) striolar rows, displayed outward rectification near resting membrane potential and did not saturate for larger positive currents. Type E cells ($n = 14$) were also strongly outwardly rectifying for depolarizing currents, with slope conductances of 3.29 ± 1.06 nS for hyperpolarizing currents and 4.27 ± 1.24 nS for depolarizing currents. In addition, they displayed a pronounced inward (or anomalous) rectification for membrane potentials more negative than approximately -100 mV (Fig. 6, *bottom*).

Electrical resonance

Most (19/22) Type E cells, unlike other utricular hair cells, were electrically resonant, producing one to three cycles of heavily damped oscillations (ringing) at the onset of depolarizing current steps. The membrane potentials of these hair cells rapidly decreased to a steady-state plateau that was maintained throughout the current step (Fig. 7, *left*). The amplitude, frequency, and quality of ringing at the onset of the current step initially increased with depolarizing current. Larger depolarizing currents increased only the first voltage peak, resulting in a disappearance of subsequent peaks and converting the ringing into a spike-like response. At the termination of depolarizing current steps, resonating Type E cells rapidly repolarized to resting levels with no hyperpolarizing undershoot.

A few (3/22) Type E cells did not exhibit ringing for any value of intracellular current. Rather, they had only spike-like responses, displaying prominent depolarizing peaks in response to depolarizing current steps. In these cells the membrane potential became increasingly depolarized toward the end of the current step (Fig. 7, *right*). The amplitude of both the depolarizing peak and the increasing membrane depolarization seen in these cells was reduced when they were held at depolarized membrane potentials by the



injection of constant current (Fig. 5, *bottom*). The repolarization of spiking Type E cells at the termination of depolarizing current steps was significantly slower than that of resonating Type E cells (Fig. 7, *right*).

Hyperpolarizing currents produced, as in Type C cells, a sag in membrane potential from an initial maximum with no associated oscillations (Fig. 7, *left and right*). This sag was reduced in amplitude by direct current depolarization (Fig. 5, *bottom*). In resonating Type E cells (Fig. 7, *left*) oscillations were also seen after the termination of the current step. These oscillations were of lower frequency than those seen at the onset of depolarizing currents. Similar oscillations were also seen in spiking Type E cells depolarized with direct current (Fig. 5, *bottom*).

I was interested in comparing the responses of electrically resonant hair cells in the utricle with those in the bullfrog sacculus, a preparation in which the ionic basis of such resonance is better understood. The responses of saccular hair cells, like those of utricular hair cells, fell into two classes. In most (10/12) saccular hair cells decaying oscillations were observed in response to depolarizing current steps. These oscillations were superimposed on a steady-state plateau and were symmetrical, i.e., ringing occurred at both the onset and termination of the current step (Fig. 8*A*). The frequency of oscillations after depolarizing currents was largely independent of current amplitude and was a measure of the cell's natural frequency (Crawford and Fettiplace 1981; Lewis and Hudspeth 1983). As in utricular hair cells the amplitude, frequency, and quality of ringing at the onset of the current step initially increased with depolarizing current. Larger depolarizing currents increased only the first voltage peak, resulting in a disappearance of subsequent peaks and converting the ringing into a spikelike response. Two hair cells, both located at the peripheral margins of the sacculus, displayed spikelike responses to depolarizing current (Fig. 8*B*). The membrane potential of these cells slowly repolarized after removal of the depolarizing current, exhibiting a prominent slow hyperpolarizing undershoot at the termination of the current step. Hyperpolarizing current steps caused large potential changes in all saccular hair cells with no associated oscillations, suggesting a strongly rectifying $I-V$ relationship (Fig. 8, *A and B*). Oscillatory changes were, however, observed at the termination of hyperpolarizing current steps. As in utricular hair cells these oscillations were of a lower frequency than those seen at the onset of depolarizing currents.

As expected, the steady-state $I-V$ relations of utricular and saccular hair cells were similar. This can be seen in Fig. 9, which illustrates the steady-state $I-V$ relations of 14 utricular (Fig. 9*A*) and 12 saccular (Fig. 9*B*) hair cells recorded at four or more values of intracellular current. As in the sacculus most utricular hair cells displayed some degree of

FIG. 6. Steady-state current-voltage ($I-V$) relations, measured 100 ms after the onset of an intracellularly injected current step, for 7 Type B, 15 Type C, 19 Type F, and 14 Type E hair cells. Symbols indicate the steady-state $I-V$ relations of hair cells whose voltage responses are shown in Figs. 5 (Types B, C, and F) and 7 (Type E). Triangles: Type B, Type C, Type F, and resonating Type E hair cells. Circles: transitional Type F hair cells. Squares: transitional Type F or spiking Type E hair cells.

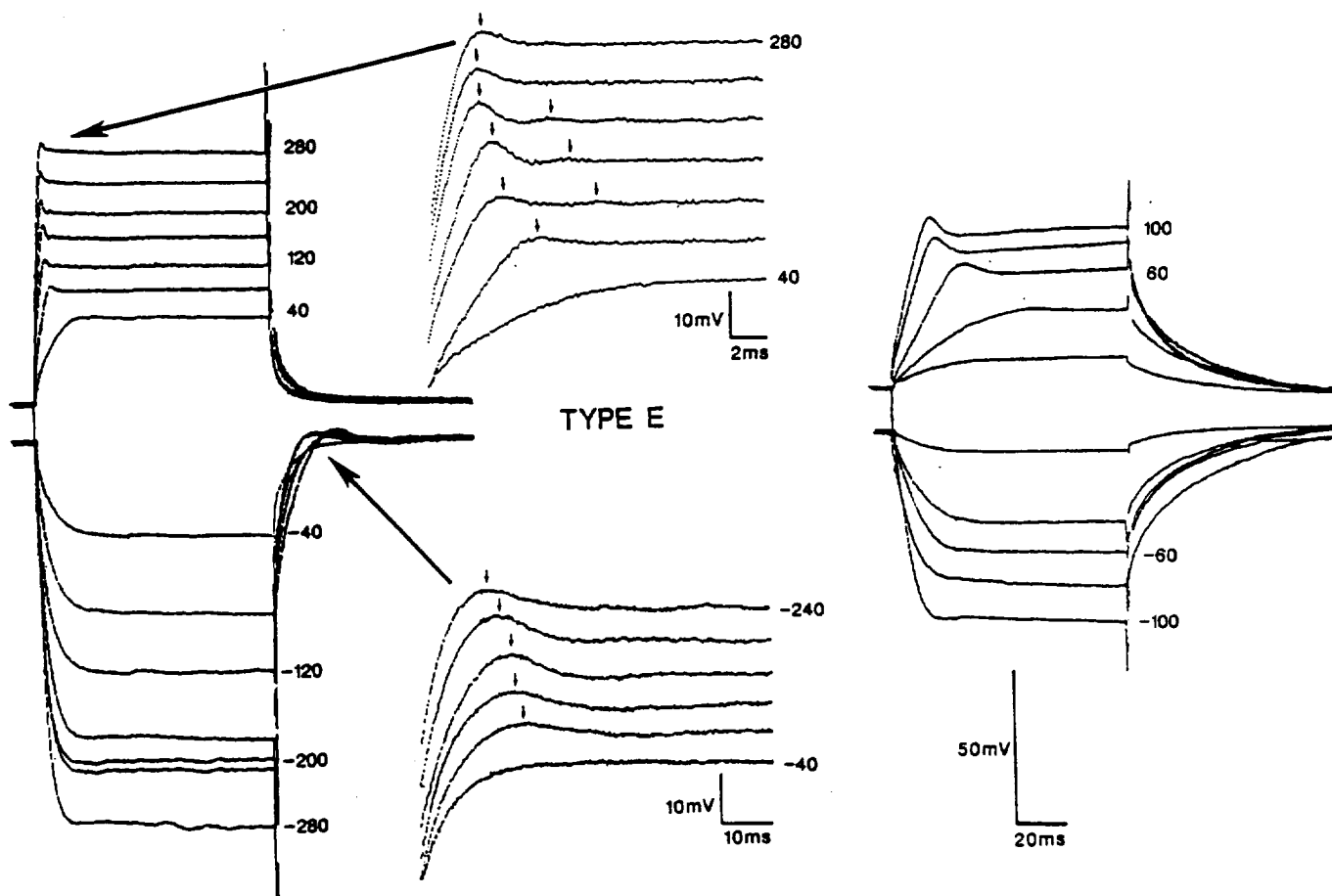


FIG. 7. Voltage responses of resonant (*left*) and spiking (*right*) Type E hair cells to depolarizing and hyperpolarizing current steps of varying amplitude. Numbers to the *right* of selected traces are the amplitude of the step stimulus (picoamperes). Detailed *insets* of membrane oscillations at the onset of depolarizing and the termination of hyperpolarizing current are shown to the *right* of the resonant Type E cell. Small arrows in the detailed *insets*: occurrence of peaks in the oscillatory voltage response.

inward (or anomalous) rectification for membrane potentials more negative than approximately -100 mV. In addition, both utricular and saccular hair cells were strongly outwardly rectifying for depolarizing voltages. The slope conductances of utricular hair cells to hyperpolarizing currents were only slightly different from those of saccular hair cells (3.29 ± 1.06 and 4.22 ± 1.22 nS, respectively). The slope conductances of utricular cells to depolarizing currents, on the other hand, were significantly lower than those of saccular cells, measuring 4.27 ± 1.24 and 8.75 ± 3.55 nS, respectively. Spiking hair cells (squares) in both endorgans had lower slope conductances to depolarizing currents than resonating cells (triangles).

Responses to intracellular current sinusoids

To simulate the *in vivo* stimulation of hair cells during hair bundle stimulation I examined the responses of utricular hair cells to sinusoidal current sweeps in the frequency range of 0.5–200 Hz. The passive membrane properties of hair cells determined from sinusoidal currents were similar to those determined from current steps. In particular, Type B and Type C cells, by virtue of their membrane time constants, had the smallest and largest bandwidths of all utricular hair cells. The responses of Type B cells were linear for a

wide range of amplitudes (Fig. 10, *top*). This was also true to a lesser extent for Type C and Type F cells (data not shown). Type E cells, although linear at low stimulus amplitudes, were strongly rectifying at higher amplitudes, resulting in pronounced DC shifts at high frequencies (Fig. 10, *bottom*).

The voltage responses of utricular hair cells to individual current sinusoids were also examined. As expected, the responses of Type B (Fig. 11, *top*) and Type C (data not shown) cells displayed little or no distortion at any frequency. Type E and, to a lesser extent, Type F cells (data not shown) displayed large nonlinear deviations during the depolarizing portion of their sinusoidal response (Fig. 11, *middle*). These deviations, indicated by arrows in Fig. 11, were most evident at low stimulus frequencies, reaching a maximum at the resonant frequency of the cell and becoming successively smaller at higher frequencies. Within a given cell the peak of these deviations also shifted with increasing frequency, occurring at different portions of the stimulus cycle. This phenomenon was also observed in saccular hair cells, although nonlinear deviations in these cells were restricted to a smaller portion of the stimulus cycle than those of utricular hair cells at all stimulus frequencies (Fig. 11, *bottom*).

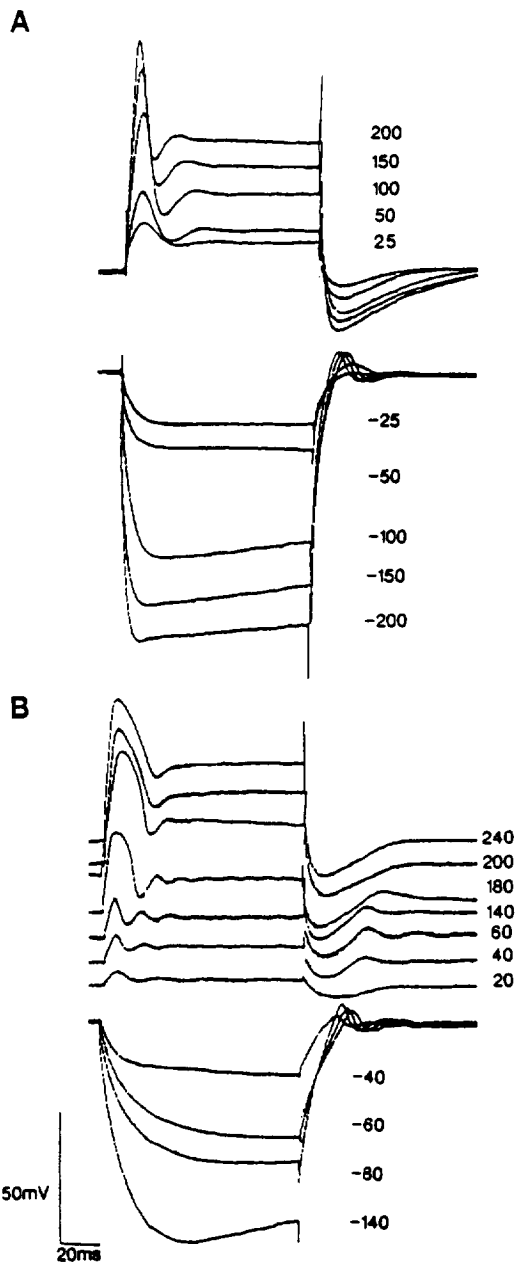


FIG. 8. Voltage responses of resonant (*A*) and spiking (*B*) saccular hair cells to depolarizing (*top*) and hyperpolarizing (*bottom*) current steps of varying amplitude. Numbers to the *right* of each trace are the amplitude of the step stimulus (picoamperes).

DISCUSSION

The results of the present study clearly demonstrate that hair cells in the bullfrog utricle, identified as Type II by cell body and synapse morphology (Wersall and Bagger-Sjoberg 1974), can be further classified into a number of types on the basis of hair bundle morphology. These hair cell types possess unique macular distributions. Recent studies have also shown that immature versions of these hair cell types exist in the regenerating bullfrog utricle (Baird et al. 1994), suggesting that these cells may represent distinct phenotypes within the vestibular otolith organs. These hair cell types differ in their passive membrane properties and voltage responses to intracellular current, sug-

gesting that they differ in their complement of basolateral membrane conductances. These conductances, by acting as frequency-dependent filters of the receptor current, determine how faithfully the membrane potential of hair cells follows their receptor current and modify the responses of hair cells to natural stimulation, regulating sensitivity, frequency selectivity, and synaptic release.

My results represent, to my knowledge, the first direct evidence of physiological differences being associated with differences in kinociliary and stereociliary morphology. There is already strong evidence that hair cells with differing cellular morphology differ in their physiological response properties. In the auditory system, for example, inner and outer hair cells in the mammalian cochlea express different ionic currents and respond differently to intracellular current (Brownell et al. 1985; Kros and Crawford 1990). A similar distinction is seen in the chick cochlea (Fuchs and Evans 1990; Murrow and Fuchs 1990), where hair cells have been divided according to cell body length into short and tall classes. In the vestibular system similar studies have shown that Type I and Type II hair cells in the pigeon (Lang and Correia 1989), guinea pig (Rennie and Ashmore 1991), and the rat (Eatock and Hutzler 1992) differ in their complement of basolateral membrane conductances. Sugihara and Furukawa (1989) have also shown that Type II hair cells in the goldfish sacculus can vary in

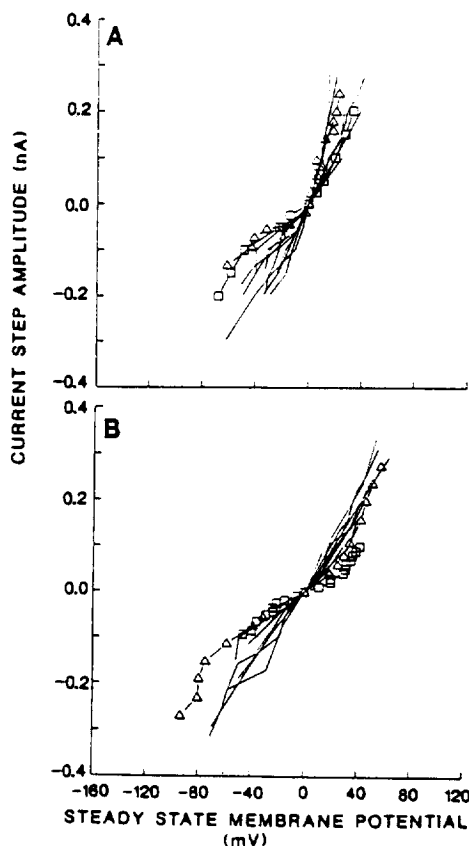


FIG. 9. Steady-state I - V relations measured 100 ms after the onset of an intracellularly injected current step, for 14 utricular Type E (*A*) and 12 saccular (*B*) hair cells. Symbols indicate the steady-state I - V relations of hair cells whose voltage responses are shown in Figs. 7 (utricular Type E) and 8 (saccular), respectively. Triangles: resonant hair cells. Squares: spiking hair cells.

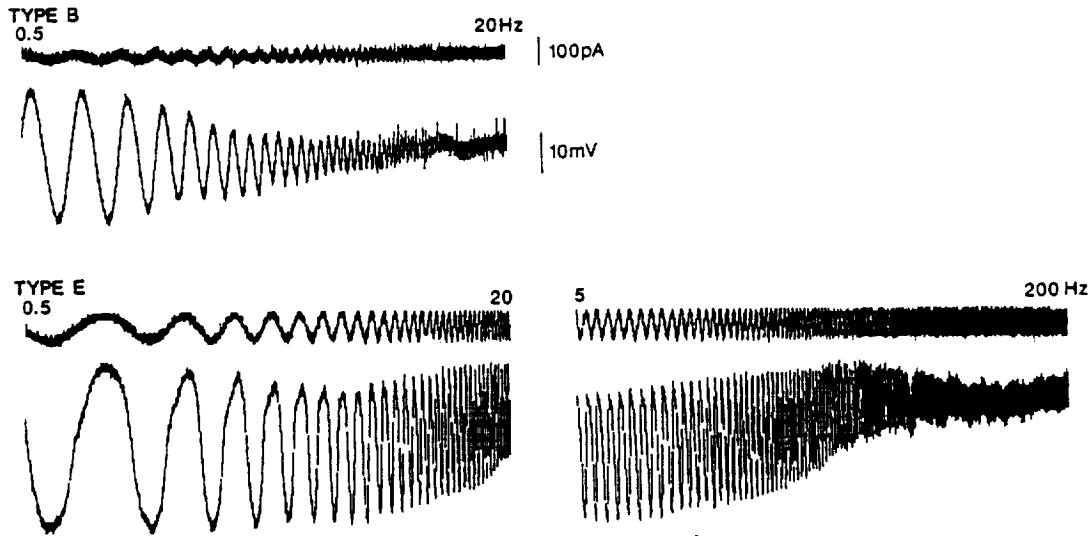


FIG. 10. Voltage responses of a Type B (*top*) and a resonant Type E (*bottom*) hair cell to logarithmic sweeps of sinusoidal current from 0.5 to 20 Hz (*left*) and 5 to 200 Hz (*right*). For each pair of waveforms *top trace*: current stimulus; *bottom trace*: resulting voltage response.

their physiological response properties, with short cells displaying oscillatory responses and tall cells displaying spike-like responses to intracellular current.

Previous studies have also demonstrated that hair cells with differing hair bundle morphology differ in their physiological response properties. The best frequencies of electrically tuned hair cells in the lizard (Turner et al. 1981) and turtle (Art and Fettiplace 1987) cochlea, for example, are correlated with their stereociliary lengths. Short and tall hair cells in the chick cochlea (Fuchs and Evans 1990; Murrow and Fuchs 1990) and the goldfish sacculus (Sugihara and Furukawa 1989) also differ, although not so systematically, in stereociliary length. In each case faster outward currents are associated with higher resonant frequencies and are found in hair cells with successively shorter stereociliary lengths.

Because hair cells in different epithelial regions often display subtle morphological differences it has proven difficult to unambiguously relate regional variations in physiological properties to different hair cell types. In the bullfrog utricle, on the other hand, differences in hair bundle morphology are more marked than in other preparations and are only weakly correlated with differences in cellular morphology. Hair cells in the inner striola, for example, were significantly longer in length than those in the extrastriolar or outer striolar rows, regardless of their hair bundle morphology. Moreover, Type B cells, the only hair cell type found in all macular regions, had similar response properties in both the striolar and extrastriolar regions. Unfortunately only a small number of Type B cells were recorded in this study and these cells were all located within the striola or immediately adjacent to its medial border. A larger and more widely dispersed sample of these hair cells would be desirable. Finally, striolar hair cells in similar macular locations, but with different hair bundle morphology, differ in their physiological response properties. Interestingly, hair cells intermediate in their hair bundle morphology were also intermediate in their physiology. Some hair cells, for example, were difficult to classify because they had kino-

cilia longer than Type F but shorter than Type C cells. These hair cells had voltage responses resembling those of Type C cells for depolarizing currents and those of Type F cells for hyperpolarizing currents.

The cellular mechanism(s) by which hair cells link the development of the hair bundle and the expression of ionic currents in their basolateral membranes are not well understood. It is not difficult, however, to see why such a linkage would be desirable. First, the hair bundle contributes significantly to input capacitance and therefore to the membrane time constant of hair cells. Second, hair bundle morphology contributes to the sensitivity and, possibly, the frequency selectivity of the hair cell to natural stimulation. This point is explored more quantitatively in a companion paper (Baird 1994).

Passive membrane properties of utricular hair cells

Differences in the responses of utricular hair cells to intracellular current could reflect differences in the leakage conductance, passive membrane properties, or the basolateral membrane conductances of hair cell types. Resting membrane potential, for example, can influence the filtering properties of cells by determining the setpoint for the activation and inactivation of ionic channels. The mean resting membrane potential of utricular hair cells is similar to that reported for vestibular hair cells in the chick (Ohmori 1984) and Type II semicircular canal hair cells from the bullfrog (Housley et al. 1989), pigeon (Correia et al. 1989), guinea pig (Rennie and Ashmore 1991), and rat (Eatock and Hutzler 1992). Surprisingly, I did not observe a difference in the resting membrane potentials of different utricular hair cell types. In other preparations the resting membrane potentials of different hair cell types vary markedly. Short and long Type II hair cells in the goldfish sacculus, for example, have resting potentials of -78 and -101 mV, respectively (Sugihara and Furukawa 1989). In the pigeon semicircular canals Type I and Type II hair cells have resting membrane potentials of -70 and -57 mV,

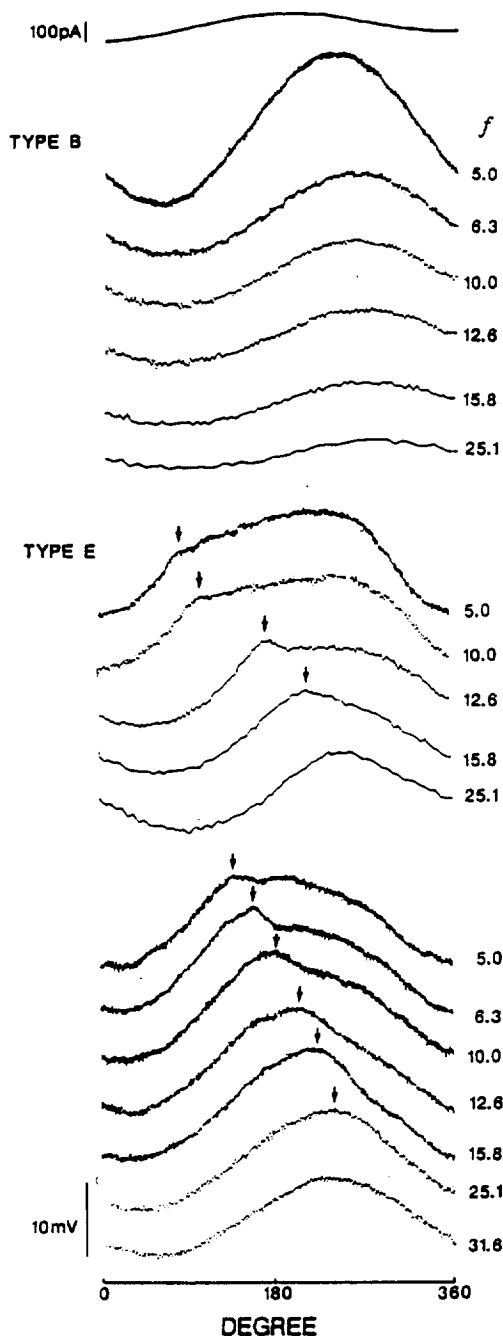


FIG. 11. Cycle histograms of the voltage responses of utricular Type B (top), utricular Type E (middle), and saccular (bottom) hair cells to sinusoidal current. Numbers to the right of each trace indicate the frequency of the sinusoidal current stimulus. Small arrows: peak distortion of the voltage response of utricular Type E (middle) and saccular (bottom) hair cells at each frequency.

respectively (Correia et al. 1989). Type I and Type II hair cells in the guinea pig (Rennie and Ashmore 1991) and rat (Eatock and Hutzler 1992), on the other hand, do not vary in resting membrane potential.

The sensitivity and frequency selectivity of hair cells are also partially determined by their passive membrane properties. R_N , along with input capacitance, determines the membrane time constant and the low-pass corner frequency of hair cells at low voltage levels. By determining

the slope conductance around resting membrane potential R_N also determines the sensitivity of hair cells to receptor current. Type B cells, for example, have high R_N that limit their low-pass corner frequencies and give them low slope conductances to small receptor voltages. Type C cells, on the other hand, have low R_N , greatly increasing their slope conductance around resting membrane potential. R_N and slope conductance can also change dramatically as hair cells depolarize. In Type E and Type F cells, for example, slope conductance decreases markedly with increasing depolarization, increasing the corner frequencies of these hair cell types for larger stimulation.

My measurements of membrane resistance in utricular hair cells are almost certainly underestimates because they ignore the leakage resistance created by the intracellular impalement of cells by sharp microelectrodes. Using whole-cell patch-clamp recordings, mean R_N of 0.4 G Ω have been reported for Type I hair cells in the pigeon semicircular canals (Correia and Lang 1990). Values of R_N for Type II hair cells in the chick vestibular organs (Ohmori 1984) and the pigeon (Correia et al. 1989) and bullfrog (Housley et al. 1989) semicircular canal have been reported to range from 1 to 10 G Ω . With the use of conventional recording techniques, however, somewhat lower values of R_N have been reported by other investigators. In the bullfrog sacculus, for example, Hudspeth and Corey (1977) measured R_N of 200–900 M Ω , values in substantial agreement with my values for utricular hair cells. The input capacitances of utricular hair cells are also similar to those reported for other preparations, which for vestibular hair cells have ranged from 3 pF for hair cells in the bullfrog (Corey and Hudspeth 1983) and goldfish sacculus (Sugihara and Furukawa 1989) to 13 pF for Type II hair cells in the pigeon semicircular canal (Correia et al. 1989). As in other neural tissue, the specific membrane capacitance of hair cells appears to be $\sim 1 \mu\text{F}/\text{cm}^2$ (Housley et al. 1989; Ohmori 1984).

Type C hair cells had significantly lower R_N than other hair cell types. I considered the possibility that these cells were selectively damaged during isolation of the utricular macula. In early experiments it was observed that Type C cells were often selectively damaged by removal of the otolith membrane. This problem was avoided in later experiments by increasing the duration of enzymatic digestion. Although I did not attempt intracellular recordings from obviously damaged hair cells it is possible that some Type C cells were damaged by my isolation procedure. The resting membrane potentials of Type C cells, however, were not significantly different from those of other utricular hair cells. Furthermore, Type C cells, despite their low R_N , displayed normal responses to hair bundle stimulation (Baird 1994).

I also considered the possibility that differences in the R_N of hair cells were an artifact created by the impalement of these cells with sharp microelectrodes. Two lines of evidence suggest, however, that differences in R_N among hair cell types were not an artifact of my recording conditions. R_N , if governed by the shunt conductance created by microelectrode impalement, should be correlated with resting membrane potential. This was not observed. In addition, damage from microelectrode impalement might be expected to be greater in smaller than in larger hair cells. On

the contrary, Type B cells, which are significantly smaller than Type C cells, were found to have the highest R_N of all utricular hair cells.

Electrical resonance

Many utricular Type E cells were electrically resonant, displaying evoked oscillations of their membrane potential in response to depolarizing current steps. Electrical resonance was first demonstrated in the turtle cochlea (Crawford and Fettiplace 1981) and has since been demonstrated in the amphibian sacculus (Ashmore 1983; Hudspeth and Lewis 1988a; Lewis and Hudspeth 1983), amphibian papilla (Pitchford and Ashmore 1987), and chick cochlea (Fuchs et al. 1988). In these auditory and vibratory endorgans high-quality oscillations are evoked by intracellular current and natural stimulation. Electrical resonance seen in the goldfish and toadfish sacculus is of a somewhat lower quality (Steinacker and Romero 1992; Sugihara and Furukawa 1989). In the vestibular organs Housley et al. (1989) have reported electrical resonance in isolated bullfrog semicircular canal hair cells but only in response to extremely large (1.0 nA) intracellular currents. A study of electrical resonance in hair cells isolated from the pigeon semicircular canal, on the other hand, revealed that 59% of Type II hair cells had resonance peaks in their impedance functions or some form of membrane ringing for potentials near their resting membrane potential (Correia et al. 1989). More recently, Rennie and Ashmore (1991) and Eatock and Hutzler (1992) have reported that Type II, but not Type I, hair cells in the guinea pig and rat semicircular canal possess highly damped resonances to intracellular current.

The responses of Type E cells closely resemble the responses of oscillatory hair cells in the pigeon semicircular canal (Fig. 6, Lang and Correia 1989) and goldfish (Fig. 3, Sugihara and Furukawa 1989) and toadfish (Steinacker and Romero 1992) sacculus. As in these other preparations, two types of responses to depolarizing current are observed. The majority of Type E cells have fast responses and relatively high resonant frequencies. These cells, like oscillatory cells from the rostral goldfish sacculus (Sugihara and Furukawa 1989), display resonant responses at all depolarizing potentials, exhibiting rapid returns to resting membrane potential after a depolarizing current step. Other Type E cells respond to depolarizing current with slow, spikelike responses followed by a slowly increasing depolarization.

The quality of electrical oscillations in utricular hair cells is less than that seen in higher vertebrates. This is at least partially due to my use of sharp microelectrodes that, during impalement, introduce large leakage conductances into hair cells. Electrical oscillations in saccular hair cells, for example, are smaller and more highly damped in my recordings than in whole-cell patch-clamp recordings (Lewis and Hudspeth 1983; Hudspeth and Lewis 1988a). There are, nevertheless, several major differences in the responses of electrically resonant utricular and saccular hair cells under the same recording conditions. One, oscillatory potential changes in utricular hair cells are only produced by larger depolarizing currents than those needed to evoke similar changes in saccular hair cells. Two, these oscillations are

smaller and more highly damped than those seen in saccular hair cells (cf. Figs. 7 and 8). Three, oscillations in utricular hair cells are always asymmetric, i.e., ringing is not seen in utricular hair cells at the termination of depolarizing current steps. Finally, unlike saccular hair cells, utricular hair cells do not exhibit hyperpolarizing undershoots at the termination of depolarizing current steps.

Presumptive membrane conductances of utricular hair cells

Several investigators have used the whole-cell variation of the patch-clamp technique (Hamill et al. 1981; Marty and Neher 1983) to study the basolateral membrane conductances of isolated hair cells. These studies have shown that hair cells possess a rich ensemble of ionic currents which determine their resting membrane potential and membrane properties. These include the inward calcium (I_{Ca}) (Eatock and Hutzler 1992; Fuchs et al. 1990; Hudspeth and Lewis 1988a; Lang and Correia 1989; Lewis and Hudspeth 1983; Ohmori 1984; Rennie and Ashmore 1991; Roberts et al. 1990) and anomalous rectifier (Ohmori 1984; Sugihara and Furukawa 1989; Fuchs and Evans 1990; Eatock and Hutzler 1992) currents and three outward potassium currents—the delayed rectifier (I_K) (Eatock and Hutzler 1992; Fuchs and Evans 1990; Housley et al. 1989; Kros and Crawford 1990; Lang and Correia 1989; Steinacker and Romero 1991, 1992), the transient rectifier (I_A) (Eatock and Hutzler 1992; Housley et al. 1989; Kros and Crawford 1990; Lang and Correia 1989; Murrow and Fuchs 1990; Rennie and Ashmore 1991; Steinacker and Romero 1992; Sugihara and Furukawa 1989), and the Ca^{2+} -activated rectifier ($I_{K(Ca)}$) (Eatock and Hutzler 1992; Fuchs and Evans 1990; Housley et al. 1989; Hudspeth and Lewis 1988a; Kros and Crawford 1990; Lang and Correia 1989; Lewis and Hudspeth 1983; Ohmori 1984; Rennie and Ashmore 1991; Roberts et al. 1990; Steinacker and Romero 1991, 1992; Sugihara and Furukawa 1989). There is also recent evidence that Type I vestibular hair cells possess a persistent outward current (Correia and Lang 1990; Eatock and Hutzler 1992; Rennie and Ashmore 1991) similar to the M-current previously described in bullfrog sympathetic neurons (Adams et al. 1982).

My results suggest that hair cell types in the bullfrog utricle possess different complements of basolateral membrane conductances. Unfortunately, because of the large leakage conductance introduced by sharp microelectrodes during cell impalement, it is not possible to achieve more than a qualitative description of the basolateral membrane conductances of hair cells with conventional current-clamp recordings. In addition, these recordings cannot detect the contribution of small conductances nor distinguish the effects of slowly activating conductances from the rapid inactivation of more transient conductances. I can, however, infer the identify of many of these conductances from theoretical considerations and the steady-state and dynamic responses of hair cells to intracellular current.

On theoretical grounds I_{Ca} is found in all hair cells and is undoubtedly involved in Ca^{2+} -dependent transmitter release from hair cells to vestibular nerve afferents (Fuchs et al. 1990; Hudspeth and Lewis 1988a; Lang and Correia 1989; Lewis and Hudspeth 1983; Ohmori 1984; Roberts et

al. 1990). This inward current, however, would not be expected to be detected with conventional current-clamp recordings. One, it is only slightly activated near resting membrane potential. Two, it is small, representing only 10% of the total membrane current of semicircular canal hair cells (Housley et al. 1989; Lang and Correia 1989), and cannot usually be detected even in whole-cell recordings without pharmacologically blocking larger potassium currents. Calcium channels appear to have similar gating kinetics in all vestibular hair cells, displaying rapid (100–200 μ s) activation and little or no inactivation to depolarizing voltages (Hudspeth and Lewis 1988a; Lang and Correia 1989; Lewis and Hudspeth 1983; Ohmori 1984; Roberts et al. 1990).

Utricular hair cells, like other hair cells, presumably possess a number of potassium currents. My results suggest that the identity of these currents is different in different hair cell types. Type B cells, in both the striolar and extrastriolar regions, have high R_N that dominate their voltage responses near resting membrane potential. The high R_N and passive responses of these cells to depolarizing and hyperpolarizing current also suggest that Type B cells have few, if any, membrane conductances activated near resting membrane potential. At larger depolarizing potentials, potentials at which outward potassium channels would presumably be strongly activated, these cells continued to exhibit slow responses with little outward rectification. This suggests that the steady-state $I-V$ relations of these hair cells are dominated by I_K , the activation kinetics of which are considerably slower than other potassium currents (Fuchs and Evans 1990; Lang and Correia 1989; Steinacker and Romero 1991).

Type C cells have low R_N and near-linear $I-V$ relations, suggesting that they possess a persistent potassium conductance. The only persistent potassium conductance previously reported in hair cells is that seen in Type I hair cells in the pigeon (Correia and Lang 1990), guinea pig (Rennie and Ashmore 1991), and rat (Eatock and Hutzler 1992). These hair cells, unlike Type II hair cells in the same preparations, display large, persistent outward currents near their resting membrane potentials with properties similar to those of the M-current described in bullfrog sympathetic neurons (Adams et al. 1982). In sympathetic neurons the time-dependent opening of M-channels introduces considerable outward rectification into the steady-state $I-V$ relations of bullfrog sympathetic neurons (Adams et al. 1982). The M-current of hair cells, however, appears to activate and deactivate much more rapidly than that in sympathetic neurons (Correia and Lang 1990; Eatock and Hutzler 1992) and time-dependent relaxation of this current is not observed for voltage steps more positive than the potassium equilibrium potential (Correia and Lang 1990). This would tend to reduce outward rectification, resulting in a linear steady-state $I-V$ relation. In response to hyperpolarizing current steps, the M-current would be expected to decrease, resulting in a sag in potential dependent on the proximity to the potassium equilibrium potential (Correia and Lang 1990; Eatock and Hutzler 1992; Rennie and Ashmore 1991).

Type C cells also display rapid responses to depolarizing currents, suggesting that they possess a potassium current with fast activation kinetics. The size of these responses did

not decrease at large positive potentials, suggesting that $I_{K(Ca)}$ was not involved in their generation. They were diminished, however, when Type C cells were held at depolarized potentials with constant current injection. This current is therefore likely to be I_A , which in other preparations reaches a steady-state value within 5–10 ms during depolarizing voltage steps. Activation of this current, unlike other potassium currents, is facilitated when a large depolarizing step is applied from hyperpolarized potentials (Hudspeth and Lewis 1988a; Lewis and Hudspeth 1983). At depolarizing potentials, I_A is either largely (Lang and Correia 1989; Sugihara and Furukawa 1989) or completely (Hudspeth and Lewis 1988a; Lewis and Hudspeth 1983) inactivated.

Type F cells, like Type B cells, have high R_N , suggesting that they have few, if any, membrane conductances activated at or below resting membrane potential. For small depolarizing currents these cells displayed slow active responses, suggesting that they are dominated by I_K current. This is consistent with the nearly linear $I-V$ relations of these cells for small depolarizing currents. At larger depolarizing potentials the peaks of Type F cells decreased in size for voltages more positive than -10 mV, suggesting that these cells may also possess $I_{K(Ca)}$. In cells dominated by this current, outward current grows with increasing depolarization until the increased driving force on potassium is offset by the decreased driving force on calcium entry. Thus there is a diminution of the outward current for potentials near the calcium equilibrium potential, resulting in an "N-shaped" $I-V$ relation. Because the $I-V$ relations of Type F cells merely saturated rather than exhibiting such pronounced N-shaped relations it is likely that this current, as in pigeon semicircular canal hair cells (Lang and Correia 1989), is small.

Type E hair cells, unlike other utricular hair cells, are electrically resonant. High-quality electrical resonance in auditory and vibratory hair cells has universally been correlated with the presence of $I_{K(Ca)}$ (Hudspeth and Lewis 1988a; Lewis and Hudspeth 1982; Steinacker and Romero 1992; Sugihara and Furukawa 1989). $I_{K(Ca)}$ is the largest ionic current in these cells, dominating their steady-state $I-V$ relations positive to their resting membrane potential. Moreover, the activation kinetics of $I_{K(Ca)}$ in individual hair cells varies and is correlated with the resonant frequency of electrical oscillations. Thus hair cells with higher resonant frequencies have faster Ca^{2+} -activated potassium channels (Art and Fettiplace 1987; Fuchs and Evans 1990; Roberts et al. 1986). Unlike cells dominated by $I_{K(Ca)}$, resonant Type E cells have small and highly damped oscillations. They therefore presumably possess other, Ca^{2+} -independent, potassium currents (Steinacker and Romero 1992; Sugihara and Furukawa 1989). These currents would increase the membrane conductance of these cells, stabilizing their membrane potential and reducing the amplitude and quality of electrical oscillations. One of these currents may be I_K , which has been shown to block the production of symmetrical electrical resonance in toadfish sacculus hair cells (Steinacker and Romero 1992). A small number of Type E cells had slow, spikelike responses. In these cells an increasing depolarization is observed during depolarizing current steps, indicative of I_A inactivation (Sugihara and

Furukawa 1989). This depolarization is not observed when these cells are held at depolarized potentials with constant current injection, lending further support to the notion that an A-type current is involved. These cells also exhibit very slow hyperpolarizations at the termination of current steps, suggesting that they also possess I_K , which, when activated by a maintained or low-frequency stimulus, is slow to inactivate (Fuchs and Evans 1990; Housley et al. 1989; Lang and Correia 1989; Steinacker and Romero 1991).

Type E cells also display a pronounced inward rectification at potentials more negative than -100 mV. One possible mechanism for this change in resistance is activation of an inward rectifier current. Similar inward rectifier currents have been observed in chick vestibular cells (Ohmori 1984) and electrically resonant hair cells in the goldfish sacculus (Sugihara and Furukawa 1989) and chick cochlea (Fuchs and Evans 1990). Hair cells exhibiting inward rectification had similar resting membrane potentials as those that did not, suggesting that this inward rectifier current is probably permeable to both sodium and potassium ions (Sugihara and Furukawa 1989).

Functional organization of the utricular macula

There is a regional organization of the utricular macula with afferents innervating the central, or striolar, zone of the endorgan having higher gains and more phasic response dynamics than those supplying the peripheral, or extrastriolar, zone (Baird and Lewis 1986; Goldberg et al. 1985, 1990). Morphological studies also indicate that the innervations of these macular zones are relatively independent (Baird and Schuff 1994). It is therefore of interest to ask whether hair cells in these regions differ in their physiological response properties. My results reveal that the responses of striolar hair cells to intracellular current differ in several respects from those of hair cells in extrastriolar regions (see below). Morphological studies in both the bullfrog (Baird and Schuff 1994) and the chinchilla (Fernandez et al. 1990) further demonstrate that afferent innervation patterns in a juxtastriolar zone, located immediately adjacent to the medial striola, differ from those in more peripheral extrastriolar regions, suggesting that hair cells in the extrastriolar regions may also differ in their physiological response properties. My results show little support for this suggestion. The number of Type B cells recorded in this study was, however, small and these cells were all from the striolar and juxtastriolar zones.

Type B cells in the striolar and extrastriolar regions have similar response properties. These cells have high R_N that make them highly sensitive to small receptor potentials but limit their bandwidths to natural stimulation around their resting membrane potentials. The responses of these cells appear to be dominated by I_K . This current is slow to turn on and is not likely to be activated during rapid or high-frequency stimulation. When activated by a maintained or low-frequency stimulus it is also slow to inactivate. Functionally, this implies that these cells are slow to repolarize and slow to return to prestimulus conditions. They are, however, well suited to encode static gravity and tonic head and body movements.

Hair cells restricted to the striolar region differ in several respects from those of Type B cells. Type C cells, for example, have low R_N , greatly increasing their slope conduc-

tance to potentials around their resting membrane potential. This would make these cells less sensitive to small receptor potentials. At the same time, it would extend their dynamic range, enabling them to encode a wider range of stimulus amplitudes. These cells also possess faster outward currents than Type B cells, enabling them to better respond to higher frequency stimulation. Thus they are well suited for encoding phasic head and body movements over a wide range of amplitudes and frequencies.

Type E cells have high R_N that increase their sensitivity to small receptor potentials but limit their bandwidths to natural stimulation. They also, however, display strong outward rectification, markedly increasing their slope conductances with increasing depolarization. This rectification increases the corner frequencies of these cells for larger stimuli, allowing hair cells to modulate transmitter release at frequencies higher than their membrane time constant. Type E cells, unlike other utricular hair cells, are also electrically resonant. Hair cells in the bullfrog can therefore be classified, as in other auditory and vestibular endorgans (Correia et al. 1989; Fuchs and Evans 1990; Fuchs et al. 1988; Steinacker and Romero 1991, 1992; Sugihara and Furukawa 1989), into resonant and nonresonant classes. This resonance presumably allows these cells, as in auditory and vibratory endorgans, to encode stimulus frequency (Ashmore 1983; Crawford and Fettiplace 1981; Fuchs et al. 1988; Hudspeth and Lewis 1988a; Lewis and Hudspeth 1983; Pitchford and Ashmore 1987).

Type E cells are selectively innervated by one class of utricular afferents (Baird and Schuff 1994), suggesting that at least some utricular afferents primarily convey frequency information to the CNS. The damped resonance of Type E cells may also allow these cells to encode temporal aspects of the stimulus signal. In auditory and vibratory endorgans, resonance in individual hair cells is restricted to a narrow range of frequencies and there is a tonotopic mapping of frequency across the endorgan. Afferents innervating these cells have very restricted innervation patterns, strongly phase-locking their discharge to the oscillations of hair cells and allowing them to transmit precise information about stimulus frequency to the CNS. Vestibular organs, by reducing the quality of electrical resonance, may allow hair cells to respond to a greater range of frequencies. Afferents innervating these cells can then achieve phase-locking over a wider frequency range. Resonating hair cells in gravisensitive endorgans may also encode both the transient and envelope of a stimulus signal (Steinacker and Romero 1991).

The functional role of Type F cells is less clear. Unlike Type E cells, they are not selectively innervated by utricular afferents and make up only a small percentage of the total innervation of striolar afferents (Baird and Schuff 1994). These cells resemble Type B cells in having high R_N and slow voltage responses. They would thus seem well suited for encoding tonic head and body movements. Like Type E cells, however, the slope conductance of these cells decreases markedly with increasing depolarization, increasing their corner frequencies for larger stimulation. They might therefore complement the responses of Type B cells, encoding small head and body movements over a somewhat higher range of frequencies.

In conclusion, the bullfrog utriculus is highly organized to extract static and dynamic information about head and

body movement. Type B cells in the striolar and extrastriolar regions of this endorgan are well suited for encoding static gravity and low-frequency linear accelerations. Hair cells restricted to the striolar region, on the other hand, are specialized to encode higher frequency information. These hair cells possess faster ionic currents and, in the case of Type E cells, are electrically tuned to further enhance their high-frequency sensitivities. As we shall see in the companion paper (Baird 1994), hair cells in the striolar and extrastriolar regions also differ in their responses to mechanical stimulation. These differences, unlike the differences discussed here, appear to be shaped by the morphological properties of the hair bundle and the adaptation kinetics of the transduction channel.

The bullfrog, unlike the mammal, possesses only Type II hair cells (Lindeman, 1969; Wersall and Bagger-Sjoberg 1974), which differ markedly in kinociliary and stereociliary morphology (Lewis and Li 1975). These differences are correlated with the physiological responses of these hair cells to intracellular current. A similar association may also be applicable to higher vertebrates. Recent studies have shown that the longest stereocilia of Type I and Type II hair cells in mammals display regional variations in morphology (Lapeyre et al. 1992). It is not known whether these regional variations are associated with differences in hair bundle physiology. It is, however, possible that such variations, more subtle than those involved in the separation of hair cells into Type I and Type II varieties, may be correlated with differences in hair cell physiology in mammalian preparations.

I am grateful to N. R. Schuff for figure preparation and assistance during electrophysiological experiments and to B. Smith for manuscript preparation.

Funding for this work was provided by National Institute of Deafness and Communicative Disorders Grants DC-00355 and DC02040, by National Aeronautics and Space Administration Grant NCC 2-651, and by grants from the Oregon Lions Sight and Hearing Foundation.

Address for reprint requests: R. A. Baird, R. S. Dow Neurological Sciences Institute, Good Samaritan Hospital and Medical Center, 1120 NW 20th Avenue, Portland, OR 97209.

Received 24 February 1993; accepted in final form 14 October 1993.

REFERENCES

- ADAMS, P. R., BROWN, D. A., AND CONSTANTI, A. M-currents and other potassium currents in bullfrog sympathetic neurons. *J. Physiol. Lond.* 330: 537-572, 1982.
- ART, J. J., CRAWFORD, A. C., AND FETTIPLACE, R. Electrical resonance and membrane currents in turtle cochlear hair cells. *Hear. Res.* 22: 31-36, 1986.
- ART, J. J. AND FETTIPLACE, R. Variation of membrane properties in hair cells isolated from the turtle cochlea. *J. Physiol. Lond.* 385: 207-242, 1987.
- ASHMORE, J. F. Frequency tuning in a frog vestibular organ. *Nature Lond.* 304: 536-538, 1983.
- BAIRD, R. A. Morphological and electrophysiological properties of hair cells in the bullfrog utricle. *Ann. NY Acad. Sci.* 656: 12-26, 1992.
- BAIRD, R. A. Comparative transduction and tuning mechanisms of hair cells in the bullfrog utricle. II. Sensitivity and response dynamics to mechanical displacement. *J. Neurophysiol.* 71: 685-705, 1994.
- BAIRD, R. A., DESMADRYL, G., FERNANDEZ, C., AND GOLDBERG, J. M. The vestibular nerve of the chinchilla. II. Relation between afferent response properties and peripheral innervation patterns in the semicircular canals. *J. Neurophysiol.* 60: 182-203, 1988.
- BAIRD, R. A. AND LEWIS, E. R. Correspondences between afferent innervation patterns and response dynamics in the bullfrog utricle and lagena. *Brain Res.* 369: 48-64, 1986.
- BAIRD, R. A. AND SCHUFF, N. R. Comparative transduction mechanisms of hair cells in the bullfrog utricle. *Soc. Neurosci. Abstr.* 16: 733, 1990.
- BAIRD, R. A. AND SCHUFF, N. R. Transduction mechanisms of hair cells in the bullfrog utricle. *Assoc. Res. Otolaryngol. Abstr.* 14: 38, 1991.
- BAIRD, R. A. AND SCHUFF, N. R. Peripheral innervation patterns of vestibular nerve afferents in the bullfrog utricle. *J. Comp. Neurol.* In press.
- BAIRD, R. A., TORRES, M. A., AND SCHUFF, N. R. Hair cell regeneration in the bullfrog vestibular otolith organs following aminoglycoside ototoxicity. *Hear. Res.* 65: 164-174, 1993.
- BOYLE, R., CAREY, J. P., AND HIGHSTEIN, S. M. Morphological correlates of response dynamics and efferent stimulation in horizontal semicircular canal afferents of the toadfish. *Opsanus tau*. *J. Neurophysiol.* 66: 1504-1521, 1991.
- BROWNELL, W. E., BADER, C. R., BERTRAND, D., AND DE RIBAUPIERRE, Y. Evoked mechanical responses in isolated cochlear outer hair cells. *Science Wash. DC* 227: 194-196, 1985.
- COREY, D. P. AND HUDSPETH, A. J. Ionic basis of the receptor potential in vertebrate hair cell. *Nature Lond.* 281: 657-677, 1979.
- COREY, D. P. AND HUDSPETH, A. J. Kinetics of the receptor current in bullfrog saccular hair cells. *J. Neurosci.* 3: 962-976, 1983.
- CORREIA, M. J., CHRISTENSEN, B. N., MOORE, L. E. AND LANG, D. G. Studies of solitary semicircular canal hair cells in the adult pigeon. I. Frequency- and time-domain analysis of active and passive membrane properties. *J. Neurophysiol.* 62: 924-934, 1989.
- CORREIA, M. J. AND LANG, D. G. An electrophysiological comparison of solitary type I and type II vestibular hair cells. *Neurosci. Lett.* 116: 106-111, 1990.
- CRAWFORD, A. C. AND FETTIPLACE, R. An electrical tuning mechanism in turtle cochlear hair cells. *J. Physiol. Lond.* 312: 377-412, 1981.
- DALLOS, P. Neurobiology of cochlear inner and outer hair cells: intracellular recordings. *Hear. Res.* 22: 185-198, 1986.
- EATOCK, R. A., COREY, D. P., AND HUDSPETH, A. J. Adaptation of mechano-electric transduction in hair cells of the bullfrog's sacculus. *J. Neurosci.* 7: 2821-2836, 1987.
- EATOCK, R. A. AND HUTZLER, M. J. Ionic currents of mammalian vestibular hair cells. *Ann. NY Acad. Sci.* 656: 58-74, 1992.
- FERNANDEZ, C., GOLDBERG, J. M., AND BAIRD, R. A. The vestibular nerve of the chinchilla. III. Peripheral innervation patterns of the utricular macula. *J. Neurophysiol.* 63: 767-804, 1990.
- FUCHS, P. A. AND EVANS, M. G. Potassium currents in hair cells isolated from the cochlea of the chick. *J. Physiol. Lond.* 429: 529-551, 1990.
- FUCHS, P. A., EVANS, M. G., AND MURROW, B. W. Calcium currents in hair cells isolated from the cochlea of the chick. *J. Physiol. Lond.* 429: 553-568, 1990.
- FUCHS, P. A., NAGAI, T., AND EVANS, M. G. Electrical tuning in hair cells isolated from chick cochlea. *J. Neurosci.* 8: 2460-2467, 1988.
- GOLDBERG, J. M., BAIRD, R. A., AND FERNANDEZ, C. Morphophysiological studies of the mammalian vestibular labyrinth. In: *Progress in Clinical and Biological Research. Contemporary Sensory Neurobiology*, edited by M. J. Correia and A. A. Perachio. New York: Liss, 1985. vol. 176, p. 231-245.
- GOLDBERG, J. M., DESMADRYL, G., BAIRD, R. A., AND FERNANDEZ, C. The vestibular nerve in the chinchilla. V. Relation between afferent response properties and peripheral innervation patterns in the utricular macula. *J. Neurophysiol.* 63: 781-790, 1990.
- GOLDBERG, J. M., SMITH, C. E., AND FERNANDEZ, C. The relation between discharge regularity and responses to externally applied galvanic currents in vestibular-nerve afferents of the squirrel monkey. *J. Neurophysiol.* 51: 1236-1256, 1984.
- HAMILL, O. P., MARTY, A., NEHER, E., SAKMANN, B., AND SIGWORTH, F. J. Improved patch-clamp techniques for high resolution current recording from cells and cell-free membrane patches. *Pfluegers Arch.* 393: 254-261, 1981.
- HILLMAN, D. E. AND McLAREN, J. W. Displacement configuration of semicircular canal cupulae. *Neuroscience* 4: 1989-2000, 1979.
- HOLTON, T. AND HUDSPETH, A. J. The transduction channel of hair cells from the bullfrog characterized by noise analysis. *J. Physiol. Lond.* 375: 195-227, 1986.
- HILLMAN, D. E. AND McLAREN, J. W. Displacement configuration of semicircular canal cupulae. *Neuroscience* 4: 1989-2000, 1979.
- HOLTON, T. AND HUDSPETH, A. J. The transduction channel of hair cells from the bullfrog characterized by noise analysis. *J. Physiol. Lond.* 375: 195-227, 1986.
- HONRUBIA, V., HOFFMAN, L. F., SITKO, S. T., AND SCHWARTZ, I. R. Ana-

- tonic and physiological correlates in bullfrog vestibular nerve. *J. Neurophysiol.* 61: 688-701, 1989.
- HONRUBIA, V., SITKO, S. T., KIMM, J., BETTS, W., AND SCHWARTZ, I. R. Physiological and anatomical characteristics of primary vestibular afferent neurons in the bullfrog. *Int. J. Neurosci.* 15: 197-206, 1981.
- HORIKAWA, K. AND ARMSTRONG, W. E. A versatile means of intracellular labeling: injection of biocytin and its detection with avidin conjugates. *J. Neurosci. Methods* 25: 1-11, 1988.
- HOUSLEY, G. D., NORRIS, C. H., AND GUTH, P. S. Electrophysiological properties and morphology of hair cells isolated from the semicircular canal of the frog. *Hear. Res.* 38: 259-276, 1989.
- HOWARD, J., ROBERTS, W. M., AND HUDSPETH, A. J. Mechano-electrical transduction by hair cells. *Annu. Rev. Biophys. Chem.* 17: 99-124, 1988.
- HUDSPETH, A. J. The cellular basis of hearing: the biophysics of hair cells. *Science Wash. DC* 230: 745-752, 1986.
- HUDSPETH, A. J. AND COREY, D. P. Sensitivity, polarity and conductance change in the response of vertebrate hair cells to controlled mechanical stimuli. *Proc. Natl. Acad. Sci. USA* 74: 2407-2411, 1977.
- HUDSPETH, A. J. AND LEWIS, R. S. Kinetic analysis of voltage- and ion-dependent conductances in saccular hair cells of the bullfrog, *Rana catesbeiana*. *J. Physiol. Lond.* 400: 237-274, 1988a.
- HUDSPETH, A. J. AND LEWIS, R. S. A model for electrical resonance and frequency tuning in saccular hair cells of the bullfrog, *Rana catesbeiana*. *J. Physiol. Lond.* 400: 275-297, 1988b.
- KOYAMA, H., LEWIS, E. R., LEVERENZ, E. L., AND BAIRD, R. A. Acute seismic sensitivity in the bullfrog ear. *Brain Res.* 250: 168-172, 1982.
- KROS, C. J. AND CRAWFORD, A. C. Potassium currents in inner hair cells isolated from the guinea-pig cochlea. *J. Physiol. Lond.* 421: 263-291, 1990.
- LANG, D. G. AND CORREIA, M. J. Studies of solitary semicircular canal hair cells in the adult pigeon. II. Voltage-dependent ionic conductances. *J. Neurophysiol.* 62: 935-945, 1989.
- LAPEYRE, P., GUILHAUME, A., AND CAZALS, Y. Differences in hair bundles associated with Type I and Type II vestibular hair cells of the guinea pig saccule. *Acta Otolaryngol. Stockh.* 112: 635-642, 1992.
- LEWIS, E. R., BAIRD, R. A., LEVERENZ, E. L., AND KOYAMA, H. Inner ear: dye injection reveals peripheral origins of specific sensitivities. *Science Wash. DC* 215: 1641-1643, 1982.
- LEWIS, E. R. AND LI, C. W. Hair cell types and distributions in the otolithic and auditory organs of the bullfrog. *Brain Res.* 83: 35-50, 1975.
- LEWIS, R. S. AND HUDSPETH, A. J. Voltage and ion-dependent conductances in solitary vertebrate hair cells. *Nature Lond.* 304: 538-541, 1983.
- LIM, D. J. Morphological and physiological correlates in cochlear and vestibular sensory epithelia. In: *Scanning Electron Microscopy*, edited by O. Johari and R. P. Becker. Chicago: IIT Research Institute, 1976, vol. 5, p. 269-276.
- LINDEMAN, H. H. Studies on the morphology of the sensory regions of the vestibular apparatus. *Ergeb. Anat. Entwicklungsgesch.* 42: 1-113, 1969.
- MARTY, A. AND NEHER, E. Tight-seal whole-cell recording. In: *Single Channel Recording*, edited by B. Sakmann and E. Neher. New York: Plenum, 1983, p. 107-122.
- MCLAREN, J. W. AND HILLMAN, D. E. Displacement of the semicircular canal cupula during sinusoidal rotation. *Neuroscience* 4: 2001-2008, 1979.
- MILLER, R. G., JR. Developments in multiple comparisons, 1966-1977. *J. Am. Statist. Assoc.* 72: 779-788, 1977.
- MURROW, B. W. AND FUCHS, P. A. Preferential expression of transient potassium current (I_A) by "short" hair cells of the chick's cochlea. *Proc. R. Soc. Lond. B Biol. Sci.* 242: 189-195, 1990.
- NUTALL, A. L. Influence of direct current on DC receptor potentials from cochlear inner hair cells in the guinea pig. *J. Acoust. Soc. Am.* 77: 165-175, 1985.
- OHMORI, H. Studies of ionic currents in the isolated vestibular hair cells of the chick. *J. Physiol. Lond.* 350: 561-581, 1984.
- PITCHFORD, S. AND ASHMORE, J. F. An electrical resonance in hair cells of the amphibian papilla of the frog *Rana temporaria*. *Hear. Res.* 27: 75-84, 1987.
- RENNIE, K. J. AND ASHMORE, J. F. Ionic currents in isolated vestibular hair cells from the guinea-pig crista ampullaris. *Hear. Res.* 51: 279-291, 1991.
- ROBERTS, W. M., HOWARD, J., AND HUDSPETH, A. J. Hair cells: transduction, tuning, and transmission in the inner ear. *Annu. Rev. Cell Biol.* 4: 63-92, 1988.
- ROBERTS, W. M., JACOBS, R. A., AND HUDSPETH, A. J. Colocalization of ion channels involved in frequency selectivity and synaptic transmission at presynaptic active zones of hair cells. *J. Neurosci.* 10: 3664-3684, 1990.
- ROBERTS, W. M., ROBLES, L., AND HUDSPETH, A. J. Correlation between the kinetic properties of ionic channels and the frequency of membrane-potential resonance in hair cells of the bullfrog. In: *Auditory Frequency Selectivity*, edited by B. C. J. Moore and R. D. Patterson. New York: Plenum, 1986, p. 89-95.
- RUSSELL, I. J., CODY, A. R., AND RICHARDSON, G. P. The responses of inner and outer hair cells in the basal turn of the guinea-pig cochlea and in the mouse cochlea grown in vitro. *Hear. Res.* 22: 199-216, 1986.
- STEINAKER, T. AND ROMERO, A. Characterization of voltage-gated and calcium-activated potassium currents in toadfish saccular hair cells. *Brain Res.* 556: 22-32, 1991.
- STEINAKER, T. AND ROMERO, A. Voltage-gated potassium current and resonance in the toadfish saccular hair cell. *Brain Res.* 574: 229-236, 1992.
- STEWART, W. W. Functional connections between cells as revealed by dye-coupling with a highly fluorescent naphthalimide tracer. *Cell* 14: 741-759, 1978.
- SUGIHARA, I. AND FURUKAWA, T. Morphological and functional aspects of two different types of hair cells in the goldfish sacculus. *J. Neurophysiol.* 62: 1330-1342, 1989.
- TURNER, R. G., MURASKI, A. A., AND NIELSEN, D. W. Cilium length: influence on neural tonotopic organization. *Science Wash. DC* 213: 1519-1521, 1981.
- WERSALL, J. AND BAGGER-SJOBACK, D. Morphology of the vestibular sense organs. In: *Handbook of Sensory Physiology, Vestibular System: Basic Mechanisms*, edited by H. H. Kornhuber. New York: Springer-Verlag, 1974, pt. 1, vol. 6, p. 123-170.

Comparative Transduction Mechanisms of Hair Cells in the Bullfrog Utriculus. II. Sensitivity and Response Dynamics to Hair Bundle Displacement

P-21

RICHARD A. BAIRD

Department of Neuro-otology and R. S. Dow Neurological Sciences Institute, Good Samaritan Hospital and Medical Center, Portland, Oregon 97209

SUMMARY AND CONCLUSIONS

1. Hair cells in whole-mount in vitro preparations of the utricular macula of the bullfrog (*Rana catesbeiana*) were selected according to their macular location and hair bundle morphology. The sensitivity and response dynamics of selected hair cells to natural stimulation were examined by recording their voltage responses to step and sinusoidal hair bundle displacements applied to their longest stereocilia.

2. The voltage responses of 31 hair cells to sinusoidal hair bundle displacements were characterized by their gains and phases, taken with respect to peak hair bundle displacement. The gains of Type B and Type C cells at both 0.5 and 5.0 Hz were markedly lower than those of Type F and Type E cells. Phases, with the exception of Type C cells, lagged hair bundle displacement at 0.5 Hz. Type C cells had phase leads of 25–40°. At 5.0 Hz, response phases in all cells were phase lagged with respect to those at 0.5 Hz. Type C cells had larger gains and smaller phase leads at 5.0 Hz than at 0.5 Hz, suggesting the presence of low-frequency adaptation.

3. Displacement-response curves, derived from the voltage responses to 5.0-Hz sinusoids, were sigmoidal in shape and asymmetrical, with the depolarizing response having a greater magnitude and saturating less abruptly than the hyperpolarizing response. When normalized to their largest displacement the linear ranges of these curves varied from <0.5 to 1.25 μm and were largest in Type B and smallest in Type F and Type E cells. Sensitivity, defined as the slope of the normalized displacement-response curve, was inversely correlated with linear range.

4. The contribution of geometric factors associated with the hair bundle to linear range and sensitivity were predicted from realistic models of utricular hair bundles created using morphological data obtained from light and electron microscopy. Three factors, including 1) the inverse ratio of the lengths of the kinocilium and longest stereocilia, representing the lever arm between kinociliary and stereociliary displacement; 2) tip link extension/linear displacement, largely a function of stereociliary height and separation; and 3) stereociliary number, an estimate of the number of transduction channels, were considered in this analysis. The first of these factors was quantitatively more important than the latter two factors and their total contribution was largest in Type B and Type C cells. Theoretical models were also used to calculate the relation between rotary and linear displacement. When expressed in terms of angular rotation, differences in sensitivity among hair cell types were increased, suggesting that these differences were not due to the manner in which hair bundles were stimulated in these studies.

5. The voltage responses of 16 hair cells to sinusoidal displacement were examined at four or more frequencies from 0.5 to 125 Hz. Type B and Type E cells had small bandwidths, with falling gains and increasing phase lags at all frequencies. In contrast, Type

C cells displayed 10- to 20-fold gain enhancements as frequency was increased and phase leads, ranging from 20 to 40°, were seen between 0.5 and 20 Hz. At higher frequencies, Type C cells had decreasing gains and increasing phase lags. Individual Type C cells displayed differing amounts of gain enhancement and phase lead at low frequencies. Rapidly adapting cells, distinguished by larger gain enhancements and larger phase leads, were more likely to be located in the outer striolar rows than slowly adapting cells. Type F cells did not adapt, displaying constant gains and near-zero phases at low frequencies.

6. Mean sinusoidal gains and phases to hair bundle displacement were fit by a transfer function, $H(s) = H_A(s) \cdot H_T(s)$, consisting of two terms thought to represent the adaptation associated with mechano-electrical transduction (H_A) and the gating kinetics of voltage-dependent membrane conductances (H_T). H_T was represented by a first- or second-order filter, with upper corner frequencies ranging from <1 to >50 Hz. H_A was best fit by a lead operator with a fractional exponent, k_A . At frequencies above an upper corner frequency ranging from <1 to 10 Hz, this operator introduced a gain that increased as f^{k_A} and a phase lead that approached $90^\circ \cdot k_A$. There was a systematic increase in this exponent from $k_A = 0$ for nonadapting hair cells to $k_A = 0.25$ – 0.40 for adapting hair cells.

7. The response dynamics of hair cells to hair bundle displacement differed in two respects from those to intracellular current. 1) hair cells that adapted to hair bundle displacement did not adapt to intracellular current. 2) the bandwidths of cells to hair bundle displacement were greater than those to intracellular current, presumably reflecting the increased conductance of transduction channels.

8. The response dynamics of 15 hair cells were examined with step hair bundle displacements. Type B cells in both the striolar and extrastriolar regions displayed little or no adaptation to step displacements. Other hair cell types displayed conspicuous response declines during step displacement and hyperpolarizing undershoots at their termination. The rate and extent of adaptation varied in different hair cell types. Type C cells, for example, were rapidly or slowly adapting, reaching steady-state levels in 50–100 ms or 100–200 ms, respectively. Type F and Type E cells adapted more slowly, reaching steady-state values in 300–500 ms. With the exception of Type E cells, rapidly adapting cells declined to a greater extent than slowly adapting cells.

9. With the possible exception of rapidly adapting Type C cells, the peak and steady-state responses of adapting hair cells were linearly related to step amplitude, suggesting that the time course and extent of adaptation were independent of displacement. The time course and extent of adaptation, however, were functions of step duration, suggesting that adaptation was activated at the onset of the step displacement but its kinetics were controlled by an intermediate process with variable response dynamics. This pro-

cess may reflect the kinetics of calcium regulation in different hair cell types.

10. These results indicate that hair cells in the utricular macula are organized to encode both static and dynamic information. This is largely accomplished by varying the rate and extent of adaptation in different hair cell types. Type B cells in both the striolar and extrastriolar regions are nonadapting. Hair cells restricted to the striolar region, on the other hand, adapt to maintained hair bundle displacement, with Type C cells adapting most rapidly and Type F and Type E cells adapting least rapidly. These results also suggest that utricular afferents derive much of their low-frequency response dynamics from the adaptation kinetics of their innervated hair cells. In particular, phasic-tonic afferents may derive tonic sensitivity from non-adapting and phasic sensitivity from adapting hair cells. Additional micromechanical factors, such as differences in the way in which individual hair cells couple to the otoconial membrane, may also be involved.

INTRODUCTION

The vertebrate utricle, one of the vestibular otolith organs, is a sensor of static gravity and dynamic linear acceleration (Lewis et al. 1982). In a companion study (Baird 1994) I studied the voltage responses of hair cells in the bullfrog utricle to intracellular current to understand how these receptor cells transduce both tonic and dynamic head and body movement. These studies were motivated by morphophysiological studies that have suggested that the diversity of physiological responses of utricular afferents is determined, at least in part, by regional variations in hair cell transduction mechanisms (Baird and Lewis 1986).

My companion studies revealed that hair cells in the bullfrog utricle, classifiable as Type II by cell body and synapse morphology (Wersall and Bagger-Sjoberg 1974), differ markedly in hair bundle morphology (Lewis and Li 1975). These hair cell types have unique macular distributions. Moreover, they differ in their passive and active membrane properties (Baird 1992, 1994), suggesting that they possess different basolateral membrane conductances. These basolateral conductances, by acting as frequency-dependent filters of the receptor current, can modify the responses of hair cells to natural stimulation, regulating sensitivity, frequency selectivity, and modulating synaptic release. My previous results suggest that the utricle is regionally organized, with hair cells in the central, or striolar, region of the utricle having faster outward potassium currents than hair cells in the peripheral, or extrastriolar, zone. Moreover, hair cells in the innermost striola, but no others, exhibit electrical resonance. This phenomenon, similar to that seen in some auditory (Crawford and Fettiplace 1981; Fuchs et al. 1988; Pitchford and Ashmore 1987) and vibratory (Ashmore 1983; Hudspeth and Lewis 1988; Lewis and Hudspeth 1983) hair cells, is known to sharpen frequency tuning.

In the present study, I was interested in seeing whether hair cell types in the bullfrog utricle might also differ in their voltage responses to hair bundle displacement. I was particularly interested in assessing the contributions of two factors to the responses of utricular hair cells. First, I was interested in examining the effect of hair bundle morphology on the sensitivity of hair cells to natural stimulation. This interest was motivated by the observation that vestibular

hair cells, unlike many auditory hair cells, are not free-standing but rather linked to an accessory cupular or otolithic membrane via the tip of their kinocilium (Hudspeth 1986; Roberts et al. 1988; Wersall and Bagger-Sjoberg 1974). Natural stimuli are initially transmitted to this accessory membrane, which in turn deflects the hair bundles of hair cells. This suggests that the morphology of the hair bundle is important for determining the sensitivities of individual hair cells to natural stimulation. I therefore used theoretical models of hair bundles to examine the contribution of geometric factors associated with these bundles to natural sensitivity in different hair cell types.

I was also interested in examining the contribution, if any, of adaptation to the response properties of utricular hair cells. As previous studies have shown, hair cells in auditory (Crawford et al. 1989, 1991) and vibratory (Assad and Corey 1992; Assad et al. 1989; Eatock et al. 1987; Hacohen et al. 1989) inner ear endorgans adapt to maintained displacements of their hair bundles, sharply limiting their low-frequency sensitivity. This adaptation is mediated by a shift in the displacement-response curve (DRC) of the hair cell along the displacement axis. Adaptation does not depend on the current through the transduction channel (Assad et al. 1989; Eatock et al. 1987). Moreover, adaptation of the receptor current proceeds when hair cells are voltage clamped to their resting membrane potential and so is not a consequence of the voltage change after hair bundle displacement. These observations suggest that the adaptation process occurs within the hair bundle and precedes mechanoelectric transduction. Recent observations of time-dependent changes in hair bundle stiffness are consistent with this conclusion (Howard and Hudspeth 1987, 1988).

Adaptation would be expected to be most useful in inner ear endorgans in which hair cells are subject to large static displacements that could potentially saturate their instantaneous response and compromise their sensitivity to high-frequency stimulation. Hair cells in these organs, by adapting to these static displacements, would restore their sensitivity to smaller, more dynamic stimuli. The adaptation process also permits hair cells to maintain their sensory hair bundle in the most sensitive portion of their DRC. In vestibular otolith organs in which static sensitivity is desirable, such as those endorgans that provide static gravitational sensitivity, any adaptation process in the hair cells may be undesirable. In these hair cells, the adaptive shift process may not exist or may proceed at a very low rate. To test this hypothesis, I measured the rate and extent of the decline of the voltage responses of utricular hair cells to step and sinusoidal hair bundle displacements. I then compared, for similar resting potentials and response amplitudes, the voltage responses of individual hair cells to both hair bundle displacement and intracellular current.

These results suggest that hair cells in the bullfrog utricle, besides differing in their basolateral membrane conductances, also differ in their sensitivity and response dynamics to hair bundle displacement. Sensitivity differences between hair cells are at least partially due to geometric factors associated with the stereociliary array. Differences in the low-frequency response dynamics of utricular hair cells, on the other hand, appear to largely reflect the time course of adaptation in individual hair cells. Moreover,

studies of the peripheral innervation patterns of utricular afferents (Baird and Schuff 1994) further suggest that the kinetics of the hair cell adaptation process also determine the tonic and phasic sensitivities of utricular afferents to head and body movement.

Preliminary accounts of portions of this data have been presented in both abstract (Baird and Schuff 1990, 1991) and short manuscript form (Baird 1992).

METHODS

Whole-mount *in vitro* preparations of the utricular macula were isolated as in the preceding paper (Baird 1994). Briefly, bisected utricular maculae were mounted flat, hair cells uppermost, within a small chamber on the fixed stage of an upright microscope (Zeiss model 16). I then positioned macular pieces so that the morphological polarization vectors of hair cells in the central macula were oriented perpendicular to a stimulating probe. The macular locations and hair bundle morphology of selected hair cells were identified on-line using Nomarski optics and a contrast-enhancement video camera (Hamamatsu C2400-07). Camera images of selected hair cells were stored on an S-VHS videotape recorder (Panasonic PV-S4864). The apical surfaces of selected utricular hair cells were impaled as in the previous paper (Baird 1994) with conventional intracellular microelectrodes pulled from thin-walled aluminosilicate glass.

Hair bundle stimulation

Hair cells were mechanically stimulated by deflecting their hair bundles with stiff borosilicate glass probes pulled to 0.5 to 1.0- μm tips (Corey and Hudspeth 1980). Stimulating probes were bent using a heated filament so that their final millimeter was parallel to the plane of the macula. After being cleaned in a sulfate-nitric acid solution and rinsed in distilled water they were mounted to a piezoelectric bimorph element (Vernitron PZT-5B) and driven via leads soldered to their nickel-plated surface by a waveform generator (Wavetek model 185). The driving signal from this generator was filtered at 1 kHz to minimize a probe mechanical resonance at ~ 10 kHz. Stimulating probes were positioned against the hair bundle of selected hair cells with a hydraulically controlled Huxley-style micromanipulator (Sutter). Probe motion in response to applied voltages was calibrated against a stage micrometer at high magnification ($\times 10,000$).

I had originally hoped to stimulate hair cells at the distal tip of their kinocilium to simulate the action of natural stimulation on the hair bundle. It proved difficult, however, to visualize and couple stimulating probes to the distal tip of the kinocilium in whole-mount preparations. Hair cells were therefore approached from the stereociliary side and stimulated at the level of their longest stereocilia. After coupling the stimulus probe to the hair bundle I made small adjustments of the stimulating probe with the Huxley-style micromanipulator or by adjusting a DC bias voltage applied to the stimulating probe. The probe position that gave the largest voltage response to a 5.0-Hz sinusoidal stimulus was taken as the resting position of the hair bundle. Stimulus probes were observed on a video monitor at high magnification ($\times 10,000$) during hair bundle displacement to verify the lack of relative motion between the probe and the hair bundle. Theoretical models of hair bundles were used to normalize the resulting responses for differences in hair bundle morphology (see below).

Data analysis

Sinusoidal hair bundle displacements at 0.5 or 5.0 Hz, presented in bursts of five to six cycles, were delivered to hair cells via stimulating probes. The amplitude of sinusoidal hair bundle dis-

placements was varied from 0.25 to 2 μm , producing peak voltage responses from <5 to 20 mV. Setting the stimulus amplitude to give a maximum response at <10 mV, I then examined the responses of hair cells to sinusoidal hair bundle displacements in the frequency range from 0.5 to 200 Hz using individual sinusoids and logarithmic frequency sweeps. If possible the responses of hair cells to sinusoidal intracellular current were also recorded. During frequency sweeps hair cells were stimulated at a start frequency (0.5 or 5.0 Hz) for several seconds before initiation of the frequency sweep. They were then stimulated successively for ~ 1 s each with 15 additional frequencies (not including the end frequency) equally spaced in frequency from the start frequency (0.5 or 5.0 Hz) to the end frequency (20 or 200 Hz). For both stimuli the responses to successive sine wave cycles were averaged; the number of averaged cycles varied with stimulus frequency, ranging from 2 at 0.5 Hz to 16 at 125 Hz. Sinusoidal gains and phases were extracted by a Fourier analysis of the averaged responses and expressed with respect to peak intracellular current or hair bundle displacement. Gain was calculated as the ratio of a hair cell's response amplitude at the fundamental frequency divided by the amplitude of intracellular current or hair bundle displacement. Nonlinear distortion was measured as the ratio of the root-mean-squared (rms) amplitude of the second to the fifth harmonics to the rms amplitude of the fundamental component.

The response dynamics of hair cells to hair bundle displacement were further assessed with step displacements of varying amplitude and duration, displacing the hair bundle both parallel and antiparallel to its vector of morphological polarization. Step displacements (100 ms to 10 s in duration) were usually alternated between positive (excitatory) and negative (inhibitory) values, starting at 1 or 2 μm and halving step amplitude with each iteration until reaching a final value of 0.25 μm . In a few cases the stimulating probe was visually observed to lose contact with the hair bundle during the return phase of a step displacement. This loss of contact was correlated with a slow return of membrane potential to its resting value rather than a distinct discontinuity at the termination of the displacement step.

Calculational procedures

DRCs. DRCs were determined from the rising or falling phases of the response to 5.0-Hz sinusoidal hair bundle displacements by plotting, for each cycle of the sinusoidal stimulus, the value of membrane voltage versus hair bundle displacement. The intersection of the DRCs derived from the rising and falling phases of the sinusoidal responses was taken to be the rest position of the hair bundle. To minimize the phase shift and hysteresis associated with the sinusoidal stimulus I then shifted the DRC derived from the rising phase of the sinusoidal response with respect to the displacement axis to place the rest position at zero displacement and normalized the result to its maximum voltage response. Normalized DRCs derived from the rising phases of the sinusoidal responses of individual cells were then averaged to obtain the mean DRCs of different hair cell types. The linear range of DRCs was defined to be the range of displacements that generated 10–90% of the normalized voltage response. Sensitivity of a hair cell to displacement was defined as the slope of its normalized DRC within its linear range.

TRANSFER FUNCTIONS. A nonlinear modeling technique was used to fit a transfer function, $H(s)$, the ratio of the Laplace transform of the voltage response to the Laplace transform of the sinusoidal stimulus, to a set of mean frequency response data given by gain and phase values at specified discrete frequencies (Seidel 1975). The general form and number of parameters of a transfer function, $H(s)$, were first specified in terms of a gain term, any number of simple or complex poles and/or zeros, and, if desired, a zero term raised to a fractional exponent. A Fortran computer

program (TRNFIT) then provided estimates of the fit parameters on the basis of a minimization of the squared error between the fit model and the mean gain and phase data. This error was weighted by the difference in frequency between succeeding data points and taken over all frequencies for which mean data was available. Fits provided by transfer functions were described in terms of rms errors in gain and phase.

Morphological analyses

To examine the hair bundle morphology of individual utricular hair cells in detail, two utricular maculae were prepared for electron microscopy. Maculae were first fixed for 2 h in a solution containing 1.25% glutaraldehyde-1.0% paraformaldehyde and 5 mM CaCl_2 in 0.1 M phosphate buffer (pH 7.25). They were then postfixed at 4°C for 1 h in a 1.0% glutaraldehyde-1.0% osmium tetroxide solution in 0.1 M phosphate buffer, dehydrated in a series of ethanol solutions, and embedded in acrylic resin (London Resin LR White). After embedding, the hair bundles of hair cells were serially sectioned at a thickness of 200 nm on an ultramicrotome (LKB Nova). Thin sections were collected on Formvar-coated grids and stained for 3 min with 10% uranyl acetate in 25% ethanol and 10–20 s with lead citrate. Thick (0.2 μm) sections were cut every 1 μm to ensure the completeness of the hair bundle, to determine the position of thin sections from the apical surface, and to allow individual hair bundles to be identified at the light microscopic level. Thin sections were examined, photographed, and videotaped in a transmitting electron microscope (Zeiss 10C/A) operated at an accelerating voltage of 80 kV.

Hair cells were identified, as in previous studies (Baird 1992, 1994), from their macular location and hair bundle morphology. This was done by examining thick sections of hair bundles at varying heights above the apical surface and noting the size of the hair bundle, the presence or absence of a bulbed kinocilium, and the relative lengths of the kinocilium and longest stereocilia. Selected hair bundles were then further examined in thin sections taken above the height of the apical surface and below the height of their shortest stereocilia. Splayed hair bundles were excluded from further analysis.

Electron photomicrographs and videotaped images of selected hair bundles were input to a computerized image analysis system (Bioquant System IV) for morphometric analysis (Fig. 1, *a* and *b*). For each identified hair bundle the number of stereocilia were counted. Mean stereociliary diameter was determined by averaging the diameter of all stereocilia in the stereociliary array. The mean spacing between adjacent stereocilia was determined by averaging the distance between stereocilia in adjacent rows.

Theoretical models of utricular hair bundles

Theoretical models of utricular hair bundles were created using morphological data from our electron microscopic studies and the previous paper (Baird 1994). I first estimated the relation between angular rotation and linear displacement for different hair cell types, assuming that the stereociliary array pivoted as a stiff beam about its base. Using simple geometry (Fig. 1*c*), the angle of rotation, Θ_r , is equal to $\sin^{-1}(x/l_s)$, where x is the linear displacement applied to the hair bundle and l_s is the length of the longest stereocilia (Table 1, Baird 1994).

The hair bundles of individual hair cell types were further characterized by three geometric factors, the product of which represents the total contribution of these factors to hair cell sensitivity. The first factor was a measure of the mechanical advantage afforded the hair bundle by the differential anchoring points of its kinocilium and longest stereocilia (Fig. 1*c*). This factor was determined from the ratio of the lengths of the kinocilium (l_k) and the

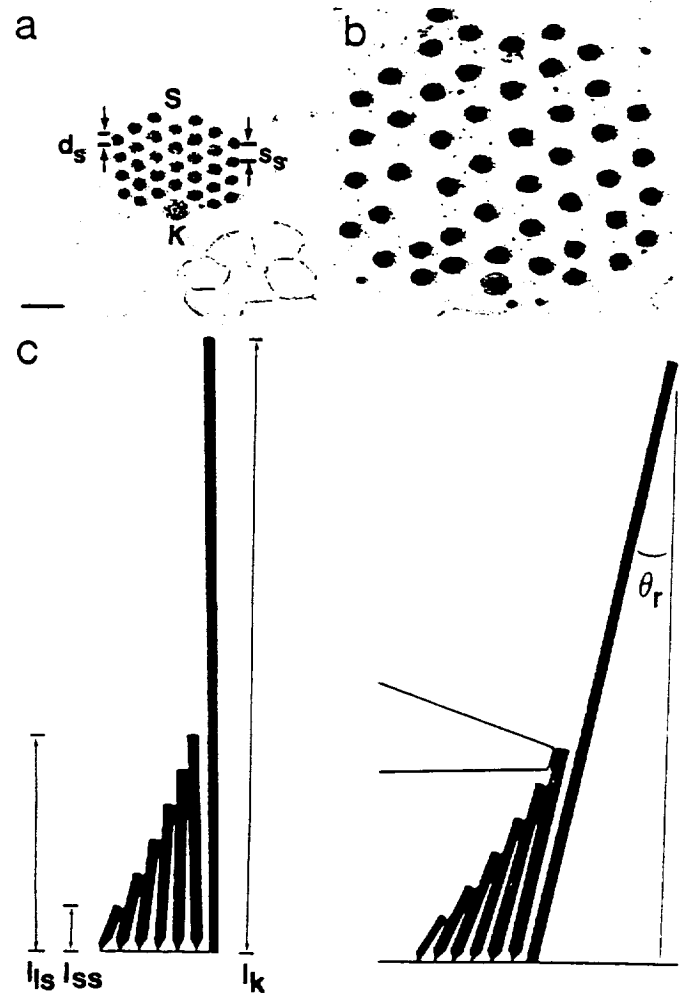


FIG. 1. Transmission electron photomicrographs of cross-sectioned Type B (*a*) and Type F (*b*) hair bundles in the medial extrastricular and striolar regions, respectively. *c*: schematic representation of hair bundle during excitatory displacement with definition of geometric variables used in theoretical modeling. K, kinocilium; l_k , kinociliary length; S, stereocilia; l_s , longest stereociliary length; l_{ss} , shortest stereociliary length; d_s , stereociliary diameter; s_s , stereociliary spacing; Θ_r , angular rotation. Bar: 1 μm .

longest stereocilia (l_s), mean values of which were obtained from the previous paper (Table 1, Baird 1994). A second factor, expressed as the amount of tip-link extension per linear displacement, was calculated using BUNDLE, a computer program created by Dr. D. Corey of the Massachusetts Eye and Ear Infirmary. In this calculation, the length, diameter, and spacing of individual stereocilia in different hair cell types were obtained from my electron microscopic studies. The resting position and resting lengths of tip links were arbitrarily assigned to typical values for saccular hair cells (D. Corey, personal communication). The third factor, a measure of the number of transduction channels, was set equal to 5 times the number of stereocilia in the hair bundle (Holton and Hudspeth 1986).

Statistical procedures

Unless otherwise stated, statistical comparisons of morphometric and physiological data were based on a one-way analysis of variance. Where appropriate, post hoc pairwise multiple comparisons were performed using the Tukey multiple comparison test, adjusting when necessary for unequal group sizes (Miller 1977).

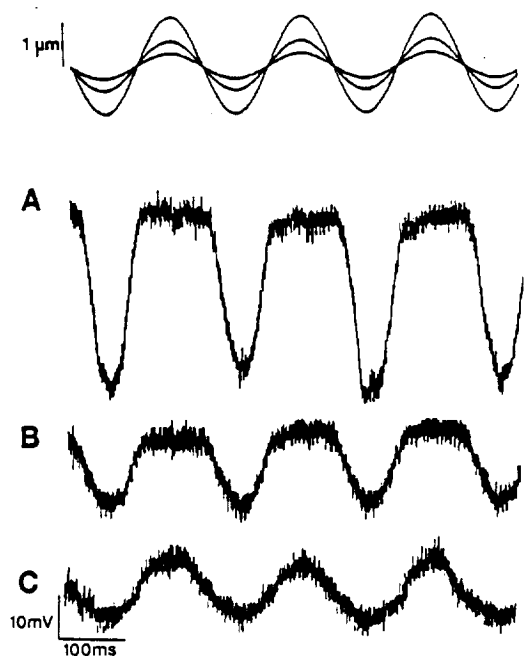


FIG. 2. Voltage responses of a Type F cell to 1.0- μm (A), 0.5- μm (B), and 0.25- μm (C) 5.0-Hz hair bundle displacements.

RESULTS

Responses to sinusoidal hair bundle displacement

The responses of 31 utricular hair cells were examined to 0.5- or 5.0-Hz sinusoidal hair bundle displacements. Of this total, 3 were Type B hair cells located in the medial extrastriola. The remaining 28 hair cells, including 4 Type B, 13 Type C, 7 Type F, and 4 Type E cells, were from the striolar region. I did not obtain the responses of any Type B cells in the lateral extrastriola to hair bundle displacement. The responses of hair cells to sinusoidal hair bundle displacements were characterized by their gains and phases, taken with respect to peak hair bundle displacement. Sinusoidal responses, even in the most sensitive hair cells, were linear for peak response amplitudes <10 mV (Fig. 2C), but become increasingly nonlinear for larger stimulus amplitudes (Fig. 2, A and B). At small stimulus amplitudes nonlinear distortion was usually near 10%. Response linearity was also studied in 10 cells by varying the amplitude of 5.0-Hz sinusoids from 0.25 to 1.0 μm . The variation of sinusoidal gain and phase with amplitude was small, averaging $\pm 10\%$ and $\pm 5^\circ$, respectively.

The sinusoidal gains and phases of 17 hair cells at 0.5 Hz and 31 hair cells at 5.0 Hz are plotted in Fig. 3, A and B, respectively. The gains of Type B cells, whether in the extrastriolar (open circles) or striolar (solid circles) region, were markedly lower than those of other hair cell types (Fig. 3, A and B). This was also true, to a lesser extent, for Type C cells (squares). Type C cells also had large phase leads at 0.5 Hz. The phases of other cells, with the exception of two transitional cells (see below), lagged hair bundle displacement. Type B cells in the striola were more phase lagged than their extrastriolar counterparts. Three hair cells (circled symbols) had transitional responses. These included a Type B cell that, like Type C cells, strongly phase-led hair bundle displacement and a Type C cell that, like Type B

cells, phase-lagged hair bundle displacement. Both these cells were located on the striolar border. In addition, one Type F cell had high gains but, like Type C cells, phase-led hair bundle displacement at both 0.5 and 5.0 Hz.

With the exception of Type C cells, gains at 5.0 Hz were less than or equal to those at 0.5 Hz. The responses of all hair cells were also more phase lagged at 5.0 than at 0.5 Hz. This is evident from Fig. 3C, which plots the gain ratio and

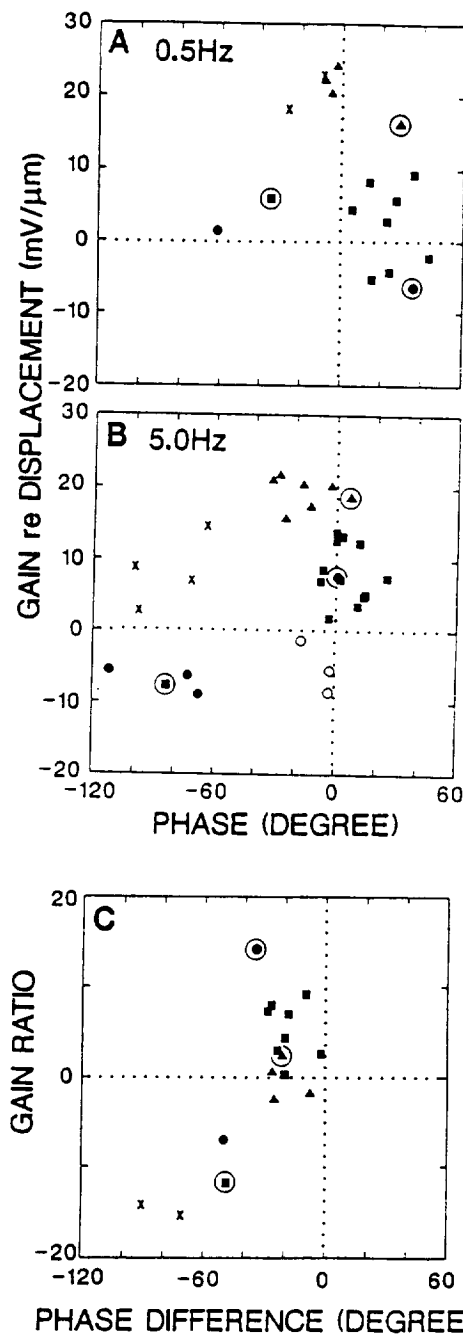


FIG. 3. A and B: gain plotted vs. phase for 17 hair cells at 0.5 Hz (A) and 31 hair cells at 5.0 Hz (B) in response to sinusoidal hair bundle displacement. C: gain ratio and phase difference between voltage responses at 5.0 and 0.5 Hz for 17 hair cells in A recorded to both 0.5- and 5.0-Hz sinusoidal hair bundle displacements. Extrastriolar and striolar cells are represented by open and solid symbols, respectively. Circled symbols: 3 transitional hair cells with intermediate response properties (see text). Circles: Type B. Squares: Type C. Triangles: Type F. Crosses: Type E.

phase difference at 0.5 and 5.0 Hz for 17 cells that were examined at both frequencies. Type B (circles) and Type E (crosses) cells had smaller gains and larger phase lags at 5.0 Hz than at 0.5 Hz, suggesting that they had smaller bandwidths than other hair cell types. By contrast, the responses of Type C cells (squares) at 5.0 Hz were larger than at 0.5 Hz, indicating the presence of low-frequency adaptation (see below). The gains and phases of Type F cells (triangles) were similar at both frequencies.

DRCs of hair cells

DRCs, determined from the rising phase of the voltage responses of hair cells to 5.0-Hz sinusoids (see METHODS), were sigmoidal in shape. They were also asymmetrical, with their resting bundle position displaced toward negative displacements and the positive response evoked by movements toward the kinocilium exhibiting a greater magnitude and more gradual saturating approach than the negative response. When normalized to their largest displacement, these curves differed in both their linear range and their sensitivity to hair bundle displacement. Type B cells, in both the striolar (open circles) ($n = 2$) and medial extrastriolar (solid circles) ($n = 1$) regions, had the largest linear ranges of utricular hair cells (Fig. 4, *top*). Type C cells ($n = 8$) had somewhat smaller linear ranges, averaging $0.75 \mu\text{m}$ (Fig. 4, *top middle*). The linear ranges of Type F ($n = 6$) and Type E ($n = 3$) cells (Fig. 4, *bottom middle* and *bottom*), with the exception of a single transitional Type F cell (open triangles), were $<0.50 \mu\text{m}$ and were significantly smaller than those of Type B and Type C cells. The DRC of the transitional Type F cell closely resembled that of Type C cells. Sensitivity, defined as the slope of the normalized DRC, ranged from <0.50 to $>1.5 \mu\text{m}^{-1}$ and was inversely correlated with linear range.

Theoretical models of hair bundles

Differences in linear range and sensitivity between utricular hair cell types could be due to geometric factors associated with their hair bundles and to the way in which hair bundles were stimulated in this study. To test these possibilities, I created theoretical models of hair bundles using morphological data obtained from light and electron microscopy. These models were used to estimate the in situ sensitivities of different hair cell types and to quantify geometric factors associated with hair bundle types that might be involved in determining the sensitivity of individual hair cells to natural stimulation.

Morphometric data obtained from light and electron microscopy are summarized in Table 1, which also includes the results of statistical tests. Measurements of kinociliary and stereociliary lengths were determined from a morphological study of 135 hair cells in the previous paper (Baird 1994). The mean number, diameter, and spacing of stereocilia in the hair bundle of each hair cell type were measured in a separate population of 88 hair cells whose cross-sectioned hair bundles were examined in the electron microscope. When Type B and Type C cells are compared with Type F and Type E cells, the kinocilia of the former are longer and the shortest and longest stereocilia shorter in length than those of the latter. The stereocilia of Type B and

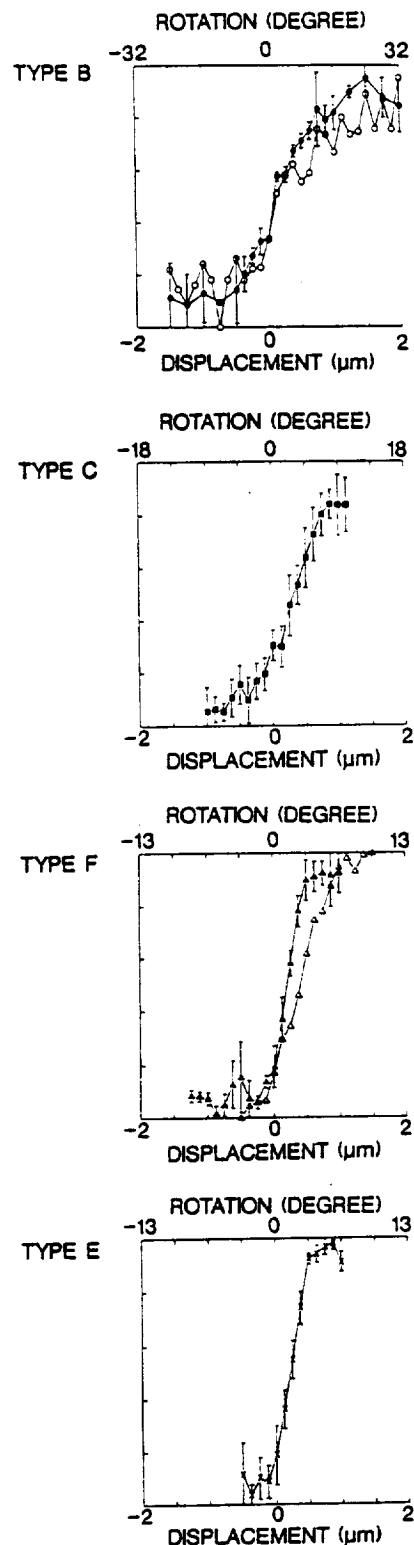


FIG. 4. Mean displacement-response curves (DRCs) of 3 Type B, 8 Type C, 6 Type F, and 3 Type E hair cells determined from the normalized voltage responses to 5.0-Hz hair bundle displacement. For Type B cells, open symbols indicate the DRC of an extrastriolar Type B cell; solid symbols indicate the mean DRC of two striolar Type B cells. For Type F cells, open symbols indicate the DRC of a transitional Type F cell whose voltage response, unlike those of typical Type F cells, demonstrated adaptation to hair bundle displacement (see text); solid symbols indicate the mean DRC of 5 typical Type F cells. Circles: Type B. Squares: Type C. Triangles: Type F. Crosses: Type E. Points: means. Bars: SDs.

TABLE 1. *Morphological properties, utricular hair bundles*

Cell Type	n	Stereociliary						
		Number	Diameter, μm	Spacing, μm	n	Shortest length, μm	Longest length, μm	Kinociliary Length, μm
Type B	22	38.0 \pm 3.9	0.19 \pm 0.03	0.33 \pm 0.04	55	1.1 \pm 0.5	3.8 \pm 1.0	12.2 \pm 1.9
MES	11	39.2 \pm 4.6	0.20 \pm 0.04	0.33 \pm 0.05	30	1.2 \pm 0.5	4.0 \pm 0.9	12.6 \pm 1.6
MS/LS	0	—	—	—	6	0.7 \pm 0.4	2.8 \pm 0.4	10.3 \pm 1.9
LES	11	36.8 \pm 3.0	0.17 \pm 0.01	0.32 \pm 0.04	19	1.1 \pm 0.4	3.9 \pm 1.0	12.1 \pm 2.0
Type C	15	42.4 \pm 6.0	0.24 \pm 0.04	0.38 \pm 0.06	41	1.3 \pm 0.6	6.3 \pm 1.2	16.6 \pm 2.3
Type F	32	46.7 \pm 5.9	0.33 \pm 0.05	0.70 \pm 0.08	23	1.9 \pm 0.9	8.2 \pm 1.3	9.3 \pm 1.2
Type E	19	34.7 \pm 6.3	0.33 \pm 0.05	0.69 \pm 0.08	16	2.1 \pm 0.7	8.9 \pm 1.1	9.8 \pm 1.1

Values are means \pm SD. *n* is number of hair bundles (*left*) or hair cells (*right*). Stereociliary number, diameter, and spacing were measured from electron micrographs of identified hair bundles. Kinociliary and stereociliary lengths were measured with light microscopy in a separate population of cross-sectioned hair cells (Baird 1994, Table 1). The following differences were statistically significant. Stereociliary number: Type F vs. Types B and E, Type C vs. Type E, $P < 0.001$. Stereociliary diameter: Types F and E vs. Types C and B, $P < 0.001$ in all cases. Stereociliary spacing: Types F and E vs. Types C and B, $P < 0.001$ in all cases; Type C vs. Type B, $P < 0.01$. Shortest stereociliary length: Type E vs. Types C and B, Type F vs. Type B, $P < 0.001$; Type F vs. Type C, $P < 0.005$. Longest stereociliary length: Types E and F vs. Types C and B, Type C vs. Type B, $P < 0.001$ in all cases. Kinociliary length: Types C and B vs. Types E and F, Type C vs. Type B, $P < 0.001$ in all cases. MES, medial extrastriola; MS, medial striola; LS, lateral striola; LES, lateral extrastriola.

Type C cells are also smaller in diameter and more closely spaced than those of Type F and Type E cells. Type F cells had greater numbers of stereocilia than other hair cell types. Regional variations in hair bundle morphology were small and insignificant.

Previous studies (Ohmori 1985, 1987) have argued that angular rotation, rather than lateral displacement, is the natural stimulus to hair cells. For technical reasons hair cells in this study were stimulated at the height of their longest stereocilia. Because this height varies for different hair cell types (Table 1) the rotary stimulus applied to hair cells was a function of stereociliary height. Using simple geometry I therefore calculated the relation between linear displacement and angular rotation to normalize the sensitivities of different hair cell types (Table 2). Assuming that each stereocilia pivots as a stiff beam about its base, the angular rotation experienced by the hair bundle, Θ_r , is equal to $\sin^{-1}(x/l_s)$, where x is the linear displacement applied to the hair bundle and l_s is the length of the longest stereocilia (Fig. 1C). Normalized sensitivities, expressed as a function of angular rotation, were markedly different in different hair cell types, with Type B, and to a lesser extent,

Type C cells having lower sensitivities to sinusoidal hair bundle displacement than Type F and Type E cells. Differences in the sensitivities of hair cell types were greatly enhanced by the normalization procedure, suggesting that differences in sensitivity between hair cell types were not due merely to the manner in which hair bundles were stimulated in these studies.

Hair bundles were also characterized by three geometric factors, the product of which represents the total contribution of these factors to hair cell sensitivity. These factors are summarized in Table 2, which also includes the results of statistical tests. The first factor, determined from the ratio of the lengths of the kinocilium and longest stereocilia, was a measure of the mechanical advantage afforded hair bundles by the differential anchoring points of their kinocilium and longest stereocilia. In this analysis I assumed that hair bundles were firmly attached to the otolith membrane by a rigid kinocilium and that displacement was conveyed to the stereociliary array via lateral linkages that attach the tallest stereocilia to the kinocilium. Under these circumstances the kinocilium would be expected to decrease the amplitude of the linear displacement experienced by the stereociliary

TABLE 2. *Normalization factors, utricular hair bundles*

Cell Type	n	Rotary/Lateral Displacement, $^\circ/\mu\text{m}$	Length Ratio, F1	n	Tip-link Extension/Lateral Displacement, F2	Number of Stereocilia, F3	Total, F1 \times F2 \times F3
Type B	55	16.4 \pm 5.0	0.32 \pm 0.08	22	0.092 \pm 0.029	38.0 \pm 3.9	1.07
MES	30	15.5 \pm 4.1	0.32 \pm 0.08	11	0.086 \pm 0.022	39.2 \pm 4.6	1.08
MS/LS	6	21.4 \pm 3.6	0.28 \pm 0.06	—	—	—	—
LES	19	16.2 \pm 5.8	0.33 \pm 0.08	11	0.090 \pm 0.032	36.8 \pm 3.0	1.09
Type C	41	9.5 \pm 1.9	0.38 \pm 0.07	15	0.062 \pm 0.014	42.4 \pm 6.0	1.18
Type F	23	7.2 \pm 1.1	0.89 \pm 0.10	32	0.087 \pm 0.017	46.7 \pm 5.9	3.62
Type E	16	6.5 \pm 0.8	0.92 \pm 0.12	19	0.076 \pm 0.010	34.7 \pm 6.3	2.43

Values are means \pm SD. *n* is number of hair cells (*left*) or hair bundles (*right*). Length into (F1) is the inverse ratio of the kinociliary and longest stereociliary lengths, obtained from the previous paper (Baird 1994, Table 1). Rotary/linear displacement is defined by $\sin^{-1}(l/l_s)$, where l_s is the length of the longest stereocilia. Stereociliary number, diameter, and spacing were measured from electron micrographs of identified hair bundles. Tip-link extension/lateral displacement (F2) is obtained from the above measurements and the computer program BUNDLE (see text). The following differences were statistically significant. Rotary/lateral displacement: Type B vs. Types C, F, and E, striolar Type B vs. MES Type B, $P < 0.001$; striolar Type B vs. LES Type B, $P < 0.01$; Type C vs. Types F and E, $P < 0.05$. Length ratio (F1): Types E and F vs. Types C and B, Type C vs. Type B, $P < 0.001$ in all cases. Tip link extension/lateral displacement (F2): Types B and F vs. Type C, $P < 0.001$; Type B vs. Type E, $P < 0.05$. Number of stereocilia (F3): Type F vs. Types B and E, Type C vs. Type E, $P < 0.001$. For abbreviations, see Table 1.

array and the in situ sensitivity of a hair cell would actually be less than that measured in this study. This reduction, which ranged in value from 0.16 to 1.08, was 2–3 times larger in Type B and Type C cells than in Type F and Type E cells (Table 2). A second factor, a measure of tip-link extension per linear stereociliary displacement, was calculated assuming that the hair bundle was stimulated at its longest stereocilia and that each stereocilia pivoted as a stiff beam about its base. This factor, which was largely dependent on the height and spacing of adjacent stereocilia in the stereociliary array, ranged in value from 0.04 to 0.18 and was larger in Type B and Type F cells than in Type C and Type E cells. Finally, I considered the possibility that hair bundles differed in their number of stereocilia and therefore the number of their transducer channels. The number of stereocilia in individual hair cells varied by a factor of two, ranging from 24 to 57. The mean number of stereocilia was significantly larger in Type F cells than in other hair cell types. On the basis of geometric factors alone, the above analysis suggests that Type B and Type C cells should have sensitivities to linear displacement 2–3 times smaller than those of Type F and Type E cells. This difference was due largely to the large mechanical advantage afforded Type F and Type E cells by their short kinocilium and long stereocilia.

Response dynamics to sinusoidal hair bundle displacements

The responses of 16 hair cells, including 2 Type B, 8 Type C, 3 Type F, and 3 Type E cells, were obtained to logarithmic sweeps of hair bundle displacement between 0.5 and 200 Hz (Fig. 5). There were striking differences in the responses of hair cells to sinusoidal hair bundle displacement. The responses of Type B cells were small and decreased sharply with increasing frequency. Type C cells had larger responses and responded to much higher frequencies than Type B cells. In addition, the responses of Type C cells showed conspicuous response declines for frequencies <5 Hz. Type F and Type E cells displayed the largest responses to hair bundle displacement. Type F cells had responses similar to those of Type C cells but did not exhibit response declines at low frequency. The responses of Type E cells declined sharply with increasing frequency, resembling the responses of Type B cells. At higher stimulus amplitudes these hair cells were also strongly rectifying, displaying a marked DC response at higher frequencies for which no fundamental response was evident. This rectification, unlike the low-frequency response declines in Type C cells (see below), was also evident in the responses of Type E cells to intracellular current (Baird 1994).

The effect of stimulus amplitude on sinusoidal gain and phase was not systematically examined at all stimulus frequencies. Rather, stimulus amplitude was adjusted between 0.5 and 2 μm to give a maximum response at <10 mV, a level of response for which the variation of sinusoidal gain and phase with stimulus amplitude at 5.0 Hz was small (Fig. 2). A similar result was seen in two Type C cells in which sinusoidal gain and phase were examined at multiple stimulus amplitudes at additional frequencies, justifying the presentation of frequency response data in the form of normalized Bode plots.

Bode plots for 16 individual hair cells for which voltage responses were obtained at four or more frequencies between 0.5 and 125 Hz are shown as solid lines in Fig. 6. Where applicable, the group means for the four hair cell types, separately calculated for gains and phases, are also shown (open circles). The responses of two Type B cells, one from the striola and the other from the medial extrastriola, are shown at the far left. For frequencies >5 Hz the extrastriolar Type B cell displayed falling gains and increasing phase lags with increasing frequency. The response of this cell was not examined at lower frequencies. The striolar Type B cell had a smaller bandwidth than its extrastriolar counterpart. In contrast, Type C cells displayed 10- to 20-fold gain enhancements as frequency was increased and phase leads, ranging from 20 to 40°, were seen between 0.5 and 20 Hz. At higher frequencies Type C cells displayed decreasing gains and increasing phase lags. Individual Type C cells displayed differing amounts of gain enhancement and phase lead at low frequencies. For higher frequencies the response dynamics of individual Type C cells were similar, suggesting that the response dynamics of Type C cells were governed by two components, one dominating their responses at lower frequency and the other dominating at higher frequencies (see below). Rapidly adapting Type C cells (heavy lines), distinguished by large gain enhancements and large phase leads, differed from more slowly adapting Type C cells (light lines) in two respects. 1) they had higher sensitivities to hair bundle displacement. 2) they displayed gain enhancements and phase leads at higher frequencies than more slowly adapting Type C cells. The degree of adaptation in Type C cells was also correlated with macular location, with rapidly adapting cells tending to be located in the outer striolar rows and slowly adapting cells in the inner striolar rows. In particular, two of three rapidly adapting Type C cells were located in the outer rows, whereas three of five slowly adapting Type C cells were located in the inner rows. Type F cells, with one prominent exception (heavy lines), had near-constant gains and phases hovering near zero at low frequencies. The exceptional cell, like Type C cells, displayed increasing gain and phase leads at low frequencies and, unlike typical Type F cells, was located in the outer striolar rows. At higher frequencies, Type F cells displayed decreasing gains and increasing phase lags. Type E cells had small bandwidths, displaying falling gains and increasing phase lags with increasing frequency.

Transfer functions

The gains and phases of individual Type B cells and the group means and phases of the hair cell types to hair bundle displacement were fit by a transfer function, $H(s) = H_A(s) \cdot H_T(s)$, made up of two components. As I will argue in the DISCUSSION, it is convenient to think of $H_A(s)$ as reflecting the dynamics of an adaptation process associated with mechanoelectric transduction and $H_T(s)$ as a dynamic component introduced by other transduction processes within the hair cell, primarily the gating kinetics of voltage-dependent conductances in the apical and basolateral membrane.

The response dynamics of adapting hair cells could not

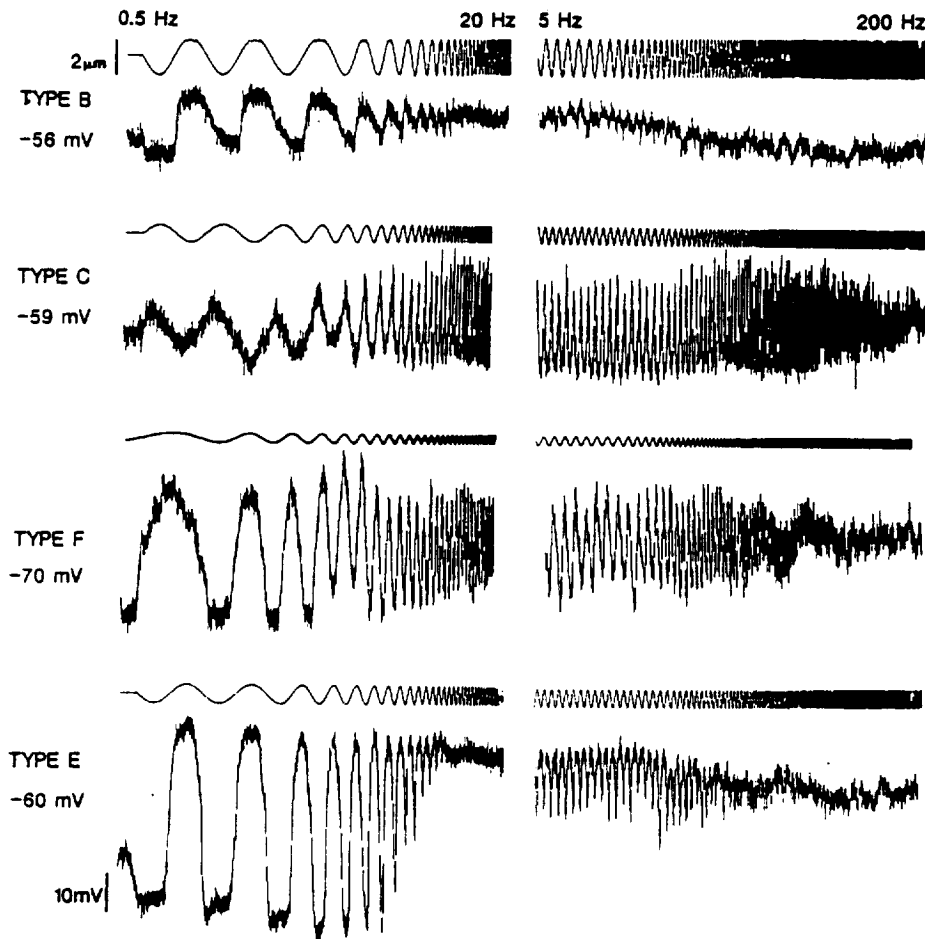


FIG. 5. Voltage responses of typical Type B, Type C, Type F, and Type E cells to logarithmic sweeps of sinusoidal hair bundle displacement in the frequency ranges of 0.5–20 and 5–200 Hz.

be fit by an integral lead operator because low-frequency gains in these cells increased as a fractional power of sinusoidal frequency and phase leads, even in the most rapidly adapting hair cells, did not approach 90° . I therefore adopted the first-order fractional-lead operator, $H_A(s) = (1 + s\tau_A)^{k_A}$, where k_A is a fractional exponent and τ_A is an adaptation time constant, to provide the gain enhancement and phase leads seen in adapting hair cells. This operator, above an upper corner frequency of $1/(2\pi\tau_A)$, introduces a gain that increases as f^{k_A} and a phase lead that approaches $90^\circ \cdot k_A$ (Thorson and Biederman-Thorson 1974). The high-frequency response dynamics of utricular hair cells were represented by a second-order lag element, $H_T(s) = 1/(1 + s\tau_{T1})(1 + s\tau_{T2})$, where τ_{T1} and τ_{T2} are time constants, because the phase lags of many cells at these frequencies were $>90^\circ$. This lag element accounts for the high-frequency phase lags observed in all hair cells and for the fact that the high-frequency phase leads seen in adapting hair cells were smaller than would be predicted solely from the fractional-lead operator.

The mean frequency response data of each hair cell type, illustrated in Fig. 7, was fit to the transfer function $H(s) = H_A(s) \cdot H_T(s)$ using a least-squares fit (see METHODS). The best-fitting transfer functions for each hair cell type in the frequency range from 0.5 to 125 Hz, shown as solid lines in Fig. 7, provided good approximations to the experimental data. The average gain and phase errors for all 16 hair cells were 9.5% and 3.7° , respectively. The small size of the fit-

ting errors implies that the Bode plots for the mean frequency response data can be summarized in terms of their transfer function parameters. The best-fitting transfer function parameters for the different hair cell types are summarized in Table 3. Type B and Type F cells (Fig. 7, A and B) had strongly overdamped response dynamics. $H_T(s)$ in these cells could be reduced to a first-order lag element, $H_T(s) = 1/(1 + s\tau_T)$, with little or no increase in fitting errors, indicating that their response dynamics in the frequency range from 0.5 to 125 Hz were dominated by a single real pole. The mean response dynamics of Type C and Type E cells (Fig. 7, C and D), on the other hand, were best fit by second-order lag elements. The gain and phase errors of Type C cells (with those for Type E cells in parentheses) for a second-order lag element were 6.2% (9.6%) and 4.4° (3.0°), respectively. The best-fitting one-term operator, $H_T(s) = 1/(1 + s\tau_T)$, with $\tau_T = 9.1$ s (13.8 s), increased these errors to 9.0% (10.8%) for gain and 7.1° (17.7°) for phase.

Differences in the low-frequency response dynamics of utricular hair cells to hair bundle displacement were largely accounted for by variations in a single parameter, k_A . Type B and Type F cells, at least for frequencies >0.5 Hz, did not exhibit adaptation and had near-zero k_A values. Type C cells, on the other hand, uniformly adapted to hair bundle displacement and had a mean k_A value of 0.24. Individual Type C cells that differed in their degree of adaptation to hair bundle displacement also differed in their values of k_A ,

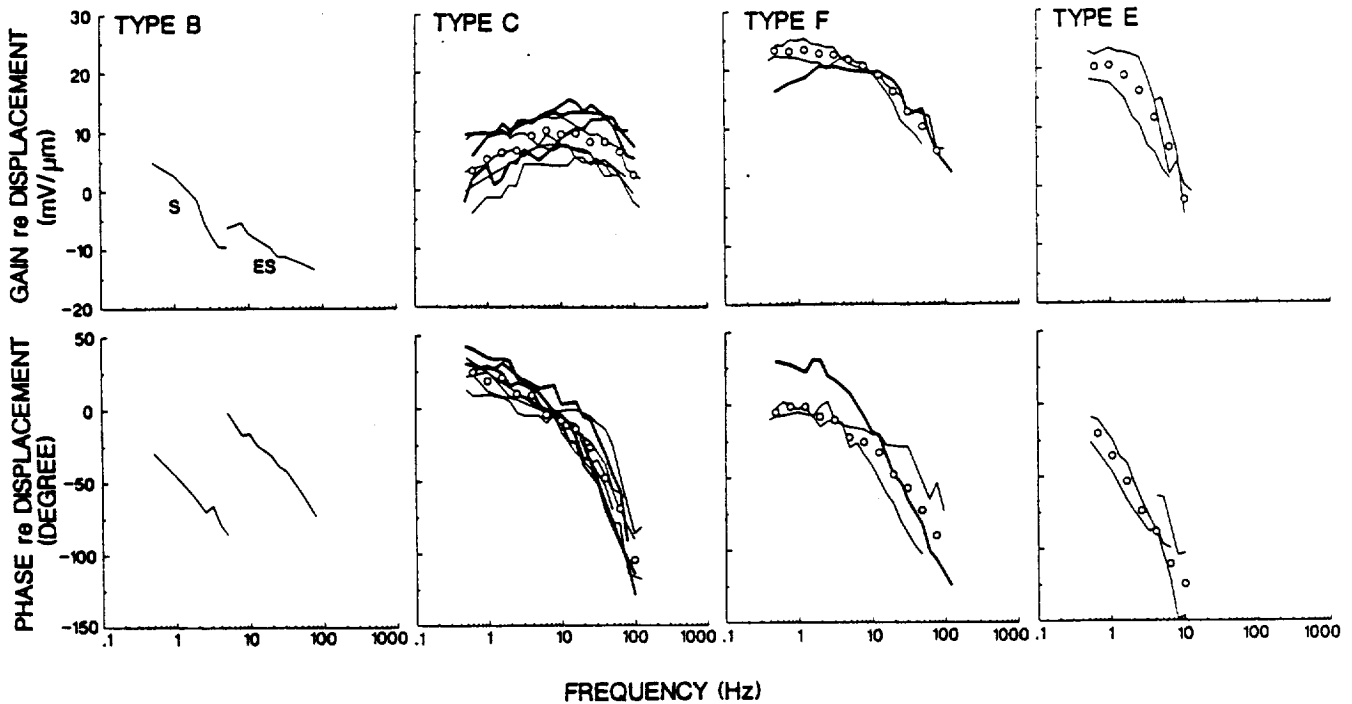


FIG. 6. Bode plots of gains (*top*) and phases (*bottom*) for 2 Type B, 8 Type C, 3 Type F, and 3 Type E cells to sinusoidal hair bundle displacement. Lines: curves for individual cells. Circles: means for all cells in each category. For Type C cells, heavy lines delineate individual curves of rapidly adapting Type C cells. For Type F cells, heavy line delineates a transitional Type F cell whose voltage response, unlike those of typical Type F cells, demonstrated adaptation to hair bundle displacement (see text). Phase leads are plotted as positive (upward) values.

with rapidly adapting Type C cells ($n = 3$) having k_A values ranging from 0.27 to 0.38 and slowly adapting Type C ($n = 5$) cells having k_A values ranging from 0.11 to 0.20. Type E

cells had intermediate k_A values, indicating that they, like Type C cells, were slowly adapting to hair bundle displacement (see below). Estimates of τ_A were only reliable when

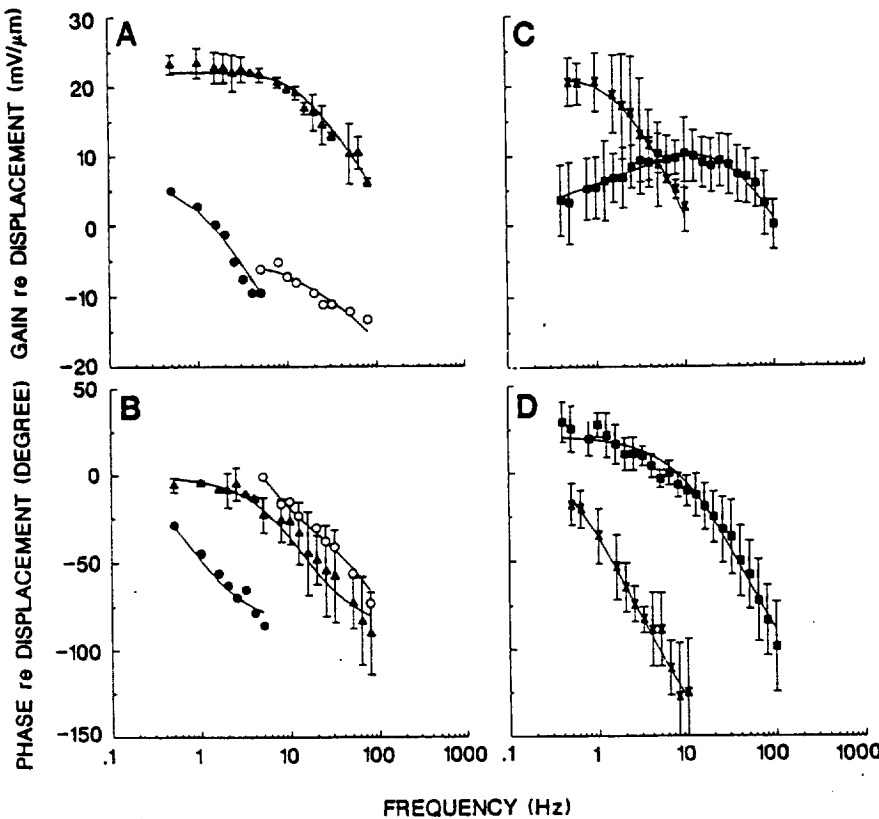


FIG. 7. Mean Bode plots of gains (*A* and *C*) and phases (*B* and *D*) for 16 hair cells in Fig. 6 to sinusoidal hair bundle displacement. Open and solid symbols: extrastriolar and striolar cells, respectively. Lines indicate best-fitting transfer functions to mean frequency response data (see text). Circles: Type B. Squares: Type C. Triangles: Type F. Crosses: Type E. Points: means. Bars: SDs.

TABLE 3. Mean transfer function parameters, hair bundle displacement

Cell Type	n	Hair Bundle Displacement			
		k_A	τ_A , s	τ_{T1} , ms	τ_{T2} , ms
Type B					
MES	1	0.00	—	5.25	0.01
MS/LS	1	0.04	—	3.00	205.0
LES	—	—	—	—	—
Type C	8	0.24	0.17	1.07	6.96
RA	3	0.35	0.12	2.35	5.61
SA	5	0.13	0.22	0.34	4.33
Type F	2	0.01	—	7.84	1982.
Type E	3	0.14	1.33	25.22	135.6

Values are means. n is number of hair cells. k_A and τ_A are the exponent and time constant of a fractional-lead operator; τ_{T1} and τ_{T2} are time constants of a 2nd-order lag operator. Three transitional cells—1 Type B, 1 Type C, and 1 Type F—are not included in the above averages (see text). RA, rapidly adapting; SA, slowly adapting. For other abbreviations, see Table 1.

the fractional-lead operator was effective (i.e., when k_A was nonzero) because large changes in τ_A could be compensated by small changes in k_A . This was true only for Type C and, to a lesser extent, Type E cells. For these cell types, estimates of τ_A were 0.17 s and 1.33 s, respectively.

Response dynamics to intracellular current and hair bundle displacement

In a previous study (Baird 1994) I examined the response dynamics of a separate population of hair cells to intracellular current. The gains of hair cells to intracellular current were constant at low frequencies and decreased with increasing frequency. These gains differed markedly, reflecting the different resistances of hair cells at resting membrane potential. The phases of hair cells in response to intracellular current hovered near zero at low frequencies and became increasingly phase lagged for increasing frequency. When possible, I examined the responses of individual hair cells to both sinusoidal intracellular current and hair bundle displacement at multiple frequencies. This was accomplished in seven cells, including six Type C cells and a Type F cell whose voltage responses closely resembled those of Type C cells. For other hair cell types this information was either unavailable or was obtained at different resting membrane potentials, preventing a direct comparison of the response dynamics to the two stimuli.

The response dynamics of hair cells to sinusoidal hair bundle displacement differed in two respects from their response dynamics to intracellular current. First, hair cells that adapted to hair bundle displacement did not adapt to intracellular current. This is seen in Fig. 8, which illustrates the Bode plots of a rapidly adapting (Fig. 8, A and B) and slowly adapting (Fig. 8, C and D) Type C cell and the mean Bode plot of six Type C cells (Fig. 8, E and F) to both intracellular current and hair bundle displacement. In each case the responses to intracellular current (open symbols) did not display the gain enhancements and large phase leads displayed by the responses to hair bundle displacement (solid symbols) at low frequencies. Rather, adapting

hair cells displayed low-pass filter characteristics in response to sinusoidal current, with constant gains and near-zero phases at low frequencies and decreasing gains and increasing phase lags at higher frequencies. Second, with the exception of one Type C cell, hair cells had higher bandwidths to hair bundle displacement than they did to intracellular current, presumably reflecting the increased conductance resulting from the opening of increased numbers of transduction channels during hair bundle displacement. This was also reflected in the time constants of the best-fitting transfer functions to individual hair cells, which were larger in response to intracellular current than to hair bundle displacement. The mean dominant time constant of six Type C cells, for example, was 2.6 s to intracellular current but only 2.2 s to hair bundle displacement.

I was unable to obtain the responses of individual Type B and Type E cells to both intracellular current and hair bundle displacement at multiple stimulus frequencies. I was, however, able to compare the responses of these cells to 5.0-Hz sinusoids of intracellular current and hair bundle displacement. In each case, hair cells displayed smaller phase lags at this frequency to hair bundle displacement than they did to intracellular current, suggesting that they had higher bandwidths to the former stimulus.

Responses to step hair bundle displacements

Because of a lack of data at low frequencies it was not always possible to determine whether hair cells were adapting using sinusoidal displacements. The low-frequency responses of hair cells to hair bundle displacement were therefore further assessed with step displacements. In general, adapting hair cells displayed adaptation to excitatory displacements that depolarized their membrane potentials. Inhibitory displacements, which hyperpolarized membrane potential, caused little or no adaptation during the step stimulus but did produce a depolarizing overshoot and subsequent adaptation at the termination of the step stimulus.

Hair cells with differing hair bundle morphology had markedly different responses to hair bundle displacement. This is illustrated in Fig. 9, which depicts typical voltage responses of each hair cell type to both excitatory hair bundle displacement (*left*) and, if available, intracellular current (*right*). Type B cells in both the striolar ($n = 1$) and extrastriolar ($n = 1$) regions displayed little or no adaptation to maintained hair bundle displacement. The responses of these cells to step displacement strongly resembled their responses to steps of intracellular current. Hair cells restricted to the striolar region, on the other hand, had different responses to hair bundle displacement and intracellular current, displaying a marked adaptation to the former but not the latter stimulus. This adaptation took the form of response declines during step displacements and hyperpolarizing undershoots at their termination. The rate and extent of adaptation differed in different hair cells. As for sinusoidal stimuli, Type C cells had either rapidly or slowly adapting responses. Rapidly adapting Type C cells ($n = 4$), after initially rising to a peak value, declined in <50–100 ms to a small steady-state level. Other Type C cells ($n = 3$) had slower rates of adaptation, declining within 100–200 ms to larger steady-state levels. The rate of

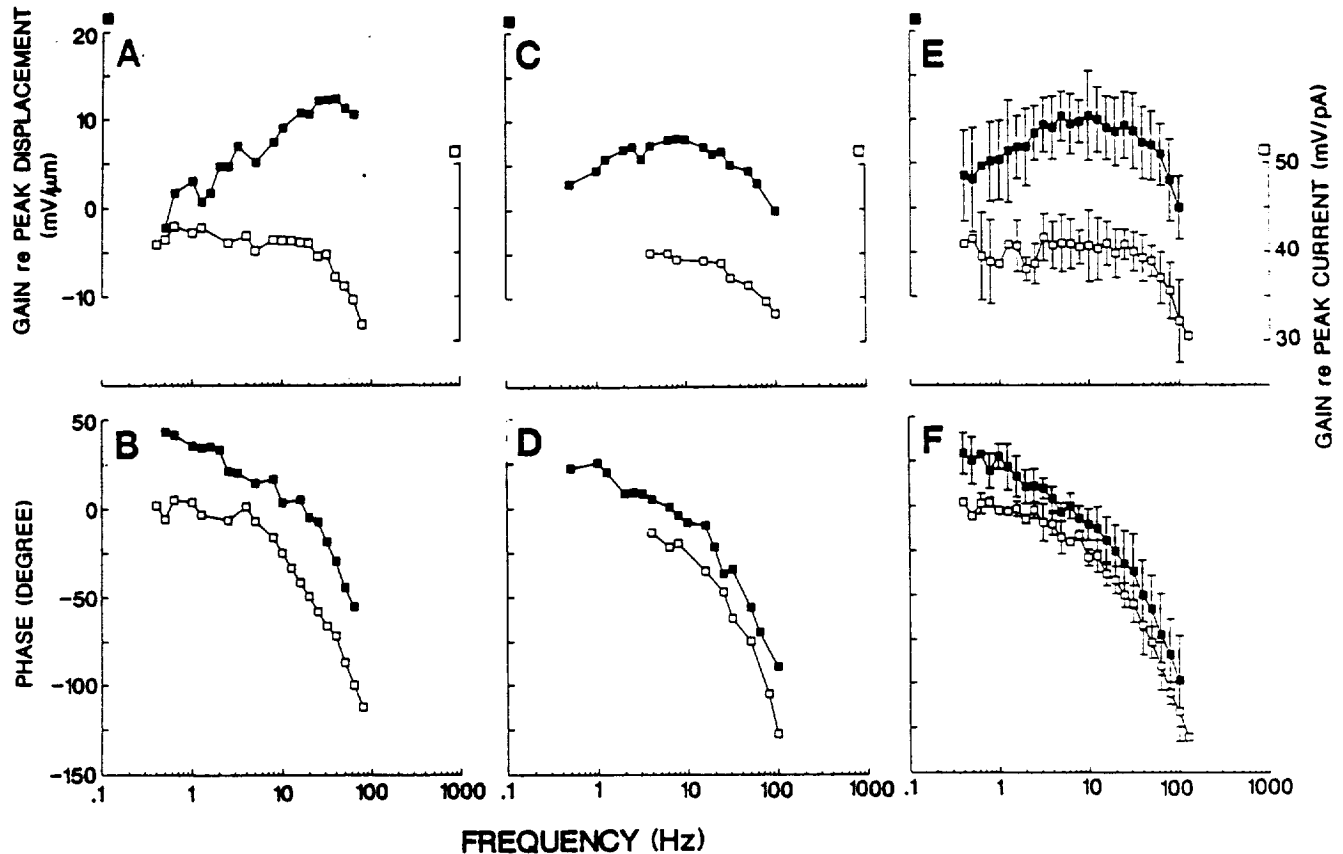


FIG. 8. Bode plots of gains and phases of individual rapidly (*A* and *B*) and slowly (*C* and *D*) adapting Type C cells and mean Bode plots of 6 Type C cells (*E* and *F*) to sinusoidal intracellular current (open squares) and hair bundle displacement (solid squares). Points: means. Bars: SDs.

adaptation of Type C cells to step displacement, as for sinusoidal stimuli, was correlated with their macular location, with rapidly and slowly adapting cells located in the outer and inner striolar rows, respectively. Type F ($n = 4$) and Type E ($n = 2$) cells adapted very slowly, reaching steady-state values in 300–500 ms, and displayed pronounced hyperpolarizing undershoots at the termination of excitatory step displacements. In Type E cells these hyperpolarizing undershoots were also seen, albeit to a smaller extent, in the responses to intracellular current. With the exception of Type E cells, rapidly adapting cells declined to a greater extent than slowly adapting cells. Type E cells, although slowly adapting, displayed large response declines to step displacement.

There was good agreement between the time constants of adaptation measured in the time and frequency domain. In four rapidly adapting Type C cells the mean time constant of adaptation to step displacement, measured as the time constant of the best-fitting exponential, was equal to 0.06 s, a value in reasonable agreement with 0.12 s, the time constant obtained from the best-fitting transfer function for three rapidly adapting Type C cells to sinusoidal stimulation (Table 3). A similar result was obtained for slowly adapting Type C cells, for which the time constants of adaptation to step and sinusoidal displacement were 0.20 s and 0.22 s, respectively. The best-fitting transfer functions for each hair cell type, summarized in Table 3, were also used to derive theoretical responses of these hair cells to step

displacement (data not shown). Parameters used in these calculations were, with the exception of a constant gain term, derived from the mean Bode plots of each hair cell type. With one exception, the predicted response declines after excitatory step displacement were close to that actually observed. The one discrepancy involved the time course of the hyperpolarizing undershoot after the response decline in rapidly adapting Type C cells, which was more pronounced than that seen in response to step displacements.

Adaptation versus step amplitude

The peak and steady-state responses of hair cells were examined to excitatory step displacements of varying amplitude (Fig. 10). For small amplitudes the peak responses of hair cells to hair bundle displacement were linearly related to the amplitude of hair bundle displacement. At larger amplitudes the peak responses of hair cells began to saturate. The range of linear response and sensitivity to hair bundle displacement was different in different hair cell types. Type B cells, for example, produced the smallest voltage responses to hair bundle displacement. These responses, however, were linear over a wide range, barely displaying saturation at 2- μm displacements. Type C cells produced larger voltage responses but only over a narrower range, displaying saturation for hair bundle displacements $> 1 \mu\text{m}$. Type F and Type E cells had the large voltage re-

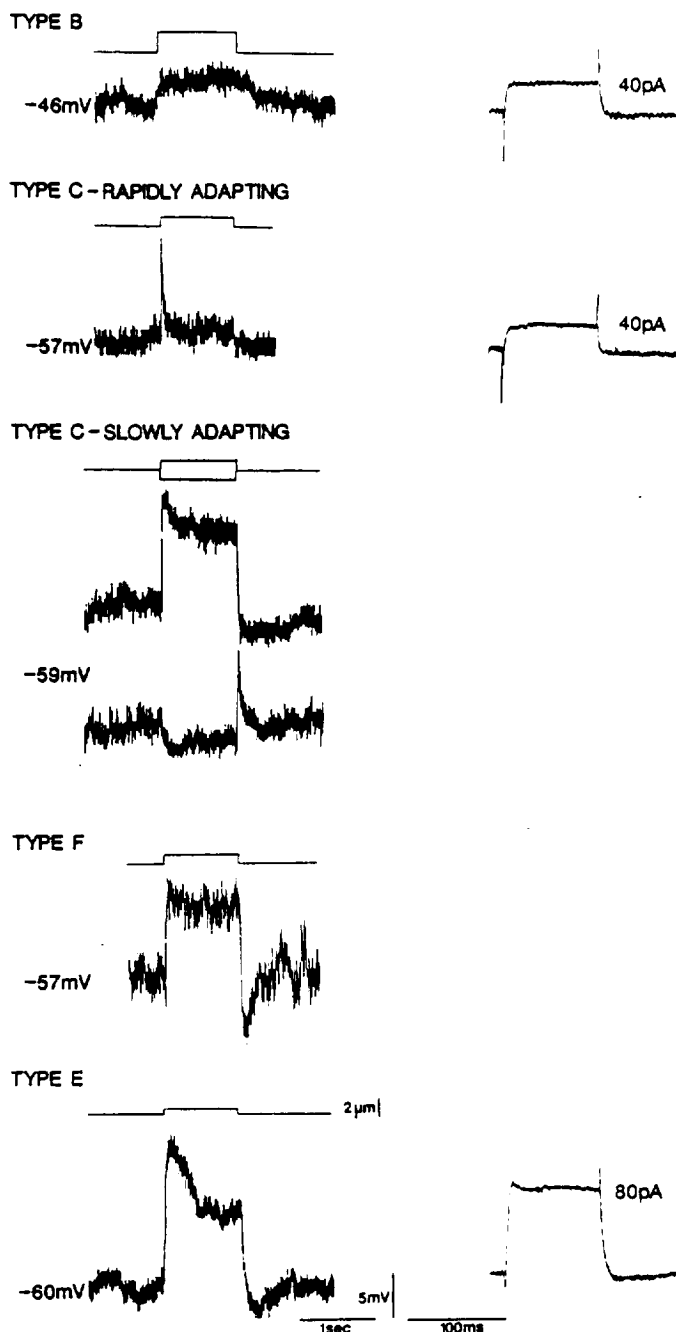


FIG. 9. Voltage responses of typical Type B, Type C, Type F, and Type E cells to steps of hair bundle displacement (*left*) and intracellular current (*right*). Numbers at *left* and *right* indicate the resting membrane potential of the cell and the amplitude of the current stimulus, respectively.

sponses but most restricted linear range of all utricular hair cells, displaying saturation for step displacements $>0.5 \mu\text{m}$. With the exception of Type B cells, the lengths of the longest stereocilia of striolar hair cells were similar (Table 1), indicating that this discrepancy was not due merely to the way in which hair cells were stimulated in this study. The time course of adaptation, at least for displacements in the linear operating range, was not a function of stimulus amplitude.

With the possible exception of rapidly adapting Type C cells, the steady-state responses of adapting hair cells, at

least for small step amplitudes, were also linearly related to step amplitude. The steady-state responses of rapidly adapting Type C cells were relatively independent of stimulus amplitude, although this was difficult to measure because of the small size of these responses. Thus the extent of adaptation, as measured by the inverse ratio of the peak and steady-state responses, was independent of stimulus amplitude. The extent of adaptation was also, as mentioned above, different in different hair cell types, being least in Type F cells and greatest in rapidly adapting Type C cells.

The steady-state sensitivities of Type B hair cells, whether in the striolar or extrastriolar region, to step stimulation were in reasonable agreement with their sensitivities to low-frequency sinusoidal stimulation (Table 4), suggesting that these cells do not adapt to maintained hair bundle displacement. The sensitivity of a Type B cell in the medial extrastriola to step displacement and 5.0-Hz sinusoidal displacement, for example, was 0.63 and 0.59 $\text{mV}/\mu\text{m}$. For a striolar Type B cell the sensitivity to step displacement and 0.5-Hz sinusoids was 1.95 and 1.18 $\text{mV}/\mu\text{m}$, respectively. The mean sensitivity of Type F cells to step displacement, on the other hand, was significantly less than their sensitivity to 0.5 Hz sinusoidal stimulation (8.58 and 13.23 $\text{mV}/\mu\text{m}$, respectively). This suggests that although little evidence of adaptation was seen in these cells in response to sinusoidal stimulation (Figs. 5-7), Type F cells do adapt to very low-frequency displacement. This suggestion is further supported by the results of studies using long-duration step displacements (see below). As expected, the sensitivities of Type C and Type E cells to step displacement were also less than their sensitivities to low-frequency sinusoidal stimulation, confirming that they also adapt to maintained hair bundle displacement. Type C cells, for example, had mean sensitivities of 1.11 $\text{mV}/\mu\text{m}$ to step displacement and 1.56 $\text{mV}/\mu\text{m}$ to 0.5-Hz sinusoidal displacement. The mean sensitivities of Type E cells to the same stimuli were 9.68 and 11.12, respectively.

Adaptation versus step duration

The effects of increasing step duration on adaptation were examined at step durations ranging from 100 ms to 10 s (Fig. 11). In nonadapting Type B cells there was no sign of adaptation to either 1- or 2-s step displacements. Other hair cell types, however, displayed increasing amounts of adaptation at longer maintained hair bundle displacements. This was seen most clearly in Type F cells, which were relatively nonadapting at 100- and 200-ms step displacements but demonstrated increasing amounts of adaptation in response to steps of longer duration. In rapidly adapting Type C cells (data not shown) the time course of adaptation was similar at all step durations, confirming that adaptation in these cells is completed before 100 ms. I did not record the responses of these hair cells to shorter step durations. More slowly adapting Type C hair cells, on the other hand, had different time courses for different step durations. In slowly adapting Type E cells adaptation continued despite a lack of maintained stimulus, suggesting that adaptation was activated by the excitatory hair bundle displacement but delayed by the kinetics of some intermediate process. This delay may reflect the kinetics of calcium regulation in dif-

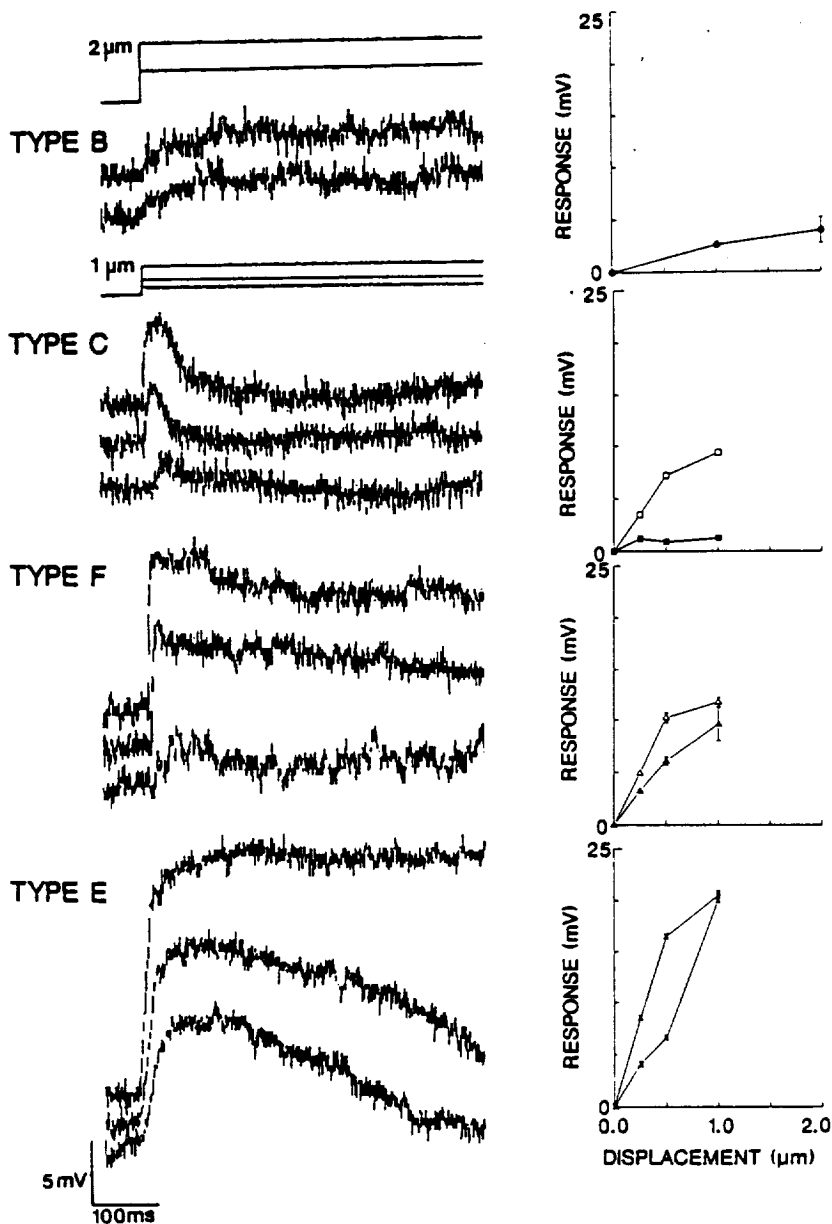


FIG. 10. Voltage responses of typical Type B, Type C, Type F, and Type E hair cells to step hair bundle displacements of varying amplitude. Peak (open symbols) and steady-state (solid symbols) responses for each hair cell are plotted vs. hair bundle displacement to the right. Circles: Type B. Squares: Type C. Triangles: Type F. Crosses: Type E. Points: means. Bars: SDs.

ferent hair cell types and may be the rate-limiting step in determining the kinetics of the adaptation process in different hair cell types (see below).

DISCUSSION

In the companion paper (Baird 1994) I demonstrated that utricular hair cells in different macular zones differed in their responses to intracellular current, implying that these cells differed in their complement of basolateral membrane conductances. In this study I demonstrate that utricular hair cells in different macular zones also differ in their sensitivity and response dynamics to hair bundle displacement. Because the response dynamics of hair cells to intracellular current differ from those to hair bundle displacement I argue that these differences arise not from the passive or active membrane properties of hair cells but rather from an adaptation process associated with mechano-electric transduction. Adaptation, by preventing tonic dis-

placements from saturating the mechano-electric response, allows hair cells to maintain sensitivity to higher-frequency displacements. More specifically I suggest that utricular hair cells vary in their rate of adaptation to maintained hair bundle displacement, regulating their sensitivity and frequency selectivity and allowing some hair cell types to encode static gravity and others to encode high-frequency linear acceleration.

Previous studies have demonstrated that adaptation is not a universal property of hair cells. Hair cells in chick vestibular endorgans (Ohmori 1985, 1987) and the mammalian cochlea (Russell et al. 1989), for example, do not adapt at all to hair bundle displacement. Hair cells in different endorgans are also known to differ in their rates of adaptation. In the turtle cochlea (Crawford et al. 1989, 1991), for example, hair cells adapt an order of magnitude faster than do hair cells in the bullfrog sacculus (Assad et al. 1989; Eatock et al. 1987; Hacohen et al. 1989). Hair cells within individual endorgans, however, tend to have similar adapta-

TABLE 4. *Response gains, step and sinusoidal hair bundle displacements*

Cell Type	Sinusoidal Displacements Gain		Step Displacements Gain	
	0.5 Hz, mV/ μ m	5.0 Hz, mV/ μ m	Peak, mV/ μ m	Steady-State, mV/ μ m
Type B	1.18 (1)	0.52 \pm 0.18 (6)	—	1.29 \pm 0.93 (2)
MES	—	0.59 \pm 0.25 (3)	—	0.63 (1)
MS/LS	1.18 (1)	0.46 \pm 0.08 (3)	—	1.95 (1)
LES	—	—	—	—
Type C	1.56 \pm 0.91 (8)	2.83 \pm 1.30 (12)	5.49 \pm 1.69 (7)	1.11 \pm 0.62 (7)
Type F	13.23 \pm 2.90 (3)	9.66 \pm 2.36 (7)	10.19 \pm 1.22 (4)	8.58 \pm 2.98 (4)
Type E	11.12 \pm 4.27 (2)	2.94 \pm 1.69 (4)	13.25 \pm 4.60 (2)	9.68 \pm 1.16 (2)

Values are means \pm SD with sample numbers in parentheses. Three transitional units—1 Type B, 1 Type C, and 1 Type F—are not included in the above averages (see text). For abbreviations, see Table 1.

tion kinetics. To my knowledge these results are the first direct evidence of large-scale regional differences in adaptation in hair cells from a single inner-ear endorgan.

Sensitivity of hair cells to hair bundle displacement

My results reveal that hair cells with differing hair bundle morphology have different sensitivities to hair bundle displacement. More specifically, Type B and, to a lesser extent, Type C cells have lower sensitivities to hair bundle displacement than Type F and Type E cells. This was not due to the manner in which hair bundles were stimulated in this study. It was, however, partially determined by geometric factors associated with the hair bundle morphology of different hair cell types. As long as hair bundle displacement is applied at the tip of the hair bundle, longer hair bundles are less sensitive to hair bundle displacement. They will, however, linearly transduce a wider range of displacements. In many vestibular hair cells this process is further extended by using a long kinocilium to effectively increase stereociliary length. Hair bundles with large numbers of short stereocilia are also more sensitive than other hair bundles, because small displacements produce large angular rotations and because more stereocilia imply more transducer channels. When normalized for these geometric factors, however, the sensitivities of utricular hair cell types were still markedly different, demonstrating that differences in hair bundle morphology can only partially compensate for intrinsic differences in sensitivity between hair cell types. Other factors, not examined in this analysis, may also contribute to differences in sensitivity between hair cell types. It is possible, for example, that utricular hair cells differ in the size of their transduction conductances, the range of tension conveyed by tip links to their transduction channels, or the probability of opening of their transduction channels.

Differences in the sensitivity of utricular hair cells to hair bundle displacement might also reflect differences in the passive membrane properties of distinct hair cell types (Baird 1994). The sensitivity of hair cells to hair bundle displacement, however, did not correlate with their sensitivity to intracellular current. Type B cells, for example, had high input resistances but low sensitivities to hair bundle displacement. Type C cells, by contrast, had low resistances

and large responses to hair bundle displacement. When normalized for differences in hair bundle morphology, the maximum sensitivities of utricular hair cells to hair bundle displacement were similar to those reported for other hair cell preparations. Hair cells in the turtle (Crawford et al. 1989) and mammalian cochlea (Russell et al. 1986) have maximum sensitivities of 30 mV/ $^{\circ}$. Vestibular hair cells have somewhat lower sensitivities. Hair cells in the bullfrog sacculus, for example, have reported sensitivities from 2–4 mV/ $^{\circ}$ (Eatock et al. 1987; Hudspeth and Corey 1977).

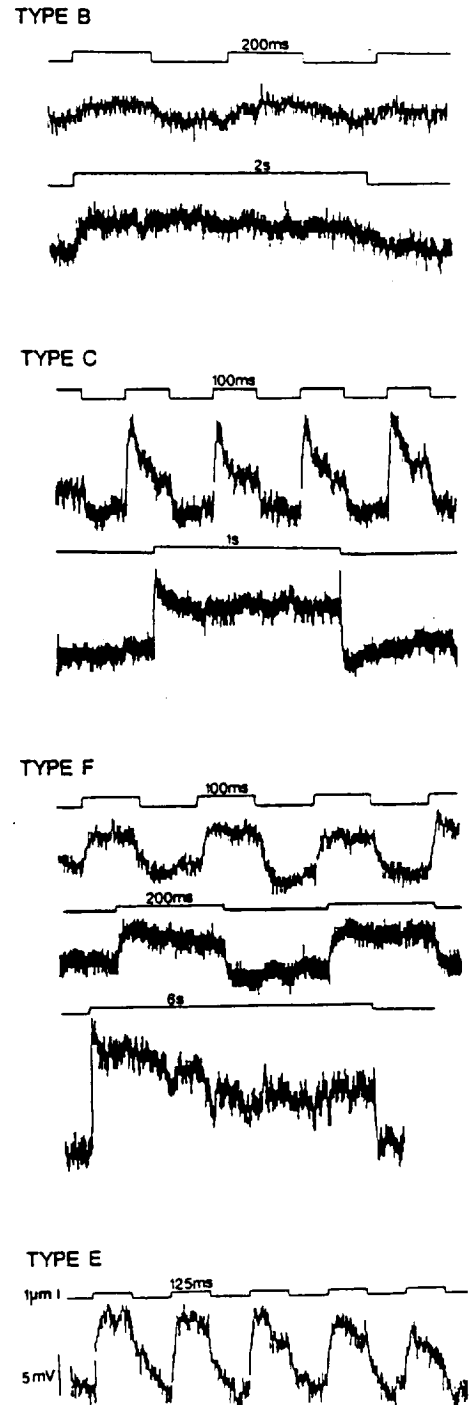


FIG. 11. Voltage responses of typical Type B, Type C, Type F, and Type E hair cells to step hair bundle displacements of varying duration.

This compares favorably with my value of $2 \text{ mV}/^\circ$ for Type F and Type E cells. Type B cells, on the other hand, had sensitivities of only $0.1 \text{ mV}/^\circ$.

Hair cells in the bullfrog utricle also differed in their linear range of transduction, suggesting that the relationship between hair bundle displacement and the probability of transduction channel opening is different in different hair cell types. Previous studies in auditory (Fuchs et al. 1988; Russell et al. 1986) and chick vestibular (Ohmori 1985, 1987) hair cells have also shown that hair cells with longer hair bundles differ in their linear range and sensitivity to hair bundle displacement. The linear range of utricular hair cells ranged from 3° in Type F and Type E cells to $\sim 25^\circ$ in Type B cells and was similar to that reported for other preparations. In the turtle cochlea, hair cells encode $<5^\circ$ of angular rotation (Crawford et al. 1989). This range is somewhat larger in vestibular hair cells, ranging from $\sim 7^\circ$ for chick vestibular hair cells (Ohmori 1984, 1985) to $\sim 15^\circ$ for hair cells in the bullfrog sacculus (Hudspeth and Corey 1977).

Response dynamics of hair cells to hair bundle displacement

The response dynamics of utricular hair cells to hair bundle displacement, measured in both the time and frequency domain, differ from those to intracellular current. More specifically many hair cells display adaptation, recognizable by conspicuous response declines to maintained step displacements and large gain enhancements and phase leads to low-frequency sinusoidal displacement. This is a function of their macular location, with striolar but not extrastriolar cells adapting to hair bundle displacement. Among adapting cells the rate and extent of adaptation differs in different hair cell types. These differences are also correlated with macular location, with rapidly adapting cells located in the outer striolar rows and more slowly adapting cells located more centrally. The step responses of Type C cells in the outer rows, for example, are rapidly adapting. Type C cells located more centrally adapt somewhat more slowly to maintained displacement. Type F and Type E cells, located only in the inner striolar rows, adapt only in response to longer-duration step displacements. With the exception of Type E cells, the rate and extent of hair cells are also correlated, with rapidly adapting cells adapting to a greater extent than more slowly adapting hair cells.

Similar response declines to step displacements are seen in intracellular recordings of receptor voltage from hair cells in the bullfrog sacculus (Eatock et al. 1987). In this preparation the responses of hair cells decline to 10–30% of their peak amplitude in response to depolarizing step displacements. Adaptation also manifests itself as a decline in the receptor current of voltage-clamped hair cells in both the bullfrog sacculus (Assad et al. 1989; Eatock et al. 1987; Hacohen et al. 1989) and turtle cochlea (Crawford et al. 1989, 1991) to maintained hair bundle displacement. The extent of adaptation is similar in auditory and vibratory hair cells. Its time course, however, is not. The responses of hair cells in the bullfrog sacculus decline to steady-state levels in $<50 \text{ ms}$ in response to depolarizing step displacements. Hair cells in the turtle cochlea adapt even more

quickly, declining within 10 ms to $\sim 20\%$ of their peak amplitude (Crawford et al. 1989). No evidence for adaptation has been seen in hair cells from the chick vestibular endorgans (Ohmori 1985, 1987) or the mammalian cochlea (Russell et al. 1989).

Adaptation in other inner ear endorgans, although it manifests itself as a progressive decline in receptor current or voltage, is not due to desensitization of the transducer channels (Assad et al. 1989; Crawford et al. 1989; Eatock et al. 1987; Hacohen et al. 1989). Rather, transduction persists with normal sensitivity, but the position at which the hair cell is most sensitive shifts from its initial resting position toward the current position of the hair bundle. Thus adaptation involves a mechanical adjustment of the tension stimulus reaching the displacement-sensitive stereocilia (Assad et al. 1989; Hacohen et al. 1989; Howard and Hudspeth 1987, 1988) or an adjustment of the open probabilities of the transduction channel (Crawford et al. 1989, 1991). This adjustment is believed to be made at the level of the tip links, fine filamentous links connecting adjacent stereocilia within the hair bundle (Osborne et al. 1988; Pickles et al. 1984). Mechanoelectric transduction is disrupted when these links are severed by removal of calcium from the external medium (Assad et al. 1991; Crawford et al. 1991). Recent physiological evidence suggests that a cytoplasmic motor, possibly a myosinlike protein (Hacohen et al. 1989; Howard and Hudspeth 1987, 1988; Shepherd et al. 1990), maintains resting tension on transduction channels, perhaps by actively moving one or both ends of the tip links.

Before concluding that response declines seen in utricular hair cells are the result of an adaptation process associated with mechanoelectric transduction I must briefly consider some potential artifacts and alternative explanations for their generation. The observed declines in these voltage responses are unlikely to be an artifact due to the slipping of the stimulus probe. First, there was no observable motion of the top of the hair bundle and stimulus probes did not appear to lose contact with the hair bundle during an adapting stimulus. Second, the steady-state voltage responses of adapting hair cells did not exhibit further changes after adaptation had taken place, even for step displacements $\leq 10 \text{ s}$ in duration, suggesting that the probe was well coupled to the hair bundle. Finally, the time course of adaptation was different in different hair cell types. Because the hair bundles of all hair cells were displaced in a similar manner, it seems unlikely that slippage of the stimulus probe would occur only for specific hair cell types.

Unlike other studies in the bullfrog sacculus (Assad et al. 1989; Hacohen et al. 1989) and turtle cochlea (Crawford et al. 1989, 1991), I did not directly record transduction current in these experiments. It is therefore possible that at least some of the response dynamics seen in response to hair bundle displacement were contributed by the gating kinetics of voltage- and ion-dependent conductances in the basolateral membrane. Differences in the response dynamics of utricular hair cells to hair bundle displacement would then reflect differences in the active membrane properties of distinct hair cell types (Baird 1994). Several lines of evidence, however, suggest that this is unlikely. The amplitude of voltage responses examined in this study was small. With the possible exception of Type C cells, which

may possess a persistent membrane conductance near resting membrane potential (Baird 1994), it is therefore unlikely that voltage-dependent membrane conductances were activated to any large extent in response to the range of hair bundle displacements used in this study. Moreover, the low-frequency response dynamics of hair cells to hair bundle displacement were markedly different from those to intracellular current. Individual hair cells that adapted to hair bundle displacement, for example, did not adapt to intracellular current. In addition, hair cells that had similar response dynamics to intracellular current had very different response dynamics to hair bundle displacement. I cannot as yet rule out the possibility that the response declines seen in the responses of utricular hair cells are due to an inactivation of their transduction channels. The most parsimonious interpretation of these results, however, is that, as in the bullfrog sacculus (Assad et al. 1989; Eatock et al. 1987; Hacohen et al. 1989) and turtle cochlea (Crawford et al. 1989, 1991), adaptation acts to reduce the mechanical input to the transducer channels, resetting the operating range of the hair bundle.

It is important to establish that differences in adaptation kinetics are not an artifact determined by variations in the physiological state of hair cells during recording. Adaptation in hair cells is known to be more labile than mechanoelectric transduction (Assad et al. 1989; Eatock et al. 1987) and has even been compromised in early whole-cell patch-clamp recordings (Holton and Hudspeth 1986). This is probably due to the known tendency for patch-clamp electrodes to dialyze cells, leaching the intracellular cytoplasm of important cofactors or second messengers necessary for many physiological phenomenon (Marty and Neher 1983). The sharp intracellular microelectrodes used in this study would not be expected to produce such an effect. Moreover, if such a mechanism were at work, one might expect to see adapting cells only at early times during an experiment or to find substantial disagreement between intracellular data acquired at different times from the same hair cell. Neither of these possibilities was observed.

There are still several potential difficulties with concluding that adaptation kinetics vary in different hair cell types. First, the number of hair cells recorded in this study was small and these cells were located only within the striola or immediately adjacent to its medial border. A larger and more widely dispersed sample of hair cells, particularly in the extrastriolar regions, would be desirable. Because of the limited data set, many of my interpretations about the rate and extent of adaptation in different hair cell types should be viewed cautiously. In addition, hair cells were not always stimulated at identical resting membrane potentials. In other preparations (Assad et al. 1989; Crawford et al. 1989; Hacohen et al. 1989), depolarizing membrane voltages have been shown to shift the resting DRCs of hair cells to the left, decreasing both the size of the response and the rate of adaptation to a given hair bundle displacement. I would therefore expect adaptation to be more difficult to detect in hair cells with more depolarized resting membrane potentials. Furthermore, the rate of any observed adaptation would be underestimated in these cells. It is therefore possible that nonadapting hair cells were simply recorded at more depolarized resting membrane potentials than rapidly

adapting cells. This was not observed. Rather, rapidly adapting hair cells often had more depolarized resting membrane potentials than more slowly adapting hair cells. Furthermore, hair cells with similar resting membrane potentials often displayed markedly different rates of adaptation to hair bundle displacement.

A second possibility is that some hair cells were driven into negative or positive saturation by the placement of the stimulating probe, obscuring the presence of adaptation to maintained hair bundle displacement. To guard against this possibility, I was careful to compare the resting membrane potential of hair cells before and after placement of the stimulating probe and to examine the form of the DRC. It is nevertheless possible that the hair bundles of some hair cells were displaced from their resting position by the stimulus probe, especially with the relatively large displacements used in these experiments. This is supported by the observation that nonadapting hair cells were extremely sensitive to resting hair bundle position and were easily driven into negative or positive saturation. Rapidly adapting hair cells, however, were not sensitive to resting hair bundle position, suggesting that utricular hair cells do differ in their adaptation kinetics.

A third potential difficulty with these studies was that hair cells were not always stimulated at identical displacements. The process underlying adaptation in auditory and vibratory hair cells is nonlinear, occurring more rapidly for excitatory than for inhibitory steps and more completely for small than for large steps (Assad et al. 1989; Crawford et al. 1989, 1991; Eatock et al. 1987; Hacohen et al. 1989). In these preparations, the time course of the response to adapting steps of varying amplitude follows roughly similar time courses, so long as hair bundle displacement is kept below a certain level. At saturating hair bundle displacements, however, the time course of the voltage response does not reflect the actual time course of adaptation. It is therefore possible that I underestimated the rate of adaptation in some hair cells. Voltage responses in Type B cells, for example, were small and, unlike other hair cell types, observed only for large hair bundle displacements. It is possible that these cells would have exhibited faster rates of adaptation at smaller stimulus amplitudes. Hair cells stimulated with similar displacements, however, still differed dramatically in their rate of adaptation to hair bundle displacement, supporting the conclusion that large variations exist in the adaptation kinetics of utricular hair cells.

Differences in the response dynamics of utricular hair cells to hair bundle displacement were correlated with differences in hair bundle morphology rather than macular location per se. Type B cells, for example, had similar response properties, whether they were located in the striolar or extrastriolar region. Moreover, hair cells in similar macular locations, but with differing hair bundle morphology, differed in their responses to hair bundle displacement. Type C cells in the inner striolar rows, for example, were more rapidly adapting than other cell types in these rows. At the same time, the relation between adaptation kinetics and hair bundle morphology was not absolute. The adaptation kinetics of Type C cells, for example, varied over a wide range. A few hair cells also had intermediate physiological properties. Hair cells on the striolar border, for exam-

ple, could be nonadapting, resembling Type B cells, or rapidly adapting, resembling the responses of Type C cells. This was also seen in the striolar region, where the responses of one Type F cell strongly resembled those of Type C cells. These transitional units may have been inadvertently misclassified. The fact that these cells were all located in transitional macular locations, however, suggests that they may represent natural variations.

Previous studies in both the bullfrog sacculus (Assad et al. 1989; Hacohen et al. 1989) and the turtle cochlea (Crawford et al. 1989, 1991) have shown that the kinetics of adaptation are a function of both membrane voltage and calcium concentration. As Assad et al. (1989) and Crawford et al. (1989) have shown, both the decline in receptor current and the shift in the DRC of adapting hair cells are slower at depolarized potentials. This voltage dependence is eliminated if extracellular calcium concentration is reduced (Assad et al. 1989), suggesting that this dependence is an indirect consequence of external calcium entry through transduction channels and that the entry of external calcium into the stereocilia facilitates the adaptation process. The rate of adaptation is also reduced by lowering extracellular calcium concentration (Eatock et al. 1987; Hacohen et al. 1989) or by including high concentrations of the calcium chelator bis-(*O*-aminophenoxy)-*N,N,N',N'*-tetraacetic acid in the interior of patch-clamp pipettes (Crawford et al. 1989). Calcium may also directly affect the kinetics of the transduction channel (Crawford et al. 1989, 1991). In either case, it appears likely that adaptation is predicated on the action of calcium at some internal site and may be slowed or prevented by limiting the access of calcium to this site. Thus the dynamics of calcium regulation within the hair bundle, which are interposed between tip-link displacement and the relaxation of tension to the transduction channels, may constitute a rate-limiting intermediate process that controls adaptation kinetics.

Calcium regulation within the hair bundle is unlikely to be accomplished entirely by passive diffusion. As Crawford et al. (1989) point out, the kinetics of adaptation are nonlinear, with the rate of adaptation being slower for larger transduction currents. This is the opposite of what would be expected from the entry of external calcium followed by passive diffusion. More likely, calcium is actively sequestered by Ca^{2+} -binding proteins that act to limit free calcium concentration within the hair bundle. The dynamics of calcium regulation would then be governed by the relative affinities of individual Ca^{2+} -binding proteins for calcium. The role of Ca^{2+} -binding proteins in regulating adaptation is not clear, although the rate of adaptation is reduced by nonselective calmodulin inhibitors (Corey et al. 1987).

Utricular hair cells with differing rates of adaptation may possess different complements of Ca^{2+} -binding proteins. Some support for this suggestion is found in the results of recent biochemical (Gillespie and Hudspeth 1991; Shepherd et al. 1989), immunocytochemical (Dechesne and Thomasset 1988; Dechesne et al. 1988; Oberholtzer et al. 1988; Rabie et al. 1983; Sans et al. 1986, 1987; Shepherd et al. 1989), and molecular biological (Dememes et al. 1991) studies. These studies have demonstrated the presence of

several Ca^{2+} -binding proteins, including calbindin (Dechesne and Thomasset 1988; Dechesne et al. 1988; Oberholtzer et al. 1988; Rabie et al. 1983; Sans et al. 1986, 1987), calmodulin (Shepherd et al. 1989), calretinin (Dechesne et al. 1991), and S-100 (Saidel et al. 1990) in auditory and vestibular hair cells. In bullfrog saccular hair cells these proteins have been localized to the hair bundle, suggesting that they are involved with mechanoelectric transduction (Gillespie and Hudspeth 1991; Shepherd et al. 1989). In addition, recent studies in our laboratory (Baird and Schuff, unpublished data) have demonstrated that utricular hair cells differ in their complement of Ca^{2+} -binding proteins.

Functional organization of the utricular macula

Hair cells in the bullfrog utricle are specialized, via a combination of mechanical and ionic mechanisms, to encode both static and dynamic acceleration. Sensitivity, for example, is determined both by mechanical factors associated with hair bundles and by the passive membrane properties of hair cells. Response dynamics, on the other hand, are governed by the kinetics of an adaptation process associated with transduction channels and of voltage-dependent conductances in the basolateral membrane. Thus Type B cells, with their long kinocilium and short stereocilia, have lower sensitivities to stereociliary displacement than other utricular hair cells. This lower sensitivity, although somewhat offset by the higher sensitivity of these cells to intracellular current (Baird 1994), allows them to faithfully transduce a wider range of hair bundle displacements than other hair cell types. Type B cells also do not adapt or adapt only very slowly to maintained hair bundle displacement. They are therefore well suited for encoding static gravity and low-frequency linear acceleration. Hair cells restricted to the striolar region, on the other hand, have higher sensitivities to natural stimulation. Moreover, they have higher frequency sensitivities than extrastriolar hair cells, and, in the case of Type E cells, are electrically tuned to further enhance their high-frequency sensitivity (Baird 1994). Type C cells, for example, resemble Type B cells in having relatively low sensitivities to hair bundle displacement. Unlike Type B cells, however, they rapidly adapt to maintained hair bundle displacement. The rapid adaptation of Type C cells has two consequences. First, it prevents static gravity from saturating their responses, allowing them to maintain high sensitivity to smaller, high-frequency linear accelerations. Second, it reduces their input conductance at the termination of depolarizing displacements, allowing them to respond to signals over a wider dynamic range (Crawford et al. 1989). In the inner striola, Type F and Type E cells have higher sensitivities and transduce a smaller range of displacement than other hair cells. They also adapt, although more slowly, to maintained hair bundle displacement. The slower time course of adaptation in these cells may enable them to retain a higher degree of sensitivity to low-frequency displacement. This would presumably reduce the sensitivity of these cells to high-frequency displacement but might allow them to retain sensitivity to both static and dynamic acceleration.

Contribution of hair cell adaptation to afferent response dynamics

Utricular afferents in bullfrog (Baird and Lewis 1986; Blanks and Precht 1976; Caston et al. 1977) and fish (Macadar et al. 1975) have previously been classified as gravity or vibratory sensitive. Gravity afferents have been further classified into three classes according to their responses to head tilt. Tonic gravity afferents respond to head position, phasic gravity afferents respond to head velocity, and phasic-tonic afferents respond to both head position and velocity. Higher vertebrates possess only tonic and phasic-tonic otolith afferents (Anderson et al. 1978; Fernandez and Goldberg 1976a,b; Goldberg et al. 1990a; Perachio and Correia 1983; Vidal et al. 1971).

Morphophysiological studies suggest that differences in afferent response dynamics are solely determined by regional variations in presynaptic transduction mechanisms (Baird et al. 1988; Goldberg et al. 1985, 1990b). In the semicircular canal, regional variations in cupular dynamics (Boyle et al. 1991; Hillman and McLaren 1979; Honrubia et al. 1981, 1989; McLaren and Hillman 1979) or the coupling of the cupula to the sensory hair bundles of hair cells (Honrubia et al. 1981, 1989; Lim 1976) may underlie the diversity in response dynamics. In the otolith organs, on the other hand, differences in afferent response dynamics may be determined by differences in the transduction mechanisms of different hair cell types. In the bullfrog utricle, the response dynamics of utricular afferents are correlated with the hair bundle morphology of their innervated hair cells (Baird and Lewis 1986), suggesting that hair cells with differing hair bundle morphology may represent independent hair cell types with distinctive physiological response properties.

These results suggest that the response dynamics of gravity afferents are largely determined by the rate of adaptation in their innervated hair cells. Tonic gravity afferents, for example, innervate Type B cells in the medial and lateral extrastriolar regions (Baird and Lewis 1986). Other afferent classes supply the striolar region, generally innervating a complex mixture of hair cell types (Baird and Schuff 1994). Phasic and phasic-tonic gravity afferents, for example, are both known to innervate hair cells in the outer striolar rows (Baird and Lewis 1986). Afferents innervating these rows largely innervate Type B and Type C cells (Baird and Schuff 1994). Moreover, the numbers of Type B and Type C hairs innervated by these afferents are inversely correlated. This suggests that striolar afferents with varying degrees of tonic and phasic gravity sensitivity differ in the number of Type B and Type C hair cells they contact. This hypothesis is supported by the results of the present study, which indicate that Type B cells, whether located in the striolar or extrastriolar region, are sensitive only to low frequencies and are nonadapting or very slowly adapting to hair bundle displacement. Type C cells, on the other hand, rapidly adapt to hair bundle displacement, suggesting that they encode head velocity rather than head position. Type F and Type E cells, which adapt only slowly and to a limited extent, may also contribute to tonic gravity sensitivity. These cells, however, represent only a small percentage of

the total innervation of most striolar afferents (Baird and Schuff 1994).

With the exception of vibratory afferents, utricular afferents in the bullfrog have peripheral innervation patterns (Baird and Schuff 1994) and physiological response properties (Baird and Lewis 1986) similar to those seen in mammals. Recent studies have also shown that the longest stereocilia of Type I and Type II hair cells in mammals display regional variations in morphology similar to those seen in the bullfrog (Lapeyre et al. 1992). Such variations, more subtle than those involved in the separation of hair cells into Type I and Type II varieties, may be associated with differences in hair cell physiology in many vertebrate species, including mammals.

I am indebted to Dr. David C. Corey for a program that predicts tip-link extensions resulting from linear stereociliary displacements. Dr. Robert R. Peterka for a program that estimates, using a least-squares criterion, the parameters of transfer functions to sinusoidal gain and phase data, and to Dr. Miriam D. Burton for assistance with electron microscopy. I am also grateful to N. R. Schuff for figure preparation and assistance during electrophysiological experiments and B. Smith for manuscript preparation.

Funding was provided by National Institute of Deafness and Communicative Disorders Grants DC-00355 and DC-02040, National Aeronautics and Space Administration Grant NCC 2-651, and by grants from the Oregon Lions Sight and Hearing Foundation.

Address for reprint requests: R. A. Baird, R. S. Dow Neurological Sciences Institute, Good Samaritan Hospital and Medical Center, 1120 NW 20th Avenue, Portland, OR 97209.

Received 24 February 1993; accepted in final form 14 October 1993.

REFERENCES

- ANDERSON, D. J., BLANKS, R. H. I., AND PRECHT, W. Response characteristics of semicircular canal and otolith neurons in cat. I. Dynamic responses of primary vestibular fibers. *Exp. Brain Res.* 32: 491-507, 1978.
- ASHMORE, J. F. Frequency tuning in a frog vestibular organ. *Nature Lond.* 304: 536-538, 1983.
- ASSAD, J. A. AND COREY, D. P. An active motor model for adaptation by vertebrate hair cells. *J. Neurosci.* 12: 3291-3309, 1992.
- ASSAD, J. A., HACHOEN, N., AND COREY, D. P. Voltage dependence of adaptation and active bundle movement in bullfrog saccular hair cells. *Proc. Natl. Acad. Sci. USA* 86: 2918-2922, 1989.
- ASSAD, J. A., SHEPHERD, G. M. G., AND COREY, D. P. Tip-link integrity and mechanical transduction in vertebrate hair cells. *Neuron* 7: 985-994, 1991.
- BAIRD, R. A. Morphological and electrophysiological properties of hair cells in the bullfrog utricle. *Ann. NY Acad. Sci.* 656: 12-26, 1992.
- BAIRD, R. A. Comparative transduction and tuning mechanisms of hair cells in the bullfrog utricle. I. Responses to intracellular current. *J. Neurophysiol.* 71: 666-684, 1994.
- BAIRD, R. A., DESMADRYL, G., FERNANDEZ, C., AND GOLDBERG, J. M. The vestibular nerve of the chinchilla. II. Relation between afferent response properties and peripheral innervation patterns in the semicircular canals. *J. Neurophysiol.* 60: 182-203, 1988.
- BAIRD, R. A. AND LEWIS, E. R. Correspondences between afferent innervation patterns and response dynamics in the bullfrog utricle and lagena. *Brain Res.* 369: 48-64, 1986.
- BAIRD, R. A. AND SCHUFF, N. R. Comparative transduction mechanisms of hair cells in the bullfrog utricle. *Soc. Neurosci. Abstr.* 16: 733, 1990.
- BAIRD, R. A. AND SCHUFF, N. R. Transduction mechanisms of hair cells in the bullfrog utricle. *Assoc. Res. Otolaryngol. Abstr.* 14: 38, 1991.
- BAIRD, R. A. AND SCHUFF, N. R. Peripheral innervation patterns of vestibular nerve afferents in the bullfrog utricle. *J. Comp. Neurol.* In press.
- BLANKS, R. H. I. AND PRECHT, W. Functional characterization of primary vestibular afferents in the frog. *Exp. Brain Res.* 25: 369-390, 1976.
- BOYLE, R., CAREY, J. P., AND HIGHSTEIN, S. M. Morphological correlates of response dynamics and efferent stimulation in horizontal semicircular canal afferents of the toadfish, *Opsanus tau*. *J. Neurophysiol.* 66: 1504-1521, 1991.
- CASTON, J., PRECHT, W., AND BLANKS, R. H. I. Response characteristics of

- frog's lagenar afferents to natural stimulation. *J. Comp. Physiol.* 118: 273-289, 1977.
- COREY, D. P. AND HUDSPETH, A. J. Ionic basis of the receptor potential in vertebrate hair cell. *Nature Lond.* 281: 657-677, 1979.
- COREY, D. P. AND HUDSPETH, A. J. Mechanical stimulation and micromanipulation with piezoelectric bimorph elements. *J. Neurosci. Methods* 3: 183-202, 1980.
- COREY, D. P. AND HUDSPETH, A. J. Kinetics of the receptor current in bullfrog saccular hair cells. *J. Neurosci.* 3: 962-976, 1983.
- COREY, D. P., SMITH, W. J., BARRIS, B. A., AND KOROSHETZ, W. J. Calmodulin inhibitors block adaptation in vestibular hair cells. *Soc. Neurosci. Abstr.* 13: 538, 1987.
- CRAWFORD, A. C., EVANS, M. G., AND FETTIPLACE, R. Activation and adaptation of transducer currents in turtle hair cells. *J. Physiol. Lond.* 419: 405-434, 1989.
- CRAWFORD, A. C., EVANS, M. G., AND FETTIPLACE, R. The actions of calcium on the mechanoelectric transducer current of turtle hair cells. *J. Physiol. Lond.* 434: 369-398, 1991.
- CRAWFORD, A. C. AND FETTIPLACE, R. An electrical tuning mechanism in turtle cochlear hair cells. *J. Physiol. Lond.* 312: 377-412, 1981.
- DECHESNE, C. J. AND THOMASSET, M. Calbindin (CaBP-28kDa) appearance and distribution during development of the mouse inner ear. *Dev. Brain Res.* 40: 233-242, 1988.
- DECHESNE, C. J., THOMASSET, M., BREHIER, A., AND SANS, A. Calbindin (CaBP 28 kDa) localization in the peripheral vestibular system of various vertebrates. *Hear. Res.* 33: 273-278, 1988.
- DECHESNE, C. J., WINSKY, L., KIM, H. N., GOING, G., VU, T. D., WENTHOLD, R. J., AND JACOBOWITZ, D. M. Identification and ultrastructural localization of a calretinin-like calcium-binding protein (protein 10) in the guinea pig and rat inner ear. *Brain Res.* 560: 139-148, 1991.
- DEMEMES, D., MONIOT, B., LOMRI, N., THOMASSET, M., AND SANS, A. Detection of calbindin-28k mRNA in rat vestibular ganglion neurones by in situ hybridization. *Mol. Brain Res.* 9: 153-156, 1991.
- EATOCK, R. A., COREY, D. P., AND HUDSPETH, A. J. Adaptation of mechanoelectric transduction in hair cells of the bullfrog's sacculus. *J. Neurosci.* 7: 2821-2836, 1987.
- FERNANDEZ, C. AND GOLDBERG, J. M. Physiology of peripheral neurons innervating otolith organs of the squirrel monkey. I. Response to static tilts and to long-duration centrifugal force. *J. Neurophysiol.* 39: 970-984, 1976a.
- FERNANDEZ, C. AND GOLDBERG, J. M. Physiology of peripheral neurons innervating otolith organs of the squirrel monkey. III. Response dynamics. *J. Neurophysiol.* 39: 995-1008, 1976b.
- FUCHS, P. A., NAGAI, T., AND EVANS, M. G. Electrical tuning in hair cells isolated from chick cochlea. *J. Neurosci.* 8: 2460-2467, 1988.
- GILLESPIE, P. G. AND HUDSPETH, A. J. High purity isolation of bullfrog hair bundles and subcellular and topological localization of constituent proteins. *J. Cell Biol.* 112: 625-640, 1991.
- GOLDBERG, J. M., BAIRD, R. A., AND FERNANDEZ, C. Morphophysiological studies of the mammalian vestibular labyrinth. In: *Progress in Clinical and Biological Research. Contemporary Sensory Neurobiology*, edited by M. J. Correia and A. A. Perachio. New York: Liss, 1985, vol. 187, p. 231-245.
- GOLDBERG, J. M., DESMADRYL, G., BAIRD, R. A., AND FERNANDEZ, C. The vestibular nerve in the chinchilla. IV. Discharge properties of utricular afferents. *J. Neurophysiol.* 63: 781-790, 1990a.
- GOLDBERG, J. M., DESMADRYL, G., BAIRD, R. A., AND FERNANDEZ, C. The vestibular nerve in the chinchilla. V. Relation between afferent response properties and peripheral innervation patterns in the utricular macula. *J. Neurophysiol.* 63: 791-804, 1990b.
- HACOHEN, N., ASSAD, J. A., SMITH, W. J., AND COREY, D. P. Regulation of tension on hair-cell transduction channels: displacement and calcium dependence. *J. Neurosci.* 9: 3988-3997, 1989.
- HILLMAN, D. E. AND MCLAREN, J. W. Displacement configuration of semicircular canal cupulae. *Neuroscience* 4: 1989-2000, 1979.
- HOLTON, T. AND HUDSPETH, A. J. The transduction channel of hair cells from the bullfrog characterized by noise analysis. *J. Physiol. Lond.* 375: 195-227, 1986.
- HONRUBIA, V., HOFFMAN, L. F., SITKO, S. T., AND SCHWARTZ, I. R. Anatomical and physiological correlates in bullfrog vestibular nerve. *J. Neurophysiol.* 61: 688-701, 1989.
- HONRUBIA, V., SITKO, S. T., KIMM, J., BETTS, W., AND SCHWARTZ, I. R. Physiological and anatomical characteristics of primary vestibular afferent neurons in the bullfrog. *Int. J. Neurosci.* 15: 197-206, 1981.
- HOWARD, J. AND HUDSPETH, A. J. Mechanical relaxation of the hair bundle mediates adaptation in mechanoelectrical transduction by the bullfrog's saccular hair cell. *Proc. Natl. Acad. Sci. USA* 84: 3064-3068, 1987.
- HOWARD, J. AND HUDSPETH, A. J. Compliance of the hair bundle associated with gating of mechanoelectrical transduction channels in the bullfrog's saccular hair cell. *Neuron* 1: 189-199, 1988.
- HOWARD, J., ROBERTS, W. M., AND HUDSPETH, A. J. Mechanoelectrical transduction by hair cells. *Annu. Rev. Biophys. Biophys. Chem.* 17: 99-124, 1988.
- HUDSPETH, A. J. The cellular basis of hearing: The biophysics of hair cells. *Science Wash. DC* 230: 745-752, 1986.
- HUDSPETH, A. J. AND COREY, D. P. Sensitivity, polarity and conductance change in the response of vertebrate hair cells to controlled mechanical stimuli. *Proc. Natl. Acad. Sci. USA* 74: 2407-2411, 1977.
- HUDSPETH, A. J. AND LEWIS, R. S. Kinetic analysis of voltage- and ion-dependent conductances in saccular hair cells of the bullfrog, *Rana catesbeiana*. *J. Physiol. Lond.* 400: 237-274, 1988.
- LAPEYRE, P., GUILHAUME, A., AND CAZALS, Y. Differences in hair bundles associated with Type I and Type II vestibular hair cells of the guinea pig sacculus. *Acta Otolaryngol. Stockh.* 112: 635-642, 1992.
- LEWIS, E. R., BAIRD, R. A., LEVERENZ, E. L., AND KOYAMA, H. Inner ear: dye injection reveals peripheral origins of specific sensitivities. *Science Wash. DC* 215: 1641-1643, 1982.
- LEWIS, E. R. AND LI, C. W. Hair cell types and distributions in the otolithic and auditory organs of the bullfrog. *Brain Res.* 83: 35-50, 1975.
- LEWIS, R. S. AND HUDSPETH, A. J. Voltage and ion-dependent conductances in solitary vertebrate hair cells. *Nature Lond.* 304: 538-541, 1983.
- LIM, D. J. Morphological and physiological correlates in cochlear and vestibular sensory epithelia. In: *Scanning Electron Microscopy*, edited by O. Johari and R. P. Becker. Chicago: IIT Research Institute, 1976, vol. V, p. 269-276.
- MACADAR, O., WOLFE, G. E., O'LEARY, D. P. AND SEGUNDO, J. P. Response of the elasmobranch utricle to maintained spatial orientation, transitions, and jitter. *Exp. Brain Res.* 22: 1-22, 1975.
- MARTY, A. AND NEHER, E. Tight-seal whole-cell recording. In: *Single Channel Recording*, edited by B. Sakmann and E. Neher. New York: Plenum, 1983, p. 107-122.
- MCLAREN, J. W. AND HILLMAN, D. E. Displacement of the semicircular canal cupula during sinusoidal rotation. *Neuroscience* 4: 2001-2008, 1979.
- MILLER, R. G., JR. Developments in multiple comparisons, 1966-1977. *J. Am. Statist. Assoc.* 72: 779-788, 1977.
- OSBERG, J. C., BUETTGER, C., SUMMERS, M. C., AND MATSCHINSKY, F. M. The 28-kDa calbindin-D is a major calcium-binding protein in the basilar papilla of the chick. *Proc. Natl. Acad. Sci. USA* 85: 3387-3390, 1988.
- OHMORI, H. Mechanoelectric transducer has discrete conductances in the chick vestibular hair cell. *Proc. Natl. Acad. Sci. USA* 81: 1888-1891, 1984.
- OHMORI, H. Mechanoelectric transduction currents in isolated vestibular hair cells of the chick. *J. Physiol. Lond.* 359: 189-217, 1985.
- OHMORI, H. Gating properties of the mechanoelectrical transducer channel in the dissociated vestibular hair cell of the chick. *J. Physiol. Lond.* 387: 589-609, 1987.
- OSBORNE, M. P., COMIS, S. D., AND PICKLES, J. O. Further observations on the fine structure of tip links between stereocilia of the guinea pig cochlea. *Hear. Res.* 35: 99-108, 1988.
- PERACHIO, A. A. AND CORREIA, M. J. Responses of semicircular canal and otolith afferents to small angle static head tilts in the gerbil. *Brain Res.* 280: 287-298, 1983.
- PICKLES, J. O., COMIS, S. D., AND OSBORNE, M. P. Cross-links between stereocilia in the guinea-pig organ of Corti, and their possible relation to sensory transduction. *Hear. Res.* 15: 103-112, 1984.
- PITCHFORD, S. AND ASHMORE, J. F. An electrical resonance in hair cells of the amphibian papilla of the frog *Rana temporaria*. *Hear. Res.* 27: 75-84, 1987.
- RABIE, A., THOMASSET, M., AND LEGRAND, C. Immunocytochemical detection of calcium-binding protein in the cochlear and vestibular hair cells of the rat. *Cell Tissue Res.* 233: 691-696, 1983.
- ROBERTS, W. M., HOWARD, J., AND HUDSPETH, A. J. Hair cells: transduction, tuning, and transmission in the inner ear. *Annu. Rev. Cell Biol.* 4: 63-92, 1988.
- RUSSELL, I. J., RICHARDSON, G. P., AND CODY, A. R. Mechanosensitivity

- of mammalian auditory hair cells in vitro. *Nature Lond.* 321: 517-519, 1986.
- RUSSELL, I. J., RICHARDSON, G. P., AND KOSSL, M. The response of cochlear hair cells to tonic displacements of the sensory hair bundle. *Hear. Res.* 43: 55-70, 1989.
- SAIDEL, W. M., PRESSON, J. C., AND CHANG, J. S. S-100 immunoreactivity identifies a subset of hair cells in the utricle and saccule of a fish. *Hear. Res.* 47: 139-146, 1990.
- SANS, A., BREHIER, A., MONIOT, B., AND THOMASSET, M. Immunoelectronmicroscopic localization of 'vitamin D-dependent' calcium-binding protein (CaBP-28k) in the vestibular hair cells of the cat. *Brain Res.* 435: 293-304, 1987.
- SANS, A., ETCHECOPAR, B., BREHIER, A., AND THOMASSET, M. Immunocytochemical detection of vitamin D-dependent calcium-binding protein (CaBP-28K) in vestibular sensory hair cells and vestibular ganglion neurons of the cat. *Brain Res.* 364: 190-194, 1986.
- SEIDEL, R. C. Transfer-function-parameter estimation from frequency response data—a FORTRAN program. *NASA Technical Memorandum.* NASA TM X-3286, 1975.
- SHEPHERD, G. M. G., BARRES, B. A., AND COREY, D. P. Bundle blot purification and initial protein characterization of hair cell stereocilia. *Proc. Natl. Acad. Sci. USA* 86: 4973-4977, 1989.
- SHEPHERD, G. M. G., COREY, D. P., AND BLOCK, S. M. Actin cores of hair-cell stereocilia support myosin motility. *Proc. Natl. Acad. Sci. USA* 87: 8627-8631, 1990.
- THORSON, J. AND BIEDERMAN-THORSON, M. Distributed relaxation processes in sensory adaptation. *Science Wash. DC* 183: 161-172, 1974.
- VIDAL, J., JEANNEROD, M., LIFSCHITZ, W., LEVITAN, H., ROSENBERG, J., AND SEGUNDO, J. P. Static and dynamic properties of gravity-sensitive receptors in the cat vestibular system. *Kybernetik* 9: 205-215, 1971.
- WERSALL, J. AND BAGGER-SJOBACK, D. Morphology of the vestibular sense organs. In: *Handbook of Sensory Physiology, Vestibular System: Basic Mechanisms*, edited by H. H. Kornhuber. New York: Springer-Verlag, 1974, pt. 1, vol. 6, p. 123-170.

